The University of Melbourne

Doctoral Thesis

The Origin of Matter and Dark Matter

Author:
Stephen J. Lonsdale

Supervisor:
Professor Raymond R. Volkas

ORCID ID : 0000-0002-2771-5458

A thesis submitted in fulfilment of the requirements
for the degree of Doctor of Philosophy

in the

School of Physics
The University of Melbourne

February 2018

They had no temples, but they had a real living and uninterrupted sense of oneness with the whole of the universe; they had no creed, but they had a certain knowledge that when their earthly joy had reached the limits of earthly nature, then there would come for them, for the living and for the dead, a still greater fullness of contact with the whole of the universe. They looked forward to that moment with joy, but without haste, not pining for it, but seeming to have a foretaste of it in their hearts, of which they talked to one another.

The Dream of a Ridiculous Man - Fyodor Dostoyevsky

THE UNIVERSITY OF MELBOURNE

Abstract

Faculty of Science
School of Physics

Doctor of Philosophy

The Origin of Matter and Dark Matter

by Stephen J. Lonsdale

The sum of all currently identified particles accounts for only a small fraction of the mass within the observable universe. Dark matter makes up a large remaining piece of the cosmos. Its theoretical origins remain largely unknown. The relatively small amount of matter that does exist today is known to be a result of a small asymmetry in the early universe between matter and antimatter. Asymmetric dark matter models consider the approximate $1:5$ ratio of matter to dark matter as evidence that the two forms of matter have connected origins. This class of model requires that the dark matter number density is generated in the early universe through a process tied directly to the origin of matter. In order to fully account for this ratio, however, we need to both explain how the connected origins generate similar abundances of matter and dark matter particles and explain why dark matter particles have individual masses comparable to the dominant form of ordinary matter throughout the universe.

In Chapter 1 we review the current picture of the universe and examine the motivations for grand unified theories that connect the matter content of the Standard Model under larger symmetries at high energy. We then examine spontaneous symmetry breaking and the history of mirror matter models which consider a copy of the Standard Model as an explanation for dark matter. With these we develop in Chapter 2 the mechanism of asymmetric symmetry breaking which spontaneously breaks mirror symmetric grand unified theories at a high energy scale. In this $SU(5) \times SU(5)$ model we find how the low energy scale theory contains the Standard Model with minimal interactions to a dark sector that contains a confining gauge group. The unified UV gauge couplings but unique fermion masses in the two sectors results in a lightest stable composite state of the dark sector that is constrained to have a mass comparable to the proton.

In Chapter 3 we extend the asymmetric symmetry breaking concept to $SO(10)$ models and explore how unique breaking chains in the two sectors can occur spontaneously. We use the gauge boson content to modify the running of gauge coupling constants and show how this can result in low energy scale universes with dark sectors that contain viable dark matter candidates.

In Chapter 4 we examine how a similar number density of matter and dark matter can arise in an asymmetric symmetry breaking model with a mirror symmetric theory using a Standard Model that contains an extra Higgs doublet. With the addition of right-handed neutrinos we explore how a thermal leptogenesis mechanism can result in a lepton asymmetry in each sector that is converted into baryon and dark matter asymmetries at low energy. The result of this is a set of possible models that generate the approximate $1:5$ ratio of matter to dark matter in a natural way.

Finally in Chapter 5 we explore how the confinement scale and fermionic content of a confining gauge theory affects the hadronic spectra of dark $SU(3)$ theories. With this we can examine the nature of dark matter particles in our unique framework of asymmetric dark matter models.

Declaration of Authorship

I, Stephen J. Lonsdale, declare that this thesis titled, 'The Origin of Matter and Dark Matter' and the work presented in it are my own. I confirm that:

- This work was done wholly or mainly while in candidature for a research degree at this University.
- Where any part of this thesis has previously been submitted for a degree or any other qualification at this University or any other institution, this has been clearly stated.
- Where I have consulted the published work of others, this is always clearly attributed.
- Where I have quoted from the work of others, the source is always given. With the exception of such quotations, this thesis is entirely my own work.
- I have acknowledged all main sources of help.
- Where the thesis is based on work done by myself jointly with others, I have made clear exactly what was done by others and what I have contributed myself.

Signed: 

Date: 28/02/2018

List of publications

- *Grand unified dark matter*, Stephen J. Lonsdale and Raymond R. Volkas
  Phys. Rev. D 90, 083501 – Published 1 October 2014; Erratum Phys. Rev. D 91, 129906 (2015) – [arXiv:1407.4192]

- *Dark matter from intermediate symmetry breaking scales*, Stephen J. Lonsdale
  Phys. Rev. D 91, 125019 – Published 16 June 2015 – [arXiv:1412.1894]

- *Asymmetric dark matter and the hadronic spectra of hidden QCD*, Stephen J. Lonsdale, Martine Schroor, and Raymond R. Volkas
  Phys. Rev. D 96, 055027 – Published 18 September 2017 – [arXiv:1704.05213]

- *Comprehensive asymmetric dark matter model*, Stephen J. Lonsdale and Raymond R. Volkas
  Phys. Rev. D 97, 103510 – Published 16 May 2018 – [arXiv:1801.05561]

Preface

Chapter 1 is an original introduction to the motivations of this thesis and contains a review of the literature. Chapter 2 is based on the work in *Grand unified dark matter* which investigated ideas developed in collaboration with R. Volkas and was predominantly written by the author. Chapter 3 is based on the work in *Dark matter from intermediate symmetry breaking scales*, written by the author and based on ideas explored in Chapter 2. Chapter 4 is based on the work in *Comprehensive asymmetric dark matter model* which explored ideas developed in collaboration with R. Volkas and was predominantly written by the author. Chapter 5 is based on the work in *Asymmetric dark matter and the hadronic spectra of hidden QCD* which was based on ideas developed in collaboration with R. Volkas and M. Schroor. The results are primarily the work of the author with M. Schroor providing consistency checks and the introduction of the published paper. An original introduction written by the author is used in Chapter 5. Chapter 6 is an original summary of the ideas in all of these chapters and how they fit together to form a cohesive work.

Acknowledgements

I am indebted firstly to my supervisor Ray for all of his continuing support, guidance and wisdom. I could not imagine a better supervisor. Thank you to the other members of my advisory committee, Jeff and Nicole, for always offering their support. I would also like to thank all of my friends and in particular Cameron Piko, Genevieve Beart, Abhishek Sharma and Danielle St Pierre. This work would not have been possible without the support of my family and my parents' encouragement to pursue my own interests. A very large thanks is due to the dedicated physicists I have been fortunate enough to share an office with, specifically Jayne, Ahmad, Iason, Amelia, Ben, Nadine, Peter, Jackson, Laurence, Rebecca, Tim, Tomasz, Leon, John, Alex, Josh, Isaac and Martine. I would also like to thank the rest of the dedicated members of CoEPP including but not limited to KG, David, Pere, Brian, Caitlin, Innes, Jason, Millie, Lucas, Nicholas, Ying, Thor, Caroline, and Sean.

Contents

List of Figures

Abbreviations

ADM	**A**symmetric **D**ark **M**atter
ASB	**A**symmetric **S**ymmetry **B**reaking
BAU	**B**aryon **A**symmetry of the **U**niverse
BBN	**B**ig **B**ang **N**ucleosynthesis
CMB	**C**osmic **M**icrowave **B**ackground
CDM	**C**old **D**ark **M**atter
DM	**D**ark **M**atter
DS	**D**ark **S**ector
EW	**E**lectroWeak
EWSB	**E**lectroWeak **S**ymmetry **B**reaking
EWPT	**E**lectroWeak **P**hase **T**ransition
GUT	**G**rand **U**nified **T**heory
MM	**M**irror **M**atter
QHPT	**Q**uark **H**adron **P**hase **T**ransition
QCD	**Q**uantum **C**hromo**D**ynamics
SM	**S**tandard **M**odel
SSB	**S**pontaneous **S**ymmetry **B**reaking
SUSY	**SU**per **SY**mmetry
VS	**V**isible **S**ector
WIMP	**W**eakly **I**nteracting **M**assive **P**article

To my friends

Chapter 1

Introduction

The Standard Model (SM) of particle physics, together with the theory of general relativity, has seen extraordinary successes in our ongoing efforts to understand the behaviour of the universe. Despite these successes, our comprehension of the world we live in is placed in a substantially smaller framework when we consider that the sum of all currently identified particles is capable of explaining only a small fraction of the mass within the observable universe. Dark matter (DM) makes up the large remaining component of matter in the cosmos. Its nature and origins are almost completely unknown.

The Standard Model is clearly an incomplete theory with the majority of the matter and energy that make up the observable universe beyond our ken. Dark matter is the term used to describe the remaining matter, though it may be composed of many different species of undiscovered particles. There is a large body of evidence for its presence in the cosmic make-up. A hidden form of matter was hypothesised as far back as 1933 when Zwicky [1] noticed this discrepancy in the expected velocity distribution of galaxies in the Coma cluster. While his conjecture of large amounts of unseen mass dominating the gravitational profile of the cluster was not immediately accepted, history has borne out that a type of mass that is not in the form of stars or conventional interstellar gas is responsible for the long list of incongruences in the night sky. Later important evidence was found in the rotation curves of galaxies, which demonstrated the velocities of stars and gas in the outer rims to be near consistent with inner systems rather than dropping off with radius as previously expected. The experimental evidence of dark matter today comes from many different sources, ranging from observations of the acoustic spectrum

of the cosmic microwave background (CMB), through gravitational lensing observations, velocity profiles of stars in galaxies and larger systems in galactic clusters, to simulations of galaxy formation [2, 3].

While dark matter's possible origins are myriad, there are some key pieces of evidence that can allow us to pursue models of dark matter with a degree of confidence. In this work we will endeavor to explore models of both the origin of matter and dark matter in a unified way guided by these critical clues. In the pursuit of explaining dark matter we draw on the work of past dark matter models and experimental constraints from both astrophysics and high energy physics. We consider the use of theories beyond the Standard Model that attempt to solve other problems inherent to both cosmology and particle physics and we explore new ideas that attempt to solve the dark matter problem in a novel way.

To this end we will pursue in this thesis an explanation for the origin and nature of dark matter using one of the most firmly established experimental results about its existence [4], the ratio of matter to dark matter mass densities throughout the universe,

$$\rho_{\mathrm{DM}} \approx 5\,\rho_{\mathrm{M}}. \tag{1.1}$$

This seemingly simple relation will serve as a useful guiding principle for developing an explanation for dark matter as it suggests two key things about dark matter and its origins. In the absence of any information about dark matter, other than the fact that it exists, there would be no reason to assume its mass density ought to be comparable to the ordinary matter density of the universe a priori. One could just as well guess the ratio of stars in the observable universe to grains of sand on earth or any other pair of unrelated large numbers.[1] This motivates the idea that the approximate ratio of five to one is not a result of a pure coincidence, but rather the result of a connected origin. This similarity must however be the result of two different connections, since the mass density, $\rho = n \times m$, is the product of the number density, n, and the mass of the particle species, m. The most natural explanation for the similarity in mass densities is then a connected origin between matter and dark matter that explains both why $n_M \sim n_{DM}$ and $m_{DM} \sim m_M$. We must first then examine in detail the origin of the density and

[1] A quick estimate yields at least 7 orders of magnitude difference for stars compared to grains of sand.

mass of the species that make up all of the matter that is visible to us. The cosmological history of the particle species that make up this visible sector (VS) is due to the efforts in astrophysical theory together with the calculations of Standard Model of particle physics that combine to make up particle cosmology. In this chapter we will examine the story of visible matter at length before turning to the implications for dark matter.

1.1 The Standard Model

The Standard Model describes all of the known types of conventional matter and their interactions. It is based primarily on the language of symmetries, which are encoded into the Lagrangian. These symmetries can be broken up into three categories. First we have the Poincaré symmetry which guarantees that all of the interactions among particles of the SM obey the principles of special relativity, and are translationally invariant in both space and time. Second we have the local gauge symmetries $SU(3)_c \times SU(2)_L \times U(1)_Y$ which describe the forces of the SM. Finally we have symmetries such as charge(C), parity(P), and time(T) and their compositions in addition to a number of global symmetries such as chiral symmetry which is only approximate due to the quark masses.

The matter of the Standard Model consists of three 'generations' of fermions. Each generation consists of two flavours of quark colour triplets, a charged lepton and a neutrino. Each of these fermions can be further separated according to its left- and right-handed components. This is a feature of massive Dirac fermions ψ, which are not their own antiparticles and can be decomposed into two distinct irreducible representations of the Lorentz group, ψ_L and ψ_R.[2] The local symmetry group of the standard model is based on the Yang-Mills theory of renormalisable gauge interactions. Using a Lie algebra such as that of SU(N) defined through the commutation relations for the group generators,

$$\left[\tau^a, \tau^b\right] = i f^{abc} \tau^c, \tag{1.2}$$

[2]The exception to this may be the right-handed neutrino, which has not yet been observed. However, recent experiments that have demonstrated neutrino flavour oscillation indicate that neutrinos do in fact have extremely small masses. It is at present unknown if neutrino mass generation proceeds through the involvement of right-handed neutrinos.

we can consider a set of fermions that transform under a representation of this group,

$$\psi_i(x) \to E_{ij}(x)\psi_j(x), \tag{1.3}$$

where E_{ij} is a group element. In moving from a global symmetry to a local gauge theory we make the choice to promote E_{ij} from a static operator to a function of space-time, $E_{ij}(x) = (e^{-\theta^a(x)\tau^a})_{ij}$. The form of the τ^a generator here is representation dependent. Modifying the covariant derivative ∂_μ of field theory to be truly covariant under the group of choice adds connection fields, $A_\mu(x) = A^a_\mu(x)\tau^a$, to form $D_\mu = \partial_\mu - igA_\mu$. Infinitesimally we have the relationship between the local variable $\theta(x)$ and gauge field A^a_μ given by

$$\delta A^a_\mu = -\frac{1}{g}\partial_\mu\theta^a + f^{abc}\theta^b A^c_\mu. \tag{1.4}$$

The commutator of these new covariant derivatives, $F^a_{\mu\nu}\tau^a = (i/g)[D_\mu, D_\nu]$, becomes the building block with which we can write down the action of a pure Yang-Mills theory through

$$S = \int d^4x \left(-\frac{1}{2}\mathrm{Tr}\left[(F^a_{\mu\nu}\tau^a)^2\right]\right), \tag{1.5}$$

while the coupling of fermions to our gauge fields can be found through the covariant action

$$S = \int d^4x\, \bar{\psi}(i\not{D} - m)\psi. \tag{1.6}$$

Within the Standard Model, the left-handed components of each of the fermions are grouped together into doublets of the weak $SU(2)_L$ gauge symmetry while the right-handed fermions are $SU(2)_L$ singlets and thus do not interact through the weak force. $SU(3)_c$ groups together the colour triplets of quarks of each flavour and does not include any interactions among the different flavours. We detail the three generations in Table 1.1.

The bosons of the Standard Model consist of the vector bosons, G^a_μ, W^i_μ, B_μ, one for each generator of the symmetries of the gauge groups described above, as well as the $SU(2)_L$ doublet of complex scalar bosons, ϕ, which are responsible for the Higgs mechanism. Three of these scalar degrees of freedom will however be removed at the scale of electroweak symmetry breaking (EWSB) to give mass to three vector bosons of the $SU(2)_L \times U(1)_Y$ electroweak sector. This mechanism generates the masses of both the quarks and leptons, a process which we will examine in the next section on symmetry breaking.

Generation I	Generation II	Generation III	Summary
$\mathbf{Q_1} = \begin{bmatrix} u_{r,b,g} \\ d_{r,b,g} \end{bmatrix}_{\mathbf{L}}$ $\mathbf{L_1} = \begin{bmatrix} e \\ \nu_e \end{bmatrix}_{\mathbf{L}}$	$\mathbf{Q_2} = \begin{bmatrix} c_{r,b,g} \\ s_{r,b,g} \end{bmatrix}_{\mathbf{L}}$ $\mathbf{L_2} = \begin{bmatrix} \mu \\ \nu_\mu \end{bmatrix}_{\mathbf{L}}$	$\mathbf{Q_3} = \begin{bmatrix} t_{r,b,g} \\ b_{r,b,g} \end{bmatrix}_{\mathbf{L}}$ $\mathbf{L_3} = \begin{bmatrix} \tau \\ \nu_\tau \end{bmatrix}_{\mathbf{L}}$	$SU(2)_L$ doublets includes: Colour $SU(3)_c$ triplet quarks with hypercharge (1/3), $SU(3)_c$ singlet leptons with hypercharge (-1).
$\left[u_{r,b,g}\right]_{\mathbf{R}}$ $\left[d_{r,b,g}\right]_{\mathbf{R}}$	$\left[c_{r,b,g}\right]_{\mathbf{R}}$ $\left[s_{r,b,g}\right]_{\mathbf{R}}$	$\left[t_{r,b,g}\right]_{\mathbf{R}}$ $\left[b_{r,b,g}\right]_{\mathbf{R}}$	Up and down type $SU(3)_c$ triplets with hypercharges of (4/3) and $(-2/3)$ respectively.
$\left[e\right]_{\mathbf{R}}$	$\left[\mu\right]_{\mathbf{R}}$	$\left[\tau\right]_{\mathbf{R}}$	Singlets of both $SU(3)_c$ and $SU(2)_L$, with hypercharge (-2).

TABLE 1.1: The fermionic field content of the Standard Model of particle physics. We list the representations under the Standard Model gauge group, $SU(3)_c \times SU(2)_L \times U(1)_Y$.

1.1.1 Spontaneous symmetry breaking

The renormalisable self-interaction terms of the Higgs field allow for it to gain a nonzero classical minimum in the Lagrangian and thus acquire a nonzero quantum expectation value throughout the universe, generally referred to as a vacuum expectation value (VEV). To see this we examine the case of the Higgs mechanism in the Standard Model. In this case we have one Higgs $SU(2)_L$ doublet of complex scalar fields which we can parameterise as four real scalar fields. The Lagrangian of this doublet is

$$\mathcal{L}_\phi = \frac{1}{2} D_\mu \phi D^\mu \phi - V(\phi). \tag{1.7}$$

The quartic potential can be written as

$$V(\phi) = -\frac{\mu^2}{2}\phi^\dagger\phi + \frac{\lambda}{4}(\phi^\dagger\phi)^2, \tag{1.8}$$

with minimum given by

$$\langle \phi \rangle = \begin{bmatrix} 0 \\ \frac{v}{\sqrt{2}} \end{bmatrix}. \tag{1.9}$$

In terms of the original parameters of the potential, the VEV has size given by $v = \mu/\sqrt{\lambda}$. Defining new fields as excitations around this minimum, the Lagrangian is no longer invariant under $SU(2) \times U(1)$ transformations. The broken symmetry has a number of consequences. Through the couplings of the Higgs doublet to fermions,

$$\mathcal{L} \supset y_l \overline{L} \phi e_R + y_d \overline{Q} \phi d_R + y_u \overline{Q} \phi^c u_R + h.c. \,, \tag{1.10}$$

we obtain the mass terms of the fermions that couple the original left and right chiral fields. Secondly, for each broken direction of symmetry, we gain a massive vector boson. The surviving direction of symmetry forms a $U(1)$ subgroup of $SU(2)_L \times U(1)_Y$ and this is identified with electromagnetism with the photon as its associated massless vector boson. Three of the real fields from the original doublet are consumed in the process of creating the new massive vector bosons $W^+, W^-$and Z^0. Finally the remaining degree of freedom from the original doublet forms a massive neutral scalar, h, known as the Higgs boson. The discovery of this particle in 2012 [5, 6] was a landmark moment in the history of physics. The electroweak symmetry breaking process explains how the original gauge symmetry of the SM evolved at low temperature to the $SU(3)_c \times U(1)_{EM}$ symmetry of the present day that defines the electric and colour charges of leptons and quarks. While the fundamental constituents of matter gain mass through EWSB it is important to note that this is not the primary origin of m_M, the mass scale of visible matter that makes up $\sim 1/6$th of the matter of the universe. In fact the Higgs mechanism causes $< 0.05\%$ of the visible matter component alone. In order to understand where most of the VS mass comes from we must examine the $SU(3)_c$ component of the modern gauge group and some of the consequences of renormalisation and running coupling constants.

1.1.2 Running coupling constants

The coupling constants that define the magnitude of the interactions of the Standard Model are not actually constant with respect to the energy scale of interactions. The gauge couplings represent the interaction strengths of the associated forces at a particular energy scale. The renormalisation group equations (RGEs) tell us how they evolve

with energy if we measure their value at the interaction energy scale available at modern collider experiments. These RGEs depend on the field content and other parameters of the operators in the Lagrangian of our model [7–9]. The coupling constant renormalisation of a gauge theory leads to expressing the constants in terms of divergent multiplicative renormalisation constants, Z, which measure the size of counter terms added to the bare Lagrangian to kill off divergences, and a factor from dimensional regularisation, $\varepsilon = d - 4$,

$$g_0 = g\mu^{\varepsilon/2}\frac{Z_1}{Z_2\sqrt{Z_3}}. \tag{1.11}$$

Solving for the renormalisation constants by calculating the divergences of loop corrections to gauge interactions lets us find expressions of the form

$$\begin{aligned} Z_1 &= 1 - \frac{g_0^2}{8\pi^2\varepsilon}\left(C_{\text{ad}} + C_f\frac{N}{d_f}\right) + \dots, \\ Z_2 &= 1 - \left(\frac{g_0^2 N C_f}{8\pi^2 d_f \varepsilon}\right) + \dots, \\ Z_3 &= 1 + \frac{g_0^2}{8\pi^2\varepsilon}\left(\frac{5}{3}C_{\text{ad}} - \frac{4}{3}C_f\right) + \dots, \end{aligned} \tag{1.12}$$

with C_f, C_{ad} the Casimir numbers or Dynkin indexes of the Lie algebra for fundamental and adjoint representations for our gauge group defined through

$$\text{Tr}\,\tau^a\tau^b = C_R\delta^{ab} \tag{1.13}$$

for the choice of representation R. The number d_f is the dimension of the representation and N is the number of generators of the group algebra. These allow us establish the multiplicative running of g if we know its value at a particular energy scale. We can then make use of the beta function defined as

$$\beta(g) = \mu\frac{dg}{d\mu}. \tag{1.14}$$

This beta function then contains the dependence on Casimir numbers and can be calculated to n-loop order without any dependence on ε. This can be seen by a power counting argument. Let

$$Z_g = \frac{Z_2\sqrt{Z_3}}{Z_1} \tag{1.15}$$

and consider its expansion in $1/\varepsilon$,

$$Z_g = 1 + \sum_n \sum_{k=1}^{n} a_k^n \frac{g^{2n}}{\varepsilon^k}. \tag{1.16}$$

The beta function with nonzero ε can be given by

$$\beta_\varepsilon(g) = -\frac{\varepsilon}{2} g + \frac{g}{Z_g} \frac{\partial Z_g}{\partial g} \beta_\varepsilon(g), \tag{1.17}$$

which gives the entire second term as $\beta(g)$ in four dimensions with $\varepsilon \to 0$. We can then consider

$$Z_g \beta(g) = -\frac{\varepsilon}{2} g^2 \frac{\partial Z_g}{\partial g} + \beta(g) \frac{\partial Z_g}{\partial g} g. \tag{1.18}$$

Inserting the expansion of Z_g and comparing powers of ε^0 we see that

$$\beta(g) = -g^2 \sum_n n a_1^n g^{2n-1}. \tag{1.19}$$

This shows that, to any order of perturbation theory, the beta function can be found from the coefficient of the first order divergence in the expansion of Z_g. It can be explicitly verified to any order that the higher order divergences in $(1/\varepsilon^2, 1/\varepsilon^3 ...)$ amazingly cancel among themselves.

In the case of $SU(3)_c$, the high energy behaviour found a natural explanation when field theorists in the 1960's realised that the asymptotically free nature of a non-Abelian gauge theory could explain the free particle behaviour of quarks at high energy while being strongly confined into hadrons such as protons and neutrons at low energy. The mass scale of baryons in quantum chromodynamics (QCD) is now understood to originate from the confining interactions within baryons. In particular we can reverse this perspective to consider the original high energy, perturbative theory. In the low energy regime this theory evolves toward a gauge coupling that becomes large, creating the phenomenon of confinement. This is sometimes called 'infrared slavery'. The critical result of this is that an energy scale common to baryons arises at the value of μ when g becomes large, that is, the scale when QCD can no longer be described by a perturbative field theory. This is referred to as the confinement scale, Λ_{QCD}, and it is the dominant contribution to the mass of protons, neutrons and therefore to the entire periodic table, stars, galaxies and indeed the dominant source of m_M, the mass scale that makes up most of the visible

matter of the universe. This completes our short review of the Standard Model. From here we embark on reviewing some of the relevant theories that go beyond the SM that will prove critical to our work.

1.2 Beyond the Standard Model

While the Standard Model has been very successful, it is an incomplete theory. There are a number of unexplained problems that extensions beyond the Standard Model typically attempt to solve. Here we will discuss briefly some of the most pressing issues, some of which we will explore further in this work:

- The aforementioned question of dark matter, the dominant form of mass in the universe.
- The baryon and lepton asymmetry. Why is the universe composed of matter rather than antimatter or some mixture?
- Do the gauge forces unify into a larger grand unified theory at a high energy?
- The unknown nature of dark energy, the source of the universe's accelerating expansion.
- The hierarchy problem. If high energy scales directly add mass corrections to the Higgs mass, why is it so small?
- Experiments show that neutrinos undergo flavour oscillation. This implies that they have nonzero masses. What is the origin of these masses and why are they so small compared to the other fermions?
- What is the origin of the three unique generations of fermions and their different couplings?
- Does supersymmetry, the unique solution of unifying spacetime symmetries with gauge symmetries, exist?
- Is quantum field theory a valid description of interactions at high energy or is it an emergent theory of an underlying structure such as string theory?
- Is there a consistent theory of quantum gravity?

In this work we are primarily interested in models that solve the dark matter and matter-antimatter asymmetries together in a natural way. Grand unified theories and ways of explaining the mass of neutrinos will also play a part. Supersymmetric variants of these models will be discussed along with discussions of the ways our model affects issues such as the hierarchy problem. In the next section we review some of these promising extensions and their motivations.

1.2.1 Grand unified theories

Models that unify the fundamental forces of the Standard Model can be traced back to the work of Georgi, Pati, Salam and Glashow following the unification of electroweak theory [10–14]. The unifying of separate forces into singular phenomena can of course be traced back further in the history of physics to Michael Faraday's pioneering work in the connection between electric and magnetic phenomena. Evidence in support of the unification of the gauge forces of the Standard Model comes from a number of different sources. One of these is the observed direction of the running gauge couplings at higher energies and the fact that the gauge forces seem to approach a common point near a scale of 10^{15} GeV. The running of these coupling constants can be seen in Fig. 1.1.

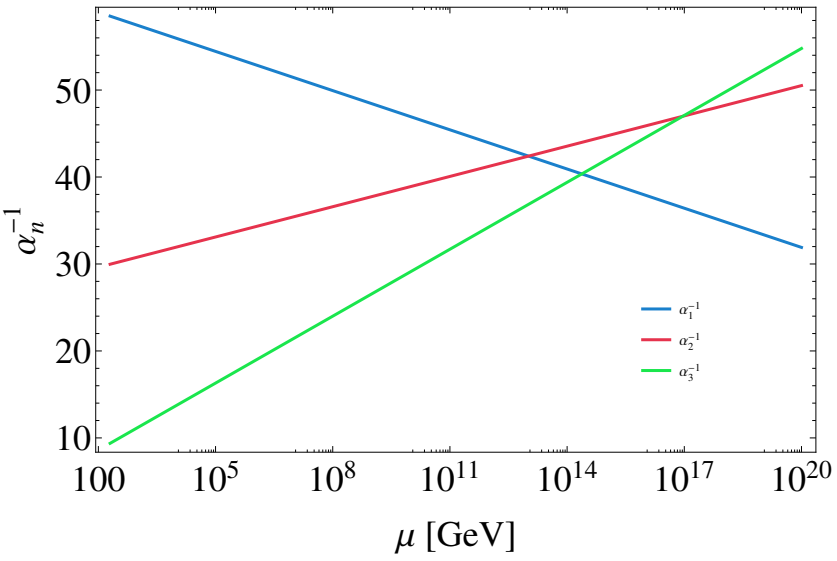

FIGURE 1.1: The evolution of the gauge couplings in the Standard Model of particle physics.

The apparent union of these couplings makes sense if at such an energy scale, a larger group that contains each of the SM gauge groups as subgroups was spontaneously broken

such that from this point three independent gauge coupling constants could then run independently. This larger group then constitutes a grand unified theory (GUT) that would unite the known forces into a single force in the early universe. That the couplings do not meet exactly may indicate that there exists new physics between the electroweak scale and the GUT scale that alters the running for one or more of the gauge forces such that they do meet precisely. As an example one can consider a model with extra Higgs doublets as in [15] where a non-supersymmetric model with eight Higgs doublets leads to gauge coupling unification. The minimal group that can accommodate all three Standard Model interactions is $SU(5)$ and this was indeed the focus of the earliest work on gauge unification. It is remarkable that a second piece of evidence then emerges when we examine how to fit the fermions into representations of $SU(5)$. Taking a single generation of fermions of the Standard Model we find that there are 15 chiral fermions. One of the smallest number of representations that $SU(5)$ could accommodate to fit these only is with just two of dimension **5** and **10**. It would then be quite a surprise to find that the unique decomposition of $\bar{\mathbf{5}} + \mathbf{10}$ under the subgroup $SU(3)_c \times SU(2)_L \times U(1)_Y$ is one of $[(1,2) + (\bar{3},1)] + [(1,1) + (\bar{3},1) + (3,2)]$. This is exactly the dimensions of the fermion representations of a single generation of the Standard Model, $[L+d]+[e+u+Q]$, and we further find a consistent assignment for left and right-handed states as well as $U(1)_Y$ charges.

Furthermore we can observe that the scale of this unification is quite close to the scale that would be required to sufficiently suppress the proton decay allowed by the unified theory, in accordance with the observed stability of the proton. The decay is predicted by interactions that make use of heavy $SU(5)$ gauge boson mediators that can convert quarks into leptons. Current experimental bounds have a half-life $> 1.67 \times 10^{34}$ years while the GUT scale in Fig 1.1 suggests a possible half-life between 10^{31} and 10^{36} years.

If we extend the SM to include neutrinos with mass, as seems to be the case based on the neutrino oscillation experiments, then extending the GUT group to $SO(10)$ becomes a compelling argument. Aside from requiring representations to accommodate all 16 chiral fermions, we can observe that the $\bar{\mathbf{5}} + \mathbf{10}$ themselves can be unified minimally into the irreducible spinorial **16** dimensional representation of $SO(10)$. A high Majorana mass scale for the gauge singlet right-handed neutrino of the seesaw model gains a natural explanation in these $SO(10)$ models when the right-handed neutrino acquires mass at the $SO(10)$ symmetry breaking scale while the rest of the 15 fermions continue to have their

zero mass protected by gauge symmetries until the electroweak (EW) scale. This then allows for an explanation of neutrino oscillations and the observed neutrinos having such small masses caused by the seesaw mechanism which we discuss further in section 1.3.2.

1.2.2 Mirror matter

We have seen that the symmetries of the universe at high energy can increase to place all of the gauge symmetries as subgroups of a single group. One of the other peculiar features of the SM is the observed fact that it is not completely invariant under the Parity symmetry (P) which interchanges spatial coordinates ($x \to -x$). This can be solved however if the Parity operator interchanges fields with symmetric copies called mirror fields. Such a theory of a high scale mirror symmetric Lagrangian can be motivated by some heterotic string theory models which in the low energy limit lead to $E_8 \times E_8$ gauge groups with equal particle content and the same gauge symmetry in two identical sectors [16]. Models of mirror matter have been used to suggest a dark matter candidate in the form of the matter of the mirror sector. These theories require that the two sectors interact only minimally with each other with gravity being the primary indication of its existence.

These mirror matter models of dark matter, Refs. [17–54], have a long history, however it is clear from the ratio in Eq. 1.1 that there must be differences between the two sectors to avoid a 1:1 ratio of matter to dark matter. If there is a hidden sector to the universe, it cannot be identical to our own and still explain the observed properties of dark matter.[3]. As we will see in this work, the theoretical motivations of a hidden mirror sector can still be satisfied with a unique dark sector if mirror symmetry, like grand unified theories, is only a symmetry of the Lagrangian at high energy and is spontaneously broken in the early universe.

1.2.3 Supersymmetry

Supersymmetric theories have their origins in the early attempts to unify gauge symmetries with spacetime symmetries. With the no-go theorem of Coleman and Mandula [55] it was shown that the two symmetry groups could not simply be subgroups of a single

[3]For exactly mirror symmetric matter at the microscopic level, the necessary asymmetry can be provided by different temperatures for the two sectors.

larger group. A side step to this problem was discovered in that a $\mathbb{Z}_2$-graded Lie-algebra could allow one to write down a theory that connected spacetime and gauge symmetry generators [56–61]. This theory is based on the algebra,

$$\begin{aligned}[P_\mu, Q_\alpha] &= 0, \\ [Q_\alpha, M^{\mu\nu}] &= \frac{1}{2}(\sigma_{\mu\nu})^\beta_\alpha Q_\beta, \\ [Q_\alpha, \overline{Q}_\beta] &= (\sigma_\mu)_{\alpha\beta} P_\mu,\end{aligned} \tag{1.20}$$

with P^μ and $M_{\mu\nu}$ the generators of spacetime symmetries of translations and rotations plus boosts and Q the generator that transforms between bosons and fermions. The irreducible representations of this algebra are the supermultiplets of supersymmetric theories and these fields contain both bosonic and fermionic degrees of freedom [62]. In fact they have the same number of degrees of freedom for each type.

The consequences of writing down a Lagrangian in terms of supermultiplets is far reaching. Unlike the potentials such as Eq. 1.8, supersymmetric theories are specified by superpotentials, W, which for the purposes of being renormalisable can only contain gauge invariant terms up to cubic order in the fields,

$$W = \sum_n \lambda_n \phi_n + \frac{1}{2}\sum_{n,m} m_{nm}\, \phi_n \phi_m + \frac{1}{3}\sum_{n,m,p} \lambda_{nmp}\, \phi_n \phi_m \phi_p. \tag{1.21}$$

The consequences for symmetry breaking with potentials such as these is examined in Chapter 2 and Chapter 3.

Supersymmetry is a very appealing extension to the SM for a number of key reasons. Firstly it provides a potential solution to the gauge hierarchy problem. If the GUT scale exists, then the quantum corrections to the Higgs mass imply that the EW scale Higgs that we observe is the result of a fine tuning between the bare mass and a correction that cancels to one part in $\sim 10^{15}$. With a symmetry between fermionic and bosonic degrees of freedom however, the loop calculations from boson and fermion loops cancel exactly and the EW scale becomes protected from GUT scale corrections, or indeed the physics of any high energy theory. It is further remarkable that restoring supersymmetry near the EW scale can adjust the running of gauge couplings to unify exactly, as in Fig. 1.2, making supersymmetric GUT extensions to the SM even better motivated than non-supersymmetric GUTs.

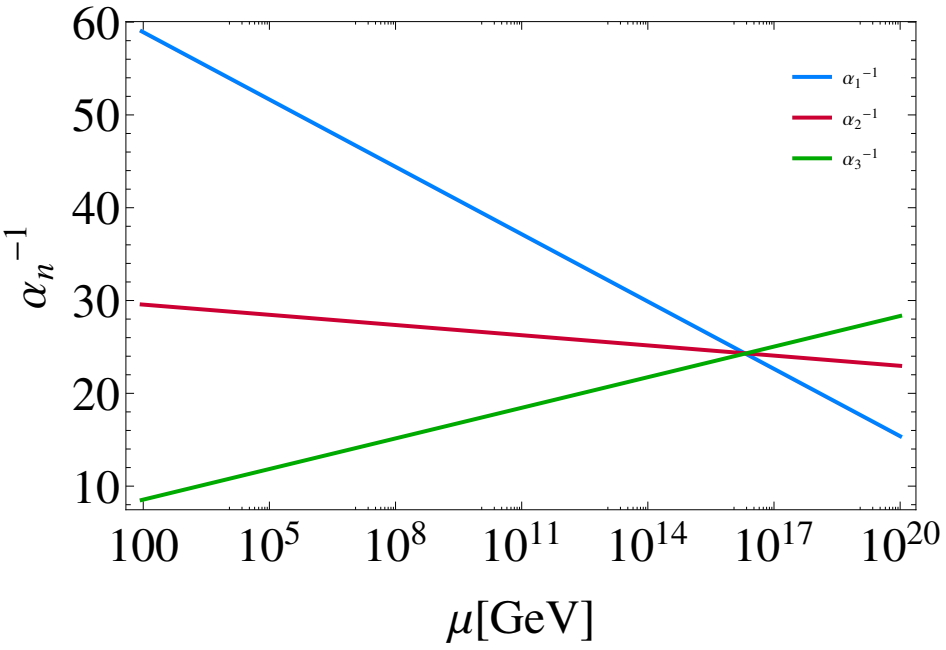

FIGURE 1.2: The evolution of the gauge couplings in the Minimal Supersymmetric Standard Model (MSSM), one of the simplest phenomenologically viable extensions to the Standard model that contains the requisite superpartners.

Going back to the early universe, beyond the restoration of the EW symmetry and possibly SUSY and GUT symmetries another possible unification arises at the Planck scale where we expect the gauge forces to have a similar strength to gravity. Reversing this perspective of symmetry restoration at higher energies leads us to consider the evolution of the universe from the beginning, at a possible moment of maximal symmetry, and the consequences for each stage of the expansion of the universe as it cooled. This constitutes the field of early universe cosmology and we will examine the Big Bang model in detail in the next section.

1.3 Big bang cosmology

The history of the universe is one of change. Since the acceptance of the big bang model of cosmic expansion, the effort to trace the timeline of the universe and its major epochs has seen great success in combining the knowledge gained from particle physics with astrophysical models and observations. This combined area of astroparticle physics has been able to construct a sequence of events that explains how the chaotic plasma of

the first moments evolves into the present day expanse of galaxies. It is however an incomplete picture. Dark matter is just one of the missing pieces.

Edwin Hubble's observations of far away galaxies receding from our own galaxy formed the basis of the expansion model which describes the universe as continuously growing in size. Today the Friedman-Lemaître-Robertson-Walker (FLRW) metric is the most accurate description of the near isotropic and homogeneous spacetime we live in. It contains an analytic solution to Einstein's field equations of general relativity, in the form of the Friedman equations, if the energy-momentum tensor is similarly assumed to be isotropic and homogeneous. We can write the metric in polar coordinates as

$$ds^2 = dt^2 - a^2(t)\left[\frac{dr^2}{1-kr^2} + r^2 d\Omega^2\right], \tag{1.22}$$

with $d\Omega^2 = d\theta^2 + \sin^2\theta d\phi^2$. The value of k parametrises whether the universe is flat($k = 0$), spherically curved($k = +1$) or hyperbolic($k = -1$). The Hubble parameter is defined by

$$H = \frac{\dot{a}}{a}. \tag{1.23}$$

We can calculate this in terms of the energy density, ρ, and pressure, P, of the universe and the expansion rate today, measured by Hubble's constant $H_0 \sim 15$km/sec per mega light year. This allows us to establish the age of the observable universe to be 13.81 billion years [4]. This is the time since all of the matter we can see was localised into a space smaller than the atom. The first Friedman equation,

$$H^2 = \frac{8\pi G}{3}\rho - \frac{k}{a^2}, \tag{1.24}$$

removes the dependency on pressure and allows us to quantify the contributions to the universe's expansion among radiation, matter, the curvature and the poorly understood dark energy which contributes to the accelerating expansion. We can label these contributions in terms of their fraction of the critical density, that is the necessary amount to make up the total energy budget today for a flat universe with $k = 0$,

$$\Omega_i = \frac{\rho_i}{\rho_{\text{crit}}}. \tag{1.25}$$

The density ratio in Eq. 1.1 can be considered as a comparison of the two fractions of the critical density, Ω_i, made up by matter and dark matter.

This FLRW cosmology does not provide a fully satisfactory account for the homogeneity and isotropy that we observe in the universe today because it involves a severe fine-tuning of the initial conditions. To explain why the early universe that we observe seems to have almost exactly the same temperature in all directions we need to add to the first moments of the universe a period of rapid inflation where a single causal patch of space was rapidly blown up exponentially in size. Following this period the universe's energy density essentially drops to zero and must undergo a period of reheating and thermalisation. This is explained in 'inflaton' models of inflation by the decay of a scalar field, the VEV of which can initially drive the rapid expansion, transferring energy back into Standard Model fields which then decay and interact until they reach equilibrium at a reheating temperature $T_{\rm rh}$ [63, 64].

If the expansion described by the FLRW metric since this period is slow enough, we can describe the early universe as being in a state of thermal equilibrium. In this hot dense early universe we can then write the number density of a species in terms of its degrees of freedom and the phase space distribution among momentum eigenstates $f(p)$,

$$n = \frac{g}{(2\pi)^3} \int d^3p f(p). \tag{1.26}$$

By combining the assumption of the homogeneity of the universe with the above we can describe the local thermal equilibrium such that the function $f(p)$ is truly independent of spatial coordinates. The phase space distribution is then described in terms of the temperature, T, and the chemical potential, μ, by the entropy maximising Fermi-Dirac and Bose-Einstein distributions,

$$f(p) = \frac{1}{e^{(E(p)-\mu)/T} \pm 1}. \tag{1.27}$$

The energy density is then given by

$$\rho = \frac{g}{(2\pi)^3} \int d^3p f(p) E(p) \tag{1.28}$$

and the pressure by

$$P = \frac{g}{(2\pi)^3} \int d^3p f(p) \frac{p^2}{3E}. \tag{1.29}$$

In the early universe when the radiation density dominates the expansion, we can find the total radiation density in terms of the number of relativistic species in the thermal

bath,

$$\rho_r = \sum_i \rho_i = \frac{\pi^2}{30} g^*(T)\, T^4, \tag{1.30}$$

where $g^*(T)$ is the total effective number of degrees of relativistic freedom in the universe at that temperature. This quantity can be calculated by counting the degrees of freedom of individual species and their respective temperatures according to

$$g^*(T) = \sum_{i=B} g_i \left(\frac{T_i}{T}\right)^4 + \frac{7}{8} \sum_{i=F} g_i \left(\frac{T_i}{T}\right)^4. \tag{1.31}$$

The first term of Eq. 1.31 counts bosonic degrees of freedom, while the second term counts those of fermions. As species become non-relativistic they are removed from the plasma and disappear from the above summation. This process continues until only the lightest states consisting of protons, neutrons, electrons, photons and neutrinos are all that remain. Neutrinos decouple from the plasma when the weak interaction rate, mediated by W bosons, falls below the Hubble rate. Following this, when the temperature drops below the mass of electrons, the energy of almost all electrons and positrons are transferred to photons. Near 0.1 MeV the light elements of the periodic table were formed in the era of big bang nucleosynthesis (BBN). As the temperature continues to drop we reach a point where photons can no longer ionise electrons that fall into proton orbits and neutral hydrogen forms, beginning the process of recombination. As the density of free charged particles drops, photons decouple and the light of this hot dense early universe is still visible today in the form of the cosmic microwave background (CMB) radiation, the redshifted photons that travelled unabated from the moment that the average energy dropped sufficiently to turn the universe transparent.

1.3.1 The matter-antimatter asymmetry

One of the most significant missing pieces in a model of particle cosmology is the origin of the baryon and lepton asymmetries in the universe. Almost all of the matter we can see is made up of protons, neutrons and electrons. Since the discovery of antimatter in the 1930s the question of why the universe is composed of one and not the other, or a mixture, has presented a great challenge. Antimatter is essentially identical to matter except that it has opposite charge. Our current understanding of the evolution of the universe details that matter and antimatter must have originated in near equal quantities. Following

a period that generates an excess of one, the symmetric components annihilate into radiation leaving a universe composed primarily of matter. The total lepton asymmetry of the universe is, however, unknown as a significant lepton asymmetry may be stored in the cosmic neutrino background, the remnant of light neutrinos from the early universe when the neutrinos decoupled from the thermal bath. This could potentially balance the asymmetry in charged leptons.

We can see that the present day density of matter is the result of the asymmetry between the production of matter and antimatter in the early universe. In particular as most of the mass of the universe comes from baryons such as protons and neutrons, it is the baryon asymmetry in the early universe that is responsible for the number density, n_M, critical to our exploration of dark matter. The study of how the baryon and lepton asymmetries originated is known as baryogenesis and leptogenesis, respectively. Such theories are often directly connected to one another. There are many models of baryogenesis, but common to all of them are some critical assumptions about generating asymmetries described by Sakharov [65]. These conditions are:

- Baryon number violation.
- C and CP symmetry violation.
- A departure from thermal equilibrium.

The first condition allows one to have interactions that create a net increase of baryons over anti-baryons. The second condition allows for these processes to occur at a different rate, else the processes that create excesses of anti-baryons over baryons would prevent an asymmetry from forming. The final condition allows for all of these processes to occur at different rates compared to the time reversed interactions. Well known models of baryogenesis include GUT baryogenesis, electroweak baryogenesis and Affleck-Dine baryogenesis. In the next section we will review one of the most appealing models, baryogenesis via leptogenesis. We focus, in particular, on thermal leptogenesis derived from the Type-1 seesaw mechanism. We will then review how electroweak sphalerons can convert the generated lepton asymmetry into the present-day baryon asymmetry.

1.3.2 Thermal leptogenesis

Thermal leptogenesis using the decays of heavy right-handed neutrino states is one of the most compelling models of generating a lepton asymmetry in the early universe [66–75]. This is due in part to the appeal of the seesaw mechanism for generating neutrino mass [76–78]. In the seesaw model, the mass eigenstates of the RH neutrinos above EWSB are $N_i = N_{R_i} + N^c_{R_i}$. The mass scale M_N of these gauge singlet states can be significantly larger than the EW scale as it is not protected by the SM gauge symmetry. When we couple the lepton doublets to these states through $y_\nu \overline{L}\phi N_{R_i}$, we acquire Dirac mass terms between the left and right-handed states in addition to the right-handed Majorana mass scale M_N. The relevant Lagrangian for neutrino mass including both the Dirac and Majorana mass terms is

$$-\mathcal{L}_\nu = y_\nu \overline{L}\phi N_{R_i} + \frac{1}{2}\overline{(N_R)^c} M_R N_R + \text{h.c.} \tag{1.32}$$

Diagonalising this mass matrix after EWSB yields a mass scale for light neutrinos

$$m_\nu \simeq -v^2 y_\nu \frac{1}{M_N} y_\nu^T. \tag{1.33}$$

While this is a remarkable result for models of neutrino mass, it was realised that it also allows us to naturally fulfil the Sakharov conditions for the creation of a lepton asymmetry.

The model comes with lepton number violating interactions involving the states N_i. CP violation can arise due to the complex phases in y_ν. The departure from thermal equilibrium can then arise if the decay rate of heavy neutrinos,

$$\Gamma_{N_i} = \frac{(y_\nu^\dagger y_\nu)_{ii} M_i}{8\pi}, \tag{1.34}$$

falls below the Hubble expansion rate of the universe. One introduces the CP parameter ϵ to measure the asymmetry in the decays to leptons and anti-leptons. It arises if we consider the interference between the tree-level and loop-level decays of heavy neutrino states shown in Fig. 1.3,

$$\epsilon_{i\alpha} = \frac{\Gamma(N \to l_\alpha H) - \Gamma(N \to \bar{l}_\alpha H^*)}{\sum_\alpha \Gamma(N \to l_\alpha H) + \Gamma(N \to \bar{l}_\alpha H^*)}. \tag{1.35}$$

In the one-flavour case this is

$$\epsilon_i = \frac{1}{8\pi}\frac{1}{(y_\nu^\dagger y_\nu)_{ii}}\sum_{k\neq i}\mathrm{Im}[(y_\nu^\dagger y_\nu)^2_{ji}]l\left(\frac{M_k^2}{M_i^2}\right), \tag{1.36}$$

with $l(x)$ a loop function [66] given by

$$l(x) = x\left[1-(1+x^2)\ln\left(\frac{1+x^2}{x^2}\right)+\frac{1}{1-x^2}\right]. \tag{1.37}$$

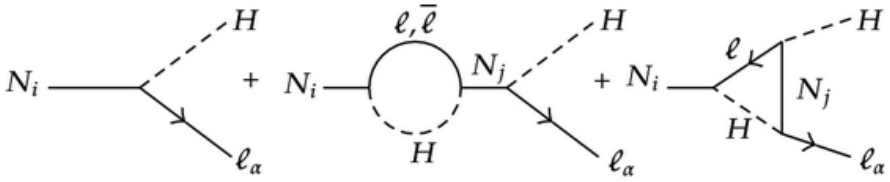

FIGURE 1.3: The interference between tree level decay and loop diagrams provides the CP asymmetry that can explain the origin of a lepton asymmetry in the early universe.

The Boltzmann equations, parametrised in terms of $z = M_1/T$, describe the competing terms in the evolution of early universe particle densities and in the case of generating a lepton asymmetry we can consider the two key rates,

$$\begin{aligned}\frac{d\mathcal{N}_{B-L}}{dz} &= -\epsilon D(\mathcal{N}_{N_1}-\mathcal{N}_{N_1^{\mathrm{Eq}}}) - W\mathcal{N}_{B-L} \\ \frac{d\mathcal{N}_1}{dz} &= -(D+S)(\mathcal{N}_{N_1}-\mathcal{N}_{N_1^{\mathrm{Eq}}}).\end{aligned} \tag{1.38}$$

The functions D, S and W measure, respectively, the rates of decays, scattering and washout processes from both scatterings and inverse decays. For sufficiently heavy right-handed neutrinos, M_N, and complex phases in the Yukawa matrix, y_ν, one can generate a net asymmetry, $\mathcal{N}_{B-L}$, in the early universe that survives until to the present day [69, 70, 72, 79–81]. At that time, this lepton asymmetry can be partially converted into a baryon asymmetry through a process we will review in the next section.

1.3.3 Electroweak sphalerons

The conversion of an initial lepton asymmetry into a baryon asymmetry through $B-L$ conserving sphalerons is a natural way to explain the baryon asymmetry in light of a possible large lepton asymmetry produced by thermal leptogenesis. In the pure gauge

configuration for $SU(2)$-Yang Mills theory where

$$A_\mu(x) = \partial_\mu U(x) U^{-1}(x), \tag{1.39}$$

the matrices $U(x)$ are elements of $SU(2)$ and x extends over S^3. Each $U(x)$ is a different vacuum state. Because $SU(2)$ is itself diffeomorphic to S^3, these mappings, and therefore the distinct vacua, can be classified by $\Pi_3(S^3) = Z$, that is, the mappings of the 3-sphere to itself. The different mappings can be categorised by their winding number, $n(U)$, which is distinct for each:

$$n(U) = \frac{1}{24\pi^2} \int d\sigma_\mu \, \epsilon_{\mu\nu\rho\sigma} \, \mathrm{tr}[(\partial_\nu U) U^{-1} (\partial_\rho U) U^{-1} (\partial_\sigma U) U^{-1}]. \tag{1.40}$$

The Cherns-Simons number is

$$N_{CS} = -\frac{1}{16\pi^2} \int d^3x K^0, \tag{1.41}$$

where $K^\mu = -2\epsilon^{\mu\nu\rho\sigma} tr(A^\nu \partial^\rho A^\sigma + \frac{2}{3} A^\nu A^\rho A^\sigma)$. This value is the same as the winding number for vacuum configurations but varies from integer values away from the true degenerate vacua. The different EW field configurations each satisfy the gauge condition above, however pure infinitesimal gauge transformations cannot transform the fields to a different vacuum state. To move from one vacuum state to another we must pass over an energy barrier since we are passing through non-vacuum states. The change in N_{CS} is given by

$$\Delta N_{CS} = \frac{1}{16\pi^2} \int_0^t dt \int d^3x \partial_\mu K^\mu \tag{1.42}$$

$$= N_{CS}(t) - N_{CS}(0). \tag{1.43}$$

Sphalerons are classical solutions to the electroweak equations of motion that describe the saddle point between two neighbouring minima. These unstable solutions to the electroweak field equations have a very low probability at the present temperature of the universe, however at the temperature above the EWPT the rate of such vacuum configuration transitions is considerably higher. Thermal fluctuations in the early universe have the potential to carry the system over the energy barrier in the classical sense. These sphaleron solutions for the interpolation between vacuum states, that pass through the saddle point, can become much more common in this era in comparison

to the low probability quantum tunneling rate [82]. Such solutions can spontaneously appear and decay in a small volume of space of size $1/M_W^2$. The anomalous divergence of the fermion currents coupled to $SU(2)_L$ is

$$\partial_\mu j_B^\mu = \partial_\mu j_L^\mu = n_f \left(\frac{g^2}{32\pi^2} \partial_\mu K^\mu - \frac{g'^2}{32\pi^2} \partial_\mu k^\mu \right), \tag{1.44}$$

where n_f counts the number of families in the Standard Model and $k^\mu = \epsilon^{\mu\nu\rho\sigma} B_{\nu\rho} B_\beta$ is associated with the $U(1)_Y$ field strengths. The integral over space for $\partial_\mu k^\mu$ yields 0. However comparing the above expression to Eq. 1.42 shows that the change between successive vacua is accompanied by a change in baryon and lepton number $\Delta B = \Delta L = n_f \Delta N_{CS}$, that preserves $B-L$ [83]. If we begin with a lepton asymmetry, rapid sphaleron processes can take the initial $(B - L)$ and reprocess it to be shared between a baryon asymmetry and lepton asymmetry,

$$B = \frac{8n_f + 4N_H}{22n_f + 13N_H}(B - L), \quad L = -\left(\frac{14n_f + 9N_H}{22n_f + 13N_H} \right)(B - L), \tag{1.45}$$

where N_H counts the number of Higgs doublets. We can now review the class of models that approaches the dark matter problem by considering how the dark matter density might be connected to the origin of the baryon asymmetry.

1.4 Asymmetric dark matter

Asymmetric dark matter (ADM) models seek to unite the efforts of understanding the origin and abundance of dark matter with theories devoted to understanding the origin of the matter-antimatter asymmetry of the universe [84–102]. Central to these models is the idea that whichever mechanism generates the matter-antimatter asymmetry in the visible sector is related to the generation of dark matter through the creation of a parallel asymmetry between dark matter and dark antimatter. Following the asymmetry generation in the dark matter species, the symmetric components must annihilate either into a form of dark radiation or into visible radiation. The dark matter density today is then the remaining asymmetric component of dark matter, with the dark antimatter removed from the universe. ADM models thus take the ratio in Eq. 1.1 to be the guiding principle in the exploration of dark matter's origins.

They further fit into the cold dark matter (CDM) hypothesis which suggests that dark matter is highly non-relativistic in the present day and can seed structure formation early in the universe as they form over-densities under their self-gravity. This is in contrast to hot dark matter (HDM) models in which dark matter is relativistic and structure forms from the fragmentation of the largest superclusters. Current evidence by the Planck experiment indicates that dark matter is made up of $\approx 85\%$ CDM [4].

Asymmetric dark matter models of CDM are directly in contrast with other popular dark matter models such as the weakly-interacting-massive-particle (WIMP) dark matter paradigm. These are motivated by the WIMP miracle, the observed coincidence that the DM critical density can result from a population of massive particles with mass $\sim$ the electroweak scale and a number density generated by a population that freezes out from the early universe plasma near the point when a weak scale interaction rate falls below the Hubble rate [103–105]. These WIMP models assume that dark matter was in thermal equilibrium with the SM species in the early universe up until the moment of freeze out when the stable DM particles chemically decoupled as their interaction rate could not keep up with the expansion. If one accepts the WIMP hypothesis, the similarity in the mass density of matter and dark matter in Eq. 1.1 remains a pure coincidence. Other DM models such as keV sterile neutrinos [106–108] and axions [109–112] have received much attention in the literature, though these too regard Eq. 1.1 as a coincidence.

For ADM the relation between the visible and dark sectors depends on the interactions between the sectors that exist within the theory. If one begins with the assumption that following inflation the two sectors are already in thermal equilibrium (an assumption which is not essential) then the two sectors will remain in thermal equilibrium so long as there remains fast interactions between particles of each sector. If we are to consider that the two sectors decouple at some temperate T_{DEC} then all such equilibrating interactions must become inefficient at that point. Reactions can fall below the required efficiency for two reasons. Firstly if the temperature of the plasma falls below the mass of one of the particles taking place in the reaction. Following the Boltzmann suppression of the number density of such particles the reaction rate falls due to the kinematic constraints as well as the number density of the suppressed species being less than the equilibrium number density of all other particles in the reaction. Secondly the reaction can be suppressed if the interaction rate as a function of temperature falls below that of the

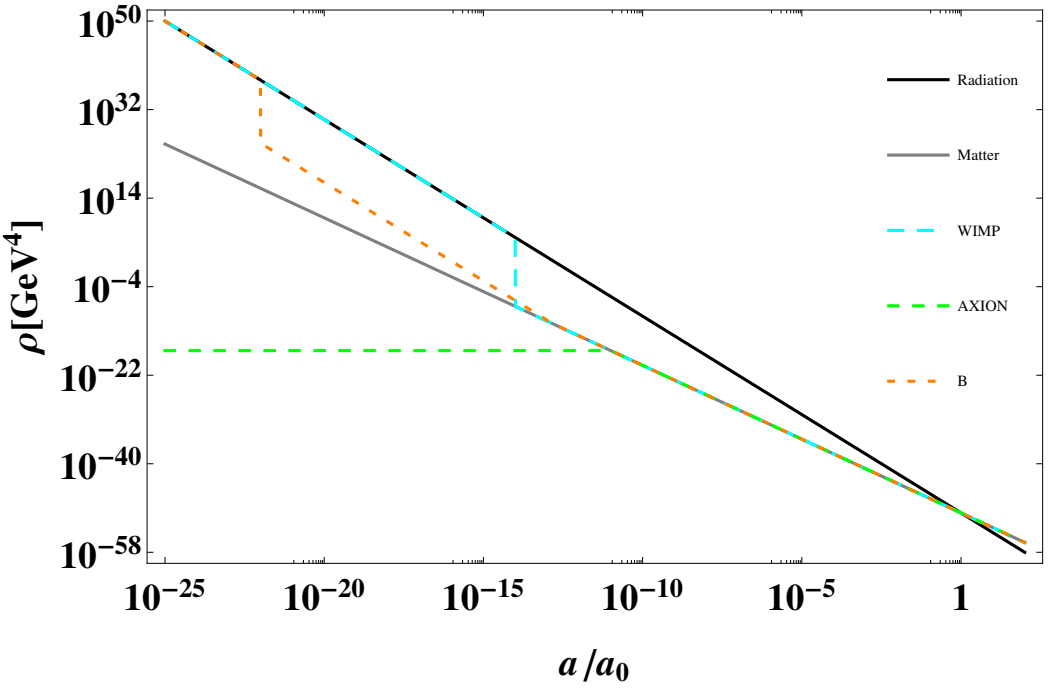

FIGURE 1.4: The evolution of the density of dark matter in various models compared to the baryon mass density. B describes the mass density initially stored in both baryons and antibaryons. The initial drop accounts for the loss in number density that follows from the annihilation of symmetric components and must reach a minimum given by the asymmetry produced by a baryogenesis mechanism. The vertical position of the matter gradient is then defined according to this observed density of visible matter today. The thermal history of WIMP models describes a fine-tuning of parameters to create a density of dark matter that freezes out with a mass density almost identical to matter. Similarly, axion models of dark matter require an initial abundance that gains mass at a particular scale in order for the mass density to evolve on the same line. Unlike the moment of matter-radiation equality, seen at the intersection in the lower right, the apparent coincidence in scale of Eq. 1.1 is a relationship which must remain true for the remainder of the universe.[4]Models of ADM consider a thermal history for DM that follows that of visible matter.

Hubble rate. In this case the equilibrating reaction cannot on average keep up with the rate at which the matter component of the universe is expanding and therefore the reaction is no longer sufficient for maintaining thermal equilibrium in the plasma. Models of ADM and WIMPS are not compatible as the generation of the DM number density is different in each case. Minimal WIMP scenarios further suggest possible direct and indirect detection signals for DM which as of this work have not been conclusively observed.

In Fig. 1.4 we compare the WIMP hypothesis with models of axion dark matter and

[4]An exception to this may arise if one or both of dark matter and the proton prove to have finite lifetimes.

asymmetric dark matter [50]. In the WIMP case, the number density scales as radiation until just after the density begins to drop when it reaches the freeze out point and stabilises on the matter gradient at almost exactly the path of the baryon density. In the case of axions, a particular preexisting axion density is produced in the early universe at the Peccei-Quinn scale. Near the QCD phase transition temperature, a specific axion mass is switched on to create a mass density for axions that begins to scale as matter at almost exactly the baryon mass density gradient. In contrast, ADM models have DM follow the same history as the baryon density. With an asymmetry between dark matter and dark antimatter, the number density drops to the amount of asymmetry after which it scales as radiation until it becomes non-relativistic and scales as matter.

The critical goal of this thesis is to utilise the extensions of the SM we have discussed to develop a new class of asymmetric dark matter models that can simultaneously explain why the mass scale of DM is similar to that of the proton. In doing so, we produce a comprehensive model of asymmetric dark matter.

1.5 Summary

This completes our overview of the status of the Standard Model, in addition to the well motivated extensions of modern physics. GUTs and supersymmetry are the primary extensions to the symmetry set of the SM Lagrangian along with mirror symmetry. Dark matter is the known missing piece of our picture and we draw from models of asymmetric dark matter that seek to explain the observed similarity in the matter and dark matter mass densities. Thermal leptogenesis and the sphaleron effects above the EWPT are the primary model we consider with regard to the creation of the matter-antimatter asymmetry of the visible universe. Table 1.2 summaries the timeline of the universe including some of the extensions to the SM we have discussed. We are now able to outline the course of this thesis in incorporating dark matter and its origins into the timeline of the universe. In Chapter 2 we will show how a mirror GUT theory can cause mirror symmetry to be spontaneously broken to create a dark sector with a composite dark matter candidate that has a mass which is naturally similar to the proton. In Chapter 3 we will examine a larger GUT theory and the possible breaking chains in the path to a low scale theory of matter and dark matter. In Chapter 4 we will study the process of generating matter and dark matter simultaneously in a model of broken

mirror symmetry and in Chapter 5 we examine in detail the mass spectra of possible confining dark sectors in detail to consider exactly what the properties of dark matter may be in all of our models. Chapter 6 then concludes with a discussion of all of these theories and what they could mean for the future of dark matter physics.

TABLE 1.2: The major epochs of the universe based on our understanding of the SM and cosmology, including some well motivated extensions. Dark matter, despite making up the majority of all matter, is absent from this timeline. In Chapter 4 we will see an example of how this timeline can be modified to provide a picture of the evolution of both matter and dark matter.

10^{19} GeV	$t \sim 10^{-43}s$	• Planck Scale era. The theorised scale where a quantum theory of gravity is necessary to model early universe dynamics.
10^{15} GeV	$t \sim 10^{-38}s$	• Inflation ends, grand unified symmetry breaking scale.
10^{12} GeV	$t \sim 10^{-30}s$	• Heavy Majorana neutrino masses.
10^{9} GeV	$t \sim 10^{-24}s$	• Thermal leptogenesis begins to produce a $B - L$ asymmetry. • Electroweak Sphalerons convert a fraction of the lepton asymmetry into a baryon excess.
10^{3} GeV	$t \sim 10^{-10}s$	• The Universe has cooled to allow the Higgs field to attain a nonzero vacuum expectation value triggering the electroweak phase transition. • Fermions gain mass.
200 MeV	$t \sim 10^{-3}s$	• The gauge coupling of $SU(3)_c$ becomes non-perturbative, breaking the approximate chiral symmetry and confining all free quarks into hadrons.
1 MeV	$t \sim 180s$	• Neutrinos decouple from the thermal bath following the weak interaction rate falling below the Hubble rate. • The neutron to proton ratio is fixed in place. • Hadrons combine into nuclei in the era of nucleosynthesis. • Free electrons and positrons annihilate, reheating photons above the temperature of the relic neutrinos. • The universe's expansion becomes dominated by matter over radiation.
1 eV	$t \sim 10^{12}s$	• Electrons and charged nuclei combine in the era of recombination. • The universe becomes transparent to photons leaving an impression of the cosmic microwave background radiation on the sky that remains today. • The newly formed atomic matter coalesces in the era of galaxy formation.

Chapter 2

Grand Unified Dark Matter: $SU(5) \times SU(5)$

2.1 Introduction

We begin by exploring a class of model that can solve the similarity between the mass scale of Standard Model nucleons and dark matter. The dependence of the running coupling constant of QCD, $\alpha_s(\mu)$, on the scale μ can be expressed in two ways. The first is as a function of a reference scale μ_0 which gives an equation of the form

$$\alpha_s(\mu) = \frac{\alpha_s(\mu_0)}{1 + (\beta_0/4\pi)\alpha_s(\mu_0)\ln(\mu^2/{\mu_0}^2)}, \tag{2.1}$$

where α_s is known at the reference scale. Alternatively the dependence can be expressed as

$$\alpha_s(\mu) = \frac{4\pi}{\beta_0 \ln(\mu^2/\Lambda^2)}, \tag{2.2}$$

in which the parameter Λ is the confinement scale, the value at which the strong coupling constant becomes large as the energy scale decreases. This is a distinct feature of asymptotic freedom in which $\beta_0 > 0$. At first order the beta function for $SU(3)$ is

$$\beta_0 = 11 - \frac{2}{3}n_f, \tag{2.3}$$

where n_f is the number of quark flavours that appear in the loop corrections at a given energy scale. If one then knows the value of the strong coupling constant at a high

energy scale U, for instance at a GUT scale, it is possible to calculate the value of the confinement scale by evolving the coupling constant and taking into account quark mass thresholds. The threshold values are actually at twice the mass of each quark as this is the amount of energy needed to switch on the relevant loop correction. The resulting equation is dependent on this high reference scale, U, α_s at said scale, and the masses of the fermions in the range between the two scales. One obtains

$$\Lambda = 2^{2/9} e^{-2\pi/9\alpha_s(U)} U^{\frac{7}{9}} m_c^{\frac{2}{27}} m_b^{\frac{2}{27}} m_t^{\frac{2}{27}}. \tag{2.4}$$

where $m_{t,b,c}$ are the top-, bottom-, and charm-quark masses. For a more general theory the confinement scale is given by

$$\Lambda = 2^{1-\frac{b_u}{b_c}} e^{-2\pi/\alpha_s(U)b_c} U^{\frac{b_u}{b_c}} m_1^{\frac{b_c-b_b}{b_c}} m_3^{\frac{b_t-b_u}{b_c}} m_2^{\frac{b_b-b_t}{b_c}}. \tag{2.5}$$

The terms labelled b_x in this form of the equation denote the values of β_0 for different numbers of contributing quark flavours. For instance, b_b is the value above twice the charm mass but below the bottom mass. We use this notation for the sake of the more generalised relationship between energy thresholds and the DM confinement scale where the number of massive quarks and the masses that they have are initially completely free parameters. Only the masses of quarks larger than Λ itself appear explicitly in the equation. It is important to note that this equation is very sensitive to the value of the scale U. This sensitivity is avoided, however, in a non-Abelian dark sector if the confining gauge group is also $SU(3)$, as we explain below. To form the alternate gauge groups we develop a systematic way of generating different dark sectors from unified origins, with both containing an unbroken $SU(3)$ factor.

The intention of this chapter is then to explore the broader possibilities of generating spontaneous differences in $G_V \times G_D$ mirror theories to answer why DM could have a mass of the same order as the proton.

In a model with unified coupling constants, and where at a high energy the gauge groups of each sector break to $SU(3)$ at the same scale, the two values of the strong coupling constant α_s and α_{s_D} are the same from the GUT breaking scale all the way down to the scale at which the number of possible fermions in the loop corrections first deviates between the two sectors or further symmetry breaking occurs. This is highly desirable

as it allows the equation of the dark confinement scale to be greatly simplified, as the high reference scale can then be chosen to be at the deviation point when α_{s_D} has just the value of the Standard Model α_s at the scale of either the top quark or the heaviest of the dark quarks depending on which of these two has greater mass. If we make the further assumption for the sake of simplicity that all heavy dark quarks have the same mass, then our equation becomes a function of just one continuous and one discrete parameter, namely the dark fermion mass scale m and the number of fermions, n_f, that are at such a scale, $\Lambda(n_f, m)$. One could devise scenarios in which some of the heavy fermions attain an intermediate mass scale and adjust the confinement scale accordingly. The baryons themselves form from the light, or massless, quarks and therefore have mass either almost or totally dominated by the confinement scale. This is similar to other models that have explored the idea of dark QCD [113–120]. These dark QCD models of recent years typically don't have a direct connection to the visible sector. If one can build a model of two connected sectors that allows for the dark sector to give masses to coloured fermions at a low enough energy scale then accordingly one can provide an explanation for the similarity in mass of visible and dark matter. We now explore fermion mass generation with a view to having the visible and dark colour $SU(3)$ gauge coupling constants evolve differently under the renormalisation group. Section 2.2 will introduce the concept of asymmetric symmetry breaking. Section 2.3 will apply this formalism to GUT symmetry breaking. Then in Section 2.4 we demonstrate the asymmetry in fermion mass generation and how this affects confinement. Section 2.5 discusses constraints in our model and Section 2.6 and Section 2.7 repeat this analysis with a supersymmetric model.

2.2 Asymmetric symmetry breaking

The journey to a comprehensive model of asymmetric dark matter begins with our description of asymmetric potentials and the concept of asymmetric symmetry breaking (ASB). In order to illustrate the range of possible asymmetric symmetry breaking models and explain the basic features that drive asymmetric symmetry breaking, we examine in this section a simple toy model that involves all of the most basic terms required and demonstrate what vacuum expectation value patterns are possible. The simple model

we use for illustration is based on four real scalars in two $\mathbb{Z}_2$ pairs,

$$\phi_1 \leftrightarrow \phi_2, \qquad \chi_1 \leftrightarrow \chi_2. \tag{2.6}$$

The general potential can be written without loss of generality as

$$\begin{aligned} V = {} & \lambda_\phi(\phi_1^2 + \phi_2^2 - v_\phi^2)^2 + \lambda_\chi(\chi_1^2 + \chi_2^2 - v_\chi^2)^2 \\ & + \kappa_\phi(\phi_1^2\phi_2^2) + \kappa_\chi(\chi_1^2\chi_2^2) + \sigma(\phi_1^2\chi_1^2 + \phi_2^2\chi_2^2) \\ & + \rho(\phi_1^2 + \chi_1^2 + \phi_2^2 + \chi_2^2 - v_\phi^2 - v_\chi^2)^2. \end{aligned} \tag{2.7}$$

Terms such as $\phi_1^3\phi_2 + \phi_1\phi_2^3$ etc. are taken to be absent because of additional discrete symmetries. If each of the parameters is positive, then each of the six terms in this potential is positive definite. Then each is individually minimised if it is equal to zero. The first four terms are thus minimised by the condition that for each $\mathbb{Z}_2$ pair, one field gains a nonzero VEV while its partner has strictly zero VEV. The fifth term is minimised by the condition that the two nonzero-valued fields do not share a subscript (sector). The last term is then already zero by the previous conditions and the entire potential is minimised by these 'asymmetric' configurations:

$$\begin{aligned} \langle\phi_1\rangle = v_\phi, \qquad & \langle\chi_1\rangle = 0, \\ \langle\phi_2\rangle = 0, \qquad & \langle\chi_2\rangle = v_\chi. \end{aligned} \tag{2.8}$$

Note that it could have been (ϕ_2, χ_1) that gained nonzero VEVs, i.e. we cannot know *a priori* which way the symmetry will break.

A key feature of these asymmetric models is the ability of one asymmetry to induce further asymmetry in additional $\mathbb{Z}_2$-related fields. If we take a second set of four fields just as in the above case,

$$\Omega_1 \leftrightarrow \Omega_2, \qquad \eta_1 \leftrightarrow \eta_2, \tag{2.9}$$

our new general potential can be written in the form,

$$\begin{aligned} V = {} & \lambda_\phi(\phi_1^2 + \phi_2^2 - v_\phi^2)^2 + \lambda_\chi(\chi_1^2 + \chi_2^2 - v_\chi^2)^2 + \kappa_\phi(\phi_1^2\phi_2^2) + \kappa_\chi(\chi_1^2\chi_2^2) \\ & + \sigma(\phi_1^2\chi_1^2 + \phi_2^2\chi_2^2) + \rho(\phi_1^2 + \chi_1^2 + \phi_2^2 + \chi_2^2 - v_\phi^2 - v_\chi^2)^2 \\ & + \lambda_\Omega(\Omega_1^2 + \Omega_2^2 - v_\Omega^2)^2 + \lambda_\eta(\eta_1^2 + \eta_2^2 - v_\eta^2)^2 + \kappa_\Omega(\Omega_1^2\Omega_2^2) + \kappa_\eta(\eta_1^2\eta_2^2) + \\ & + \sigma_1(\Omega_1^2\eta_1^2 + \Omega_2^2\eta_2^2) + \rho_1(\Omega_1^2 + \eta_1^2 + \Omega_2^2 + \eta_2^2 - v_\Omega^2 - v_\eta^2)^2 \\ & + \sigma_2(\Omega_1^2\chi_1^2 + \Omega_2^2\chi_2^2) + \rho_2(\Omega_1^2 + \chi_2^2 + \Omega_2^2 + \chi_1^2 - v_\Omega^2 - v_\chi^2)^2 \\ & + \sigma_3(\phi_1^2\eta_1^2 + \phi_2^2\eta_2^2) + \rho_3(\phi_1^2 + \eta_2^2 + \phi_2^2 + \eta_1^2 - v_\eta^2 - v_\phi^2)^2 \\ & + \rho_4(\Omega_1^2 + \phi_1^2 + \Omega_2^2 + \phi_2^2 - v_\Omega^2 - v_\phi^2)^2 + \sigma_4(\Omega_1^2\phi_2^2 + \Omega_2^2\phi_1^2) \\ & + \rho_5(\chi_2^2 + \eta_2^2 + \chi_1^2 + \eta_1^2 - v_\eta^2 - v_\chi^2)^2 + \sigma_5(\chi_2^2\eta_1^2 + \chi_1^2\eta_2^2). \end{aligned} \tag{2.10}$$

These more complex ASB potentials will be discussed further in the next chapter when we consider larger GUT groups. As before, with each term positive definite, the potential is minimised for the following pattern of VEVs:

$$\begin{aligned} \langle\phi_1\rangle &= v_\phi \ , \qquad \langle\chi_1\rangle = 0 \ , \\ \langle\phi_2\rangle &= 0 \ , \qquad \langle\chi_2\rangle = v_\chi \ , \\ \langle\Omega_1\rangle &= v_\Omega \ , \qquad \langle\eta_1\rangle = 0 \ , \\ \langle\Omega_2\rangle &= 0 \ , \qquad \langle\eta_2\rangle = v_\eta \ . \end{aligned} \tag{2.11}$$

As usual this vacuum is degenerate with its $\mathbb{Z}_2$ transform. The potential has been constructed in such a way that the minima are when nonzero ϕ, Ω VEVs share a sector, and the same is true for χ, η. This associated asymmetry allows us to link together particular subgroups from gauge symmetry breaking with appropriate Higgs multiplets for that specific sector to give different masses to fermions. Large systems of many representations of scalar fields can take an initially mirrored GUT group and naturally populate each sector with nonzero VEVs of different scales which are given to different representations thus making the two sectors highly divergent in their features though identical in their origins. This toy model will serve as a proof of concept for the more involved scenarios that we move on to, that is, replacing these singlet fields with representations of GUT groups.

2.3 GUT symmetry breaking

We now consider how an asymmetric VEV structure allows for separate mechanisms to generate fermion masses in each sector. This chapter will explore an illustrative model of asymmetrical symmetry breaking that uses the $SU(5)$ GUT candidate. As noted in the introduction, $SU(5)$ was one of the first and most promising candidates to unify the forces and matter of the Standard Model though its promise has waned with little experimental support. Paired with a discrete symmetry, our $SU(5)_v \times SU(5)_d$ will be broken to different gauge groups in the two sectors but with both featuring unbroken $SU(3)$ subgroups which have quantitative differences. This then allows a numerical difference in the value of the dark sector confinement scale. To accomplish this we build a symmetry breaking potential out of four scalar multiplets making use of two different representations of $SU(5)$, namely the **24** and the **10**, each of which will have one of two multiplets become the sole attainer of a nonzero VEV in just one sector thus facilitating the different symmetry breaking patterns. In its most basic form this is just an extension of the simple model of the previous section in which the two sectors are the visible and dark and the fields ϕ_1, ϕ_2 are now **24** dimensional multiplets while χ_1, χ_2 become two copies of the **10** representation of $SU(5)$,

$$\begin{aligned} \phi_v &\sim (24, 1) \ , \qquad \chi_v \sim (10, 1) \ , \\ \phi_d &\sim (1, 24) \ , \qquad \chi_d \sim (1, 10) \ . \end{aligned} \tag{2.12}$$

Consider firstly the **10** representation of $SU(5)$ which one uses to spontaneously break

$$SU(5)_d \to SU(3) \ \times \ SU(2) \tag{2.13}$$

by appropriate choice of the sign of parameters in a general quartic scalar potential. The general renormalisable potential for a scalar multiplet $\chi \sim 10$ is ,

$$V_{10} = -\mu_t^2 \chi_{ij} \chi^{ji} + \lambda_{t1} (\chi_{ij} \chi^{ji})^2 + \lambda_{t2} \chi_{ij} \chi^{jk} \chi_{kl} \chi^{li}. \tag{2.14}$$

Note that $i, j = 1, ..., 5$ are $SU(5)$ gauge indices with $\chi_{ij} = -\chi_{ji}$, and the subscript t denotes 'ten'. Choosing the parameter λ_{t2} to be negative produces a VEV that breaks $SU(5)$ to $SU(3) \times SU(2)$ [121].

In the other sector the method of breaking $SU(5)$ to the Standard Model is to use scalar fields in the adjoint representation. The quartic potential is

$$V_{24} = -\mu_a^2 \phi_j^i \phi_i^j + \lambda_{a1}(\phi_j^i \phi_i^j)^2 + \lambda_{a2} \phi_j^i \phi_k^j \phi_h^k \phi_i^h, \tag{2.15}$$

where the subscript a is for 'adjoint', and ϕ is Hermitian traceless. Choosing λ_{a2} to be positive gives us the breaking

$$SU(5)_v \to SU(3) \times SU(2) \times U(1). \tag{2.16}$$

In this model we have four representations of scalar fields in the two $\mathbb{Z}_2$ pairs of Eqs. 2.14 and 2.15. The complete, general fourth-order, gauge-invariant scalar potential invariant under the discrete symmetry is written in Appendix A. It contains two copies of each of the above two potentials for the multiplets in each sector as well as all possible gauge-invariant contractions between the **24** and **10** in each individual sector, that is, of the style $\chi_v \chi_v \phi_v \phi_v$.

We can take these basic potentials written above and use them to write a simple outline of the full potential. We first duplicate each of the above potentials to accommodate each one's dark counterpart, and add in the cross terms such as $\mathrm{Tr}(\phi_v^2)\mathrm{Tr}(\phi_d^2)$. We term these

$$V_A = V_{24} + V'_{24} + \kappa_a \mathrm{Tr}[\phi_v^2]\mathrm{Tr}[\phi_d^2] \tag{2.17}$$

and

$$V_T = V_{10} + V'_{10} + \kappa_t \chi_{v\,ij} \chi_v{}^{ji} \chi_{d\,nm} \chi_d{}^{mn}. \tag{2.18}$$

To this there are five remaining contractions that we must add to write the general renormalisable potential. A portion of this potential, displayed in full in Appendix A, can then be written as

$$V = V_A + V_T + C_0(\chi_{d\,nm} \chi_d{}^{mn} \mathrm{Tr}[\phi_v^2] + \chi_{v\,ij} \chi_v{}^{ji} \mathrm{Tr}[\phi_d^2]) + \dots \tag{2.19}$$

Extending the analysis of Section 2.2 we find that for a particular region of parameter space in this potential, the global minimum is at

$$\begin{aligned}
\langle \phi_v \rangle &= v_v \begin{pmatrix} 1 & 0 & 0 & 0 & 0 \\ 0 & 1 & 0 & 0 & 0 \\ 0 & 0 & 1 & 0 & 0 \\ 0 & 0 & 0 & -3/2 & 0 \\ 0 & 0 & 0 & 0 & -3/2 \end{pmatrix}, \\
\langle \chi_v \rangle &= 0, \\
\langle \phi_d \rangle &= 0, \\
\langle \chi_d \rangle &= v_d \begin{pmatrix} 0 & 1 & 0 & 0 & 0 \\ -1 & 0 & 0 & 0 & 0 \\ 0 & 0 & 0 & 0 & 0 \\ 0 & 0 & 0 & 0 & 0 \\ 0 & 0 & 0 & 0 & 0 \end{pmatrix}.
\end{aligned} \tag{2.20}$$

By using the principles of the simple model and its parameter space from Section 2.2, this potential is seen to induce the two $SU(5)$ gauge groups to indeed break differently in each sector. In one sector the **10** representation attains a VEV breaking $SU(5)$ to $SU(3) \times SU(2)$ and the positive definite contraction terms push the **24** in that sector to attain a VEV of zero. In the other sector, the **10** representation is driven to have a VEV of zero by contraction terms with its counterpart and this forces the **24** to attain a VEV that breaks this second $SU(5)$ to the Standard Model gauge group. There is once again no way of knowing which is the visible and which is the dark sector prior to symmetry breaking. Once the symmetry is broken to the lowest state it shall simply be that we label the $SU(5)$ which is broken to the Standard Model group the gauge symmetry of the visible sector and the alternatively broken symmetry is then the dark sector gauge group.

2.4 Fermion masses

In $SU(5)$ theories the fermions of the Standard Model are assigned to the $\overline{\mathbf{5}}$ and **10** representations. The product of these allows for mass generation through Yukawa couplings to Higgs fields in **5**, **10**, **45** or **50** dimensional representations. As an example, we aim

to have two different representations for our mass generation, a **5** to accommodate the Standard Model Higgs doublet in the visible sector and another representation which attains a nonzero VEV in the dark sector to give a different form of mass generation for the dark sector quarks.[1]

The **10** representation already employed in the symmetry breaking only gives mass to leptons and is thus unsuitable. We therefore choose to examine how a **5** and a **45** in each sector can allow for a difference in the scale of quark and dark-quark masses. The **45** has the interesting property of automatically leaving one dark quark massless [122], which is a very useful feature for our application. The fermion multiplets are the same in each sector, again respecting our initial mirror symmetry:

$$\begin{aligned} \psi_{v_5} &\sim (\overline{5}, 1) \ , \qquad \psi_{d_5} \sim (1, \overline{5}) \ , \\ \psi_{v_{10}} &\sim (10, 1) \ , \qquad \psi_{d_{10}} \sim (1, 10) \ , \end{aligned} \tag{2.21}$$

and the Higgs multiplets which take the place of the fields Ω, η from Section 2.2 are

$$\begin{aligned} H_{v_5} &\sim (5, 1) \ , \qquad H_{d_5} \sim (1, 5) \ , \\ H_{v_{45}} &\sim (45, 1) \ , \qquad H_{d_{45}} \sim (1, 45) \ . \end{aligned} \tag{2.22}$$

The Yukawa Lagrangian is

$$\mathcal{L}_F = y_1 \overline{\psi_{v_5}} H^*_{v_5} \psi_{v_{10}} + y_2 \overline{\psi_{v_{10}}} H_{v_{45}} \psi_{v_{10}} + y_1 \overline{\psi_{d_5}} H^*_{d_5} \psi_{d_{10}} + y_2 \overline{\psi_{d_{10}}} H_{d_{45}} \psi_{d_{10}} + h.c. \tag{2.23}$$

The methodology of Section 2.3 can be extended to include the $\mathbb{Z}_2$ scalar pairs responsible for fermion mass generation. The asymmetric symmetry breaking described in Section 2.2 can induce consecutive asymmetries in more sets of fields. The dependence for which way the asymmetry in the second set will fall is entirely dependent on the weighting of the cross terms between the two sets.

It is in this manner that we arrange for the H_{45} in the visible sector to have a zero VEV, while in the dark sector it gives mass to five of the six quarks at an indeterminate scale

[1] The idea of a non-Abelian gauge sector responsible for confining DM has been detailed in a number of different works such as [115] in which the range of $SU(N)$ groups and ultraviolet boundary conditions of the coupling constants that allow for TeV-scale-confined DM were investigated. In [118] the scale of gluinos and glueballs in an $SU(N)$ hidden sector was seen to be adjustable to produce TeV scale glueball DM that could agree with a number of astrophysical constraints of self-interacting DM.

v_d and reduces the dark sector symmetry from $SU(3) \times SU(2)$ to $SU(3)$. The invariant component of $H_{d_{45}}$ is

$$\langle H_{d_{45}} \rangle_a^{b5} = v_d \begin{pmatrix} 1 & 0 & 0 & 0 & 0 \\ 0 & 1 & 0 & 0 & 0 \\ 0 & 0 & 1 & 0 & 0 \\ 0 & 0 & 0 & -3 & 0 \\ 0 & 0 & 0 & 0 & 0 \end{pmatrix}. \tag{2.24}$$

On the other hand the H_5 has a VEV of zero in the dark sector and a nonzero VEV in the visible sector as per the minimal $SU(5)$ model of giving mass to the fermions:

$$\langle H_v \rangle = v_v(0, 0, 0, 0, 1), \qquad \langle H_d \rangle = 0. \tag{2.25}$$

The scale v_d can then be compared to the top line in Fig. 2.1 from Section 2.4 in which we have five heavy dark quarks and a single massless dark quark. In such a scenario, if the masses of the quarks are less than 1000 TeV then they produce dark confinement scales less than 14 GeV. The remaining massless quark, a dark up-quark, forms a set of neutral Δ(uuu) baryon-like states, lighter than all other possible dark colour singlets and with mass completely dominated by the confinement scale. We will discuss such states further in Chapter 5. This forms a dark analogue of the visible sector nucleon but with mass that is an order of magnitude greater. If we consider minimal differences in the magnitude of the mass generating VEVs, which is quite natural to obtain if parameters are of similar order, then at around the electroweak scale, $\sim$246 GeV, a confinement scale of 2.1 GeV is generated in the dark sector. This is around an order of magnitude higher than the Standard Model QCD scale of 0.217 GeV.

2.5 Phenomenological issues

It is important to note that we merely assumed in the previous analysis that the gauge coupling constants of the sectors unify at a high GUT scale. While the scenario of a non-supersymmetric asymmetric model that we have described does not automatically have gauge coupling unification, it is possible to bring the three coupling constants of the Standard Model together at the GUT scale by the addition of extra Higgs multiplets. One must also consider the constraints from the experimental lower bounds

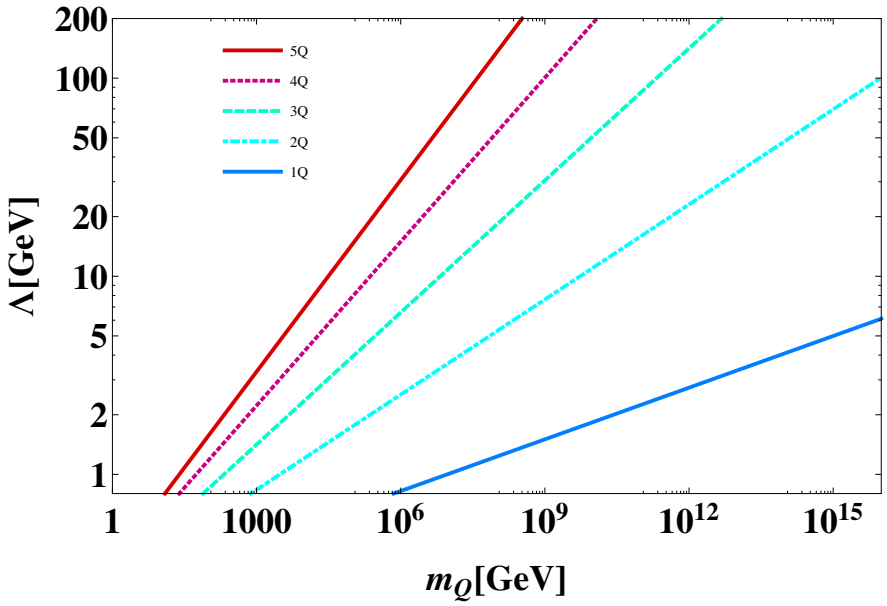

FIGURE 2.1: The confinement scale of a dark sector as a function of the common mass scale, m_Q, for 1,2,3,4 or 5 dark quarks. This assumes a common origin of the gauge coupling of the dark $SU(3)$ theory and QCD at the UV scale. The vast range of possible mass scales for fermions leads to only small changes in the dark confinement scale and a reason why dark matter, consisting of dark baryons, should have a mass that is so near that of the proton.

of proton decay. Decay modes from minimal $SU(5)$ models have quite high bounds, $\tau(p \to \pi^0 e^+) \gtrsim 10^{34}$ years [123] and the order of magnitude estimation for the width

$$\Gamma \approx \alpha^2 \frac{m_p^5}{M_X^4}, \tag{2.26}$$

demands that we must have at least $M_X \approx 4 \times 10^{15}$. In [124] it was shown that consistent proton decay limits and unification could be obtained with the addition of Higgs multiplets in a non-supersymmetric $SU(5)$.

Bounds on the dark baryons as DM from the bullet cluster observation are similar to that in [125] where the self-interaction cross section of these nucleons $\sigma \sim 10^{-26}$ cm^2 is compared to the upper bound of the DM self-interaction cross section $\leq 10^{-23}$ cm^2 [125–127]. The scale that v_d can take is something that we have not followed in full detail opting to simply take as a guide the range of scale differences that we can accommodate in the simple model in Section 2.2. These lead us to see that the scale of v_d for a factor of five difference between ordinary and dark baryons would need to be between ~ 30 GeV to 10^4 TeV depending on how many of the heavy quarks are given mass. The **45** representation of $SU(5)$ would observe the lower bound of ~ 30 GeV as the mass scale

would give this exact ratio. If, on the other hand, one only gave mass to a single quark in the dark sector then a very high mass would be compatible with a confinement scale of order the Standard Model.

Since the achievement of gauge coupling constant unification in non-SUSY GUT models is somewhat *ad hoc* and, more importantly, suffers from the gauge hierarchy problem, we now turn to SUSY models where these problems are absent.

2.6 Supersymmetric asymmetric symmetry breaking

We now develop a supersymmetric analogue of the model in Section 2.3, that is an $SU(5)$ theory with scalar fields in the **10** and **24**. In building the supersymmetric potential we will have to introduce another chiral supermultiplet in the $\overline{\mathbf{10}}$ representation, Y, to make it possible to include gauge invariant terms containing $X \sim 10$ in the superpotential. We must of course also introduce a counterpart field Y_d for the sake of the discrete symmetry.

This allows for the construction of a potential including all of the fields from the non-SUSY case. However, in order to facilitate asymmetric symmetry breaking it is key that we have both terms that mix the fields under different representations in each sector and cross terms between the two sectors. This is not possible with the set of fields as they are. To achieve this we add a singlet scalar superfield S which transforms into itself under the discrete symmetry. Doing so allows for the superpotential to generate all of the necessary cross terms for asymmetric symmetry breaking through the F-terms of the scalar potential. The chiral supermultiplets involved are then

$$\begin{aligned} &\Phi_v \sim (24, 1), \qquad X_v \sim (10, 1), \qquad Y_v \sim (\overline{10}, 1), \\ &\Phi_d \sim (1, 24), \qquad X_d \sim (1, 10), \qquad Y_d \sim (1, \overline{10}), \end{aligned} \tag{2.27}$$

and

$$S \sim (1, 1). \tag{2.28}$$

The general superpotential

$$\begin{aligned} W = & s_1(X_v Y_v + X_d Y_d) + s_2(\Phi_v \Phi_v + \Phi_d \Phi_d) + s_3(\Phi_v \Phi_v \Phi_v + \Phi_d \Phi_d \Phi_d) \\ & + s_4(X_d \Phi_d Y_d + X_v \Phi_v Y_v) + s_5(\Phi_v \Phi_v S + \Phi_d \Phi_d S) + s_6(X_v Y_v S + X_d Y_d S) \\ & + s_7 S + s_8 SS + s_9 SSS \end{aligned} \tag{2.29}$$

satisfies $SU(5)_v \times SU(5)_d$ gauge invariance and the $\mathbb{Z}_2$ discrete symmetry. The symmetry breaking possibilities with this potential are discussed in more detail in Appendix A.

The complete potential has contributions from the F-terms of the superpotential, the D-terms from those fields which are charged under one of the $SU(5)$ symmetries and soft mass and trilinear terms. Since we have a complete singlet S, the non-holomorphic trilinear terms are taken to be absent [62]. The equation is

$$\begin{aligned} V &= W^{i*} W_i + \frac{1}{2} \sum_a (g \Phi_i T_a \Phi^i)^2 - m_X (X_{vij} X_v{}^{ji} + X_{dij} X_d{}^{ji}) \\ &- m_Y (Y_{vij} Y_v{}^{ji} + Y_{dij} Y_d{}^{ji}) - m_\Phi (\Phi_v \Phi_v + \Phi_d \Phi_d) - m_S S^2 \\ &- a_1 (\Phi_d \Phi_d \Phi_d + \Phi_v \Phi_v \Phi_v) - a_2 (X_d Y_d \Phi_d + X_v Y_v \Phi_v), \end{aligned} \tag{2.30}$$

where

$$W^i = \frac{\partial W}{\partial \phi_i} \tag{2.31}$$

and each ϕ_i is one our fields. There are nine parameters from the superpotential (s_1,..., s_9), six parameters from the soft terms m_Φ, m_X, m_Y, m_S, a_1, a_2 as well as the $SU(5)$ coupling constant present in the D-terms. With this field content we find that the scalar potential then has the capacity to display asymmetric symmetry breaking by appropriate choice of the parameters. The singlet field S is important here. Without it we could not arrive at a scalar potential that has terms such as $\Phi_v \Phi_v \Phi_d \Phi_d$, that is, terms which mix the two sectors. Without these it is not possible to create the necessary dependence between sectors for VEV development to be opposing. There are non-minimal choices one could make for the additional fields that would allow for these terms but for now we choose to simply focus on the simplest case.

Consider a parameter choice with s_4 and s_5 large compared to the other superpotential parameters, and with nonzero values of m_X, m_Y and m_Φ. F-terms of the style $(\Phi_v^2 \Phi_d^2)$ or $(X_v X_v \Phi_v \Phi_v)$ can then serve as the cross terms that create the asymmetric acquisition

of VEVs. With largely positive quartic terms coming from the D-terms and negative quadratic terms in the form of the soft masses, these cross terms can drive one variety of each multiplet of a given dimensionality to zero in the same manner as the non-SUSY case. It is however the case that many other W terms can spoil this pattern and so many of the other superpotential parameters must be kept relatively small, at least an order of magnitude. The parameter s_9 we can allow to be large, as it will serve to bring the value of S to zero. In one scenario one can generate a nonzero VEV for Φ_v in the visible sector, again breaking

$$SU(5)_v \to SU(3) \times SU(2) \times U(1), \tag{2.32}$$

and in the dark sector we have Φ_d developing a VEV of zero. Then the multiplets X_d and Y_d together acquire nonzero VEVs which break

$$SU(5)_d \to SU(3) \times SU(2). \tag{2.33}$$

Being a pair of conjugate representations, they will induce breaking to the maximal stability group of $SU(5)$ according to Michel's conjecture [128, 129] which states that this is the case for a potential containing only a real representation or a pair of conjugate representation. This does not strictly apply in this scenario, of course, because we have other fields involved in the potential. However, we invoke it as numerical analysis shows that symmetry breaking of this type occurs within the parameter space that gives asymmetric VEV patterns. Appendix A contains further details of this parameter space. For the **10** dimensional representation, the maximal stability group, or maximal little group, is $SU(3) \times SU(2)$ as it is the only maximal group which observes a singlet within the **10** of $SU(5)$.

The supersymmetric case is more constrained in its ability to display asymmetric configurations, though with suitable additions in particle content we have found that it is a feature that a unified supersymmetric theory can have. Many of the parameters in the superpotential must be kept quite small so as to not overpower the terms essential for guaranteeing asymmetric VEV arrays. It would be interesting to explore this issue further in developing a complete theory and examining more of the possibilities for asymmetric SUSY sectors, however that is beyond the scope of this chapter.

We now discuss the dependence of the confinement scale with various parameters in a general supersymmetric theory.

2.7 Supersymmetric confinement

In the case of supersymmetric theories, the running coupling is modified by the additional particle content. For $SU(3)$ we are however only interested in those particles with colour charge. Note that this analysis is not dependent on any particular choice of GUT group, relying only on an $SU(3)_v \times SU(3)_d$ structure after GUT breaking.

In the MSSM the one-loop beta function for $SU(3)$ is altered by the addition of the gluinos and sfermions as per

$$\beta_0 = 11 - \frac{2}{3}n_f - C_g - \frac{2}{6}n_s, \tag{2.34}$$

where n_f (n_s) is the number of quarks (squarks) and $C_g = 2$ is due to the gluinos. The calculation of the dependence of confinement scale is more model dependent here as one must first of all take into account the mass that visible sector gluinos and squarks take to consider what value the coupling will take at the GUT or high reference scale μ_0. This will alter the precise calculation of the value of α_{3d} at the scale at which the visible and dark sector couplings unify. One can also consider in the dark sector how we might separate the scales of the quarks and squarks. If we take the assumption that the SUSY breaking scale is no higher than the mass scale of the dark quarks in the dark sector then this provides a rough upper bound on the scale at which we place the supersymmetric partners in that sector. This assumption is favourable also as it allows for a similar analysis as before in that, if the two sectors have $SU(3)$ gauge symmetry with the same number of particles of each kind all the way down in energy to the mass of the heaviest dark quark, then we can choose this as our high reference scale and take the value of the coupling at this scale to be the same in both supersymmetric sectors. Then we can establish a range of possible confinement scales that supersymmetric dark QCD could have. We will examine the relationship between the confinement scale and these mass scales as we did in the non-SUSY case. In this case we take the squarks and gluinos of the dark sector to be quite light (under a TeV) and in such a scenario the dependence is similar to the non-SUSY case but with a larger confinement scale, shown in Fig. 2.2

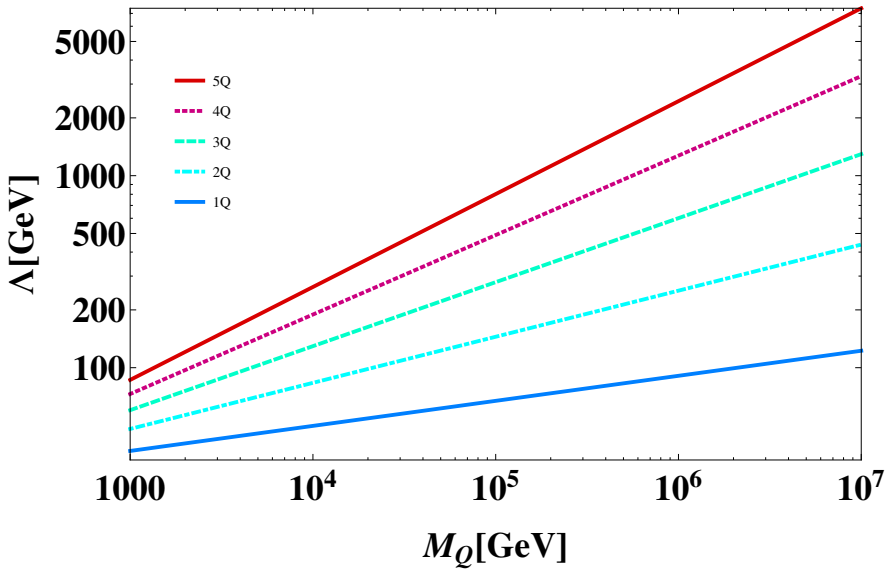

FIGURE 2.2: Confinement scale dependence on fermion masses, in simple SUSY case, almost identical to non-SUSY, but with the confinement scale axis multiplied by ~ 10.

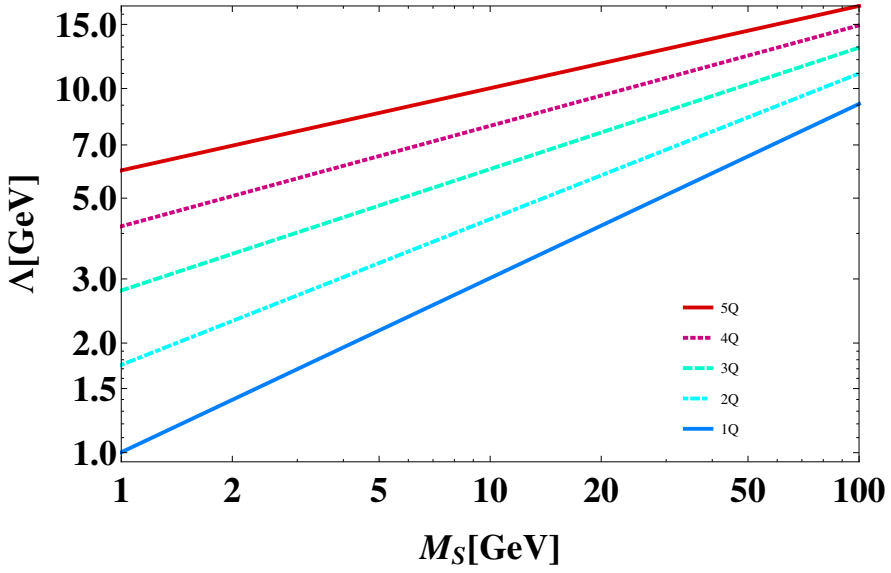

FIGURE 2.3: Confinement scale dependence on SUSY breaking scale for fixed dark-quark mass scale of 100 GeV. The number of heavy quarks at the dark-quark mass scale ranges from five at the top to one at the bottom.

We now examine the dependence of the dark confinement scale on the dark SUSY breaking scale for a range of different dark-quark masses.

The scale of dark-quark masses is taken to be higher than the SUSY breaking scale in each case. It must be noted however that the superpartners of heavy dark quarks with masses above the SUSY breaking scale have the same masses as these dark quarks

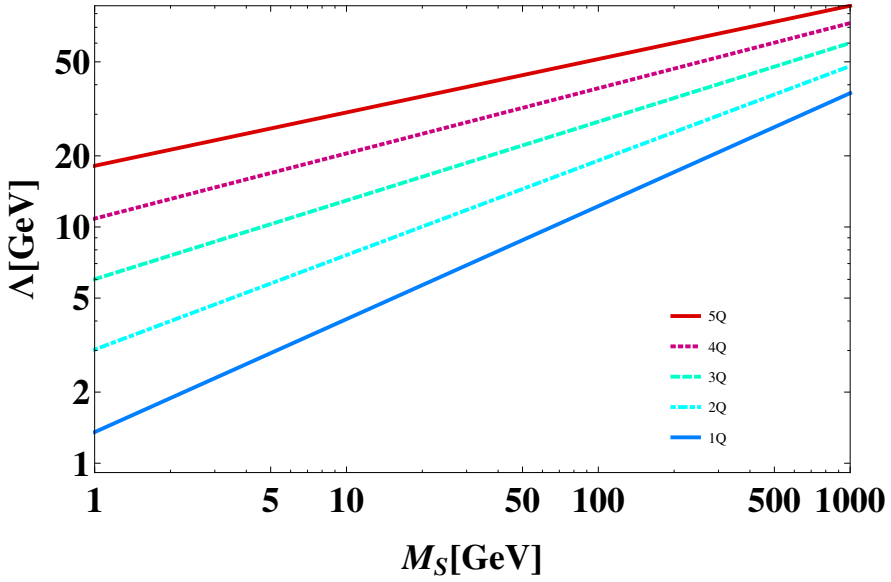

FIGURE 2.4: As for Fig. 2.3 but with a dark-quark mass scale of 1000 GeV.

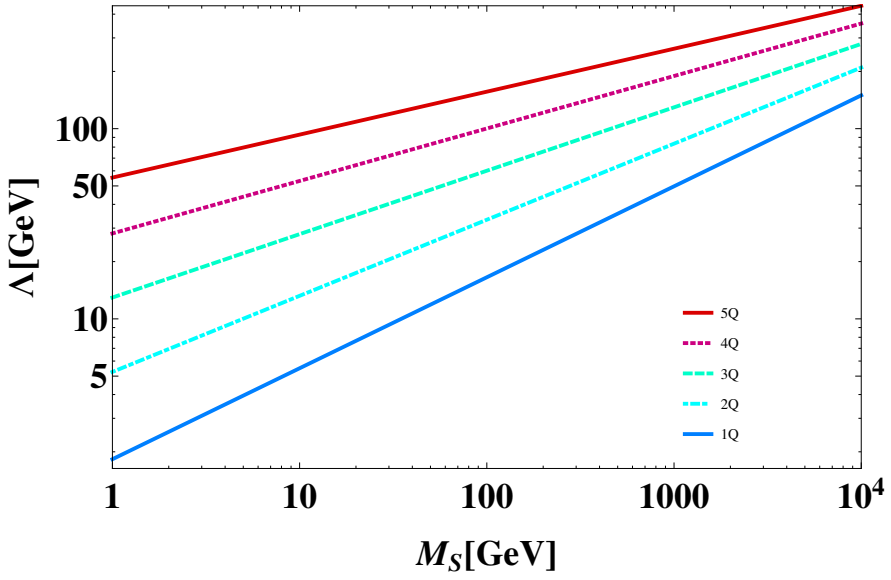

FIGURE 2.5: As for Fig. 2.3 but with a dark-quark mass scale of 10^4 GeV.

and therefore switch off in the running prior to the other superpartners. This has the additional effect of a more pronounced change in the running at these quark mass thresholds as multiple bosonic degrees of freedom are switching off at the same energy scale. Figures 4-6 show this dependence for different numbers of heavy dark quarks. The value of the confinement scale is in general higher than the non-SUSY case though we do have additional parameters to contend with in the form of the mass scales of the squarks and gluinos.

2.8 Summary

We have demonstrated in this chapter that asymmetric symmetry breaking can take a mirror symmetric grand unified theory and spontaneously break it to form distinct sectors that generate masses for fermions at different energy scales. We have further examined how the mass scales of particle species in a dark sector can alter the running of the gauge coupling constant of a confining non-Abelian gauge group. Critically we have shown that if the gauge coupling of a dark confining group is constrained to equal that of $SU(3)_c$ at the Planck scale, then the variation of a dark confinement scale compared to that of QCD is very insensitive to the mass scales of fermions in the dark sector. This provides a compelling explanation for why dark matter, in the form of composite states of a dark confining group, must have a mass similar to that of the proton. We have also shown that asymmetric symmetry breaking is compatible with supersymmetry and explored how the confinement scale of a dark sector is affected by the scale at which supersymmetry is broken. In the next section we will examine how we can extend this idea of generating a dark sector with a confinement scale similar to that of QCD.

Chapter 3

Breaking Chains of $SO(10) \times SO(10)$

In this chapter we explore the ability of spontaneous symmetry breaking to generate similar results from different GUT breaking chains in the two sectors in an $SO(10) \times SO(10)$ theory. These different gauge symmetry breaking chains can result from a simple extension of the mechanism of ASB and allows one to create regions where the coupling evolution differs in the two sectors without considering fermion mass generation. The models that we explore here are larger extensions to mirror symmetric models which have been explored in many contexts [17–24, 26, 29, 30, 32–34, 36–38, 47], where in this chapter the mirror symmetry serves only at high energy and the low energy features of the two sectors can be vastly different. We use this to develop a new way of explaining the similarity of DM mass. The next section will review the motivation for such models by examining how the running of coupling constants in gauge theories with unification can be used to link the colour confinement scales of the two sectors. From there, Section 3.2 will discuss $SO(10)$ models and their appeal as the choice of GUT group to be implemented with this method. Following this, Section 3.3 will discuss the paths of symmetry breaking that we can take within $SO(10)$ models and how these can be used in asymmetric symmetry breaking models to create the SM in one sector with an $SU(3)$ group in the dark sector. We will then move on to Section 3.5 where we will explore similar models within the supersymmetric framework, while Section 3.6 will examine the results from a broad range of these possible scenarios and their effect

on the dark QCD scale. Finally in Section 3.7 we will discuss the constraints on some of these models and the outlook for such theories.

3.1 Dimensional transmutation

Our objective is to develop $SO(10) \times SO(10)$ models that can account for the similarity in mass of visible and dark matter. We have seen that the overwhelming majority of the mass of visible matter comes from dimensional transmutation where a dimensionful parameter is created at the scale at which a coupling begins to diverge and the theory becomes non-perturbative. The masses of the protons and neutrons which dominate the visible sector in the present universe come from the confinement scale of QCD where the coupling constant of the colour force becomes large at low energy. As in the previous chapter, this feature of asymptotically free theories presents an elegant way to introduce mass scales into a theory. The capacity to yield such scales at low energy comes from the negative sign of the beta function of a non-Abelian gauge theory. The running coupling evolution is again described by the logarithmic dependence on energy scale,

$$\alpha_s(\mu) = \frac{\alpha_s(\mu_0)}{1 - (b_0/4\pi)\alpha_s(\mu_0)\ln(\mu^2/\mu_0{}^2)}, \tag{3.1}$$

such that at low energy scales the value of α_s grows exponentially. This asymptote sets the energy scale of the proton mass after chiral symmetry breaking when coloured particles are confined to bound states. We can now consider a general non-Abelian gauge theory for a group G where the full beta function at one-loop is given by

$$\begin{aligned}\beta(g)_{(1\,\text{Loop})} = \frac{g^3}{16\pi^2}\Bigg(&-\frac{11}{3}R_{\text{Gauge}} + \frac{4}{3}R_{\text{Dirac}} + \frac{2}{3}R_{\text{Majorana}} \\ &+ \frac{2}{3}R_{\text{Weyl}} + \frac{1}{3}R_{\text{C.Scalar}} + \frac{1}{6}R_{\text{Scalar}}\Bigg),\end{aligned} \tag{3.2}$$

where $\beta(g)_{(1\,\text{Loop})} = \frac{g^3}{16\pi^2}b_0$ and the factors of R are the indices for the choice of multiplet(m) defined as

$$\text{Tr}(\tau^a\tau^b) = \delta^{ab} \times R(m), \tag{3.3}$$

and are calculated for each copy of the gauge fields, which are necessarily in the adjoint representation of G, followed by the Dirac, Majorana, and Weyl fermions and finally complex and real scalars. For the familiar QCD group $SU(3)$, the beta function becomes

the original

$$b_0 = -11 + \frac{2}{3} n_f, \tag{3.4}$$

with n_f the number of flavours. In the following sections we will continue to seek explanations for the similarity of visible and dark matter masses by assuming that DM similarly gains its mass by dimensional transmutation and that the confinement scales of the two sectors are linked to each other by their different symmetry evolution from a common starting point at the GUT scale. These differences can occur spontaneously from a completely mirror symmetric model thanks to asymmetric symmetry breaking where the absolute minima of the potential are such that the vacuum structure of each sector is necessarily different. The goal of this chapter is to construct a broad outline of the possible models in which a GUT theory with a discrete $\mathbb{Z}_2$ symmetry can naturally explain the similarity of visible and dark matter masses by spontaneously breaking the symmetries of the two sectors through different subgroups while ending with at least one copy of $SU(3)$ in each sector. In this manner the confining scale of the dark QCD is related to that of the Standard Model through the unified couplings at high scale, but within intermediate symmetry breaking scales the coupling constants run differently due to the contribution from the gauge bosons of their respective groups. It thus becomes effectively the first term in Eq. 3.2 that changes at particular mass scales allowing for the generation of different confinement scales rather than the second term in Eq. 3.2 at the quark mass thresholds as in the previous chapter. In this chapter we will not examine any differences resulting from quark mass thresholds though of course the two effects could be utilised in a single theory. We will focus on those cases where, after the altered running of the two QCDs is established, the dark QCD coupling will confine at a higher energy scale as this is more suited to ADM where mass scales of around one order of magnitude higher are compatible. Figure 3.1 shows the divergence of the two $SU(3)$ theories after running at different rates for a segment of the high energy regime.

A number of other models have explored similar concepts of generating the confinement scale of a dark QCD in order to explain the DM mass coincidence. In particular this work is related to that of [130–133] where $\mathbb{Z}_2$ symmetric $SU(5)$ and $SO(10)$ GUTs were explored for generating confined states at low scales. The present chapter however seeks to expand the technique of asymmetric symmetry breaking beyond $SU(5)$ theories to the $SO(10)$ gauge group and so we move on to a discussion of its features.

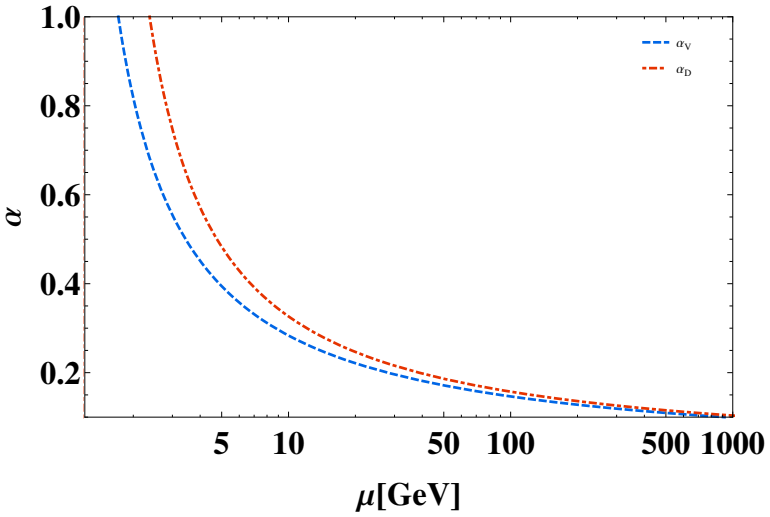

FIGURE 3.1: The confinement of the dark sector QCD occurs at a higher scale than its visible counterpart after asymmetric symmetry breaking. The top line shows α_D after running as $SU(4)$ for two orders of magnitude at a high energy scale while α_V remains $SU(3)$.

3.2 $SO(10) \times SO(10)$ models

The group $SO(10)$ presents an appealing avenue for GUT extensions to the Standard Model beyond the minimal cases. It has the benefit of allowing each generation of fermions to fit within a single $SO(10)$ multiplet including the right hand neutrino. Most $SO(10)$ models require at least two Higgs multiplets to break the full symmetry down to the Standard Model. Typical choices include one set of fields in **45** or **54** representations and another in **10**, **16** or **126** dimensional representations [122]. The choice of **126** for the second is appealing as it allows the generation of fermion masses by Yukawa coupling to the 3 copies of 16_f which contain the fermions of the Standard Model. Since there are two multiplets required to break $SO(10)$ to the Standard Model gauge group, the work of Chapter 2 can be naturally extended to $SO(10)$ where the visible and dark sectors required two Higgs representations in each sector to carry out asymmetric symmetry breaking. By giving a nonzero VEV to all four representations in such a manner that representations paired under the $\mathbb{Z}_2$ symmetry gain VEVs of different sizes, the gauge group of each sector will be different for small segments of the range between the GUT scale and the low energy theory. The parameter space of this particular type of model can be quite small and therefore leads us to consider non-minimal multi-step breaking chains in $SO(10)_V \times SO(10)_D$ models for more than four Higgs multiplets. We are chiefly concerned with paths that can break $SO(10)$ to a gauge sector containing $SU(3)$

in the dark sector while breaking to the SM gauge group in the VS. Since our primary goal is to generate dark confinement scales only slightly above that of the visible sector, we will limit ourselves to models where this is the result, that is $\Lambda_{\rm DM} > \Lambda_{\rm QCD}$. The case of $\Lambda_{\rm DM} = \Lambda_{\rm QCD}$ can also appear, often in the limiting cases where the intermediate scales approach the GUT scale.

To illustrate the concept consider the case where

$$SO(10)_V \underset{M_X}{\to} SU(4) \times SU(2) \times SU(2) \underset{M_I}{\to} SU(3) \times SU(2) \times U(1), \tag{3.5}$$

while in the dark sector

$$SO(10)_D \underset{M_X}{\to} SU(5) \underset{M_I}{\to} SU(3) \times SU(2) \times U(1). \tag{3.6}$$

In the visible sector this could be done with a Higgs multiplet which transforms as a **54** and which gains a VEV at the scale M_X while in the dark sector we have a **45**. Then a pair of **16** + $\overline{\mathbf{16}}$ or **126** + $\overline{\mathbf{126}}$ representations could gain VEVs in both sectors at the scale M_I where each sector becomes Standard Model-like. The use of a pair of conjugate representations allows for such fields to be included in the superpotential in supersymmetric theories and also allows us to invoke Michel's conjecture which states that for conjugate pairs such as these, or for real irreducible representations, the symmetry breaking must be to a maximal little group [128, 129]. This pair of breaking chains is a particularly simple example where we have only two scales, M_X and M_I, however in general it is possible for the intermediate scales of the two sectors to be independent. In such a scenario we have only the distance between the two scales M_X and M_I that determines the size of the difference between the confinement scales between the two sectors. This difference can be approximately determined by calculating the value of the dark sector's Λ after running upward in energy from $\Lambda_{\rm QCD}$ to the lowest breaking scale M_I and then to the second, M_X, before evolving back down in energy until we reach the confinement regime. Using this it can be calculated that at one-loop the ratio of the confinement scales is given by

$$\frac{\Lambda_{\rm DM}}{\Lambda_{\rm QCD}} = \frac{M_X}{M_I}^{\frac{b_D - b_V}{b_0}}, \tag{3.7}$$

where the beta functions here are for the intermediate gauge groups in the intermediate

range $M_I \leq M \leq M_X$ for the two sectors, and b_0 is the $SU(3)$ beta function given in Eq. 3.4. This calculation allows us to see that similar but different confinement scales can be generated from a model with different gauge symmetries at high energy, and for this reason we wish to consider the full set of possible symmetry breaking scenarios. In the next section we will examine what breaking chains are possible in each sector.

3.3 Multi-step breaking chains

We wish to systematically explore all the possibilities for the different breaking chains that can occur in each sector for an $SO(10)$ model in order to examine which chains allow for realistic models of both sectors. There are a number of paths through which $SO(10)$ can break down to a gauge theory containing the SM with two of the most notable being through the Pati-Salam $SU(4) \times SU(2) \times SU(2)$[134] and the Georgi-Glashow $SU(5)$ [135] subgroups. For the visible sector we are mostly concerned with these particular models, however for the dark sector we are free to choose any breaking which leaves unbroken an $SU(3)$ theory at low energy. This opens up a large number of choices of Higgs multiplet representations in the dark sector. We will limit ourselves to the cases of one and two intermediate scales as additional scales add complexity without necessarily offering more insight into possible outcomes. Below we list all of the possible breaking chains we can consider for the colour force in the dark sector. We consider first of all chains with just one intermediate scale, M_I, between the confinement scale, Λ_{DM}, and the GUT scale M_X. These are

$$\begin{aligned} SO(10) &\to SO(9) \to SU(3) \quad (I) \\ SO(10) &\to SO(8) \to SU(3) \quad (II) \\ SO(10) &\to SO(7) \to SU(3) \quad (III) \\ SO(10) &\to SU(5) \to SU(3) \quad (IV) \\ SO(10) &\to SU(4) \to SU(3) \quad (V) \end{aligned} \tag{3.8}$$

and secondly we consider models with two intermediate scales, M_I and M_J, between M_X and the low energy theory, with $M_J \geq M_I$. These are

$$\begin{aligned} SO(10) \to SO(9) \to SO(8) \to SU(3) \ \ (VI) \\ SO(10) \to SO(9) \to SO(7) \to SU(3) \ \ (VII) \\ SO(10) \to SO(9) \to SU(4) \to SU(3) \ \ (VIII) \\ SO(10) \to SO(8) \to SO(7) \to SU(3) \ \ (IX) \\ SO(10) \to SO(8) \to SU(4) \to SU(3) \ \ (X) \\ SO(10) \to SO(7) \to SU(4) \to SU(3) \ \ (XI) \\ SO(10) \to SU(5) \to SU(4) \to SU(3) \ \ (XII). \end{aligned} \tag{3.9}$$

The chains we consider in the visible sector are most often IV and V as well as the case where the two intermediate scales are close enough that the symmetry breaking effectively happens at one scale, as per $SO(10) \to SU(3)$. We consider this variety as the limiting case for the magnitude of the difference between the two groups' one-loop beta functions and is useful for cases where the symmetry breaking chains of the two sectors are in fact the same except for the scales at which breaking occurs. This can be seen as delayed symmetry breaking where at one or more of the scales, M_X, M_I and M_J, one sector breaks to a subgroup but the other does not. The analysis is no different than other examples, it is simply that we contrast some intermediate gauge group's running with that of, for instance, the group $SO(10)$ itself. In examining results we choose a breaking chain for each sector from the list, but we will limit ourselves to only those choices for which the dark scale runs faster in the intermediate range of the running for the case of one intermediate scale. These cases demonstrate the key aspect of these theories, that the gauge group of the intermediate energy scale can change the final scale of dimensional transmutation in two $SU(3)$ theories that originate from an originally $\mathbb{Z}_2$ symmetric $G \times G$ theory.

For the sake of proton decay limits the intermediate scale of the visible sector M_I must be above experimental constraints. Additionally it is important for consideration of gauge coupling constant unification in the visible sector which we will return to in Section 3.7. The scale at which the dark sector becomes $SU(3)$ is not so constrained, however if it is significantly lower the confinement scales will distance themselves beyond the desired amount. It may also have consequences for the stability of dark matter depending on

other features of the hidden sector. It is also natural to consider the models mentioned where Higgs multiplets that gain the same VEV in each sector allow for the lower intermediate scale to be the same in the two sectors. Beyond this, the next highest intermediate scale M_J is constrained only from above in that $M_J < M_X < M_{\text{Planck}}$. In the next section we present a proof that for non-SUSY models asymmetric symmetry breaking can be realised in potentials that give minima which describe any of the model types we discussed above.

3.4 Multi-Step asymmetric symmetry breaking

We will now outline how a Higgs sector can accommodate a large variety of symmetry breaking chains in a GUT model of two sectors. As in Chapter 2, asymmetric symmetry breaking can induce nonzero VEVs in Higgs multiplets which have $\mathbb{Z}_2$ partners in the opposing sector that retain a VEV of zero. We consider again the simplest example that has just two pairs of scalar singlet fields that transform under the $\mathbb{Z}_2$ symmetry as

$$\phi_1 \leftrightarrow \phi_2, \qquad \chi_1 \leftrightarrow \chi_2. \tag{3.10}$$

We can then write down the general potential without loss of generality as

$$\begin{aligned} V = {} & \lambda_\phi({\phi_V}^2 + {\phi_D}^2 - v_\phi^2)^2 + \kappa_\phi({\phi_V}^2{\phi_D}^2) \\ & + \lambda_\chi({\chi_V}^2 + {\chi_D}^2 - v_\chi^2)^2 + \kappa_\chi({\chi_V}^2{\chi_D}^2) \\ & + \sigma({\phi_V}^2{\chi_V}^2 + {\phi_D}^2{\chi_D}^2) \\ & + \rho({\phi_V}^2 + {\chi_V}^2 + {\phi_D}^2 + {\chi_D}^2 - v_\phi^2 - v_\chi^2)^2, \end{aligned} \tag{3.11}$$

where cubic terms are initially taken to be absent by additional discrete symmetries. If all of the parameters in Eq. 3.11 are positive then each term in the potential is positive definite and thus minimised if it is equal to zero. The total potential is then minimised by VEVs that break the $\mathbb{Z}_2$ symmetry in such a way that

$$\begin{aligned} \langle\phi_1\rangle = v_\phi, \qquad \langle\chi_1\rangle = 0, \\ \langle\phi_2\rangle = 0, \qquad \langle\chi_2\rangle = v_\chi. \end{aligned} \tag{3.12}$$

This minimum is also degenerate with its $\mathbb{Z}_2$ partner where it is ϕ_2 and χ_1 that gain nonzero VEVs. We can then extend this idea to larger representations of gauge groups by replacing the singlet fields with Higgs multiplets. The set of Higgs multiplets responsible for symmetry breaking in each sector can thus be entirely independent for an arbitrary number of representations we add to the theory. Let us firstly take the case of a set of $2n$ singlet scalar fields, $H_{V1}, H_{D1}, ..., H_{Vn}, H_{Dn}$, where under the $\mathbb{Z}_2$ symmetry,

$$H_V \leftrightarrow H_D. \tag{3.13}$$

We then consider general potentials where again all of the parameters are positive and each individual term is positive definite and cubic terms are taken to be absent by discrete symmetries. For the case of $n = 3$ we have

$$\begin{aligned} V = {} & \lambda_{H_1}(H_{V1}^2 + H_{D1}^2 - v_{H_1}^2)^2 + \lambda_{H_2}(H_{V2}^2 + H_{D2}^2 - v_{H_2}^2)^2 + \lambda_{H_3}(H_{V3}^2 + H_{D3}^2 - v_{H_3}^2)^2 \\ & + \kappa_{H_2}(H_{V2}^2 H_{D2}^2) + \kappa_{H_1}(H_{V1}^2 H_{D1}^2) + \kappa_{H_3}(H_{V3}^2 H_{D3}^2) \\ & + \sigma_1(H_{V1}^2 H_{V2}^2 + H_{D1}^2 H_{D2}^2) + \rho_1(H_{V1}^2 + H_{V2}^2 + H_{D1}^2 + H_{D2}^2 - v_{H_1}^2 - v_{H_2}^2)^2 \\ & + \sigma_3(H_{V1}^2 H_{D3}^2 + H_{D1}^2 H_{V3}^2) + \rho_3(H_{V1}^2 + H_{V3}^2 + H_{D1}^2 + H_{D3}^2 - v_{H_1}^2 - v_{H_3}^2)^2 \\ & + \sigma_2(H_{V3}^2 H_{V2}^2 + H_{D3}^2 H_{D2}^2) + \rho_2(H_{V3}^2 + H_{V2}^2 + H_{D3}^2 + H_{D2}^2 - v_{H_3}^2 - v_{H_2}^2)^2. \end{aligned} \tag{3.14}$$

In this case the minimum is given by

$$\begin{aligned} &\langle H_{V1} \rangle = v_{H_1}, \qquad \langle H_{D1} \rangle = 0, \\ &\langle H_{V2} \rangle = 0, \qquad \langle H_{D2} \rangle = v_{H_2}, \\ &\langle H_{V3} \rangle = v_{H_3}, \qquad \langle H_{D3} \rangle = 0. \end{aligned} \tag{3.15}$$

The above minima could have been the reverse where the V and D subscripts are interchanged of course. This potential demonstrates the general procedure by which we can generate non-supersymmetric asymmetric symmetry breaking multi-step chains. The first two sets of fields form an asymmetric set as in Eq. 3.11 and for any additional field, such as H_3 we can choose for it to align with either the visible or dark sector based on these choices: For coupling between fields that we want to break similarly we set σ to couple fields in opposing sectors and the ρ term to be that which allows for same sector terms. In this case we choose for H_3 to break the same as H_1 so σ_3 couples fields of different sectors. Then for mixing between H_3 and fields that break differently we set σ

to couple the same sector fields, where in Eq. 3.14 we have σ_2 coupling same sector fields since H_2 is aligned with the opposite sector to H_1. Following this simple prescription allows us to add an arbitrary number of multiplets to each sector with the asymmetry determining which sectors will gain the symmetry breaking aspects of that multiplet. We can then consider representations of $SO(10)$ where now each $H_{Vn} \sim (R_n, 1)$ and its $\mathbb{Z}_2$ partner transforms as $H_{Dn} \sim (1, R_n)$. The general potential will contain additional couplings, however it will always contain an analogous set of terms to those above for which we can always generate an asymmetric array of VEVs. These will then drive the symmetry breaking of the two sectors to be completely different.

As we mentioned earlier the simplest variety of $SO(10)$ model is one where the asymmetry in the VEVs of the potential is not limited to distinguishing between zero and nonzero, but rather creates an asymmetry in the size of the VEVs which are all nonzero. Consider a potential of just two pairs as in Eq. 3.11 but with each of $\kappa_\phi, \kappa_\chi < 0$. In this scenario we can create asymmetries of the form

$$\langle \phi_1 \rangle = \langle \chi_2 \rangle \,, \qquad \langle \chi_1 \rangle = \langle \phi_2 \rangle \,. \tag{3.16}$$

We found it possible to generate a ratio of $\langle \phi_1 \rangle \,/\, \langle \chi_1 \rangle \approx 10^3$ for a very constrained region of parameter space. Such a potential can minimally accommodate exactly the number of Higgs multiplets necessary to break two copies of $SO(10)$ to the same final gauge group but with different gauge groups in the intermediate range depending on the choice of Higgs multiplet. While simple in the number of multiplets, this minimal theory suffers from a much smaller allowed parameter space than the previously discussed ASB mechanisms. In particular the size of parameters must be fine-tuned slightly such that we very nearly have $\kappa_\chi \simeq \kappa_\phi$ and $-\kappa_\phi - \kappa_\chi \simeq \sigma$. If we remove the condition of having just two breaking scales and allow each of the four fields to attain different VEVs then a much broader range of the parameter space is compatible.

We can also develop models in which additional pairs of multiplets that transform under the $\mathbb{Z}_2$ symmetry are added as in Eq. 3.14 but break in such a way that they both gain nonzero VEVs and thus both contribute to the symmetry breaking in each sector. This is in fact the simplest method in select cases where the same dimensional representation is useful for the symmetry breaking needed in each sector. This can be always be accomplished by, for example, having these added fields couple only weakly to the previously

added fields.

We illustrate this asymmetric breaking with a particular $SO(10) \times SO(10)$ potential which breaks the mirror symmetric GUT group to $[SU(4) \times SU(2) \times SU(2)]_V \times [SU(5) \times U(1)]_D$. Within the context of the Standard Model, such a theory would need at least one more Higgs multiplet in order to break the Pati-Salam group to $SU(3) \times SU(2) \times U(1)$. Within our variety of models we would require at least one additional mirror symmetric pair of representations to break the symmetry in each sector to one containing $SU(3)$. Since the important results from this chapter are the generation of different symmetries in the intermediate range we focus on constructing a potential that asymmetrically generates the first step of the breaking chain. We consider a set of fields transforming as

$$\begin{aligned} \phi_V &\sim (45, 1), \qquad \chi_V \sim (54, 1), \\ \phi_D &\sim (1, 45), \qquad \chi_D \sim (1, 54). \end{aligned} \tag{3.17}$$

With these we can follow the procedure detailed in the toy model and construct an asymmetric potential. Each of the terms in the toy model has a direct analogue and in addition to these there will be new terms from unique contractions of the Higgs multiplets. The general renormalizable fourth order potential is

$$\begin{aligned} &- \frac{\mu_\phi^2}{2}(\phi_{V\,ij}\phi_{V\,ji} + \phi_{D\,ij}\phi_{D\,ji}) + \frac{\lambda_\phi}{4}((\phi_{V\,ij}\phi_{V\,ji})^2 + (\phi_{D\,ij}\phi_{D\,ji})^2) \\ &+ \frac{\alpha_\phi}{4}(\phi_{V\,ij}\phi_{V\,jk}\phi_{V\,kl}\phi_{V\,li} + \phi_{D\,ij}\phi_{D\,jk}\phi_{D\,kl}\phi_{D\,li}) + \kappa_\phi(\phi_{D\,ij}\phi_{D\,ji}\phi_{V\,kl}\phi_{V\,lk}) \\ &- \frac{\mu_\chi^2}{2}(\chi_{V\,ij}\chi_{V\,ji} + \chi_{D\,ij}\chi_{D\,ji}) + \frac{\lambda_\chi}{4}((\chi_{V\,ij}\chi_{V\,ji})^2 + (\chi_{D\,ij}\chi_{D\,ji})^2) \\ &+ \frac{\alpha_\chi}{4}(\chi_{V\,ij}\chi_{V\,jk}\chi_{V\,kl}\chi_{V\,li} + \chi_{D\,ij}\chi_{D\,jk}\chi_{D\,kl}\chi_{D\,li}) + \kappa_\chi(\chi_{D\,ij}\chi_{D\,ji}\chi_{V\,kl}\chi_{V\,lk}) \\ &+ \frac{\beta\mu_\chi}{3}(\chi_{V\,ij}\chi_{V\,jk}\chi_{V\,ki} + \chi_{D\,ij}\chi_{D\,jk}\chi_{D\,ki}) \\ &+ c_1(\phi_{D\,ij}\phi_{D\,ji}\chi_{V\,kl}\chi_{V\,lk} + \phi_{V\,ij}\phi_{V\,ji}\chi_{D\,kl}\chi_{D\,lk}) \\ &+ c_2(\phi_{D\,ij}\phi_{D\,ji}\chi_{D\,kl}\chi_{D\,lk} + \phi_{V\,ij}\phi_{V\,ji}\chi_{V\,kl}\chi_{V\,lk}) \\ &+ c_3(\phi_{D\,ij}\phi_{D\,jk}\chi_{D\,kl}\chi_{D\,li} + \phi_{V\,ij}\phi_{V\,jk}\chi_{V\,kl}\chi_{V\,li}) \\ &+ c_4(\phi_{D\,ij}\phi_{D\,jk}\chi_{D\,ki} + \phi_{V\,ij}\phi_{V\,jk}\chi_{V\,ki}) \\ &+ c_5(\mathrm{Tr}[(\phi_{V\,ik}\chi_{V\,km} - \chi_{V\,il}\phi_{V\,lm})^2] + \mathrm{Tr}[(\phi_{D\,ik}\chi_{D\,km} - \chi_{D\,il}\phi_{D\,lm})^2]). \end{aligned} \tag{3.18}$$

The addition of the cubic term is necessary for the pattern of symmetry breaking we have chosen. This differs from the toy model cases where an additional $\mathbb{Z}_2$ symmetry protected the potentials from such cubic terms. Relaxing this condition still allows for asymmetric solutions for the VEVs of the two sectors however as discussed in Appendix B. For the sake of simplicity we also set the parameters c_3, c_4, c_5 to be zero as large values will remove the asymmetric VEV structure. The analysis can be simplified by transforming the fields into a simplified VEV form. For the adjoint representation this becomes a block diagonal matrix with each block being a 2×2 antisymmetric matrix. For the **54** we have a traceless diagonal matrix. For the region of parameter space discussed in Appendix B the potential is minimised with VEVs

$$
\begin{aligned}
\langle \phi_V \rangle &= M_i \begin{pmatrix}
0 & a & 0 & 0 & 0 & 0 & 0 & 0 & 0 & 0 \\
-a & 0 & 0 & 0 & 0 & 0 & 0 & 0 & 0 & 0 \\
0 & 0 & 0 & a & 0 & 0 & 0 & 0 & 0 & 0 \\
0 & 0 & -a & 0 & 0 & 0 & 0 & 0 & 0 & 0 \\
0 & 0 & 0 & 0 & 0 & a & 0 & 0 & 0 & 0 \\
0 & 0 & 0 & 0 & -a & 0 & 0 & 0 & 0 & 0 \\
0 & 0 & 0 & 0 & 0 & 0 & 0 & a & 0 & 0 \\
0 & 0 & 0 & 0 & 0 & 0 & -a & 0 & 0 & 0 \\
0 & 0 & 0 & 0 & 0 & 0 & 0 & 0 & 0 & a \\
0 & 0 & 0 & 0 & 0 & 0 & 0 & 0 & -a & 0
\end{pmatrix} \\
\langle \phi_D \rangle &= 0 \\
\langle \chi_V \rangle &= 0 \\
\langle \chi_D \rangle &= M_j \begin{pmatrix}
b & 0 & 0 & 0 & 0 & 0 & 0 & 0 & 0 & 0 \\
0 & b & 0 & 0 & 0 & 0 & 0 & 0 & 0 & 0 \\
0 & 0 & b & 0 & 0 & 0 & 0 & 0 & 0 & 0 \\
0 & 0 & 0 & b & 0 & 0 & 0 & 0 & 0 & 0 \\
0 & 0 & 0 & 0 & b & 0 & 0 & 0 & 0 & 0 \\
0 & 0 & 0 & 0 & 0 & b & 0 & 0 & 0 & 0 \\
0 & 0 & 0 & 0 & 0 & 0 & c & 0 & 0 & 0 \\
0 & 0 & 0 & 0 & 0 & 0 & 0 & c & 0 & 0 \\
0 & 0 & 0 & 0 & 0 & 0 & 0 & 0 & c & 0 \\
0 & 0 & 0 & 0 & 0 & 0 & 0 & 0 & 0 & c
\end{pmatrix}.
\end{aligned}
\tag{3.19}
$$

In the above, $SO(10)_V$ breaks by the VEV of the **54** to $SO(6) \times SO(4) \sim SU(4) \times SU(2) \times SU(2)$ and the **45** serves to break $SO(10)_D$ to $SU(5) \times U(1)$ [136, 137]. Following this symmetry breaking we would then need additional Higgs multiplets to break each of the gauge groups to $SU(3)$ colour theories after which the running couplings will be parallel. Due to the complexity of analysing potentials with increasing numbers of large dimensional Higgs multiplets we leave such detailed models to more specific theories. We have however completed our stated objective of constructing an $SO(10)$ asymmetric potential, built according to the principles of ASB, and showing that by choosing the breaking scales in the two sectors and the breaking chains listed previously, asymmetric potentials can be constructed such that exactly that scenario is the minimum of the potential. In the next section we attempt to generalise such possibilities for supersymmetric models. We specifically look at the general case of real representations which we can examine in an illustrative model.

3.5 Supersymmetric theories

As in Chapter 2 this analysis is predicated on the unification of coupling constants and for this, among other reasons such as the gauge hierarchy problem, we will explore supersymmetric varieties of these models in this section. Supersymmetric ASB requires more fields than the non-SUSY case, specifically gauge singlets. Here we will outline a general scheme to create asymmetric symmetry breaking chains from the superpotential. In general, additional fields are required to allow for the scalar potential to have the necessary terms that drive ASB since only including non-singlet Higgs multiplets does not allow us to couple fields from the different sectors at all in the scalar potential. The method that we outline below is not necessarily the simplest way to generate such breaking for any specific choice of representations or breaking chains; indeed for many simple models as few as one additional singlet is required. The purpose of this discussion is to provide an existence proof that for any symmetry breaking chain we may consider in Section 3.6, a scalar potential can be created which allows for such a vacuum solution.

We wish to consider a supersymmetric extension to the argument of the previous section wherein pairs of Higgs multiplets can be added one at a time to a model in a $\mathbb{Z}_2$ symmetric manner while allowing us to choose which sector its VEVs will favor by appropriate choice of couplings. Take the case of the fields $H_{1V}, H_{1D}, H_{2V}, H_{2D}, H_{3V}, H_{3D}$,

$X_1, X_2, Y_1, Y_2, Z_1, Z_2, \phi, \theta$, where under the $\mathbb{Z}_2$ symmetry

$$X_1 \leftrightarrow X_2, \qquad Y_1 \leftrightarrow Y_2, \qquad Z_1 \leftrightarrow Z_2,$$
$$\phi \leftrightarrow \phi, \qquad \theta \leftrightarrow \theta. \tag{3.20}$$

We then consider the general, renormalizable, gauge invariant superpotential that respects the $\mathbb{Z}_2$ symmetry between the sectors. In this case we are assuming that the Higgs multiplets form real representations though a similar argument likely exists for complex representations as well. We do not write down all of the terms in such a superpotential, only those which directly contribute to the asymmetric symmetry breaking terms as in Eq. 3.14:

$$\begin{aligned} W = {} & \rho_1(H_{2_V}^2\phi + H_{2_D}^2\phi) + \rho_2(H_{2_V}^2 Y_1 + H_{2_D}^2 Y_2) + \rho_3(H_{1_V}^2 Z_2 + H_{1_D}^2 Z_1) \\ & + \rho_4(H_{2_V}^2 Z_2 + H_{2_D}^2 Z_1) + \rho_5(H_{1_V}^2\theta + H_{1_D}^2\theta) + \rho_6(H_{1_V}^2 X_1 + H_{1_D}^2 X_2) \\ & + \rho_7({Z_1}^3 + {Z_2}^3) + \rho_8\theta^3 + \rho_9\phi^3 + \rho_{10}({X_1}^3 + {X_2}^3) + \rho_{11}({Y_1}^3 + {Y_2}^3) \\ & + \rho_{12}(H_{3_V}^2 X_2 + H_{3_D}^2 X_1) + \rho_{13}(H_{3_V}^2 Y_1 + H_{3_D}^2 Y_2) + \rho_{14}(H_{3_V}^2\theta + H_{3_D}^2\theta) \\ & + \rho_{15}(H_{3_V}^2\phi + H_{3_D}^2\phi) + ... \end{aligned} \tag{3.21}$$

The scalar potential then comes from the sum of soft terms and $W^{i*}W_i$ where we ignore the D-terms for this analysis, though in general such terms will add positive definite quartic interactions among those fields which are non-singlets which will not negatively affect the results discussed here. We examine the extreme case of the parameter space where the terms shown dominate and all other parameters in the superpotential are at or very close to zero. In this case the scalar potential minimally contains only those terms that would exist without the purely singlet fields, as in Eq. 3.14 and which are necessary for ASB, in addition to a number of other terms which contain the purely singlet fields. If the sum of the soft mass terms and mass terms from the superpotential F-terms for the singlet fields X, Y, Z, θ, ϕ is positive then these fields can maintain a VEV of zero at the minimum. In this case the dependencies among the remaining fields is entirely that of N pairs of fields under the $\mathbb{Z}_2$ symmetry exactly like that of the previous section where the symmetry breaking of added fields can be chosen by the couplings to the previously added fields and we only have quartic and quadratic terms to deal with. Again we have that the symmetry breaking of an added multiplet such as H_3 can be chosen by its coupling strength to previously added fields, in this case the X and Y

fields. In Eq. 3.21 we have chosen to include the couplings for which, upon taking the derivatives with respect to X_1, Y_1, X_2, Y_2 create the terms that follow the prescription discussed in Chapter 2. If one wished to have the field H_3 break similarly to H_2 instead of H_1 we simply reduce the magnitude of the parameters $\rho_{12,13}$ and replace them with larger couplings for the terms $(H_{3_V}^2 X_1 + H_{3_D}^2 X_2)$ and $(H_{3_V}^2 Y_2 + H_{3_D}^2 Y_1)$ which were previously among the omitted terms. Z_1 and Z_2 set the initial asymmetry between the first two pairs of fields $H_{1V,D}$ and $H_{2V,D}$ while the F-terms from θ and ϕ create the remaining couplings in the ρ terms from Eq. 3.14. The magnitude of the VEVs of the Higgs multiplets will however depend on the size of the soft mass terms that we add and so it may be difficult to construct models with very different mass scales. This may however work to our benefit as large differences in the values of $\Lambda_{\rm QCD}$ can be generated in short ranges if the difference in the beta functions is large. One can take this example as a proof of concept that asymmetric models of any number of Higgs multiplets can be built in SUSY with the addition of singlet fields. Now that we have demonstrated such possible models in both supersymmetric and non supersymmetric cases we will move on to displaying the numerical results for the dark confinement scale for different choices of representations of the Higgs multiplets.

3.6 Dark QCD scale from asymmetric symmetry breaking

We firstly consider the set of models with just one intermediate scale which allows just one energy range over which the beta functions of the two $SU(3)$ groups differ. In this case we are thus only considering models where the group in the dark sector has a larger beta function. We consider both SUSY and non-SUSY models here since for this part of the analysis the only discerning feature is the size of the beta functions which for the SUSY case contains supersymmetric partners to consider as per Eq. 3.2. We take the unification point to be where both sectors become $SO(10)$, the GUT scale M_X in our context. We can however have cases where the dark sector remains as an $SO(10)$ for the range between M_X and the intermediate scale M_I while the visible sector changes group. The analysis is the same with the intermediate gauge group of the dark sector being simply $SO(10)$.

There are three possibilities for the visible sector's QCD parent group. It can remain $SU(3)$ up until M_X while the dark sector changes at M_I or it can become $SU(4)$ or

$SU(5)$ at the M_I and continue to the unification point. For the dark sector group we examined the cases of the chains from Section 3.3. For the case of just two scales M_X and M_I we plot the ratio of confinement scales by using Eq. 3.7. We look at the scale M_I and the difference between the two scales $\delta M = M_X - M_I$. We display in Figure 3.2 and Figure 3.3 the minimal and maximal cases in terms of group choice, that is the largest and smallest difference in beta functions for each of the possible breaking chains in the VS. The colour scale of each graph gives the ratio $\xi = \frac{\Lambda_{\rm DM}}{\Lambda_{\rm QCD}}$. We see in these figures that quite a large range in the distance between the breaking scales is acceptable if the beta functions are not very different in size, for example in the case of $SU(3)$ and $SU(4)$. The magnitude of this difference may be smaller depending on the particle content of a specific theory though the $\mathbb{Z}_2$ symmetry between the sectors prevents these matter terms in Eq. 3.2 from generating large differences. For the limiting case of $SU(3)$ and $SO(10)$, on the other hand, we have a much more constrained parameter space for the choice of breaking scales.

In these cases the results follow from that of the one intermediate scale case, that is, the final difference in the confinement scales is a function of length of the range over which the couplings run at different rates, and the magnitude of the difference between the beta functions. Because of this it is possible to create a dark sector with an acceptable confinement scale for any breaking chain that is needed to satisfy visible sector GUT constraints. For example, if a specific model requires a large range between the $SO(10)$ scale M_X and the $SU(5)$ scale M_I in a theory like that of breaking chain IV, then we can choose the scale that the dark sector breaks to $SU(5)$ to be similar to M_X and run as $SU(5)$ down to a lower scale than M_I. We have seen that there are a large number of possible cases for the breaking chains in each sector where the confinement scale in the dark sector is just larger than that of the visible sector. We have however been treating our GUT scale M_X and intermediate scaleM_I as free parameters and so in the next section we will look to constraining the realistic models and look towards possible future work in this area.

3.7 Phenomenological constraints

The methods detailed here for generating dark sectors with baryons of a mass scale just above that of the proton are generalisable to many breaking chains and GUT models,

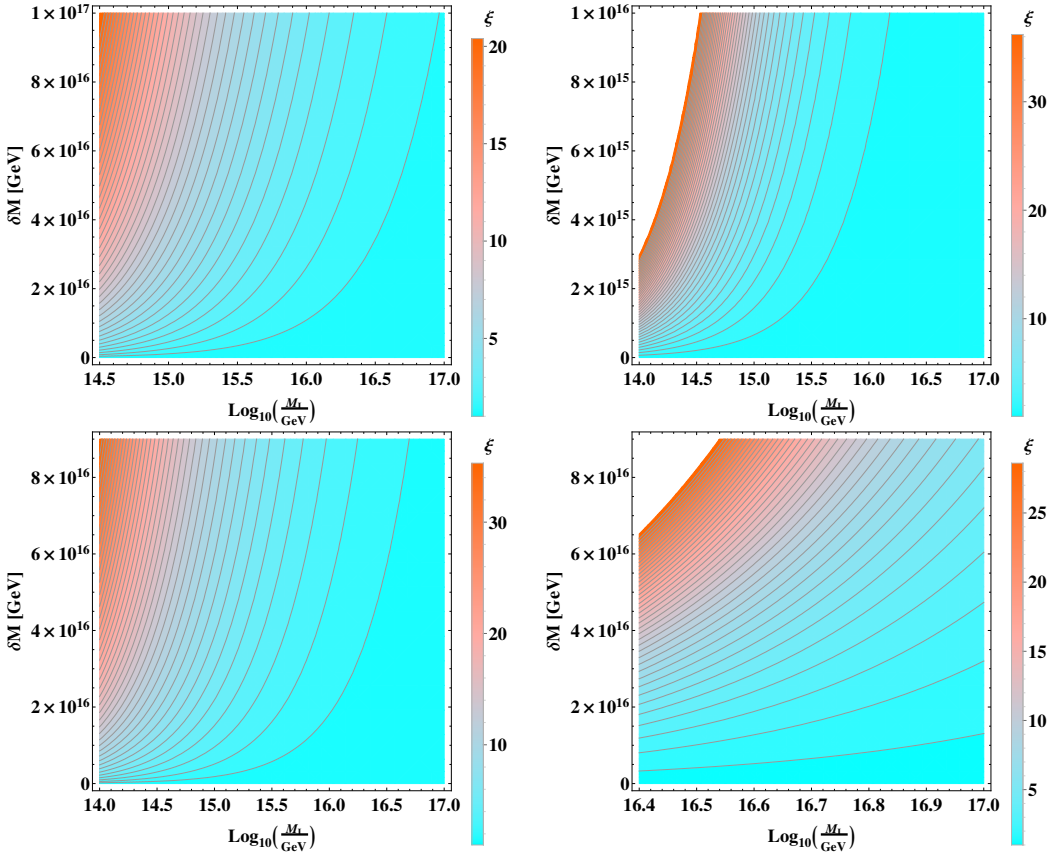

FIGURE 3.2: The ratio of confinement scales $\xi = \Lambda_{\rm DM}/\Lambda_{\rm QCD}$ in the two sectors for a sample of non-supersymmetric breaking chains. The top left figure is generated from $SU(3)_V$ and $SU(4)_D$ as the groups above the scale M_I. The top right features $SU(3)_V$ and $SU(5)_D$ above M_I while the bottom left has $SU(4)_V$ and $SU(5)_D$ followed by the bottom right with $SU(3)_V$ and $SO(10)_D$. In each graph the vertical scale is δM while the horizontal scale is M_I below which both sectors contain $SU(3)$ subgroups.

not all of which will satisfy phenomenological constraints such as current proton decay limits. Here we briefly review some of the recent $SO(10)$ GUT models which can satisfy proton decay constraints in the visible sector. Proton decay bounds typically push the scale of unification in $SU(5)$ theories up to energy regimes consistent with the unification of the gauge coupling constants. In some works such as [124] the $SU(5)$ scale is as low as $M_X \approx 4 \times 10^{15}\,\text{GeV}$ after the addition of extra Higgs multiplets. In particular we examine some of the recent work on proton decay constraints in GUT models from [123], [138] where while minimal $SU(5)$ theories are ruled out, supersymmetric $SU(5)$ theories may still be viable while both supersymmetric and non-supersymmetric $SO(10)$ models can generate cases where proton decay is within experimental limits. We have not gone into any depth on any specific choice of representations in this chapter so it remains an open question how a particular model of ASB can work in the context of

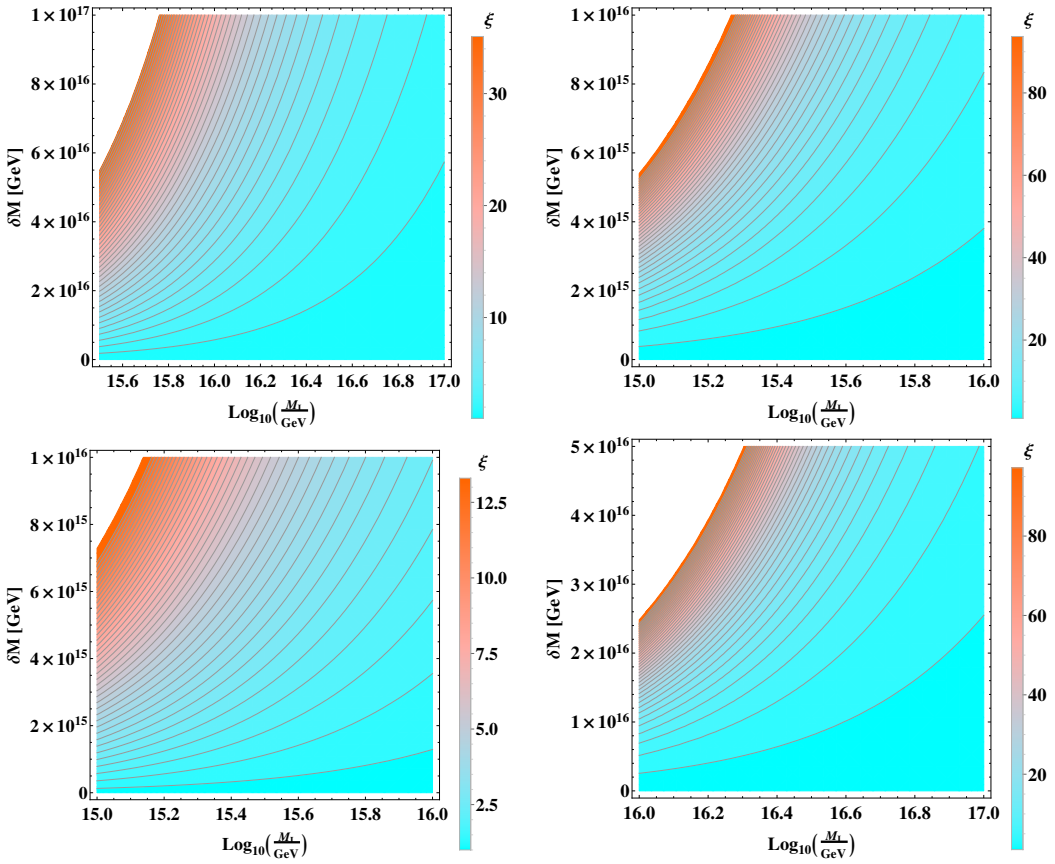

FIGURE 3.3: The ratio of confinement scales $\xi = \Lambda_{\rm DM}/\Lambda_{\rm QCD}$ in the two sectors for a sample of supersymmetric breaking chains. The top left figure is generated from $SU(3)_V$ and $SU(4)_D$ as the groups above the scale M_I. The top right features $SU(3)_V$ and $SU(5)_D$ above M_I while the bottom left has $SU(4)_V$ and $SU(5)_D$ followed by the bottom right with $SU(5)_V$ and $SO(10)_D$.

these phenomenological constraints. The construction of realistic models also requires the unification of the coupling constants which places strict constraints on the scale at which the visible sector's QCD parent group starts. We examine such examples for the MSSM running and a non-SUSY case. Below we examine the development of a dark QCD in an extension of this model where the SM gauge couplings unify at an intermediate scale and the two sectors unify closer to the Planck scale. Figure 3.4 shows the case where we have chain IV in the VS and chain X in the DS. This could be accomplished with **45** and **16** or **126** Higgs multiplets in the VS, together with a **54** or **210'** and **16** or **126** in the DS. Figure 3.5 shows the direct breaking $SO(10) \to SU(3)$ for the colour force in the VS and chain XII in the DS which was discussed in Section 3.2.

In the MSSM, once we have fixed the scale at which the VS $SU(3)$ is absorbed into $SU(5)$, M_X and any intermediate scale of the dark sector can then be treated as free

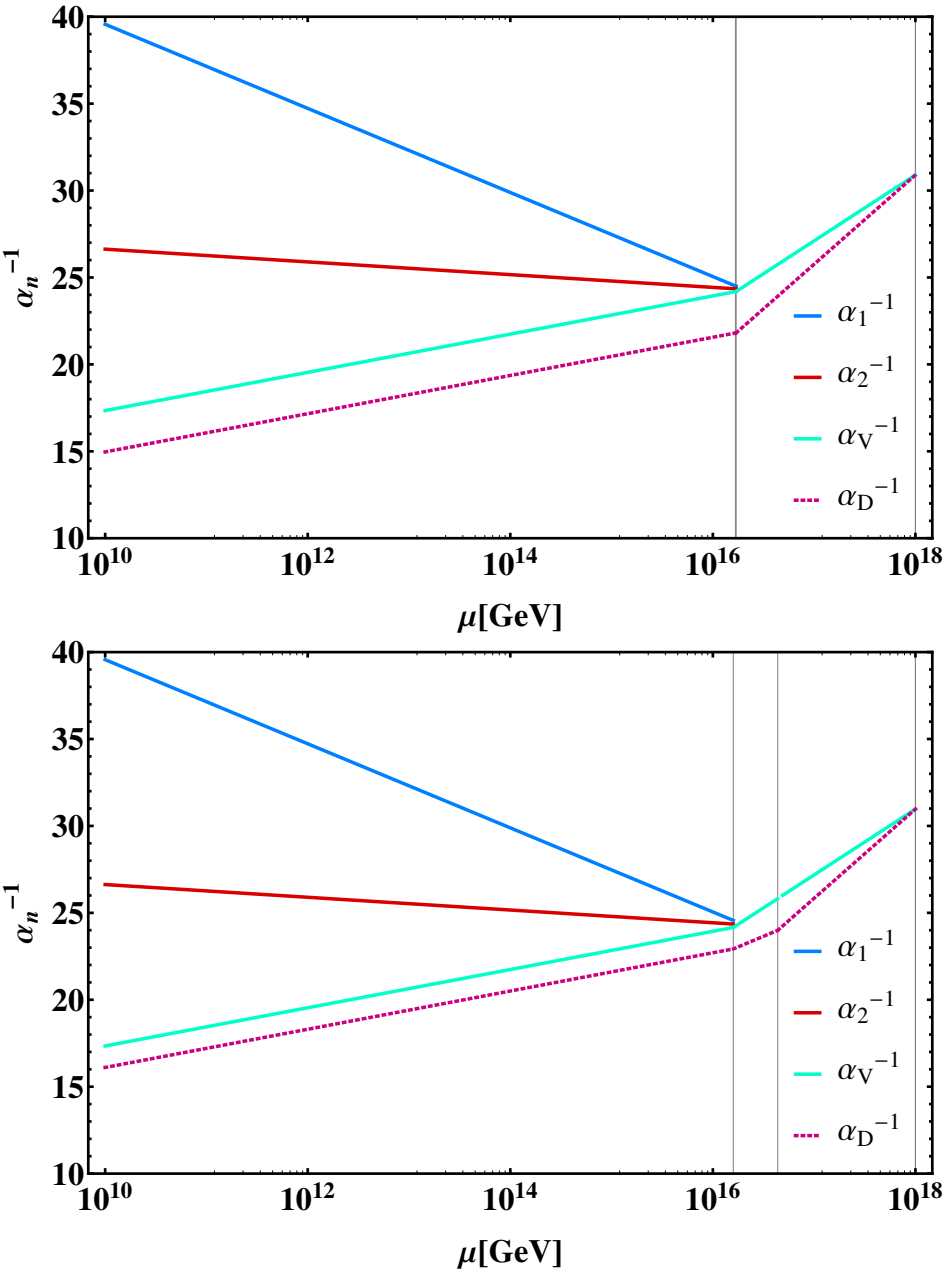

FIGURE 3.4: Supersymmetric model with one and two intermediate scales. In the top plot we have $SU(5)$ in the visible sector and $SO(8)$ in the dark above the scale $M_X \approx 10^{16}$ GeV while the bottom plot shows $SU(5)$ in the visible sector and $SO(8)$ breaking to $SU(4)$ at the scale $M_J \approx 10^{17}$ GeV in the dark sector. Each graph displays the running coupling of the SM forces $(\alpha_1, \alpha_2, \alpha_V)$ from top to bottom and that of the colour force in the dark sector(the lowest line). The value of the dark confinement scale is 4.1 GeV and 1.9 GeV for the top and bottom cases, respectively.

parameters to generate the dark confinement scale. For the non-SUSY case we examine the work of [139] in which a non-SUSY $SO(10)$ model with a colour sextet allows for the unification of the gauge coupling constants. In this case we can also examine a two step process which has one segment working to diverge the couplings after $SO(10)$ breaking,

while the next part of the breaking regime brings the couplings closer again to result in a dark QCD scale just one order of magnitude greater than the SM for breaking scales which span over four orders of magnitude.

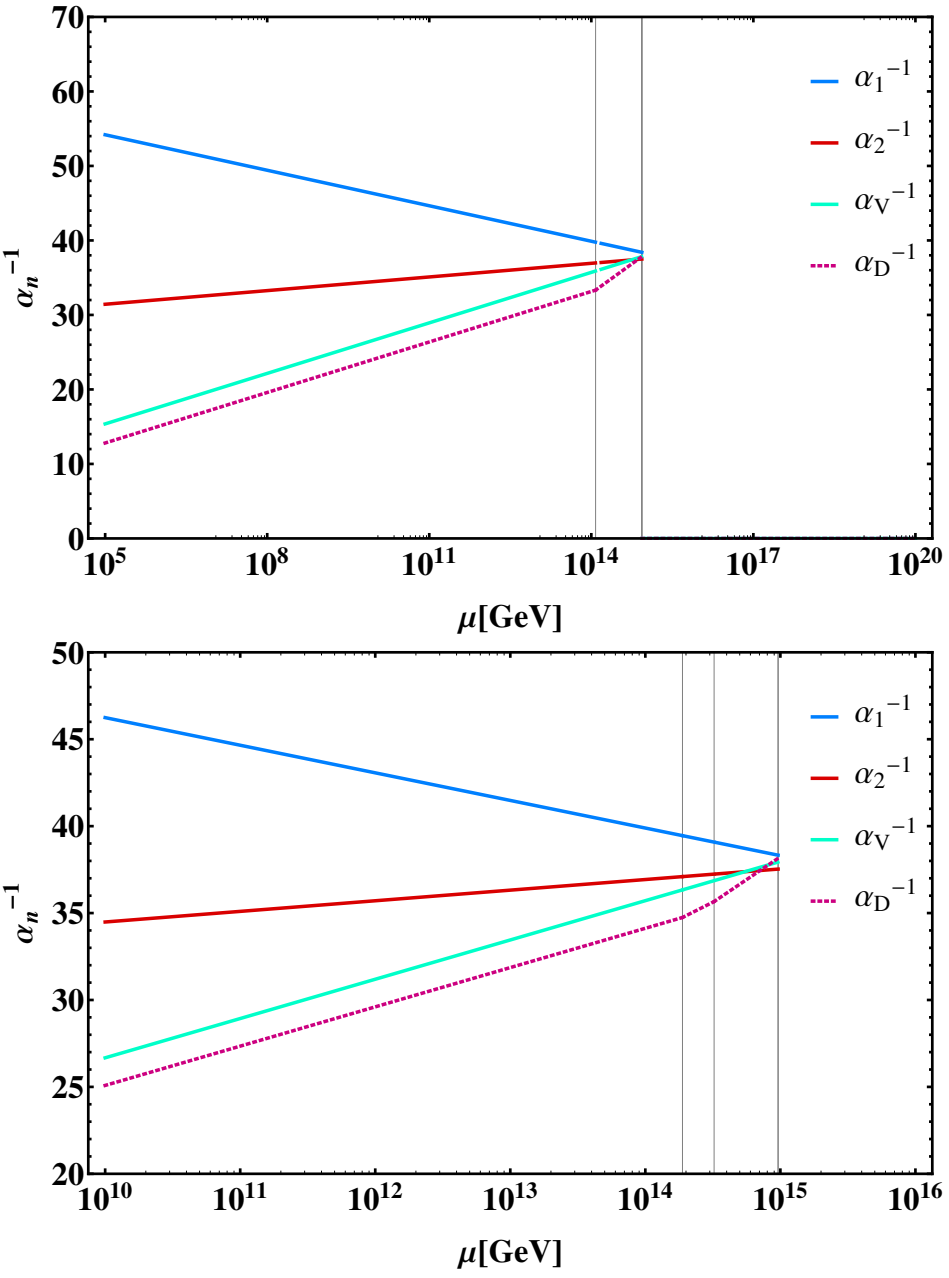

FIGURE 3.5: Non-supersymmetric model with one and two intermediate scales. In the top plot we have $SU(3)$ in the visible sector and $SU(5)$ in the dark sector above the scale $M_X \approx 10^{15}$ GeV while the bottom plot shows $SU(3)$ in the visible sector and $SU(5)$ breaking to $SU(4)$ at a scale $M_J > M_I$ in the dark sector. Each graph displays the running coupling of the SM forces $(\alpha_1, \alpha_2, \alpha_V)$ from top to bottom and that of the colour force in the dark sector(the lowest line). The value of the dark confinement scale is 3.2 GeV and 2.5 GeV respectively.

One could examine a limitless number of such models in this context, extending the

number of breaking scales, however we can see that for almost any choice in the number of such scales and breaking chains in the VS, a model can be constructed which allows a dark confinement scale through the effect of asymmetric symmetry breaking. In this sense it would be interesting to move on to developing a detailed model which resolves a significant number of other issues associated with GUTs in the VS and then adapt it to an ASB model in the pursuit of explaining dark matter also. A full theory of baryogenesis in the two sectors can also place strict limits on the size of these intermediate scales particularly in the case of baryogenesis via leptogenesis or GUT baryogenesis where the symmetry breaking scale can affect the amount of baryon number violation in the early universe. In addition to these constraints we must also consider the current DM constraints on self-interaction where the bullet cluster observation sets results on self-interaction for nucleon-nucleon like scattering in [125]. As we mentioned in the previous chapter, nucleon-like scattering has a cross section of $\sigma \sim 10^{-26}$ cm^2 and can be compared to the upper bound of the DM self-interaction cross section $\leq 10^{-23}$ cm^2 [125–127]. In the cases we have considered we were only concerned with maintaining an $SU(3)$ symmetry in the DS and so in many of these models the DM candidate only interacts with itself through short range strong forces and gravity. Such neutral baryon dark matter particles are thus compatible with current detection limits. We will discuss these dark baryons in more detail in Chapter 5.

3.8 Summary

We have shown in this chapter that independent breaking chains for a mirror symmetric GUT can lead to two distinct sectors that each have a confining gauge theory at low energy. Asymmetric symmetry breaking allows us to build potentials which break the symmetry in exactly this way, and furthermore, allow for multi-step breaking chains where the intermediate gauge groups can be different and the intermediate symmetry breaking scales of the two sectors can differ by orders of magnitude. Ultimately the mass scale of dark matter, coming from the confinement scale of the dark sector, is constrained to be similar to the mass scale of the proton by the insensitivity of the confinement scale to these symmetry breaking scales and the small changes in the beta function that come from the number of vector bosons of different gauge symmetries. We have shown that these potentials are compatible with supersymmetry, as in Chapter 2.

The combined results of Chapter 2 and Chapter 3 demonstrate a large parameter space for mirror symmetric grand unified theories that allow for a composite dark matter candidate which naturally solves the mass coincidence of the asymmetric dark matter paradigm. We can now turn to a comprehensive model of asymmetric dark matter in the next chapter that will use the previous ideas and combine them with a model that can generate a similar number density of matter and dark matter.

Chapter 4

Comprehensive Asymmetric Dark Matter

4.1 Introduction

That our universe appears to consist almost entirely of matter rather than antimatter is a remarkable state of affairs. And yet it is this asymmetry that allows for the rich structure in our observable domain of space, for without this asymmetry, all particles and antiparticles might have annihilated into photons in the early stages of the universe when all degrees of freedom were coupled together in the thermal plasma. We examined in Chapter 1 how thermal leptogenesis is an ideal way to generate the matter-antimatter asymmetry of the universe. In our mirror model paradigm, following the violation of lepton number in each sector, a baryon asymmetry can be generated at low energy through the sphaleron processes all the way down to the electroweak phase transition. If a lepton number asymmetry exists, it can be partially converted to a baryon asymmetry. If the lepton asymmetry generation takes place above the scale at which mirror parity is broken we can then have a model that provides both critical pieces of the dark matter puzzle, the number density and the mass.

We explore in this chapter a model of mirror sectors with two Higgs doublets in each sector where we can utilise the ASB mechanism to see just one of the two Higgs doublets responsible for mass generation in each sector. Critically, these doublets responsible for EWSB in each sector will not however be mirror partners. We then have that the Yukawa

couplings that generate mass for fermions in the two sectors will also be independent of each other while, above the scale of EWSB, the mirror symmetry imposes that any CP violation from the Yukawa Lagrangian will be the same. This results in equal lepton asymmetries being created in the visible and dark sectors and following the EW phase transitions in each sector the result is near-equal baryon asymmetries following the end of rapid sphaleron processes.

In the context of mirror GUT groups we follow the work in the previous chapters, though in this model, mirror symmetry remains following any GUT breaking phase transitions. We thus focus in this chapter on both of the stated aims of generating a similar abundance of visible and dark matter and explaining how the mass of dark matter has a similar mass scale to the proton. For the first task, we use baryogenesis via leptogenesis resulting from the decay of heavy Majorana neutrino states to realise a lepton asymmetry generating mechanism. For the second task we use ASB to explain the similarity of confinement scales.

In these two approaches our work follows from past theories of leptogenesis in a mirror matter context. In particular, the use of a set of three right-handed neutrinos and mirror partners was explored in [140] with temperature difference between the sectors generated after electroweak symmetry breaking. In that work the temperature difference is brought about by the asymmetric reheating of the universe with the Higgs, mirror Higgs and a pure singlet scalar after they settle into the vacuum state. In Ref. [141] a mirror model that relied on explicit breaking in different Yukawa couplings between the sectors was considered. Similar models have considered simply a common set of singlet neutrinos shared between the sectors [125, 142, 143]. In [125], thermal contact between the sectors is maintained indefinitely by the Higgs portal term and kinetic mixing in $U(1)$ gauge bosons and their mirror counterparts. In such equal temperature scenarios, one must remove relativistic degrees of freedom from the mirror sector prior to the scale of BBN to be consistent with the constraints on $\Delta N_{\rm eff}$. Recently [144] suggested that in such models as the above, the two sectors could maintain thermal equilibrium down to a temperature range with a large enough difference in the degrees of freedom of the two sectors, after which the subsequent rate of cooling in each sector would generate a temperature difference sufficient to allow for some relativistic species in the dark sector to remain while being consistent with constraints from BBN. This can be seen by entropy conservation. While the two sectors maintain equilibrium, if one sector undergoes a

sudden drop in the number of degrees of freedom, much of its entropy density will be transferred to the opposite sector.

After breaking mirror symmetry and thermally decoupling the two sectors we examine how this type of model can allow for two distinct sectors that explain both the mass and number density of dark matter. The chapter is structured as follows. In Section 4.2 we outline the field content of the model and Yukawa structure. In Section 4.3 we examine the scalar potential and symmetry breaking of the model. Then in Section 4.5 we examine the neutrino mass matrix and comment on the ordering of massive neutrino states before and after mirror parity is broken. In Section 4.6 we analyse the generation of lepton and baryon asymmetries from the CP violating decays of the heavy right-handed neutrinos. Finally in Section 4.7 we see the evolution of temperature in each of the two sectors and examine the constraints on this model from astrophysical sources and high energy physics. This includes a discussion of the thermal history of all species in both sectors and an examination of possible sources of indirect detection of dark matter in this model. We consider the details of nucleosynthesis in each sector and examine the timeline of early universe cosmology in our combined model of matter and dark matter.

4.2 The model

Previous chapters have explored asymmetric symmetry breaking with mirror symmetric GUT groups such as $SU(5)\times SU(5)$ and $SO(10)\times SO(10)$. In this work we will start with a high energy scale mirror symmetric $[SU(3)\times SU(2)\times U(1)]\times[SU(3)'\times SU(2)'\times U(1)']$ theory that duplicates the content of the Standard Model. A discrete $\mathbb{Z}_2$ symmetry interchanges visible sector (VS) particles with dark sector (DS) counterparts. For fermions, left-handed fields are interchanged with right-handed fields of the dark sector and vice versa,

$$\phi \leftrightarrow \phi', \qquad G^\mu \leftrightarrow G'_\mu, \qquad f_L \leftrightarrow f'_R, \tag{4.1}$$

where ϕ, G^μ and f refer to scalar, gauge and fermion fields. This requires a mirror counterpart for every fermion of the Standard Model. In addition to these we have three right-handed singlet neutrinos, N_R^i, and the corresponding left-handed states of the DS sector, $(N_L^i)'$. We also add a second Higgs doublet, Φ_2, with its own $\mathbb{Z}_2$ partner, Φ_2'. This second Higgs doublet allows us to use the mechanism of asymmetric symmetry breaking

to spontaneously break mirror symmetry and have Φ_2' be the instigator of EWSB in the dark sector while Φ_1 takes on the usual role in our sector. While Φ_1 and Φ_2 carry the same quantum numbers, their self couplings and the size of their couplings to fermions will differ. In this respect our model is significantly different to [125] and [140] where there existed only a VS Higgs and a mirror counterpart. We will examine in Section 4.6 how this second doublet also allows for successful thermal leptogenesis without potential concerns from heavy neutrino mass corrections to the squared Higgs boson mass. The principle motivation for the two Higgs doublets is however our decision to implement the ASB mechanism into a complete model of ADM. By using ASB we can break the mirror parity symmetry and give discernible differences to each of the sectors. The absolute minimum breaks the symmetry of the two sectors in different ways and we switch from a theory of two identical sectors to a model composed of a visible sector, which carries the observable properties of the Standard Model, and a dark sector with a phenomenology of its own that yet retains an origin which guarantees that the mass content of the dark universe will ultimately be highly similar. The total field content of the two sectors is listed in Table 4.1.

TABLE 4.1: Field content and their representations under the mirror symmetric gauge group, $[SU(3) \times SU(2) \times U(1)] \times [SU(3)' \times SU(2)' \times U(1)']$. In addition to a mirror counterpart to all of the SM fields listed in Chapter 1, both sectors contain an additional Higgs doublet to facilitate asymmetric symmetry breaking.

$L_L^i \sim (1, 2, -\frac{1}{2})(1, 1, 0)$	$(L_R^i)' \sim (1, 1, 0)(1, 2, -\frac{1}{2})$
$e_R^i \sim (1, 1, -1)(1, 1, 0)$	$(e_L^i)' \sim (1, 1, 0)(1, 1, -1)$
$Q_L^i \sim (3, 2, \frac{1}{6})(1, 1, 0)$	$(Q_R^i)' \sim (1, 1, 0)(3, 2, \frac{1}{6})$
$u_R^i \sim (3, 1, \frac{2}{3})(1, 1, 0)$	$(u_L^i)' \sim (1, 1, 0)(3, 1, \frac{2}{3})$
$d_R^i \sim (3, 1, -\frac{1}{3})(1, 1, 0)$	$(d_L^i)' \sim (1, 1, 0)(3, 1, -\frac{1}{3})$
$N_R^i \sim (1, 1, 0)(1, 1, 0)$	$(N_L^i)' \sim (1, 1, 0)(1, 1, 0)$
$\Phi_1 \sim (1, 2, \frac{1}{2})(1, 1, 0)$	$(\Phi_1)' \sim (1, 1, 0)(1, 2, \frac{1}{2})$
$\Phi_2 \sim (1, 2, \frac{1}{2})(1, 1, 0)$	$(\Phi_2)' \sim (1, 1, 0)(1, 2, \frac{1}{2})$.

4.2.1 Yukawa couplings

The use of additional Higgs doublets in extensions to the SM has a history ranging from minimal extensions of a single extra Higgs doublet to larger extensions in which the observed Higgs state discovered at the LHC is the lightest state of a largely decoupled Higgs sector [145]. Models such as supersymmetry require at least two Higgs doublets to generate mass for the fermions. In this work we will explore the implications of

having two Higgs doublets in the VS and associated mirror partners in the DS. Models of just two Higgs doublets are typically separated into three generic types based on the discrete symmetries they impose. Type-I has just one of the doublets coupling to all fermions while Type-II models have one couple to the up-type quarks and the other the down-type. Type-III, which is the model that matches our own within the context of the visible sector, gives both doublets the same quantum numbers and therefore allows each of them to couple to all flavours of quarks and leptons. In Type-III models the fields can be expressed in a basis where only one doublet gains a nonzero VEV while the second doublet retains a vanishing VEV. This is known as the Higgs basis [145]. This variety of model with a second Higgs doublet introduces highly constrained flavour changing neutral currents (FCNC) at tree level due to the fact that couplings between the fermions and multiple Higgs doublets cannot in general be simultaneously diagonalised.

Our work can be compared to other models of additional Higgs fields in addressing the nature of dark matter such as Inert Higgs doublet models [146, 147]. In this work however we gain a dark matter candidate from the stable baryons of a dark sector with the additional Higgs fields facilitating the mirror parity breaking of the two sectors and the associated asymmetric gauge symmetry breaking. The second doublet is also a second source of CP violating decays for heavy neutrino states in each sector at the scale of thermal leptogenesis. The leptonic Yukawa couplings are

$$\begin{aligned} L_{\text{Lepton}} = {} & \eta^L_{1\,ij}\,\overline{L^i_L} e^j_R \Phi_1 + \eta^L_{1ij}\,\overline{L^i_R}' e^{j\,\prime}_L \Phi'_1 + y_{1ij}\,\overline{L^i_L} N^j_R \tilde{\Phi}_1 + y_{1ij}\,\overline{L^i_R}' N^{j\,\prime}_L \tilde{\Phi}'_1 \\ & + \eta^L_{2\,ij}\,\overline{L^i_L} e^j_R \Phi_2 + \eta^L_{2\,ij}\,\overline{L^i_R}' e^{j\,\prime}_L \Phi'_2 + y_{2ij}\,\overline{L^i_L} N^j_R \tilde{\Phi}_2 + y_{2ij}\,\overline{L^i_R}' N^{j\,\prime}_L \tilde{\Phi}'_2 \\ & + f_{1ij}\,\overline{L^i_L} N^{j\,c\prime}_L \tilde{\Phi}_1 + f_{1ij}\,\overline{L^i_R}' N^{j\,c}_R \tilde{\Phi}'_1 + f_{2ij}\,\overline{L^i_L} N^{j\,c\prime}_L \tilde{\Phi}_2 + f_{2ij}\,\overline{L^i_R}' N^{j\,c}_R \tilde{\Phi}'_2 + \text{h.c.} \end{aligned} \tag{4.2}$$

Mirror parity enforces that the coupling of the doublets is the same as their mirror counterparts however terms such as y_1, and y_2 will not be the same and may differ by orders of magnitude. In addition to these we have the ordinary Majorana mass terms along with a cross-sector mass term,

$$M_{ij}\left(\overline{(N^i_R)^c} N^j_R + \overline{(N^i_L)^c}' N^{j\,\prime}_L\right) + P_{ij}\overline{N^i_R} N^{j\,\prime}_L + \text{h.c.} \tag{4.3}$$

For the quark Yukawas we have,

$$L_{\text{Quark}} = \eta^u_{1\,ij}\,\overline{Q^i_L}u^j_R\Phi_1 + \eta^u_{1\,ij}\,\overline{Q^i_R}'u^j_L{}'\Phi'_1 + \eta^d_{1ij}\,\overline{Q^i_L}d^j_R\tilde{\Phi}_1 + \eta^d_{1\,ij}\,\overline{Q^i_R}'d^j_L{}'\tilde{\Phi}'_1 + \eta^u_{2\,ij}\,\overline{Q^i_L}u^j_R\Phi_2 + \eta^u_{2\,ij}\,\overline{Q^i_R}'u^j_L{}'\Phi'_2 + \eta^d_{2ij}\,\overline{Q^i_L}d^j_R\tilde{\Phi}_2 + \eta^d_{2\,ij}\,\overline{Q^i_R}'d^j_L{}'\tilde{\Phi}'_2 + \text{h.c.} \quad (4.4)$$

We also consider the various other ways that the two sectors can interact. The photon-mirror photon kinetic mixing term,

$$\epsilon_{\gamma\gamma'}F^{\mu\nu}F_{\mu\nu}{}', \quad (4.5)$$

allows for visible sector states to have dark $U(1)$ millicharges. This parameter is constrained by orthopositronium decay experiments [148] to the degree of $\epsilon_{\gamma\gamma'} \leq 1.55\times10^{-7}$. Such terms are naturally absent in GUT contexts where they could only be generated by scalars that provide a mediating interaction between the sectors that persists in the mirror GUT regime. We also consider Higgs portal interactions. These will be explored further in the next section and later in the discussion of the thermal history. Neutrino interactions that mix the two sectors will also be present, which we will further discuss in Section 4.5. As we elaborate on in Section 4.7, the two sectors can only maintain any rapid interactions until a temperature T_{DEC}. This limits the size of any portal terms in our model and these individual limits will depend on the interaction rate's scaling with temperature. This means that no interaction between the sectors can maintain thermal equilibrium indefinitely. This further constrains the kinetic mixing term $\epsilon_{\gamma\gamma'}$ due to the scaling of photon-mirror photon interactions with temperature.

While many models of dark sectors consider the possibility of the dark sector at a lower temperature from the outset, for example in [149], this work has the benefit that the separate Higgs doublets which facilitate EWSB in each sector can spontaneously break mirror symmetry which later causes a separation in the temperature of the visible and dark sectors. This and the other differences between the two sectors is accomplished without the need for any soft symmetry breaking mass terms.[1]

[1]The domain wall problem caused by the existence of our $\mathbb{Z}_2$ symmetry may ultimately require a solution such as soft breaking terms. A soft breaking that gives some separation in the squared mass terms of Φ_i and Φ'_i could be considered. Another possibility is a small difference between the Majorana masses of N_R and N'_L as in [140]. Other solutions include non-restoration of one or both EW symmetries [150], embedding the $\mathbb{Z}_2$ symmetry within a continuous symmetry, or the possibility of breaking mirror symmetry prior to inflation in order to make the typical domain wall separation larger than the horizon distance[151].

4.3 Higgs potentials

The scalar potential of our model consists of our four Higgs doublets $\Phi_1, \Phi_1', \Phi_2, \Phi_2'$. In the simplest model of asymmetric symmetry breaking, only one Higgs multiplet gains a nonzero vacuum expectation value for each copy of the $SU(2) \times U(1)$ gauge group. Such a potential can be constructed using the minimal asymmetric potential,

$$\begin{aligned} V_{\text{ASB}} = \lambda_1 \left(\Phi_1^\dagger \Phi_1 + \Phi'^\dagger_1 \Phi'_1 - \frac{v^2}{2} \right)^2 + \lambda_2 \left(\Phi_2^\dagger \Phi_2 + \Phi_2'^\dagger \Phi_2' - \frac{w^2}{2} \right)^2 + \kappa_1 (\Phi_1^\dagger \Phi_1)(\Phi_1'^\dagger \Phi_1') \\ + \kappa_2 (\Phi_2^\dagger \Phi_2)(\Phi_2'^\dagger \Phi_2') + \sigma_1 \left((\Phi_1^\dagger \Phi_1)(\Phi_2^\dagger \Phi_2) + (\Phi_1'^\dagger \Phi_1')(\Phi_2'^\dagger \Phi_2') \right) \\ + \sigma_2 \left(\Phi_1^\dagger \Phi_1 + \Phi_2^\dagger \Phi_2 + \Phi_1'^\dagger \Phi'_1 + \Phi_2'^\dagger \Phi_2' - \frac{v^2}{2} - \frac{w^2}{2} \right)^2 . \end{aligned} \tag{4.6}$$

In this simplest potential, the condition of asymmetric breaking is given by requiring that each of the parameters, $[\lambda_1, \lambda_2, \kappa_1, \kappa_2, \sigma_1, \sigma_2]$, are real and positive definite. In this case the potential is minimised when each of the terms in the potential is zero which is given by the vacuum state,

$$\begin{aligned} \langle \Phi_1 \rangle = \begin{bmatrix} 0 \\ \frac{v}{\sqrt{2}} \end{bmatrix}, \qquad \langle \Phi_1' \rangle = 0, \\ \langle \Phi_2 \rangle = 0, \qquad \langle \Phi_2' \rangle = \begin{bmatrix} 0 \\ \frac{w}{\sqrt{2}} \end{bmatrix}. \end{aligned} \tag{4.7}$$

In the unitary gauge we can then introduce the definitions,

$$\begin{aligned} \Phi_1 = \begin{bmatrix} 0 \\ \frac{1}{\sqrt{2}}(v+h) \end{bmatrix}, \qquad \Phi_1' = \begin{bmatrix} H_D^+ \\ \frac{1}{\sqrt{2}}(H_D + iA_D) \end{bmatrix}, \\ \Phi_2 = \begin{bmatrix} H^+ \\ \frac{1}{\sqrt{2}}(H + iA) \end{bmatrix}, \qquad \Phi_2' = \begin{bmatrix} 0 \\ \frac{1}{\sqrt{2}}(w + h_D) \end{bmatrix}, \end{aligned} \tag{4.8}$$

and obtain a 2×2 mass matrix

$$\frac{1}{2} \begin{pmatrix} h \ , \ h_D \end{pmatrix} \begin{bmatrix} 2(\lambda_1 + \sigma_2)v^2 & \sigma_2 v w \\ \sigma_2 v w & 2(\lambda_2 + \sigma_2)w^2 \end{bmatrix} \begin{pmatrix} h \\ h_D \end{pmatrix}. \tag{4.9}$$

We can see that the eigenstate fields are admixtures of visible and dark states. For the remaining eigenvalues we have,

$$m_H = m_A = m_{H^\pm} = \sqrt{\frac{1}{2}\kappa_2 w^2 + \frac{1}{2}\sigma_1 v^2}, \tag{4.10}$$

$$m_{H_D} = m_{A_D} = m_{H_D^\pm} = \sqrt{\frac{1}{2}\kappa_1 v^2 + \frac{1}{2}\sigma_1 w^2}. \tag{4.11}$$

We can see in Eq. 4.9 that we recover a Standard Model physical Higgs mass formula in the limit that $\sigma_2 \to 0$ as the matrix becomes diagonal and the Standard Model Higgs boson loses the extra term. This is the same limit that switches off the only off-diagonal mass term that couples the two sectors, $\sim vw\sigma_2 h\, h_D$). If the EW scales of the two sectors are different, it is necessary to take the limit that σ_2 does not mix the two energy scales. In this limit, the asymmetric VEV is still the minimum and we can see that the massive states besides h all have mass terms that are proportional to w. This is significant in that the scale w, in the asymmetric configuration, can raise the masses of all the scalars of both sectors except for the SM Higgs boson in the case that $w > v$. We now consider this feature in the context of a full mirror symmetric potential with two Higgs doublets in each sector. In contrast with previous chapters, which dealt exclusively with potentials that made use of the fact that the multiplets in each sector were in two different sized representations of the gauge group, in this work we are considering identical representations. The most general potential in this case,

$$\begin{aligned}
V_{\text{M2HDM}} = &+m_{11}^2\,(\Phi_1^\dagger\Phi_1 + \Phi_1^{'\dagger}\Phi_1') + m_{22}^2\,(\Phi_2^\dagger\Phi_2 + \Phi_2^{'\dagger}\Phi_2') \\
&+ \left(m_{12}^2\,(\Phi_1^\dagger\Phi_2 + \Phi_1^{'\dagger}\Phi_2') + h.c.\right) + \frac{1}{2}z_1\,\left((\Phi_1^\dagger\Phi_1)^2 + (\Phi_1^{'\dagger}\Phi_1')^2\right) \\
&+ \frac{1}{2}z_2\,\left((\Phi_2^\dagger\Phi_2)^2 + (\Phi_2^{'\dagger}\Phi_2')^2\right) + z_3(\Phi_1^\dagger\Phi_1\Phi_2^\dagger\Phi_2 + \Phi_1^{'\dagger}\Phi_1'\Phi_2^{'\dagger}\Phi_2') \\
&+ z_4\,(\Phi_1^\dagger\Phi_2\Phi_2^\dagger\Phi_1 + \Phi_1^{'\dagger}\Phi_2'\Phi_2^{'\dagger}\Phi_1') + \frac{1}{2}z_5\,\left((\Phi_1^\dagger\Phi_2)^2 + (\Phi_1^{'\dagger}\Phi_2')^2 + h.c.\right) \\
&+ \left[(z_6\,\Phi_1^{'\dagger}\Phi_1' + z_7\,\Phi_2^{'\dagger}\Phi_2')\Phi_1^{'\dagger}\Phi_2' + (z_6\,\Phi_1^\dagger\Phi_1 + z_7\,\Phi_2^\dagger\Phi_2)\Phi_1^\dagger\Phi_2 + h.c.\right] \\
&+ z_8\Phi_1^\dagger\Phi_1\Phi_1^{'\dagger}\Phi_1' + z_9\,\Phi_2^\dagger\Phi_2\Phi_2^{'\dagger}\Phi_2' + (z_{10}\,\Phi_1^\dagger\Phi_2\Phi_1^{'\dagger}\Phi_2' + h.c.) \\
&+ (z_{11}\,\Phi_1^\dagger\Phi_2\Phi_2^{'\dagger}\Phi_1' + h.c.) + z_{12}(\Phi_1^\dagger\Phi_1\Phi_2^{'\dagger}\Phi_2' + \Phi_1^{'\dagger}\Phi_1'\Phi_2^\dagger\Phi_2) \\
&+ \left[(z_{13}\,\Phi_1^{'\dagger}\Phi_1' + z_{14}\,\Phi_2^{'\dagger}\Phi_2')\Phi_1^\dagger\Phi_2 + (z_{13}\,\Phi_1^\dagger\Phi_1 + z_{14}\,\Phi_2^\dagger\Phi_2)\Phi_1^{'\dagger}\Phi_2' + h.c.\right],
\end{aligned} \tag{4.12}$$

features a large number of new terms which we must consider carefully. While such a potential increases the possible minima configurations, we can always perform individual

basis rotations of the doublets in each sector to return the doublets to a 'Higgs Basis' where only one doublet has a nonzero VEV. What we then require in the context of asymmetric symmetry breaking is that the mixing in the two sectors are asymmetric. In other words, applying the Higgs basis transformation to each pair of doublets simultaneously will only put one sector in the Higgs basis. In this context we will consider the above general mirror 2HDM where the global minimum is given by

$$\langle \Phi_i \rangle = \begin{bmatrix} 0 \\ \frac{v_i}{\sqrt{2}} \end{bmatrix}, \qquad \langle \Phi_i' \rangle = \begin{bmatrix} 0 \\ \frac{w_i}{\sqrt{2}} \end{bmatrix}. \tag{4.13}$$

We then define

$$v = \sqrt{|v_1|^2 + |v_2|^2}, \;\; w = \sqrt{|w_1|^2 + |w_2|^2}, \;\; \rho = \frac{w}{v}. \tag{4.14}$$

We can then form what we term the dual Higgs basis starting with ,

$$H_1 = \frac{v_1^* \Phi_1 + v_2^* \Phi_2}{v}, \qquad H_2 = \frac{-v_2 \Phi_1 + v_1 \Phi_2}{v}, \tag{4.15}$$

and then consider new fields in the dark sector H_i' formed from VEVs w_1, w_2,

$$H_1' = \frac{w_1^* \Phi_1' + w_2^* \Phi_2'}{w}, \qquad H_2' = \frac{-w_2 \Phi_1' + w_1 \Phi_2'}{w}. \tag{4.16}$$

The fields H_1 and H_1' have nonzero VEVs given by v and w, respectively, while the orthogonal combinations have vanishing VEVs. The two field rotations result in a potential that is not obviously mirror symmetric prior to symmetry breaking. The obvious mirror symmetry would however re-appear if we expand back to the original Φ basis. After symmetry breaking we will have in this new basis fields H_1 and H_1' which break the mirror symmetry in each sector. They are not mirror partners and have different VEVs, masses and Yukawa couplings to fermions. What we then require is a vacuum configuration which was previously discussed in Chapter 3 where the asymmetry is given by the conditions

$$v_1 \gg v_2, \quad w_2 \gg w_1, \tag{4.17}$$

which breaks mirror symmetry. In general we will also be considering the case that $w_2 \gg v_1$ such that the VEVs in the dual Higgs basis obey $w \gg v$ and $\rho \gg 1$. The mirror symmetry is broken in such a way that not only is the EW scale of the dark

sector at a higher energy scale, but the fermion Yukawa couplings relevant to mass generation are independent. This is due to the fact that H_1 is mostly Φ_1 while H_1' is mostly Φ_2'. We can consider this as asymmetric symmetry breaking promoting the ratio of the two quantities $\tan(\beta) = v_2/v_1$ and $\tan(\beta') = w_2/w_1$ to a relevant quantity. The Yukawa terms relevant to quark masses, and those relevant to FCNC, in the Higgs basis are given by diagonal and non-diagonal matrices,

$$\begin{aligned} \tilde{\eta}_1^Q &= c_\beta V_L^Q \eta_1^Q V_R^{Q\dagger} + s_\beta V_L^Q \eta_2^Q V_R^{Q\dagger} \\ \tilde{\eta}_2^Q &= -s_\beta V_L^Q \eta_1^Q V_R^{Q\dagger} + c_\beta V_L^Q \eta_2^Q V_R^{Q\dagger}, \end{aligned} \tag{4.18}$$

where $Q = u, d$ and $V_{L,R}^Q$ are the left- and right-handed diagonalisation matrices. For couplings in the dark sector we have the different set of a diagonal and non-diagonal matrix,

$$\begin{aligned} \tilde{\eta}_1^{Q'} &= c_{\beta'} W_L^Q \eta_1^Q W_R^{Q\dagger} + s_{\beta'} W_L^Q \eta_2^Q W_R^{Q\dagger} \\ \tilde{\eta}_2^{Q'} &= -s_{\beta'} W_L^Q \eta_1^Q W_R^{Q\dagger} + c_{\beta'} W_L^Q \eta_2^Q W_R^{Q\dagger}, \end{aligned} \tag{4.19}$$

with $Q' = u', d'$ referring to quark flavours of the dark sector, and with W denoting the unique diagonalisation matrices. We can then see that in the limit of asymmetric VEVs in Eq. 4.17 that we have four different η terms for each of the up and down type couplings. In particular the mass eigenvalues of the two sectors are almost entirely independent. The leptonic sector follows the same procedure. The presence of the non-diagonal matrix for H_2 in the visible sector is the origin of FCNC, as in the visible sector, the model resembles that of the Type-III 2HDM. This is a necessary part of our model as we use the mirror partner of the second doublet to play a similar role to the SM Higgs doublet in the dark sector. The current constraints on such Type-III 2HDM impose significant restrictions on the masses of the additional scalars of the visible sector and the η_2 Yukawa matrix. The decoupling of the additional scalars in the VS from their coupling to the scale w seen in the minimal asymmetric model will occur in the full potential as well and this will be critical in suppressing the size of these FCNC. We can see already that it is the parameters z_8 and z_9 that play the role of κ_1, κ_2 from the minimal model. These terms will decouple the second doublet in the VS while the parameter z_{12} must be small in this basis to prevent the Standard Model Higgs from coupling to the higher mass scale just as the parameter σ_2 was kept small. It is

important to note that these terms are cross-sector couplings. Because of this the limit that these couplings approach zero may be technically natural due to the enhancement of symmetry originating in the two sectors gaining independent Poincaré groups as in Ref. [152]. Some of these cross-sector terms are however necessarily nonzero if we wish that the asymmetric VEV pattern should be the guaranteed global minimum and so the naturalness of such models is a delicate issue. In this potential this term is already necessarily small to ensure the asymmetric configuration. We can now examine how the mass scales of such a potential form. We label the fields within the doublets in the original basis as

$$\Phi_1 = \begin{bmatrix} G_1^+ \\ \frac{1}{\sqrt{2}}(v_1 + \phi_1 + iG_1) \end{bmatrix}, \qquad \Phi_2 = \begin{bmatrix} I_2^+ \\ \frac{1}{\sqrt{2}}(v_2 + \phi_2 + ia_2) \end{bmatrix} \tag{4.20}$$

and

$$\Phi_1' = \begin{bmatrix} I_1^+ \\ \frac{1}{\sqrt{2}}(w_1 + \phi_1' + ia_1) \end{bmatrix}, \qquad \Phi_2' = \begin{bmatrix} G_2^+ \\ \frac{1}{\sqrt{2}}(w_2 + \phi_2' + iG_2) \end{bmatrix}. \tag{4.21}$$

The label G denotes the states that dominate the admixtures defining the Goldstone bosons. We then consider the 6×6 symmetric neutral mass matrix in Appendix C and six neutral mass eigenstates. In the limit of no mixing between the sectors, in a 2HDM one typically labels these as h^0, H^0, A^0 and $H^\pm$ in the visible sector as in the minimal asymmetric model. In the mirror sector one would then have A_D^0, H_D^0, h_D^0 and $H_D^\pm$. In our model however these are not mirror partners. Some of these mirror partners have in fact been been absorbed via the Higgs Mechanism into the massive gauge boson states. Since we make use in the VS of the decoupling limit of the second Higgs doublet, we have that all other physical scalars would acquire masses much larger than the SM Higgs state, $m_{H^\pm}, m_{A^0}, m_{H^0} \gg m_{h^0}$. In this case the physics at low energy approaches that of just the SM Higgs state. Our approach to the decoupling limit is different from both this minimal asymmetric case and the typical Type-III model in a number of key ways. First, while a typical method in Type-III would be to flip the sign of the m_{22}^2 mass squared parameter in order to give positive masses to all other scalars, in our model we are constrained to keep the sign the same as m_{11}^2 by the principles of asymmetric symmetry breaking and our mirror symmetry. Second, the additional cross-sector terms in the full potential in Eq. 4.12 will generate mixing between scalars of the two sectors and in

general mass eigenstates may be composed of visible and dark interaction eigenstates. In this work decoupling follows from the minimal model in that w_2 lifts the mass eigenstates of all scalars except for one of the mass eigenstates which we identify with the physical Higgs. This decoupling limit also generates the alignment limit in that this lowest mass eigenstate has couplings which align with SM values.

We will label the six neutral mass eigenstates as $h_1^0, h_2^0, A_1^0, A_2^0, J_1^0, J_2^0$. We note that the first two have minimal cross-sector mixing. It is important here that the field corresponding to the Standard Model Higgs boson not mix heavily with mirror states, however we find it possible to have minimal visible-dark mixing in the low mass Higgs state with SM couplings while the heavy additional scalars do mix. This comes from terms such as

$$z_{10}\,\Phi_1^\dagger \Phi_2 \Phi_1^{\prime\dagger} \Phi_2^\prime \tag{4.22}$$

which in the limit of Eq. 4.17 only contains large mass terms of the form

$$\frac{v_1 w_2}{2}\left(\mathrm{Im}[z_{10}](-a_1\phi_2 + a_2\phi_1^\prime) + \mathrm{Re}[z_{10}](a_1 a_2 + \phi_2\phi_1^\prime)\right). \tag{4.23}$$

Making this term large also does not interfere with the asymmetric minimum. In Table 4.2 we list a set of parameters and the EW scales and masses they give for the mass eigenstates of the theory. Since in this region of parameter space the asymmetric VEV configuration is the global minimum, we have positive masses at the new minima and indeed we find for a region of the parameter space in Table 4.2 that the couplings of Φ_2 to the mirror sector EW scale w can make these positive mass terms sufficiently large while keeping the SM Higgs boson light at tree level and separating the EW scales of the two sectors, v and w. An estimate of the necessary mass scale for avoiding FCNC

TABLE 4.2: Higgs Potential parameter sample and associated masses of physical scalars in each sector. Masses are in units of GeV.

$m_{11}^2 = -87^2$	$m_{22}^2 = -2600^2$	$m_{12}^2 = -90^2$	$z_1 = 0.13$	$z_2 = 0.13$
$z_3 = 0.8$	$z_4 = .01$	$z_5 = .01$	$z_6 = .01$	$z_7 = .01$
$z_8 = .8$	$z_9 = 0.8$	$z_{10} = 0.8$	$z_{11} = .01$	$z_{12} = 10^{-8}$
$z_{13} = .01$	$z_{14} = .01$	$m_h = 125$	$m_{h_D} = 3696$	$m_{A_1} = 5965$
$m_{A_2} = 6912$	$m_{J_1} = 5965$	$m_{J_2} = 6512$	$m_{H^+} = 5965$	$m_{H^{+\prime}} = 6512$
$v = 246$	$w = 7276$	$\tan(\beta) = 4 \times 10^{-5}$	$\tan(\beta^\prime) = 18190$	$\rho = 30$

is given by [145] where $K - \overline{K}$ oscillations are avoided if $m_{H_2^0} > 150\,\mathrm{TeV}$. This assumes however that all Yukawas are similar to that of the top quark. In our case the coupling

of the second Higgs doublet, H_2, may have Yukawa couplings that are much smaller than the SM Higgs coupling to the top. The size of these Yukawas are constrained by a number of sources in the model. Among them are the Higgs portal term that maintains thermal equilibrium and the relevant scattering terms in the era of leptogenesis. In particular as we will see in Fig. 4.1 the necessary confinement scale of the dark sector may require that the most massive dark quark has a mass such that it's Yukawa coupling may be comparable to the SM up and down quarks, which are at least 10^4 smaller than the top coupling. This constraint then directly limits the size of the couplings to H_1' and therefore to H_2 in the asymmetric limit such that FCNC bounds are satisfied.

We consider the mixing of neutral states by examining the rotation matrix U in, $U^T M^2 U = D^2$. This transforms the $(\phi_1', a_1, \phi_2', \phi_2, a_2, \phi_1)$ basis into the $(J_2, A_2, J_1, A_1, h_2, h_1)$ mass-basis. For the numerical sample in Table 4.2 we have,

$$U_{II} = \begin{pmatrix} -0.999996 & 0 & -0.00265105 & 0 & 0.000447771 & 0 \\ 0 & -0.999997 & 0 & -0.00260254 & 0 & 0 \\ -0.000447834 & 0 & 0 & 0 & -1. & 0 \\ -0.00265104 & 0 & 0.999996 & 0 & 0 & 0 \\ 0 & -0.00260254 & 0 & 0.999997 & 0 & 0 \\ 0 & 0 & 0 & 0 & 0 & 1. \end{pmatrix}, \quad (4.24)$$

which shows how the mixing $U_{\phi_1 h_1}$ can be 1, while the remaining states have larger mixing between the sectors. This mixing can also allow for a Higgs portal term without affecting the couplings of the Standard Model Higgs boson and maintaining the decoupling limit for the additional scalar degrees of freedom. We will return to this possible connection between the two sectors in Section 4.7.2. In Table 4.3 we list a set of parameters for another section of parameter space with a larger ratio of the EW scales of the two sectors.

TABLE 4.3: Higgs Potential parameter sample and associated masses of physical scalars in each sector. Masses are in units of GeV. This example point in parameter space for $\rho = 3000$ will be used throughout this work to exemplify the large ρ case.

$m_{11}^2 = -6.7^2$	$m_{22}^2 = -183150^2$	$m_{12}^2 = -6.7^2$	$z_1 = 0.13$	$z_2 = 0.13$
$z_3 = 0.8$	$z_4 = .01$	$z_5 = .01$	$z_6 = .01$	$z_7 = .01$
$z_8 = .01$	$z_9 = 0.8$	$z_{10} = 0.8$	$z_{11} = .01$	$z_{12} = 10^{-9}$
$z_{13} = .01$	$z_{14} = .01$	$m_h = 125$	$m_{h_D} = 366300$	$m_{A_1} = 590729$
$m_{A_2} = 645018$	$m_{J_1} = 590729$	$m_{J_2} = 645018$	$m_{H^+} = 590729$	$m_{H^{+\prime}} = 645018$
$v = 246$	$w = 738000$	$\tan(\beta) = 10^{-4}$	$\tan(\beta') = 10^7$	$\rho = 3000$

The mixing matrix in the case of 4.3 is then given by

$$U_{III} = \begin{pmatrix} -1. & 0 & 0 & 0 & 0.000184443 & 0 \\ 0 & 1. & 0 & 0 & 0 & 0 \\ -0.000184443 & 0 & 0 & 0 & -1. & 0 \\ 0 & 0 & -1. & 0 & 0 & -0.000147143 \\ 0 & 0 & 0 & 1. & 0 & 0 \\ 0 & 0 & -0.000147143 & 0 & 0 & 1. \end{pmatrix}. \tag{4.25}$$

We can see that these potentials allow for ASB that can give significant differences to the two sectors while beginning with a mirror symmetry. In the next section we will focus on how the independent Yukawa couplings and the dark EW scale w can vary without significantly changing the confinement scale of the $SU(3)'$ gauge group when compared to that of the visible $SU(3)$.

4.4 Dark confinement

As in Chapter 2, at high energy the mirror symmetry between the sectors imposes the condition that the gauge coupling of the $SU(3)$ and $SU(3)'$ groups are the same above the dark electroweak scale, after which the mirror symmetry is broken and the couplings may become differentiated.

In particular we have very different masses for the dark quarks, which result from a combination of the larger electroweak VEV of H_1' and Yukawa couplings which are independent almost entirely independent of the couplings to H_1. This will in turn set the scale of quark mass threshold corrections in the running of α_3' such that it will become non-perturbative at an energy scale above that of the Standard Model. This follows the analysis in Chapter 2. The reason for this is to leave two dark quarks with small masses to form our dark baryons, a point we will return to in Section 4.7. The principle goal of examining the quark Yukawa hierarchies is to examine which cases will allow for a dark confinement scale, $\Lambda_{\rm DM}$, that is approximately five times that of the Standard Model value, $\Lambda_{\rm QCD}$. As Section 4.6 will explore how to obtain near equal number densities of visible and dark baryons, this difference between confinement scales will be the cause of dark matter's larger role in the universe's mass density.

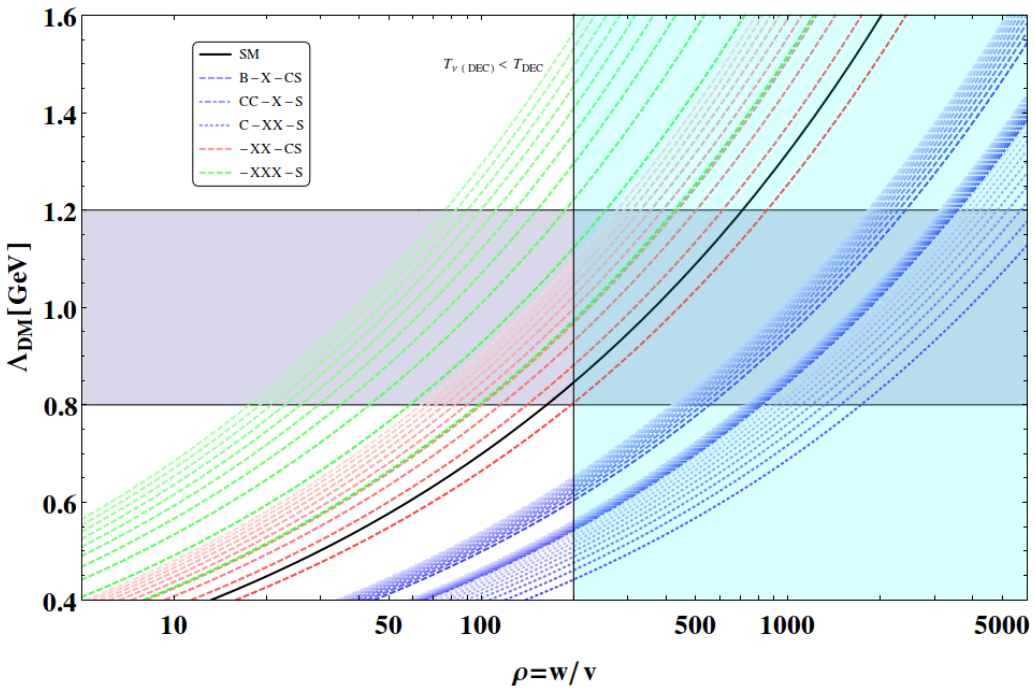

FIGURE 4.1: The confinement scale as a function of ρ, the ratio of EW scales, for a variety of Yukawa coupling hierarchies. The SM Yukawa range is shown for reference in the black curve. Each of the sets of Yukawa couplings is divided into ranges where one common coupling for one, two or three dark quark flavours varies between a maximum at the SM Yukawa coupling constant listed first and a minimum at the SM Yukawa coupling constant listed last. Yukawa coupling constants vary from left to right in each colour band in ten even divisions. For example, C-XX-S indicates that the largest coupling is equal in magnitude to the SM charm Yukawa, then there are two identical Yukawa couplings that vary between the SM charm and strange Yukawas, and a fourth Yukawa with a magnitude equal to that of the SM strange quark. Each of these examples includes two light quarks which have masses far below the confinement scale. The red- and green-dashed cases have a Yukawa coupling constant upper value set equal to that of the SM top quark. The blue shaded region indicates the divide between two different regions of parameter space that we explore, one with light mirror neutrinos in the present day (left of vertical line), and one without. The grey shaded region indicates the desired range for the dark confinement scale to explain the similarity between dark matter and proton mass scales.

We consider in this work the case of variations on the mass hierarchy of quarks in the DS. This extends the work in Chapter 2, where a common mass scale for heavy quarks was considered for the sake of simplicity. Now that we have a model with independent Yukawa couplings, it is useful to consider the larger parameter space involved in moving all six dark quarks independently. This approach of completely free dark quark mass parameters and the possible effects will be considered further in Chapter 5. The critical result is that we can see as a function of the ratio of the VEVs in each sector what, for instance, the mirror bottom Yukawa would need to be in divisions between the SM

charm and top Yukawa couplings to result in a dark confinement scale ~ 5 times that of ordinary QCD. Figure 4.1 shows a sample of which Yukawa hierarchies can give a $\sim 5\,\text{GeV}$ dark baryon. As the size of the dark EW scale affects the entire dark quark mass spectrum, we see what the dark confinement scale is for a variety of hierarchies at each value of ρ, the ratio of dark to visible electroweak scales. Also shown in Fig. 4.1 is the SM Yukawa hierarchy for reference. As we will discuss in Section 4.7, depending on the assumptions of the model with regard to the thermal history, different limits on ρ come from constraints on the abundance of charged dark baryons as well as from constraints on VS flavour physics and successful leptogenesis.

4.5 Neutrino masses

The neutrinos of our model consist of the left-handed states of the visible sector, heavy right-handed states with Majorana mass terms along with all of the associated mirror counterparts. These are heavy left-handed states of the DS and light right-handed states. Above the mirror breaking scale we have only the mixing between the heavy Majorana states given by Eq. 4.3. The cross-sector mixing, given by the parameter P, must be suppressed in order to prevent too much mixing between light neutrinos in each sector once the heavy degrees of freedom are integrated out. This aligns with technical naturalness from independent Poincaré symmetries discussed in Section 4.3. If P is the product of a small dimensionless cross-sector coupling and a right-handed neutrino mass scale $\sim M$ that develops near the GUT scale, then we expect $M \gg P$. However it must be noted that any nonzero value of P will induce maximal mixing for the heavy mass eigenstates as mirror parity commutes with the Hamiltonian. The heavy states that undergo CP violating decays to produce the lepton asymmetry of both sectors are equal admixtures of visible and mirror matter states. This follows the case in [142] of an $SO(10) \times SO(10)$ model. Below the scale of symmetry breaking we can consider both the heavy and light neutrino states of the theory. For the Lagrangian given by Eqs. 4.3

and 4.2, we have mass terms in the basis $(\overline{\nu_L}, \overline{\nu_R^c}', \overline{N_R^c}, \overline{N_L}')$ given by

$$\mathbb{M} = \begin{pmatrix} 0 & 0 & y_1 v & f_1 v \\ 0 & 0 & f_2^* w & y_2^* w \\ y_1^\dagger v & f_2^T w & M & P \\ f_1^\dagger v & y_2^T w & P^T & M \end{pmatrix}. \tag{4.26}$$

Above the scale at which parity is broken, where the mass eigenstates must also be parity eigenstates, the matrix only contains the lower right 2×2 matrix and we can write the heavy Majorana states as linear combinations of visible and dark sector flavour states [153–155].

$$N^\pm = \frac{1}{\sqrt{2}} \left((N_L')^C \pm N_R \right). \tag{4.27}$$

These have masses $M_N^\pm = M \pm P$ however by taking the cross-sector mass P to be small, they become near degenerate at a scale $M_N \simeq M$. For each generation we gain two near degenerate mass eigenstates with masses $M_N = (M_1, M_2, M_3)$. We see directly that taking this cross-sector mass to be small also sets the mixing of light visible and mirror neutrinos to be minimal once the heavy neutrinos are integrated out. In the three generational case, above the scale of mirror symmetry breaking, the heavy Majorana mass eigenstates, N_i will be divided into parity-even and parity-odd states,

$$\begin{aligned} N^+_{1,2,3} &= \alpha_i^+ (N_{R_1} + N'_{L_1}) + \beta_i^+ (N_{R_2} + N'_{L_2}) + \gamma_i^+ (N_{R_3} + N'_{L_3}) \\ N^-_{1,2,3} &= \alpha_i^- (N_{R_1} - N'_{L_1}) + \beta_i^- (N_{R_2} - N'_{L_2}) + \gamma_i^- (N_{R_3} - N'_{L_3}), \end{aligned} \tag{4.28}$$

with $|\alpha_i|^2 + |\beta_i|^2 + |\gamma_i|^2 = 1$ and $i = (1, 2, 3)$. We will consider a hierarchical case of thermal leptogenesis where the near equal masses $M_1 \pm \frac{P}{2}$ of the lightest heavy states will be relevant to the temperature where out of equilibrium CP violating decays generate a lepton asymmetry in each sector.

4.5.1 Small cross-sector coupling case

We first consider the case where the cross-sector Yukawa couplings satisfy $y_i \gg f_i$. Below the scale of symmetry breaking, where mirror parity has been broken, the mass eigenvalues effectively result in two independent seesaw mechanisms [156] with masses

given by

$$m_\nu \simeq \frac{(y_1 v)^2}{M_N}\left(1+\mathcal{O}\left(\frac{P}{M_N}\right)\right), \qquad m_{\nu'} \simeq \frac{(y_2 w)^2}{M_N}\left(1+\mathcal{O}\left(\frac{P}{M_N}\right)\right). \tag{4.29}$$

The light neutrino states of the dark sector will gain a mass larger than the VS counterparts from the Dirac mass term while being suppressed by the same Majorana mass scale. The Dirac mass will differ on two accounts. Firstly, the larger electroweak scale w and secondly the different couplings of y_2 compared to y_1. The limit on the number of effective relativistic degrees of freedom will limit how many dark neutrino flavours can be relativistic.

As we have two seesaw mechanisms, one in each sector, that rely on different Yukawa couplings we now turn to parameterising the couplings and masses of the three light flavours. Following the Casas-Ibarra [157] parametrisation, the visible sector has mass matrix $m_\nu = v^2 y_1 D_M^{-1} y_1^T$ while in the dark sector we have $m_{\nu'} = w^2 y_2 D_M^{-1} y_2^T$. Each of these is independently diagonalised into D_m and $D_{m'}$ by different matrices which we will label U and U' respectively. We then have in the exact asymmetric vacuum configuration,

$$y_1 = \frac{1}{v} U D_m^{\frac{1}{2}} R D_M^{\frac{1}{2}}, \quad y_2 = \frac{1}{w} U' D_{m'}^{\frac{1}{2}} R' D_M^{\frac{1}{2}}. \tag{4.30}$$

Here R and R' are orthogonal matrices and are independent as U and U' are. In particular U' will contain phases from the rotation of charged mirror leptons which gain mass from H_2 such that

$$U' = (W_L^l)^\dagger U^{\nu'}, \tag{4.31}$$

where $U^{\nu'}$ diagonalises the low energy $m_{\nu'}$. W_L^l also depends strongly on the texture of η_2^l. In solving the Boltzmann equations for the related Yukawa couplings above, sample η_2^l matrices are chosen such that the mass eigenstates are in accordance with the thermal history assumptions for dark lepton masses in that region of parameter space while $U^{\nu'}$ is an unconstrained unitary matrix as the PMNS matrix of the dark sector is not known. At the scale of thermal leptogenesis y_2 can be the dominant coupling for the creation of a population of heavy neutrino states and the subsequent decay when $T < M_1$. It can also be the major contribution to the lepton asymmetry created in both the visible and the dark sector. We can see that successful thermal leptogenesis may ultimately impose more constraints on the dark sector's low temperature light neutrino parameter space in contrast with ordinary thermal leptogenesis. In the next section we will examine how

this L asymmetry can form in both sectors within the mirror symmetric temperature regime.

4.5.2 Significant cross-sector coupling case

We now consider the case where the cross-sector terms, f_i, are comparable to the other Yukawa couplings. These will create Dirac mass terms that induce some mixing between light neutrinos of the two sectors. We will see in the next two sections that the requirements on the number of effective relativistic degrees of freedom in the dark sector require one of two possibilities. First the dark EW scale, w, can be small enough that any relativistic neutrino species of the dark sector remain in thermal equilibrium until the temperature drop of the dark sector, and therefore fall to a lower temperature along with the dark photon. The second possibility is that the dark EW scale is large enough such that any dark neutrinos become non-relativistic and subsequently decay from the plasma prior to any temperature shift. In this latter case we will require that the neutrinos of the dark sector are heavy enough that they decay to SM species with a short enough lifetime. We examine the masses and mixing in this case. Points in the parameter space such as

$$\left[f_1 = 0.05,\ f_2 = 0.0005,\ \rho = 3000,\ y_2 = .005,\ y_1 = 10^{-6},\ M_1 = 1 \times 10^7 \text{GeV}\right] \quad (4.32)$$

allow for heavy states that are still approximately even admixtures of N and N' and there now exists a small amount of mixing between the light states of the two sectors. With the much larger EW scale of the dark sector we can have all three flavours of dark neutrino in the 100 MeV range and mixing between the two light species of order $\delta_{\nu\nu'} = 10^{-3}$ where $\tilde{\nu} = \nu + \delta_{\nu\nu'}\nu'$. This is similar to that of Ref. [125], except that in this case it is mixing between the light neutrinos of one sector with the heavy states of the opposing sector. The light neutrinos of the dark sector then decay to visible sector species via $(\nu' \to \nu e^+ e^-)$ just prior to BBN and the only remaining light degree of freedom in the dark sector will be the dark photon. With these larger f_i couplings we can examine the subsequent additional terms in the Boltzmann equations in there era of thermal leptogenesis. Since we will consider at that temperature a population of mass eigenstates $N^{\pm}$, this will amount to an extra pair of terms to the total decay rate,

$\Gamma(N \to \phi l)$, in each sector and modify the washout rates and CP asymmetry parameter. We explore this and the first case in detail in the next section.

4.6 Symmetric leptogenesis

We now consider how the visible and dark sectors generate a comparable amount of baryon asymmetry. As with all models of Baryogenesis we require the fulfilment of the Sakharov conditions, that is, a B violating mechanism, C and CP violation, and a departure from thermal equilibrium. Mirror symmetry can then provide an associated mechanism in the DS though the exact process will differ once mirror symmetry is broken. Ultimately it is necessary for the two sectors to be different to explain why there is more dark matter than visible matter in the universe. Either DM is more massive than the proton or the dark sector contains a higher concentration, or it is a combination of each, to such a slight degree that the mass densities remain within the same order of magnitude. The dark sector must also have a mechanism for the symmetric components of the plasma to annihilate, for example through dark photons. In order to create this B and B' asymmetry we consider the creation of a baryon asymmetry through sphaleron effects that partially convert a lepton asymmetry generated through high scale thermal leptogenesis. As most of the lepton asymmetry will develop at a scale above the mirror parity breaking scale, the generation of the mirror lepton asymmetry will proceed almost identically. Following this the sphaleron effects in each sector will convert these lepton asymmetries into similar amounts of B and B' asymmetry in each sector. The amount of B and B' will not be identical as sphaleron effects will take place at different temperatures when the sectors are no longer connected by mirror parity and may therefore have different thermal populations.

Since the second Higgs doublet in the visible sector can provide a way to generate a sufficient amount of lepton asymmetry while not contributing to the squared Higgs mass corrections usually seen in the thermal leptogenesis case, the associated naturalness bound might be avoided. This can be compared to recent work in [158] which examined how the tension between Higgs mass corrections and the requirements of vanilla leptogenesis can be solved with a second Higgs doublet. The squared mass correction from

the right-handed neutrino mass scale can be written as

$$\delta\mu^2 \approx \frac{1}{4\pi} y_1^2 M_N^2. \tag{4.33}$$

The mass corrections to the heavier bosons will be larger if y_2 is, however since the mass scale of the dark Higgs, dark EW scale, and the other decoupled scalars is orders of magnitude larger also, the quantum corrections have the capacity to still be natural if one adopts the criteria that such corrections should be no larger than of order $1\,\mathrm{TeV}^2$ [159] for the SM Higgs. Then this translates to an upper bound of $\sim 3 \times 10^7\,\mathrm{GeV}$ for the Majorana mass in a single flavour case.

In the simplest case of leptogenesis from the decay of heavy right-handed neutrinos the amount of asymmetry produced can be expressed in terms of the CP asymmetry ϵ and the efficiency factor κ_f, which measures the asymmetry destroying processes during the era of leptogenesis. For the case of a single doublet, the CP asymmetry factor for the lightest right-handed state N_1 is

$$\epsilon_1 = \frac{\Gamma(N_1 \to l\phi^*) - \Gamma(N_1 \to l^c\phi)}{\Gamma(N_1 \to l\phi^*) + \Gamma(N_1 \to l^c\phi)}. \tag{4.34}$$

Adding a second doublet allows for two relevant CP factors from y_1 and y_2. Including the mirror sector adds a decay channel through f_1 and f_2 that can generate asymmetry in the opposite sector. In a standard seesaw model, with the CP parameter calculated, the decay parameter is defined as

$$K = \frac{\Gamma_D(z=\infty)}{H(z=1)}, \tag{4.35}$$

where $z = M_1/T$ and Γ_D is the decay width. This is typically done in order to set bounds on the mass of light neutrinos in most models however in this case some of the CP asymmetry is being generated by the coupling of heavy neutrino states to Φ_2 and Φ_2' and so in the visible sector, the Yukawa coupling relevant to mass is not important in terms of the generation of a lepton asymmetry. The factor K can still serve as a useful parameter in measuring the ratio of relevant parameters, that of the CP violating couplings and the heavy neutrino mass scale M_1.

We consider in this work the generation of a $B-L$ asymmetry in the one-flavour approximation. While this approximation is typically only completely accurate at temperatures

of lepton asymmetry generation above the scale at which the tau charged lepton Yukawa interactions are in equilibrium, so that the value of M_1 violates the Vissani bounds on naturalness, in this case the role of flavour effects will be more complicated. In particular the thresholds for when charged lepton Yukawa interactions are in equilibrium will depend on the couplings to Φ_2, as well as to Φ_1. Additionally the charged lepton Yukawa coupling matrices to Φ_1 and Φ_2, which contribute to the thermal masses, cannot in general be simultaneously diagonalised. A full analysis of possibly significant flavour effects in this case would need to carefully consider the relative rates among six interactions of lepton doublets l involving $(N\Phi_1, N\Phi_2, N'\Phi_1, N'\Phi_2, \Phi_1 e_R, \Phi_2 e_R)$ as well as the Hubble rate at each temperature range in order to determine the coherent state evolution. For the present analysis, we make the simplifying assumption that the combination of y_1, y_2, f_1, f_2 channels for washout is similar in magnitude for each individual flavour and so the unflavoured approximation may yield a more accurate result for the total $B - L$ asymmetry with $T < 10^{12}\,\text{GeV}$ in this case than ordinary Type-1 seesaw thermal leptogenesis models.

We will consider two separate regions of parameter space that are compatible with all of the other features in the model. We can classify these as the small ρ regime with $\rho < 200$ and the large ρ regime. These different cases require different treatments for a number of key reasons. In the small ρ regime, dark EW interactions are still in equilibrium at the time of the temperature decoupling of the two sectors. This will allow the light neutrinos of the dark sector to undergo a temperature change along with the dark photon as they have not yet decoupled. Because of this, it is possible to have light neutrinos in the dark sector and still satisfy the constraints on N_{eff} as we will discuss in the next section.

4.6.1 Small cross-sector coupling case

We first consider the case with $y_i \gg f_i$ and a hierarchical relationship among the Majorana masses, $M_2, M_3 \gg M_1$. The heavy states decay to visible and dark leptons with equal rates and their asymmetry in these rates is also the same. We must also account for the fact that each of Φ_1 and Φ_2 can appear in the self-energy and vertex diagrams. We then obtain the expression for the CP parameters $\epsilon_1^{\phi_1}$ and $\epsilon_1^{\phi_2}$ from decays, $N_1 \to l\phi_1$ and $N_1 \to l\phi_2$. These can be expressed as functions of the form

$$\epsilon_1^{\phi_1} \simeq \sum_{i=1,2}\sum_{k\neq 1}\frac{1}{16\pi}\frac{M_1}{M_k}\left[\frac{\mathrm{Im}\left[(y_1^\dagger y_i)_{k1}(y_i^\dagger y_1)_{k1}+2(y_1^\dagger y_1)_{k1}(y_i^\dagger y_i)_{k1}\right]}{(y_1^\dagger y_1)_{11}}\right], \tag{4.36}$$

$$\epsilon_1^{\phi_2} \simeq \sum_{i=1,2}\sum_{k\neq 1}\frac{1}{16\pi}\frac{M_1}{M_k}\left[\frac{\mathrm{Im}\left[(y_2^\dagger y_i)_{k1}(y_i^\dagger y_2)_{k1}+2(y_2^\dagger y_2)_{k1}(y_i^\dagger y_i)_{k1}\right]}{(y_2^\dagger y_2)_{11}}\right].$$

Note that there is an additional term proportional to M_1^2/M_k^2 which is neglected in this hierarchical case. Such terms are ordinarily exactly zero after summing over lepton flavours however y_2 allows one of these to survive [80]. The lepton asymmetry can be generated through the out of equilibrium decays of heavy neutrinos, N. From the Yukawa couplings we have CP violating decays both in $(N \to \phi_1 l)$, $(N \to \phi_2 l)$ and in the mirror sector $(N \to \phi_1' l')$ and $(N \to \phi_2' l')$.

The tree level total decay rate of the heavy states, including cross-sector decay in this visible sector channel is given by

$$\Gamma_{N_i} = \frac{1}{8\pi}\left[(y_1^\dagger y_1)_{ii}+(y_2^\dagger y_2)_{ii}+(f_1^\dagger f_1)_{ii}+(f_2^\dagger f_2)_{ii}\right]M_i. \tag{4.37}$$

In order for these decays to take place out of equilibrium we can consider each of the strong and weak washout cases. In the weak regime ($K < 1$), inverse decays will create an abundance of heavy neutrino states which surpasses the equilibrium number density and the subsequent out of equilibrium decays will produce an asymmetry which depends on the initial conditions. The size of the initial population will determine the opposite sign asymmetry produced during inverse decays as the equilibrium density is reached. The final asymmetry will then be a combination of the asymmetry produced in each phase. In the strong washout regime ($K > 1$) the high coupling will bring an initial population of heavy N states quickly to the equilibrium density. The strong coupling leads to a high rate of decays and inverse decays that washes out any initially formed asymmetry after which a final asymmetry is produced when inverse decays become suppressed as $T < M_1$ and non-relativistic heavy neutrinos undergo CP violating decays. We make use of the variable $z = \frac{M_1}{T}$ and write $[D, S, W] = \Gamma_{[D,S,W]}/Hz$.

It is useful to consider the limiting case by taking the contribution from y_1 terms to be small enough that the dominant contribution to the CP violating decays comes from just y_2. In this case we can take the usual strong washout efficiency factor κ_f, defined

by

$$\mathcal{N}_{B-L} = -\frac{3}{4}\kappa_f \epsilon_1^{\phi_2}, \tag{4.38}$$

where this has an approximate analytical expression in terms of K in the limit that y_2 dominates [160],

$$\kappa_f \simeq \frac{2}{z_B K}\left[1 - \exp\left(-\frac{1}{2} z_B K\right)\right], \tag{4.39}$$

$$z_B(K) \simeq 1 + \frac{1}{2}\ln\left[1 + \frac{\pi K^2}{1024}\left(\ln\left(\frac{3125\pi K^2}{1024}\right)\right)^5\right]. \tag{4.40}$$

This is a useful check for the numerical solutions in the limit that y_2 dominates however in the general numerical solutions later we do not neglect the role of y_1. In the more general case we will write the Boltzmann equations for the generation of a lepton asymmetry for one sector in the following and take $\mathcal{N}_1$ to be the combined population of states N_1^+ and N_1^- at mass scale M_1. With light neutrinos in the dark sector, $y_i \gg f_i$, and two seesaw mechanisms we can have an orthogonal complex matrix R' such that the scale of $(y_2^\dagger y_2)_{11}$ is not so large that the N_1 mediated scattering $l\phi \leftrightarrow \bar{l}\bar{\phi}$ destroys the created lepton asymmetry. The light neutrinos of the DS have their masses constrained by the requirement that they do not significantly contribute as a hot dark matter candidate. This imposes limits on the size of y_2 in this case. These constraints will also depend on the temperature of these light mirror neutrino states which will be lower than VS neutrinos. In the next section we see these limits on $m_{\nu'}$ in the low ρ case depend on the thermal history assumptions. We consider the cases of the heaviest dark light neutrino limited by upper bounds of $1.1\,\text{eV}, 3.2\,\text{eV}, 5.6\,\text{eV}$. Sample R and R' matrices for the two seesaw mechanisms are then explored in cases A and B in Fig. 4.2 for the first two bounds while the largest temperature difference that allows $5.6\,\text{eV}$ has three sample pairs of matrices R and R' for $C - E$.

4.6.2 General cross-sector coupling case

The previous case can be contrasted with the model for large ρ case. This scenario has fewer constraints from FCNC however above $\rho = 200$ the neutrinos of the dark sector decouple prior to the sectors thermally decoupling, such that all of the light neutrinos of the dark sector must be non-relativistic. Clearly multiple things must change. In this large ρ case, the requirements on the dark confinement scale will necessitate smaller Φ_2

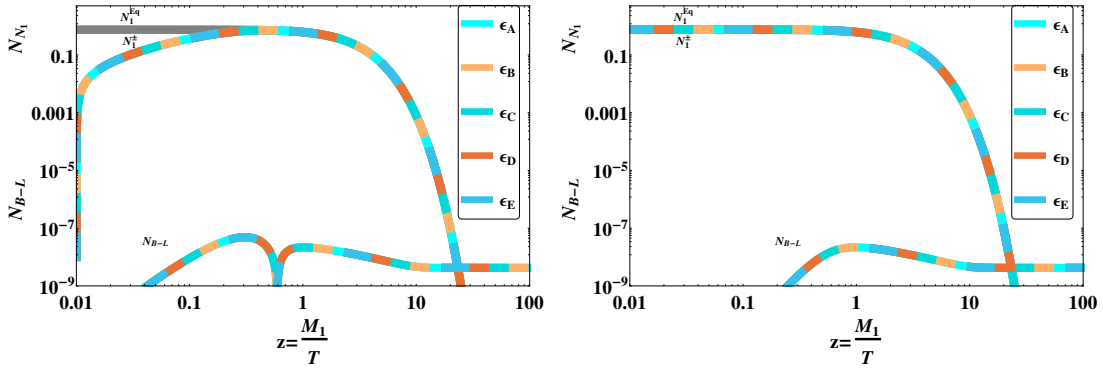

FIGURE 4.2: Evolution for the N_1 number density (the sum of the densities of N_1^+ and N_1^- divided by two) and the $B-L$ asymmetry for the small ρ case for different choices of the mass of the heaviest dark light neutrino. The left panel has zero initial N_1 abundance, while the right panel has an initial thermal abundance. In all cases, the observationally required $B-L$ asymmetry is produced at the low temperature end, and is independent of the initial abundance because we work in the strong washout regime. Case A corresponds to 1.1 eV, case B to 3.2 eV, while cases $C-E$ have 5.6 eV for the dark neutrino mass upper limit. Each curve illustrates an allowed choice for the Casas-Ibarra R and R' matrices with $\rho = 30$ and $M_1 = 10^9$ GeV. The small ρ case allows for larger quark scattering rates to ϕ_2 and is comparable to past works in thermal leptogenesis. The limits on the CP parameters ϵ_{A-E} come from limiting the amount of dark matter composed of hot dark neutrinos.

quark couplings than the SM in general. In the case that all three of the light neutrinos are $\sim 100\,\mathrm{MeV}$ and $\rho > 200$, the constraints on parameters such as in Eq. 4.32 on washout require that the CP parameter be much larger. At the same time with f_i and y_i comparable and P nonzero such an enhancement is immediate. We consider the CP parameter now in the case of individual populations of N^+ and N^-. Rewriting in terms of $Y_i = y_i + f_i, F_i = y_i - f_i$ we have

$$\epsilon_{1^+}^{\phi_1} = \sum_{i=1,2}\sum_k \frac{1}{16\pi}\left[\mathrm{R}(M_i^+, M_k^-)\frac{\mathrm{Im}\left[2\left((Y_1^\dagger F_1)_{k1}(Y_i^\dagger F_i)_{k1}\right) + 2\left((Y_1^\dagger Y_1)_{k1}(Y_i^\dagger Y_i)_{k1}\right)\right]}{(Y_1^\dagger Y_1)_{11}}\right.$$
$$+\mathrm{I}\left(\frac{M_1}{M_k}\right)\frac{\mathrm{Im}\left[(Y_1^\dagger Y_1)_{k1}(F_i^\dagger F_i)_{k1} + (Y_1^\dagger Y_i)_{k1}(Y_i^\dagger Y_1)_{k1}\right.}{(Y_1^\dagger Y_1)_{11}}$$
$$\left.\left.\frac{+(F_1^\dagger F_i)_{k1}(Y_i^\dagger Y_1)_{k1} + (Y_1^\dagger Y_1)_{k1}(F_i^\dagger Y_i)_{k1}\right]}{(Y_1^\dagger Y_1)_{11}}\right], \qquad (4.41)$$

$$\epsilon_{1^+}^{\phi_2} = \sum_{i=1,2}\sum_{k}\frac{1}{16\pi}\left[\mathrm{R}(M_i^+, M_k^-)\frac{\mathrm{Im}\left[2\left((Y_2^\dagger F_2)_{k1}(Y_i^\dagger F_i)_{k1}\right)+2\left((Y_2^\dagger Y_2)_{k1}(Y_i^\dagger Y_i)_{k1}\right)\right]}{(Y_2^\dagger Y_2)_{11}}\right.$$
$$+\mathrm{l}\left(\frac{M_1}{M_k}\right)\frac{\mathrm{Im}\left[(Y_2^\dagger Y_2)_{k1}(F_i^\dagger F_i)_{k1}+(Y_2^\dagger Y_i)_{k1}(Y_i^\dagger Y_2)_{k1}\right.}{(Y_2^\dagger Y_2)_{11}}$$
$$\left.\left.\frac{+(F_2^\dagger F_i)_{k1}(Y_i^\dagger Y_2)_{k1}+(Y_2^\dagger Y_2)_{k1}(F_i^\dagger Y_i)_{k1}\right]}{(Y_2^\dagger Y_2)_{11}}\right],$$

where

$$l(x) = x\left[1-(1+x^2)\ln\left(\frac{1+x^2}{x^2}\right)+\frac{1}{1-x^2}\right], \tag{4.42}$$

and

$$R(M_i^+, M_k^-) = \frac{M_i^+(M_i^{+2}-M_k^{-2})}{(M_i^{+2}-M_k^{-2})^2+M_i^{+2}\Gamma^2_{N_k^-}}. \tag{4.43}$$

The CP parameters for the ϵ_{1^-} terms can easily be found by interchanging F and Y. The relevant diagrams for these CP parameters are in Fig. 4.3. Note that the sum can now extend to $k = 1$ and we have a nonzero CP parameter for some of these terms. This can be compared to the case of the double seesaw mechanism of leptogenesis [161]. However in this case again we have a symmetric asymmetry generated in the dark sector.

Similar to double seesaw mechanisms we have in this case the fact that P, the cross-sector masses, being small automatically places us in a parameter space near resonance between N_1^+ and N_1^-. This comes with the nonzero CP violation originating from the interference of diagrams that involve both N^+ and N^-. With $P/M_N \approx 10^{-9}$ we are within the range of resonant effect through the interference in the self-energy diagram with N_1^+ and N_1^- for the Yukawas in Eq. 4.32. In Figure 4.4 we see that resonant increase in the CP parameter for this large ρ case.

Note that this differs from [125] in that the resonance comes from adjusting the single small parameter P which was previously constrained to be small rather than adjusting M_1 and M_2 to bring their difference close to the decay width. The resonant boost can allow for a smaller value of M_N such that in the high ρ case we bring M_N down to $\sim 10^7$GeV.

In Fig. 4.5 we can examine the scattering rate and total washout rate in the different cases of quark mass hierarchies in the dark sector. With general cross-sector couplings we can examine the more complex set of decays, scatterings and inverse decays. We

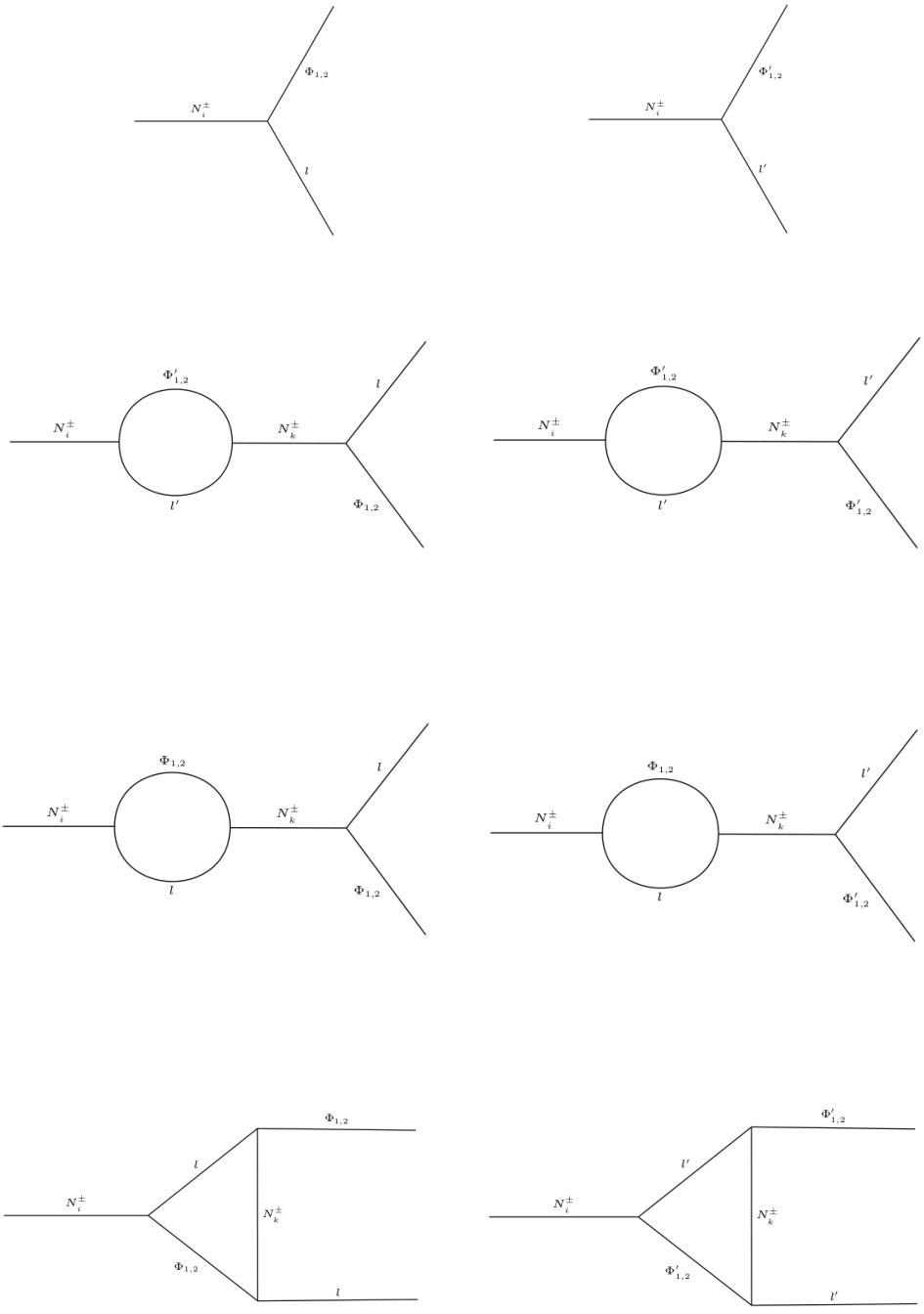

FIGURE 4.3: The interference of all diagrams in the left column for a fixed final state Φ_1 and initial state $i = 1^+$ contributes to $\epsilon_{1^+}^{\phi_1}$ while fixing Φ_2 and $i = 1^+$ allows us to calculate $\epsilon_{1^+}^{\phi_2}$. Choosing $i = 1^-$ yields $\epsilon_{1^-}^{\phi_{1,2}}$. Likewise the right column gives the interference among mirror counterpart diagrams in the dark sector.

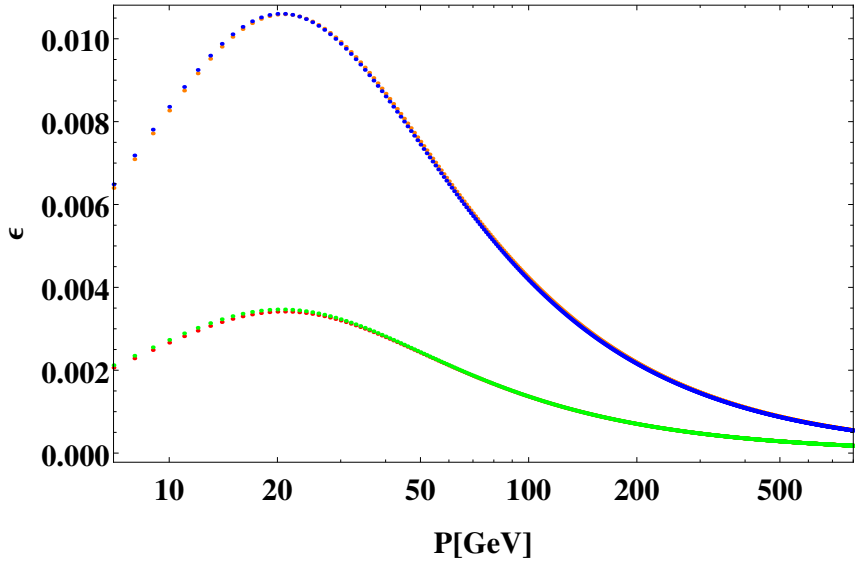

FIGURE 4.4: The resonant increase in the CP parameters $\epsilon_{1^+}^{\phi_1}, \epsilon_{1^+}^{\phi_2}, \epsilon_{1^-}^{\phi_1}, \epsilon_{1^-}^{\phi_2}$ (Blue, Orange, Red, Green) as a function of P in GeV, the cross-sector neutrino mass term.

consider simultaneously the variables, $\mathcal{N}_1^+$ and $\mathcal{N}_1^-$ and asymmetries of both sectors, $\mathcal{N}_{B-L}$ and $\mathcal{N}'_{B-L}$. The considered interactions of the decay and inverse decay type are

$$N_1^{\pm} \leftrightarrow \phi_1^* l,$$
$$N_1^{\pm} \leftrightarrow \phi_1 l^c,$$
$$N_1^{\pm} \leftrightarrow \phi_2^* l,$$
$$N_1^{\pm} \leftrightarrow \phi_2 l^c,$$

and their mirror analogues

$$N_1^{\pm} \leftrightarrow \phi_1'^* l',$$
$$N_1^{\pm} \leftrightarrow \phi_1' l'^c,$$
$$N_1^{\pm} \leftrightarrow \phi_2'^* l',$$
$$N_1^{\pm} \leftrightarrow \phi_2' l'^c.$$

For scattering processes, it is known that the dominant ones in the standard leptogenesis case are leptons with top quarks, so in our situation we must consider if the Yukawa couplings to quarks of the second Higgs doublet are in a similar range. We thus consider

the following processes into the Boltzmann equations:

$$N_1^{\pm} l^c \leftrightarrow t\bar{q},$$
$$N_1^{\pm} q \leftrightarrow t l,$$

driven by virtual ϕ_1 exchange in the s- and t-channels, and the ϕ_2-driven counterparts,

$$N_1^{\pm} l^c \leftrightarrow u_i \bar{q},$$
$$N_1^{\pm} q \leftrightarrow u_i l,$$

where $q = d, s, b$ and u_i is any charge $+2/3$ quark flavour that has a significant Yukawa coupling to ϕ_2. The mirror analogues of these processes also must be included. For the strong-washout regime, processes such as $\phi_1 l \leftrightarrow \phi_1^* l^c$ and the like can be small due to the large mass of the exchanged virtual heavy neutral lepton compared to the temperature at which the asymmetries are generated.

If we again consider the case of the strong washout regime where gauge scattering can be ignored, due to only being effective in the $T > M_1$ era, then the relevant Boltzmann equations only contain washout from inverse decays and quark scattering [74],

$$\begin{aligned}
\frac{d\mathcal{N}_{B-L}}{dz} =& -(\epsilon_{1+}^{\phi_1} D_+^{\phi_1} + \epsilon_{1+}^{\phi_2} D_+^{\phi_2})(\mathcal{N}_{N_1^+} - \mathcal{N}_{N_1^{\mathrm{Eq}}}) \\
& -(\epsilon_{1-}^{\phi_1} D_-^{\phi_1} + \epsilon_{1-}^{\phi_2} D_-^{\phi_2})(\mathcal{N}_{N_1^-} - \mathcal{N}_{N_1^{\mathrm{Eq}}}) - W_T \mathcal{N}_{B-L}, \\
\frac{d\mathcal{N}_{B'-L'}}{dz} =& -(\epsilon_{1+}^{\phi_1} D_+^{\phi_1} + \epsilon_{1+}^{\phi_2} D_+^{\phi_2})(\mathcal{N}_{N_1^+} - \mathcal{N}_{N_1^{\mathrm{Eq}}}) \\
& -(\epsilon_{1-}^{\phi_1} D_-^{\phi_1} + \epsilon_{1-}^{\phi_2} D_-^{\phi_2})(\mathcal{N}_{N_1^-} - \mathcal{N}_{N_1^{\mathrm{Eq}}}) - W_T \mathcal{N}_{B'-L'}, \\
\frac{d\mathcal{N}_{N_1^+}}{dz} =& -(D_+ + S_+)(\mathcal{N}_{N_1^+} - \mathcal{N}_{N_1^{\mathrm{Eq}}}), \\
\frac{d\mathcal{N}_{N_1^-}}{dz} =& -(D_- + S_-)(\mathcal{N}_{N_1^-} - \mathcal{N}_{N_1^{\mathrm{Eq}}}).
\end{aligned} \tag{4.44}$$

The scaled decay, scattering and washout rates are detailed in Appendix C. We consider the large ρ case with strong washout and with both a vanishing and a thermal population of heavy neutrino states as initial conditions in Fig. 4.6. The different cases $(F - J)$ describe different sample points in parameter space of the matrix in Eq. 4.26 that satisfy the condition that non-relativistic light neutrinos of the dark sector have masses of order 100 MeV and decay into SM species prior to BBN. In Section 4.7 we will see that the

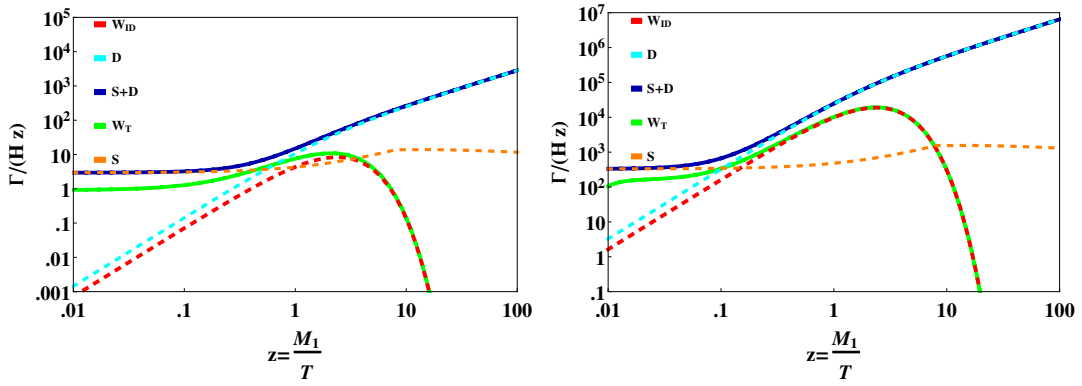

FIGURE 4.5: Scaled Rates $(D_+, S_+, W_{ID}, W_T, S_+ + D_+)$ in the Boltzmann equations for the cases of small (left panel) and large (right panel) ρ. The parameter points are as for Fig. 4.2 and Fig. 4.6, respectively. As the quark Yukawa couplings to the second doublet Φ_2 can be smaller than those to Φ_1 in the large ρ case, the $(qt \leftrightarrow \phi_2 l)$ scattering rates in the Boltzmann equations can be minimal. In the strong washout regime, $(K > 1)$ we see in the large ρ case significant washout rates, the natural resonance that can arise in the CP parameter can allow the necessary asymmetry to survive at the point the washout rates become ineffective.

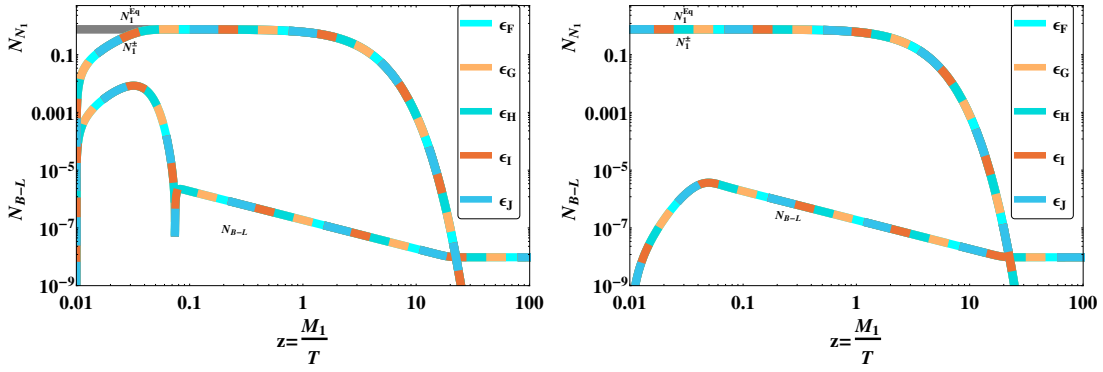

FIGURE 4.6: $B - L$ asymmetry and N abundance in the visible sector for the large ρ case for the parameter point of Eq. 4.32. The N_1^+ and N_1^- number densities are almost indistinguishable. Each graph displays five distinct choices for the matrices y_1, y_2, f_1 and f_2, labelled $F - J$. These solutions gain an enhanced $B - L$ from the resonance effect between the N^+ and N^- mass eigenstates. The CP parameter additionally varies from the coupling to both Higgs doublets. Each case has different initial abundances for N_1: vanishing (left panel) and thermal (right panel).

bounds on N_{eff} from BBN can easily accommodate the dark photon that remains as the only relativistic degree of freedom in this regime.

4.7 Cosmological history

We now focus on examining the consequences of this type of model on the thermal history of both the visible and dark sectors. In particular we examine how the two sectors can be consistent with the current evidence of BBN and the constraints on the number of relativistic degrees of freedom. In the dark sector we consider how, after the breaking of mirror parity, a clear dark matter candidate can form which satisfies all of the current astrophysical evidence of dark matter.

4.7.1 Baryogenesis in the visible and dark sector

The lepton asymmetry of each sector is converted to a baryon asymmetry beginning at the temperature at which the $B-L$ asymmetry is produced by thermal leptogenesis. Immediately after this, the relation between the B, L and $B-L$ asymmetries of each sector can be related by

$$\begin{aligned} \mathcal{N}_B &= \frac{24+4N_H}{66+13N_H}\mathcal{N}_{B-L}\ , \\ \mathcal{N}_L &= -\frac{42+9N_H}{66+13N_H}\mathcal{N}_{B-L}\ , \end{aligned} \tag{4.45}$$

where N_H is the number of Higgs doublets that remain in equilibrium [162]. Following the EWPT of the dark sector, sphaleron processes of the dark sector are no longer rapid and the relation between B', L' and $B'-L'$ is fixed at the values as in Eq. 4.45 with $N_H = 2$. At this point, one of the Higgs doublets of the visible sector gains a large positive squared mass value sufficient to decouple one the doublets of the visible sector while sphaleron effects of the visible sector are still rapid. The $B-L$ asymmetry in the visible sector is then reprocessed to satisfy Eq. 4.45 with $N_H = 1$ and this will be the value that remains when visible sphaleron processes are no longer rapid following the visible sector's EWPT. The modern baryon asymmetries are therefore given by

$$\mathcal{N}_B = \frac{28}{79}CN_{B-L}\,, \quad \mathcal{N}'_B = \frac{8}{23}CN'_{B-L} \tag{4.46}$$

where $C = g^*(T_0)/g^*(T)$ accounts for the variation in photon density between the onset of leptogenesis and now. We therefore have an abundance ratio from the symmetric leptogenesis phase that is slightly less than 1 which still suggests a mass ratio of dark

baryons that are ~ 5.57 that of the proton. In Fig. 4.1 this is considered as a range for the dark confinement scale with the exact mass of any heavy baryons having a range depending on the dark coloured quark masses. Further discussion of such hidden QCD models and the exact relationship between confinement scale and baryon masses will be explored in Chapter 5. We can now consider some of the broader consequences of the dark sector.

4.7.2 Thermal decoupling

As discussed previously we will examine the case that the two sectors should decouple within the temperature region between the confinement scales of the two sectors. By doing so, we can reduce the number of degrees of freedom in the DS while the two sectors are still in thermal contact and thus transfer the majority of the entropy density of the universe to the visible sector. This allows for the DS to cool at a faster rate and acquire a lower temperature at the time of BBN when constraints on the number of effective neutrino species are stringent. This idea was explored in past works on dark QCD models and in particular Ref. [144]. In models of two sectors the exact relationship between the temperature of each sector has important limits imposed by the effect of additional radiation components of the universe on the BBN and acoustic oscillations in the CMB. This is usually quantified through an effective excess neutrino number defined by

$$N_{\rm eff} = 3\left(\frac{11}{4}\right)^{4/3}\left(\frac{T_\nu}{T_\gamma}\right)^4 + \frac{8}{7}\left(\frac{11}{4}\right)^{4/3}\frac{g_D^*}{2}\left(\frac{T_D}{T_\gamma}\right)^4, \tag{4.47}$$

with the entire second term constituting $\Delta N_{\rm eff}$. The terms g_D^* and T_D are the degrees of freedom of the dark sector and their temperature. Recent measurements have obtained the bound $\Delta N_{\rm eff} = 0.11 \pm 0.23$ at the 68% confidence limit level[4]. The ratio of the temperatures of the two sectors at the scale of BBN is a function of the degrees of freedom in each sector compared to the value at the time of decoupling,

$$\frac{T_V^3}{T_D^3} = \frac{g_D}{g_V}\left(\frac{g_V}{g_D}\right)_{\rm DEC}. \tag{4.48}$$

In mirror symmetric models where the two sectors remain in thermal contact such as [125] the constraints on the dark degrees of freedom are strong enough that it is necessary that all mirror relativistic particles must be removed prior to the era of big bang

nucleosynthesis (BBN). If the temperature of the DS sector is less than the VS then the BBN constraint may be satisfied with at least a massless photon and possibly additional species still present in the dark sector.

In order to decouple to the two sectors in the energy range between $\Lambda_{\rm QCD}$ and $\Lambda_{\rm DM}$ we require a particle interaction that proceeds fast enough at high energy and becomes ineffective shortly after the DS becomes confining. We then require that either one or more of the species involved must become Boltzmann suppressed or the rate of the reaction as a function of temperature must drop below the Hubble rate. There are multiple distinct cases in which this can work in our model, depending on the value of ρ and the masses of the particle species in the DS.

4.7.2.1 Large ρ

In the first case all three of the dark sector's light neutrino species have non-relativistic masses, which is possible in this work given the independent y_2 and with w sufficiently larger than v such that $m_{\nu_1'}, m_{\nu_2'}, m_{\nu_3'} \sim 100\,\text{MeV}$. We thus consider the first case of only a relativistic dark photon in the region of parameter space where $\rho > 200$ as mentioned previously. From the temperature difference generated by the drop in degrees of freedom between the confinement scales we obtain

$$\Delta N_{\rm eff} = \frac{2}{0.45}\left(\frac{T_D}{T_V}\right)^4 \simeq 0.17, \tag{4.49}$$

where the factor of 2 counts the degrees of freedom of the single dark photon. This is well within the observationally allowed limits. The thermal history of the universe in this case is summarised in Table 4.4 at the end of the chapter. Figure 4.7 shows the degrees of freedom in each sector in this timeline.

4.7.2.2 Small ρ

The other case keeps all three dark neutrinos relativistic and has a sufficient temperature difference to allow for all four of these species. In order for neutrinos to undergo the temperature change from the above mechanism, it is critical that the lightest neutrino population not decouple from the dark plasma prior to the thermal decoupling of the two sectors. As the dark weak interaction rate scales down with the increasing mass of

the dark electroweak gauge bosons, an upper bound of $\rho < 200$ can be placed assuming that the maximum value of $T_{\rm DEC}$ is just below the dark confinement scale. While in Ref. [144] the large change in g^* following the dark QHPT is only large enough to allow for one light neutrino species of the dark sector, the independent Yukawa couplings of the dark sector allows for a more complex thermal history. In particular any asymmetry between the two sectors in whether a species annihilates into photons before or after $T_{\rm DEC}$ can further the temperature difference.

- Consider in particular the $\mu^{+\prime} + \mu^{-\prime} \leftrightarrow \gamma' + \gamma'$ annihilations after the temperature of the plasma drops below the dark muon mass, but at a temperature above $T_{\rm DEC}$. The energy density is shared between the two sectors. After $T_{\rm DEC}$ when T_V falls below the mass of SM muons the visible plasma is heated but the dark plasma is not. This asymmetry in muon annihilation together with the entropy shift between the confining phase transitions, and with three light mirror neutrinos leads directly to $\Delta N_{\rm eff} = 0.50$.

- We can take this further by considering the dark pions. If these have a mass that is above $\Lambda_{\rm QCD}$ and above $T_{\rm DEC}$ then they too will share the entropy density. The scaling of pion mass will depend more significantly on the bare masses of the lightest dark quarks and in particular will increase with more massive bare dark quarks. With the asymmetric photon injection from both dark pions and dark muons one obtains $\Delta N_{\rm eff} = 0.387$.

- If in addition to dark muons and pions we also have that all of the dark electron energy is shared between the sectors, this yields $\Delta N_{\rm eff} = 0.229$, which is well within the current constraints. We can also have a thermal portal that decouples the two sectors when the temperature falls below the mass of dark electrons, due to dark electrons being reactants in the portal term. In this case only a fraction of dark electron energy will be transferred to SM species while the thermal portal is still active, so that $\Delta N_{\rm eff}$ will therefore be between 0.229 and 0.387

Each of these thermal histories for relativistic light dark neutrinos sets a different final temperature for the dark neutrino species and therefore contributes a different limit to how massive the light neutrinos of the dark sector can be before contributing too much hot dark matter to the model. Taking the limit that $\Omega_{\rm HDM} < .011$ we obtain for the

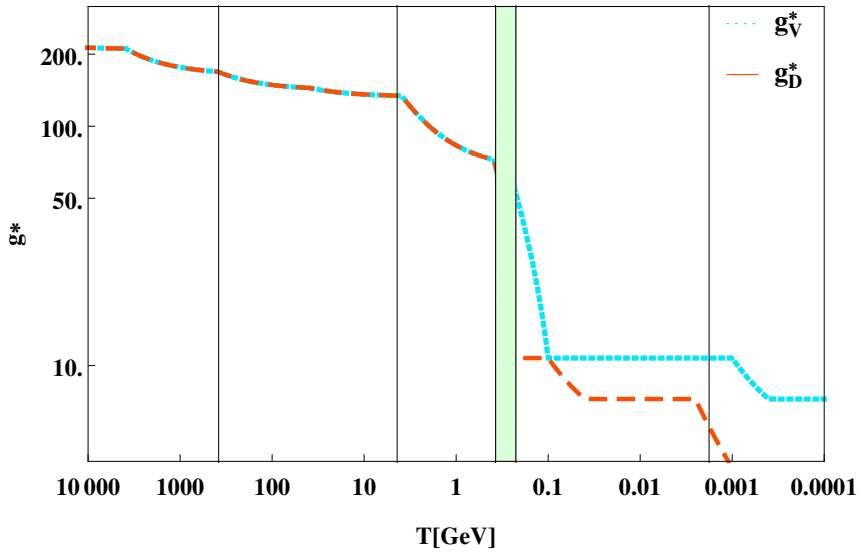

FIGURE 4.7: The degrees of freedom in the two sectors as a function of T. Initially they constitute one sector. After the thermal decoupling the two sectors are independent and the degrees of freedom have separate histories. For $\Lambda_{\rm QCD} < T_{\rm DEC} < \Lambda_{\rm DM}$ the ratio of temperatures after decoupling can fall to $T_D < 0.5T_V$ as the entropy density of the dark sector is shifted to the visible sector in the shaded region. The effective g^*_D contributing to the expansion rate is then suppressed by this temperature difference. The arrangement of dark quark masses is not significant to this picture. Any dark quarks that become suppressed prior to $\Lambda_{\rm DM}$ will contribute to the difference in g^*, however any that are still in equilibrium will hadronise at $\Lambda_{\rm DM}$ and thus their degrees of freedom will be removed in any case. The temperature shift can be affected by mass scales of dark leptons and the dark pion mass scale.

above three cases a limit of $\sum m_{\nu'} < 1.1\,\text{eV}, 3.2\,\text{eV}, 5.6\,\text{eV}$ respectively. This sets a limit on how large a role y_2 can take in the low ρ regime of thermal leptogenesis.

4.7.2.3 Decoupling mechanism

In the relativistic decoupling case it is natural to examine the effective interactions between the sectors that our model contains to observe if any of these can maintain contact until the appropriate region. Since the scaling of the Hubble rate is of the form

$$H(T) = \sqrt{\frac{4\pi^3}{45}}\frac{\sqrt{g^*}T^2}{M_{\rm pl}}, \tag{4.50}$$

we require that such reactions scale with temperature at a faster rate. It would be preferable to have a portal that naturally switched off at the appropriate energy scale. One appealing possibility is a dimension-9 quark interaction, that constitutes a neutron portal operator,

$$\frac{1}{M^5}\,\overline{u}\overline{d}d\,u'd's' + h.c. \tag{4.51}$$

The u', d' and s' states here could in fact be other quark flavours, what is important is that the two flavours that make up the dark neutron are involved and a third with mass below 1 GeV. This ensures that dark neutrons do not decay into ordinary neutrons. Studying such an operator within the regime where one sector has become confining and the other has not becomes difficult due to the chaotic nature of the quark hadron phase transition. It is possible however that the QHPT itself can be held responsible for breaking the thermal contact between the sectors. In such a scenario once the dark quarks of the DS have formed bound neutron states, these can then decay into VS quarks, which are still unconfined, transferring a sufficient amount of entropy density from the DS to the VS. Since the dark neutrons have a mass greater than than the dark confinement scale they immediately begin being suppressed in their numbers following the chiral phase transition, and at the time of confinement in the VS, when quarks of the SM form bound baryonic states, the abundance of reactants is sufficiently small that thermal equilibrium between the sectors has ended. While this argument contains a natural explanation for a lower temperature DS, it is speculative. We can also consider a six-fermion leptonic interaction between the sectors that could accomplish a similar goal.

$$\frac{1}{M^5}\overline{l}\overline{l}\overline{e^c}\, l' l' e^{c\prime} + h.c. \tag{4.52}$$

This type of operator can become ineffective at the temperature when the dark charged lepton e' becomes Boltzmann suppressed. This requires that the mass of this species is tuned to be in the specific range between the confinement scales. In the large ρ case we will see that we require an electron like species to have mass much smaller than this scale and so we can again consider a particular flavour structure for the operator in Eq. 4.52 such as $l'l'\mu^{c\prime}$ for the dark sector. This allows us to choose dark muons to be the species that becomes suppressed between $\Lambda_{\rm QCD}$ and $\Lambda_{\rm DM}$. If, however, we are in the low ρ regime, the original portal involving electrons can be involved which can allow all three light dark neutrinos and a dark photon to be consistent with the extra radiation bounds during BBN and the CMB formation. Such an operator could fall below the Hubble rate due to the lightest charged leptons becoming Boltzmann suppressed at the requisite temperature range. Efficient weak interactions of the dark sector can then remove the remaining asymmetric component of dark electrons along with the more massive dark protons and store the lepton asymmetry of the dark sector in the dark cosmic neutrino background.

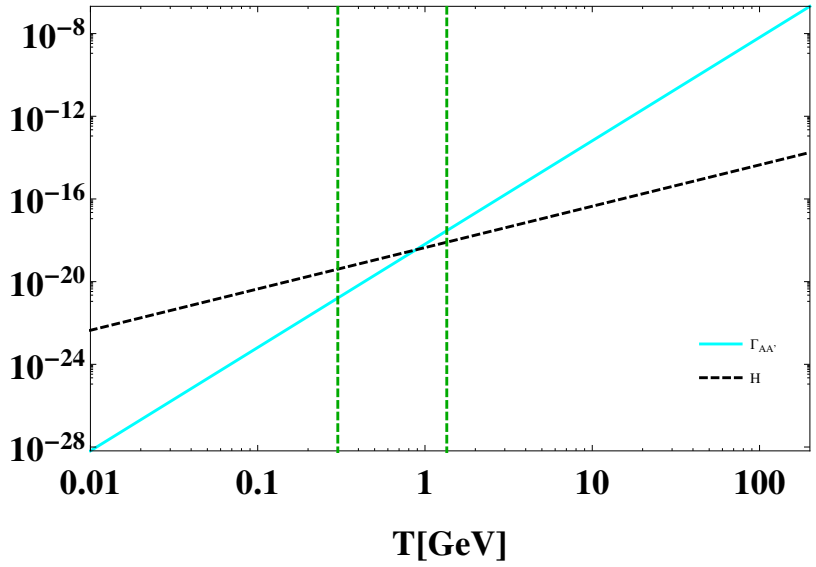

FIGURE 4.8: Higgs mediated four fermion interaction rate as a function of temperature falling below the Hubble rate between the confinement scales (Green) of the two sectors. The rate uses $[\eta_1 = 0.6, \eta_2 = 0.6, z_{10} = 0.1, m_{A_1} = 3525\,\text{GeV}, v_1 = 246\,\text{GeV}, w_2 = 7380\,\text{GeV}]$

We can also consider the Higgs mediated interaction that survives below our EWSB scales consisting of the mixing between heavy neutral scalars of the two sectors. The four fermion interaction rate can be written as

$$\Gamma_{AA'} \simeq {\eta_2}^2 {\eta_1}^2 z_{10} \frac{v_1^2 w_2^2 T^5}{m_{A_1}^8}. \tag{4.53}$$

This term can provide a way to couple the two sectors without altering the global minima of the potential and removing the asymmetric configuration or mixing the weak scales of the two sectors. Additionally, such a Higgs mediated interaction can thermally couple the two sectors down to $\sim 1\,\text{GeV}$ in a way that an ordinary mixing of a Higgs with a mirror partner cannot. In our model, using a typical Higgs mediated interaction in order to maintain thermal equilibrium to a low enough temperature, the Yukawa couplings would need to be sufficiently large. However if these same Yukawa coupling give mass to the fermions involved in the cross-sector interaction, then they will be Boltzmann suppressed prior to $T \sim 1\,\text{GeV}$ and hence the interaction cannot remain above the Hubble rate at this low a temperature range. In our model, since the interaction utilises those Higgs doublets that are not responsible for mass generation in their respective sectors, such a coupling can work if the mass hierarchies permit some low mass fermions of the SM to have heavy mirror partners in the dark sector and vice versa. In Fig. 4.8

we examine the scaling of such a Higgs mediated interaction with temperature in the small ρ regime. Other portal operators have been explored. Setting the ZZ' mixing to a suitable value forces the photon kinetic mixing to keep the two sectors in thermal contact to the present day which is unacceptable for our theory.

4.7.3 Dark big bang nucleosynthesis

In the dark sector, the confinement scale is approximately five times higher than its visible sector counterpart while the electroweak scale can span a much broader allowed parameter space given by ρ. With the larger EW scale in the dark sector we also have larger masses for the W' and Z' bosons. The independence of the Yukawa couplings that generate mass for fermions in each sector also allows for the lightest baryon of the dark sector to be neutral under $U(1)'_Q$. For ordinary baryons, the mass difference of the proton and neutron, $\delta m = m_n - m_p$, can be considered as the sum of two components. The first is from QCD which can be approximated by the mass difference of the up and down quarks $\delta_{\rm QCD} \simeq m_d - m_u \approx 2.51$ MeV. The second is from EM interactions and is given by $\delta_{\rm EM} \approx -1.00$ MeV. We then have $\delta_m = \delta_{\rm QCD} + \delta_{\rm EM} \approx 1.51$ MeV. By reducing the difference in mass of the lightest of up and down type dark quarks, we can reduce the QCD contribution until $|\delta_{\rm QCD}| < |\delta_{\rm EM}|$ for dark baryons. The variation of the dark electroweak scale does impact the size of the QED correction to the proton through the change in $\alpha_{\rm EM}$, however this correction is insignificant. This can be seen by the matching condition $\frac{1}{\alpha_{\rm EM}} = \frac{1}{\alpha_1} + \frac{1}{\alpha_2}$, and the fact that the $U(1)$ and $SU(2)$ gauge couplings run in opposing directions such that variations in the symmetry breaking scale only minimally alter the value of $\alpha_{\rm EM}$.

The lightest baryon of the dark sector is then the dark neutron n' and the decay rate of the dark proton p' into the dark neutron is suppressed by the larger mass of the dark sector W' bosons. If the dark weak interaction rate now falls below the Hubble rate at an earlier point, it is possible to find a situation in which the dark BBN produces a maximal amount of dark helium, by contrast with the visible sector, despite the dark neutron being the most stable baryon. This is because the n'-p' ratio will be sensitive to the interactions that are still in equilibrium in the dark sector as well as the mass difference between them. However, the formation of nuclei through primordial synthesis may not take place at all if the dark deuteron is unbound. It is a well known feature of

conventional BBN that the deuteron, the bound state of one proton and neutron, is only very weakly bound [163]. Its function in BBN is essential, however, in that it forms the intermediate step between hydrogen and heavier elements such as helium. A sufficient abundance of deuterium only appears at temperatures lower than 2.2 MeV due to its low binding energy. The binding energy of the deuteron can be related to the ratio of $\frac{m_\pi}{m_p}$ which has been estimated to need to be < 0.16 for the deuteron to be stable. We can reconsider this ratio in terms of the factor $x_D = \frac{(m_u+m_d)}{\Lambda_{\rm QCD}}$. In Ref. [164], a conservative estimate of the required ratio to make the deuteron unstable was found to be that x_D should increase by a factor of 2.5. Such an increase can be readily achieved in our model provided that the low mass dark quark masses are larger than ~ 35 MeV, where ΛDM is ~ 5 times the SM value. If the dark deuteron were to be unbound, its absence in the primordial era of statistical nuclear equilibrium would disallow the formation of helium and heavier elements. The makeup of dark matter is then dependent on a number of free parameters in our theory. We summarise these distinct cases below.

4.7.3.1 Large ρ

In this case, with $\rho > 200$, we have the fact that dark weak interactions are suppressed by the time of the dark QHPT and the light dark neutrinos have a mass scale $\sim 100\,$MeV. The dark lepton and baryon asymmetries are fixed at their values following the sphaleron conversion and dark weak interactions prior to 1 GeV similar to [141]. This yields the initial relations $\mathcal{N}'_B = (8/23)\mathcal{N}'_{B-L}$ and $\mathcal{N}'_L = -(15/23)\mathcal{N}'_{B-L}$. If we assume that the lepton asymmetry in this phase is evenly divided among relativistic lepton flavours then the distribution between charged and neutral leptons can be found by solving the series of equations that relate the chemical potentials after the dark EWPT until dark EW interactions freeze. Using the conservation of lepton and baryon number, conservation of charge and the enforced relations from weak interactions such as $\mu_d = \mu_u + \mu_e - \mu_{\mu_e}$ we solve these equations at the point just prior to when this last weak interaction condition is removed and the charge distribution between the baryon and lepton sectors is set [165]. This is dependent on how many fermion species have been removed from the plasma when the dark weak freeze-out occurs. For all dark fermions in the plasma at freeze-out we have that the ratio of the asymmetry stored in charged leptons compared to neutral leptons of 82 : 83, while removing the two heaviest quarks yields 13 : 17. Additionally removing a third quark and a single charged lepton yields 2 : 3. Dark

QED charge conservation guarantees that the dark proton asymmetry equals the dark charged lepton asymmetry. This yields an abundance of charged leptons equal to that of charged protons such that we have a mix of dark neutral hydrogen atoms and dark neutrons after the dark QHPT. This asymmetry is then equal to the value of the lepton asymmetry stored in charged leptons just above the dark weak freeze-out temperature. The lepton asymmetry stored in the light neutrinos of the dark sector at the point of dark weak freeze-out will ultimately be transferred to the visible sector's neutrino background following the decays of these states to visible species. We can then write the number densities of dark species in terms of the B', L' and $B'-L'$ number densities with $n'_p = n'_e$ and $n'_p + n'_n = (8/23)n'_{B-L}$ such that $n'_n = (8/23)n'_{B-L} - n'_p$. The cases listed above then give neutral atoms and dark neutrons in ratios of 15:31, 13:29 and 3:7 respectively. This assumes that the dark charged-lepton that is part of dark atoms has both a small enough mass to survive to low temperatures and to not be an important contributor to the overall dark matter mass density. We can thus have a component of mirror atoms among the dark neutrons.

The later distribution between dark atoms and dark neutrons depends significantly on a number of further assumptions we make for dark sector parameters. If the mass difference between dark protons and dark neutrons, $Q = m'_p - m'_n$, is larger than the sum of the masses of dark electrons and dark neutrinos, dark protons may decay with a lifetime dependent on both the increased EW scale of the dark sector and a phase space factor which can be compared to that of the SM neutron. We can consider the case where the value of Q becomes larger than 100 MeV, while keeping the dark electron mass negligible and the dark neutrino mass fixed at 100 MeV [166]. Dark protons can then all decay prior to the matter-dominated era. Increasing ρ necessitates larger values of Q to achieve this as the weak suppression increases the lifetime by a factor of $\sim \rho^4$.

In the case that dark protons are stable due to $m'_e + m'_\nu$ exceeding Q we must also ensure that by the onset of structure formation at matter-radiation equality, $T_V \approx 1$ eV, the dark matter is no longer undergoing long range interactions and can form the early inhomogeneities. This requires that the dark matter-radiation decoupling have taken place prior to the moment of matter-radiation equality. While the lower temperature of the dark sector can bring the moment that free-streaming charged dark particle numbers are suppressed by recombination earlier in time, the dynamic temperature ratio we considered in the large ρ timeline is insufficient alone. However matter-radiation decoupling

in the dark sector may take place at a higher value of T_D compared to the visible sector case. With the Saha equation's exponential dependence on the binding energy of hydrogen we can see that raising the ionisation energy of dark hydrogen through the increased mass of dark electrons directly increases the temperature at which dark hydrogen is no longer ionised [30, 32, 100]. The ratio of T_D/T_V then satisfies the condition that dark matter-radiation decoupling takes place in the radiation dominated era of the universe provided that $T_D/T_V < 0.336\, r$ where r is the ratio of photon decoupling temperatures $r = T_D^{\gamma'}/T_V^{\gamma}$ and is dependent on the ratio of binding energies $r \simeq B'_H/B_H = m'_e/m_e$ if one uses the same condition for sufficiently small fractional ionisation in each sector.

While protons may be stable in this latter case it remains possible for the dark hydrogen atoms to undergo electron capture and decay via $e' + p' \to n' + e^+ + e^- + \nu$ due to the mixing in the neutrino sector considered in Eq. 4.32. This can be compared to muon capture in protons in short-lived μ-hydrogen atoms. Such decays are suppressed by the electron capture probability and the large dark EW scale and have lifetimes approximated by

$$\tau(e' + p' \to n' + e^+ + e^- + \nu) \sim \left(|\psi(0)|^2 \frac{{G'_F}^2 |V'_{ud}|^2}{2\pi} \frac{E_{\rm VS}^2}{M^2} (M - m'_n)^2 \right)^{-1}, \qquad (4.54)$$

where $|\psi(0)|^2 = m_r^3 \alpha'^3/\pi$ measures the wave function at the origin with m_r the reduced mass [167, 168]. The Fermi constant, G'_F, scales with W', $E_{\rm VS}$ is the combined energy of visible sector decay products, V'_{ud} is a dark-sector CKM element and M is the mass of the dark hydrogen atom. With a dark electron $\sim$ 10 times the SM electron, and dark protons and dark neutrons at $\sim$ 5 GeV, this suggests a lifetime for these dark atoms between $\sim 10^{14}$ seconds for $\rho = 200$, that is around the time of reionisation in the visible sector, to beyond the current age of the universe for $\rho > 2500$. The decays of such states could be a promising source of indirect detection for dark matter if their lifetime is between these values. The above formula holds for an on-shell dark neutrino ν', and thus is an approximate lower bound on the lifetime for the general case where ν' is off-shell.

4.7.3.2 Small ρ

In this regime with efficient dark weak interactions, a light relativistic species of neutrino and a sufficiently light associated dark charged lepton we would have charged baryons of the dark sector all decay into neutral single baryon states, due to $m_{p'} > m_{n'}$, which are then the dark matter component of our universe and so we have a complete population of dark neutrons. In order to calculate the relative abundance of n' to p' in the dark sector during BBN we begin by taking the initial abundance of these species after the dark QHPT to be near equal, given the small mass difference between them. The value of ρ will determine the ratio of dark protons to neutrons. With the mass difference, $Q = m'_p - m'_n$, we can write

$$X_p = n'_p/(n'_p + n'_n) = e^{-Q/T'}/(1 + e^{-Q/T'}). \tag{4.55}$$

The thermal freeze-out of dark protons occurs when dark weak interactions freeze-out at a temperature of $T_{DWF} \sim 0.8\rho^{4/3}$MeV. Figure 4.9 shows the how close the ratio is to 1:1 as ρ increases.

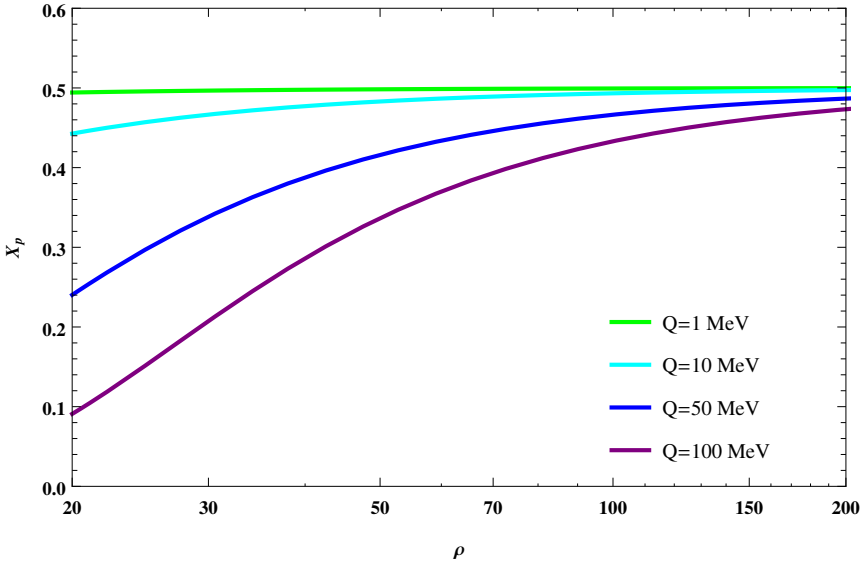

FIGURE 4.9: The ratio of dark protons to dark neutrons, X_p, as a function of ρ for a given mass difference, $Q = m'_p - m'_n$. In the large ρ limit $X_p \to 0.5$.

The lifetime of any remaining dark protons will depend on the mass difference Q and the value of ρ. Assuming a light charged lepton mass and a value of $Q \sim 1\,\text{MeV}$ we have

that in the limiting case of $\rho = 200$ the remaining dark protons will have a lifetime of $\sim 10^{12}\,s$ such that X_p will approach zero at the time of structure formation.

4.7.4 Dark matter self-interaction constraints

The possibility of self-interacting dark matter is constrained by a number of sources. In particular, ellipticity, substructure mergers and cluster collisions [2, 126] impose upper bounds ranging from $0.7 - 2.0\,\mathrm{cm}^2/g$. On the other hand, issues in simulations of ellipticity of galaxy structures, and the core-cusp problem can be solved by interacting dark matter, though the required cross section may in some cases be in conflict with upper bounds [169]. If dark matter interacts according to nucleon scattering where the cross section is set approximately by the size of the nucleon itself, then we can consider this model in the context of other models of dark neutron dark matter. As noted in [169], if the length scale and mass, m_n, of the nucleonic state is scaling with increasing Λ_{DM} then the dark self-interaction per unit mass can be considered as

$$\sigma/m \sim 3\,\mathrm{cm}^2/g \times \left(\frac{\Lambda_{\mathrm{DM}}}{m_n}\right)\left(\frac{\Lambda_{\mathrm{DM}}}{a^{-1}}\right)^2\left(\frac{100\,\mathrm{MeV}}{\Lambda_{\mathrm{DM}}}\right)^3, \tag{4.56}$$

where a is the scattering length which should obey $a \sim \Lambda_{\mathrm{DM}}^{-1}$. If the dark sector is made up of both dark neutrons and neutral dark atoms we can consider the dark neutron-atom interactions and dark atom-atom interactions as well. Since these are neutral we can consider possible magnetic self-interactions, to be discussed later in the analysis in Chapter 5 where we show that dipole-dipole interactions can be below the self-interaction bounds for a dark $\alpha'_{\mathrm{EM}} = \alpha_{\mathrm{EM}}$ and dark matter particles of mass 1 GeV. Compact object formation such as dark stars may also reduce the density of objects in galaxy clusters such that the diffuse gas assumptions which set limits on cross sections are not applicable. The details of dark first generation star formation will depend on the thermal history assumptions and critically on the composition of the dark sector, i.e. the ratio of dark hydrogen to dark helium to stable dark neutrons. In the case of a pure population of dark neutrons, we expect that with small self-interactions compact object formation will not take place. With a mixture of neutral dark atoms and dark neutrons, it is likely that with an unbound deuteron dark stars would not be able to survive without this link

in the nucleosynthesis chain and so would still not be able to achieve the production of heavier dark elements just as in the BBN era.

4.8 Summary

We have demonstrated a class of models that can both solve the number density similarity and provide an explanation for the similar confinement scales of the visible and dark sectors. In this model of dark matter, we have considered the possibility that the gauge group and fermionic content that we observe govern the dynamics in one of two similar sectors. In particular, drawing on the concept of a $\mathbb{Z}_2$ mirror symmetry connecting two copies of the SM gauge group we have seen how symmetric potentials can break mirror symmetric $G_{\rm SM} \times G'_{\rm SM}$ to create two markedly different sectors. One which sets the abundance of visible matter in the universe, and a dark copy with a high EW scale, slightly higher confinement scale and unique fermion flavour mass hierarchy which together sets the larger abundance of dark matter mass in the universe, made up of stable dark baryons. A summary of the universe's timeline that includes both matter and dark matter is shown in Table 4.4 and can be compared to the timeline in Table 1.2. In the next section we will examine in detail the hadronic physics of the dark composite theories we have been discussing throughout this thesis.

TABLE 4.4: The major epochs of the universe including dark matter.

10^{19} GeV	$t \sim 10^{-43}s$	• Planck scale era. Mirror symmetric sectors. $E_8 \times E_8$?
10^{15} GeV	$t \sim 10^{-38}s$	• Inflation ends, Grand unified symmetry breaking scale.
10^{12} GeV	$t \sim 10^{-30}s$	• Majorana neutrinos begin to populate both sectors.
10^{9} GeV	$t \sim 10^{-24}s$	• Thermal leptogenesis produces a $B - L$ asymmetry in the visible and dark sector. • Visible and dark sphalerons create the baryon asymmetries.
10^{5} GeV	$t \sim 10^{-10}s$	• Universe has cooled to allow the Higgs fields of the dark sector to attain a nonzero vacuum expectation value, triggering the dark electroweak phase transition. Dark fermions gain mass. • Mirror symmetry is broken. Thermal interactions between the two sectors are maintained. • One of the visible doublets gains a large positive squared mass term from the cross-sector couplings.
10^{2} GeV	$t \sim 10^{-10}s$	• Asymmetric symmetry breaking VEV breaks the EW symmetry of the visible sector. • Visible fermions gain mass.
1 GeV	$t \sim 10^{-3}s$	• The gauge coupling of the dark $SU(3)$ becomes non-perturbative, breaking chiral symmetry and confining all free dark quarks into hadrons. • The difference in degrees of freedom creates a transfer of entropy to the visible sector.
~ 500 MeV	$t \sim 10^{-3}s$	• Thermal decoupling. The interactions between the two sectors fall below the expansion rate. Each sector evolves independently.
200 MeV	$t \sim 10^{-3}s$	• Visible quarks form nucleons following the QHPT.
1 MeV	$t \sim 180s$	• Dark hadrons persist as individual nucleons. • Dark protons decay into dark neutrons. • The universe's expansion becomes dominated by matter over radiation.
1 eV	$t \sim 10^{12}s$	• Dark neutrons dominate the hadrons of the dark sector forming dark matter and seeding visible structure formation. • Visible atoms coalesce into stars.

Chapter 5

Hadronic Spectra of Dark QCD

5.1 QCD bound states

We have seen that a dark analogue of QCD provides a compelling candidate for the nature of dark matter. In this chapter we will examine more closely the properties that such a dark $SU(3)$ theory might possess. As seen in the previous chapter, the number of quarks and the mass hierarchy among them can be different to that of the Standard Model with asymmetric symmetry breaking. The implications of this freedom and its impact on the possible spectra of dark hadrons will be explored in this chapter.

The study of QCD can be traced back to the hypothesis of the colour quantum numbers in the work of Gell-Mann and Zweig [170]. The wavefunctions of QCD can be expressed as the product

$$\Omega = \Psi_{space}\ \psi_{spin}\ \phi_{flavour}\ \eta_{colour}. \tag{5.1}$$

The total wavefunction must be totally antisymmetric due to the fermion constituents. In the development of the quark model and QCD it was the observation of the symmetric form of the neutron wavefunction without colour that led to the theory of colour charge. As the colour wavefunction is taken to be the antisymmetric colour singlet, the remaining components must combine to be symmetric. We take the ground states of the theory to be symmetric in space leaving the combination of spin and flavour to be symmetric. This forms the famous baryon octet and decuplet of QCD describing the lowest lying states composed of the u, d and s quarks. The states of a QCD-like theory in a hidden sector will follow a similar logic, though the flavour structure will depend on some key

assumptions. For our purposes it will be useful to list these states by the number of flavours. One can imagine a formulation of QCD with only two light quarks, containing only those states that possess an up and a down quark, a down and a strange quark or an up and a charm quark.

In order to calculate the details of these exotic $SU(3)$ theories, we consider in this chapter the zeroth order approach to the hyperspherical non-relativistic constituent quark model for calculating the hadronic spectra, namely the hypercentral model [171–174].

In this case we take the masses of light quarks to be approximately equal at a scale m_l. As such the constituent masses of these quarks will be expressed as m_q. This constituent quark mass can be taken, in the approximation that $m_l \ll \Lambda$, to be one third of the degenerate baryon mass scale E_0. The mass scale is in turn proportional to Λ which we treat as a free parameter of the theory. In the case of $G \times G$ symmetric theories it is a function of the running of α_3 and the heavy quark mass thresholds at scales above Λ. In the hypercentral approach the inter-quark potential is a function only of the hyperradius $x = \sqrt{\rho^2 + \lambda^2}$, where ρ and λ are the Jacobi coordinates. The spatial wavefunction is factorised as

$$\psi_{\gamma n}(\rho, \lambda) = \psi_{\gamma n}(x) Y_{[\gamma] l_\rho l_\lambda}(\Omega_\rho, \Omega_\lambda, \phi), \tag{5.2}$$

where the angular part is written in hyperspherical harmonics and $\phi = \tan^{-1}(\rho/\lambda)$.

$$Y_{[\gamma] l_\rho l_\lambda}(\Omega_\rho, \Omega_\lambda, \phi) = Y_{l_\rho, m_\rho}(\Omega_\rho)\, Y_{l_\lambda, m_\lambda}(\Omega_\lambda)\, P_N^{l_\rho, l_\lambda}(t). \tag{5.3}$$

For the hyperradial part we can write down the Schrödinger equation for a given interaction potential $V(x)$,

$$[\frac{d^2}{dx^2} + \frac{5}{x}\frac{d}{dx} - \frac{\gamma(\gamma+4)}{x^2}]\, \psi_{\gamma n}(x) = -2m_q[E - V(x)]\, \psi_{\gamma n}(x). \tag{5.4}$$

In the next section we will discuss how these methods for ordinary QCD can be adapted to solve for composite theories of the dark sector.

5.2 Hadronic spectra

While the constituent quark model has achieved considerable success in replicating the ground states of the baryon spectrum, in adapting this method to the exploration of a

hidden QCD we have to deal with the fact that the parameters of the theory are taken from the experimental spectra, which are unavailable in the dark sector. In the case of hyperspherical potential models we adopt a method of exploring the possible dark matter spectra by considering simplified models that depend on only a few parameters, and then deducing how those parameters change for the dark QCD case. In particular we consider models in which the lightest dark quarks have near degenerate mass and where the baryon mass scale $E_0 \sim \Lambda_{\rm DM}$ is a free parameter. This is based on our treatment of $\Lambda_{\rm DM}$ itself as a free parameter of the theory following the work in previous chapters. In such models of asymmetric dark matter the UV value of $\alpha_{\rm DM}$ was fixed by the $\mathbb{Z}_2$ symmetry imposed on the $G \times G_{\rm mirror}$ theory. $\Lambda_{\rm DM}$ will then vary from $\Lambda_{\rm QCD}$ by the location of mass thresholds of dark quarks with mass greater than $\Lambda_{\rm DM}$, making the latter parameter different from the SM value, $\Lambda_{\rm QCD} \sim 200\,\text{MeV}$, following the mechanism of asymmetric symmetry breaking in Chapter 2 and Chapter 3. In these models, the heavy dark quarks may have masses significantly larger than the dark confinement scale: $m_q \gg \Lambda_{\rm DM}$. As these very massive degrees of freedom have no effect, except through their production of a given $\Lambda_{\rm DM}$, on the ground state of the dark $SU(3)$ theory, the locations of the thresholds can be made to produce a given low scale value of $\Lambda_{\rm DM}$ and thus E_0. The lightest dark quarks with negligible bare mass then have a dressed mass of $\sim E_0/3$.

With the variation of $\Lambda_{\rm DM}$ we also vary accordingly the length scale of the inter-quark potential and any other dimensional parameters associated with $\Lambda_{\rm DM}$ in the theory. One of the simplest quark interaction forms is described by the Cornell-type potential,

$$V(x) = -\frac{\tau}{x} + kx, \tag{5.5}$$

consisting of a hyperCoulombic and a linear term. As in the bag model of QCD, where the length scale of confinement scales inversely with the energy scale, we will vary the length scale of the potential and constituent quark masses with $\Lambda_{\rm DM}$. The parameters of the reference potential will be fitted to the Standard Model's ordinary QCD spectra and a number of different potential forms will be used for comparison. We will focus on the ratio of confinement scales in the two sectors used previously,

$$\xi = \frac{\Lambda_{\rm DM}}{\Lambda_{\rm QCD}}. \tag{5.6}$$

In a model with high scale mirror symmetry, large values of ξ are less likely since mass thresholds only vary the rate of running slightly and so similar QCD mass scales for the two sectors are well motivated by the insensitivity of the scale of dimensional transmutation to higher mass scales in the theory. In such models, the Yukawa couplings of the two sectors are also independent despite the high scale mirror symmetry. This can be seen as an effect of both the different running couplings and the fact that the Higgs mechanisms responsible for mass generation in the two sectors can involve scalar states that are not mirror partners. In this work we similarly take the Yukawa coupling constants of the dark quarks to be effectively unrelated to those of the corresponding ordinary quarks.

If $\xi > 1$ and the lightest dark quark bare masses are comparable to the up and down quark of the SM, then the approximate chiral flavour symmetry becomes more exact as ξ increases. This can be compared with our own QCD where it is the small quark masses relative to the confinement scale that generates the isospin symmetry. No symmetry connecting the bare up and down quark masses is necessary for strong isospin, only that they are small enough to be insignificant compared to the near equal constituent masses the quarks gain from chiral symmetry breaking within the bound states in the constituent quark model. It is in this sense that a dark QCD with n_l light flavours with masses $m_l \ll \Lambda_{\rm DM}$ can form an $SU(n_l)$ analogue of strong isospin. The assumption of near degenerate dark quarks is then seen to refer to constituent masses. This dark isospin is then a consequence of any hidden QCD where fermions gain mass via a Higgs-like mechanism and the product of the hidden sector Higgs VEV v_D and any dark quark Yukawa couplings are small in relation to the dark confinement scale. As the light dark quarks form the lightest bound states of a dark QCD, any coloured fermions more massive than the confinement scale will decay to lighter states of the theory and only be produced in small numbers following the dark quark hadron phase transition. We also consider states analogous to the strange quark of QCD which have a mass which can be less than $\Lambda_{\rm QCD}$ but can still contribute a significant amount to hadronic masses. There also exists the limiting case of when all of the dark quarks have mass above $\Lambda_{\rm DM}$, which has been explored in models such as [175–177] where the possibility of glueball dark matter is examined. In the case of six massless quarks and a baryonic mass scale $E_0 \sim \Lambda_{\rm DM}$, [1] the meson states will have zero mass as genuine Goldstone bosons. The

[1] The effects of the strange quark as a virtual state contributing to the mass of the proton has a long history. It is estimated that a massless strange quark may lower the nucleon mass scale of QCD by between $\sim 1 - 20\%$ [178].

exception is the Goldstone Boson associated with the breaking of the anomalous $U(1)$ axial symmetry. In QCD it is the η'. Importantly, in one flavour QCD, the only meson of the theory will gain an anomalous mass and so even in a dark QCD model with a single massless quark, there will be no massless Goldstone bosons. We will briefly discuss this particular case in the next section.

To compute the mass spectra of a dark QCD, we apply the hCQM and scale relevant parameters with the confinement scale. In the simplest potential model with an inter-quark interaction as in Eq. 5.5, the size of the bound state can be compared to the radius at which the potential transitions from Coulomb-like to linear. This follows directly from our treatment of the confinement scale as a free parameter, in that we are adjusting the scale at which the hidden QCD theory transitions from perturbative to non-perturbative. This transition radius then decreases inversely with ξ. This can be seen directly in the case of Eq. 5.5 where k has units of $(\mathrm{E})^2$ and so becomes $\xi^2 k$ in a scaled potential. The crossing point is then $r_c = \sqrt{\frac{\tau}{k}}\frac{1}{\xi}$. This relationship can be seen in Fig. 5.1. The shape of

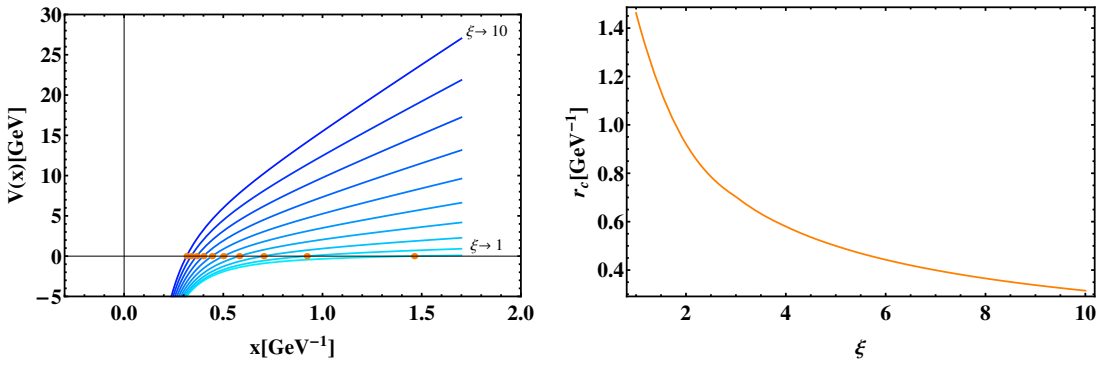

FIGURE 5.1: The variation of an example hypercentral potential V(x) with ξ (left) and the value of r_c, an estimate of the radius of confinement, as a function of ξ (right). By scaling the dimensionful parameters of the interaction potential with confinement scale, we are directly scaling the range at which the interaction transitions from perturbative to non-perturbative.

the potential directly affects the masses of bound states and in particular has important consequences for resonance states and the size of the hyperfine corrections. We now turn to the computation of the dark hadron spectra of different cases of a hidden QCD. The masses also depend on the reference potential that we can scale from and which is taken from past work on potential models of QCD in order to replicate the masses of the hadrons of the Standard Model.

5.2.1 Baryon spectra

We distinguish the cases by the number of light dark quarks in the theory and examine how the spectra change with the confinement scale. Including electromagnetic effects we can consider that as $\Lambda_{\rm DM}$ increases and r_c decreases the size of the EM mass contribution to neutral and charged states will be more significant. In particular, if we consider the simple expression for the scaling of the EM self-energy of a neutron as [179]

$$\Delta_{EM} \sim -\frac{\alpha}{\langle x^2 \rangle^{1/2}}, \tag{5.7}$$

then this term will scale upwards with ξ as the distance becomes smaller. The proton by comparison has a positive mass contribution that also scales with ξ and the difference between these will push charged states above the masses of neutral states for the case of light quarks of equal mass. Such contributions are not however to be subtracted from the calculated neutral ground states in the hypercentral analysis as they are in theory already factored in by the Coulombic term scaling of the potential and the fact that the potential was fitted to the experimental neutral masses from the PDG for $\xi = 1$. For this reason, our work is most applicable to theories of a dark QCD with an EM $U(1)$ coupling strength the same as that of ordinary electromagnetism. In models of broken mirror symmetries the value of the dark sector's EM coupling constant is constrained to be very close to that of the SM value due to the opposite direction of the running of $U(1)_Y$ and $SU(2)_W$ and so the model in this work is directly applicable to the QCD spectra of these models. In a theory without an EM gauge group, the EM mass contribution to the effective potential must be separated in order to remove its effect from the mass ordering.

For larger confinement scales the effect of EM $U(1)$ force in the theory will create mass differences pushing any charged states well above any light neutral ground states if the set of light quarks allows for them. The only counter to this is if the bare dark quark mass differences compensate for the EM mass difference as in the case of the proton-neutron mass splitting of ordinary QCD. This can be contrasted with the effect of ξ on the chromomagnetic spin-spin interactions that we employ and which scale inversely with the dark confinement scale and thus increase the degeneracy between the doublet and quartet in two flavour dark isospin, and between the octet and decuplet in three flavour dark isospin. This term crucially depends on the spatial wavefunction and the contact

term for overlapping quark coordinates $\langle\delta^{(3)}\rangle = |\psi(0)|^2$. The spin-spin interaction in the form of the chromomagnetic contact term is [180]

$$V_{ss} = \sum_{i<j} \frac{4}{9\pi} \frac{\alpha_s}{m_i m_j} \delta^{(3)}(r_{ij})\, \sigma_i.\sigma_j\,. \tag{5.8}$$

Note the inverse scaling with constituent masses $m_i m_j$ which will increase degeneracy between the mixed symmetry and totally symmetric baryon multiplets. This term is analogous to the magnetic spin-spin contact interaction that gives rise to the hyperfine splittings in atomic theory however in this case is motivated by the colour-magnetic moments. This term is important in understanding the $\Lambda^0 - \Sigma^0$ and $\Delta^0 - N$ mass differences in QCD where the flavour composition is identical and the spin-flavour wavefunction is different, a unique feature for baryon wavefunction ground states when the number of flavours exceeds two. They are then similarly important for the present work as they contribute to the mass splitting between the different ground state wavefunctions allowed in the constituent quark model. One could also consider the spin-flavour and spin-orbit interactions and depending on the choice of potential these may contribute more or less significantly. We discuss these possibilities further in Appendix D. In this work we consider models where the spin-spin interaction is the dominant source of these mass differences. In the hypercentral assumption with only one hyperradius we lose the ability to directly calculate the full value of the contact term $\langle\delta^{(3)}\rangle$ for the full coordinate system of three quark wavefunction. The Gaussian-smeared contact term with a functional form

$$\delta^{(3)}(x) = \kappa\, e^{x^2/r_0^2}, \tag{5.9}$$

that is treated perturbatively, is an approximation which has been applied successfully to fitting the light baryons in [171, 181] among others and we similarly use it in this work for the extrapolation to dark QCD states.

In fitting the form of the potential we compare parameter fits done in similar models for standard hadronic spectra. We consider primarily potentials generalising that of Eq. 5.5,

$$V(x) = -\frac{\tau}{x} + kx^{\rho}, \tag{5.10}$$

as well as a perturbative hyperfine interaction given by Eq. 5.8. The eigenstates are then given by $E_{N\gamma}$. This follows the work on visible QCD in [181–183] as well as [184]. The masses of the baryons are then given by $M_B = E_0 + E_{NL}$ where $E_0 = 3m_q$, i.e. it is

the quantity that scales directly with ξ along with the dressed light quark masses. With these different potentials, which all fit the experimental spectra to varying degrees, we can examine the variation of dark baryon masses with the choice of potential. Following the potentials given in [181–184] we list in Table 5.1 three sets of parameters that with Eq. 5.10 provide a good fit to the hadronic spectra. While our starting point was these potentials, our exact choice of parameters prioritises the fit to the ground states over the resonances as these are the most relevant to this work. We are then assuming that such a potential, when scaled, provides the more accurate prediction of dark QCD ground states.

TABLE 5.1: Parameter sets of the three choices of potentials in the fitting to ground states of QCD. The three parameter sets (P1, P2, P3) are taken from the works in [181–183] respectively. The choice of units reflects the units used in the original works.

Model	τ	k	ρ	κ	m_q	r_0	E_0
P1	102.67MeV.fm	940.95MeV/fm	1	616.02MeV.fm	337MeV	0.45fm	913.5MeV
P2	0.5069	0.1653GeV^2	1	1.8609	0.315GeV	2.3GeV^{-1}	0.8321GeV
P3	0.4242	$0.3898\text{GeV}^{5/3}$	2/3	1.8025	0.277GeV	2.67GeV^{-1}	1.1313GeV

We can then calculate the same states for a dark QCD model as a function of the number of light quarks and a value of ξ. The parameters $(\tau, k, \rho, \kappa, m_q, r_0, E_0)$ then all scale appropriately according to the mass dimensions of the chosen potential as discussed in Fig. 5.1. Figure 5.2 shows the fit to ground states of the N and Δ baryons in QCD while Fig. 5.3 shows a scaled version for a value of $\xi = 5$, chosen for the sake of example.
In the one flavour quark case, the baryon spectrum consists of a lightest stable Δ baryon with ground state spin 3/2. In the case of dark electromagnetic $U(1)_Q$ symmetry consistent with the SM it would have EM charge +2 in the case of a single up type quark. It could also be a single down type and so be singly charged with opposite sign. For the mass of this state we can compare with standard QCD in that we calculate the mass from the constituent quarks and the potential energy from the scaled potential including the spin interactions that lifts the ground state according to the chromomagnetic hyperfine interaction in Eq. 5.8. The mesonic states will likewise contain only one state however this lightest meson will be unique in that it has the feature of an anomalous mass from the breaking of the anomalous axial $U(1)$. The size of this anomalous mass in these models of dark QCD with one light flavour is beyond the scope of this work.

In the two flavour quark case, with an isospin symmetry among the light states, the baryon sector will have a spin-flavour $SU(4)$ symmetry. The spectrum then consists of a

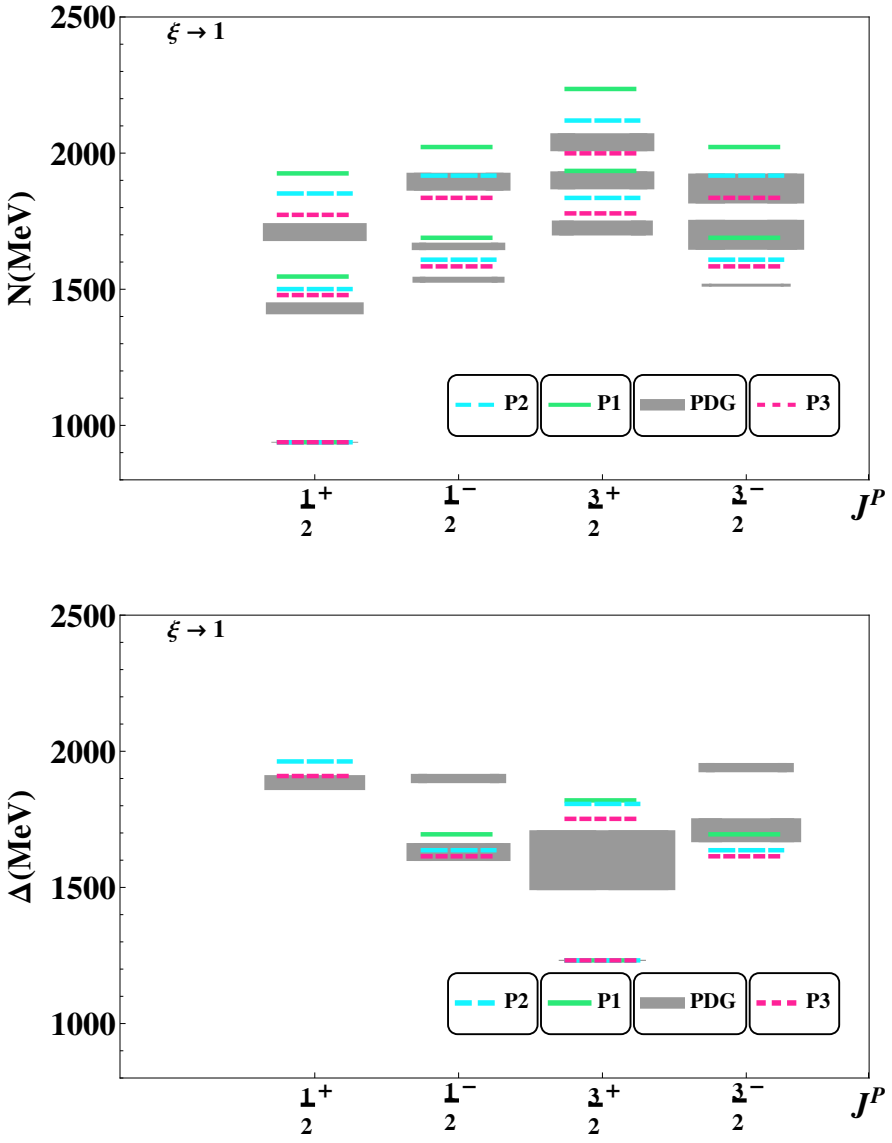

FIGURE 5.2: The resonances of the N and Δ^0 states compared to PDG. The spin 1/2 ground state of the neutron and spin 3/2 ground state of the Δ^0 are fitted to match the experimental ground states exactly in each case. These values serve as the reference for dark QCD calculations.

Δ quartet of spin 3/2 states as well as a spin 1/2 pair (N, P). However we can also consider the cases where this doublet and quartet have charges that follow the possibility of the two light dark quarks being both up type or both down type. The splitting between the doublet and quartet in any scenario is modelled again with the spin-spin contribution which gives the spin 3/2 states larger mass than similar spin 1/2 states while EM effects will make the neutral states lighter in general. For sufficiently light quarks with near equal masses we can consider the spin 1/2 (N, P) doublet as the lightest states in the first case, and with $U(1)_Q$ corrections selecting the neutral state as the lightest ground state. In the case of two up-like or down-like dark quarks, we have degenerate states with equal EM contributions which we label $(\Sigma_c^{++}, \Xi_c^{++})$ and (Ξ^-, Σ^-) following the naming conventions of standard QCD where in this case the flavour content of the theory is taken to consist of near degenerate (u,c) or (d,s) dark quarks.

In the three flavour case we can compare directly with QCD, however again we can distinguish the cases according to other quantum numbers. With three flavours we recover the familiar octet and decuplet however with near degenerate quark masses the spectrum will be near degenerate in flavour unlike the strange quark mass splitting seen in QCD. Again we can consider EM mass differences where flavour content allows for neutral and charged states. In the case of three or more flavours we gain two ways of forming a spin 1/2 wavefunction for ground states as in the case of the Σ, Λ. The differences in terms of Eq. 5.8 are the values of the $\sigma.\sigma$ terms. It remains true however that in the degenerate u, d, s case that N, Σ, Λ have the same mass and share the place of the lightest state.

In Figure 5.4 we show as a function of ξ the lightest spin parity states for each of the lightest baryons in the cases of only one light quark and two light quarks. The case of two light quarks however provides the mass scale of the lightest state for any number of light quarks greater or equal to two.

By observing the spin and flavour symmetries of a given set of light quarks one can construct an equation with a functional form similar to that of the Gell-Mann-Okubo equation which was used to make sense of the mass splittings of ground state hadrons in the quark model. For a dark variant of such an equation, the unknown parameters cannot be extracted from experiment though we can consider how these parameters change from ordinary QCD for a choice of dark QCD. We introduce the additional free

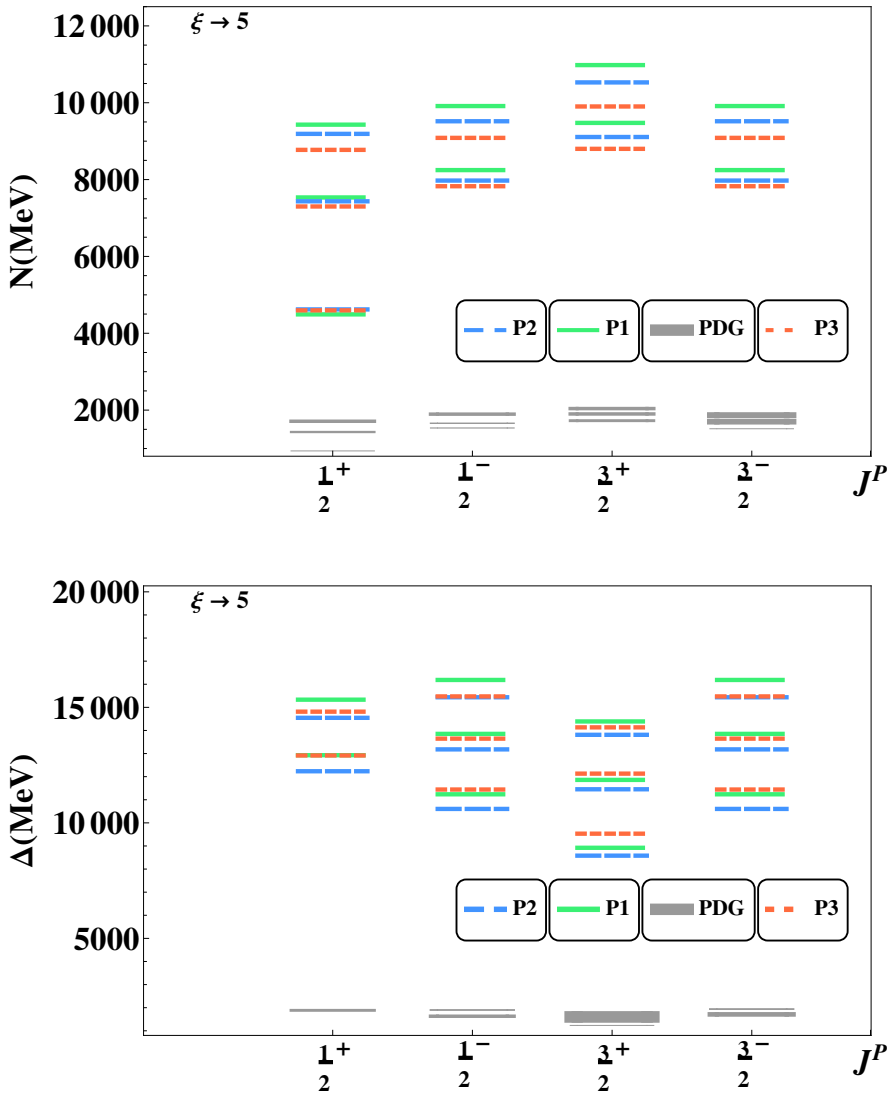

FIGURE 5.3: Spin 1/2 and spin 3/2 for a confinement scale ratio $\xi = 5$ and three light quarks. Dimensional parameters scale with ξ displayed in the upper left. The PDG values for the experimental spectra are shown for reference to the scale of the $\xi = 1$ case. Each of the results (P1,P2,P3) corresponds to a choice of parameters for the $\xi = 1$ potential given in Table 5.1.

parameter δm_s as the mass difference between the constituent quark mass of the light states and the constituent mass of a semi-light state, analogous to the position of the strange quark in QCD. In particular we consider the spin, and hypercharge symmetries of the set given by the $SU_S(2)$ and $U_Y(1)$ groups. We also include the generalisation of isospin, $SU_I(n_l)$ where n_l is the number of light flavours. This leads us to the form of the Gürsey-Radicati mass formula, which was used to explain the Gell-Mann-Okubo

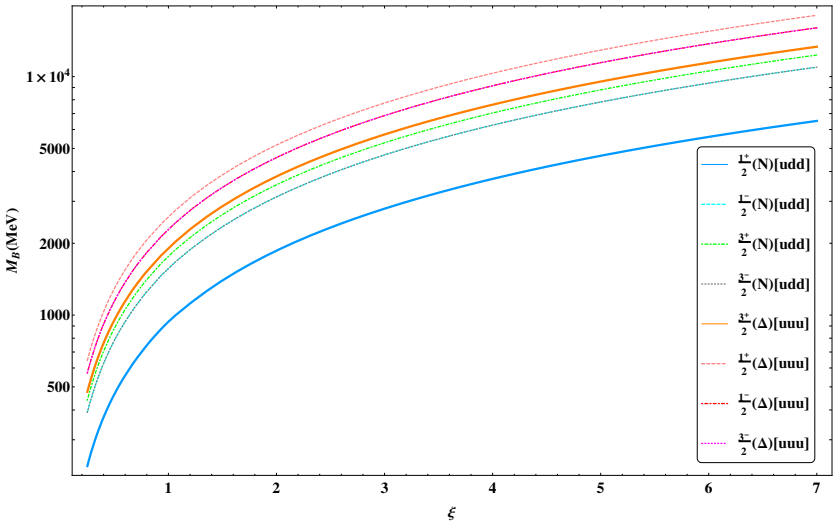

FIGURE 5.4: Spin 1/2 and spin 3/2 states as a function of the parameter ξ, the ratio of confinement scales. The direct scaling with confinement scale becomes more significant at large ξ as one expects from dimensional analysis. This uses an average of the three parameter regimes P1, P2 and P3. Using this plot we can see at each value of ξ the lowest lying baryon in a dark QCD spectrum for models of: one flavour (uuu, orange), or with two or more flavours (udd, blue).

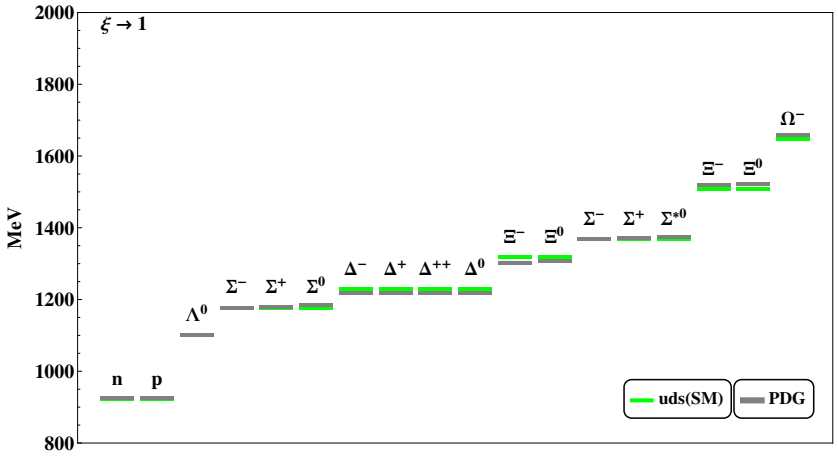

FIGURE 5.5: Baryon states in our model for visible QCD compared to PDG values [185]. Parameters for the Gürsey-Radicati formula are fitted from the baryon mass results of the hypercentral Schrödinger equation.

mass relations [186], which is written as

$$M = M_0 + C\,C_2\left[SU_S(2)\right] + D\,C_1\left[U_Y(1)\right] + E\left(C_2\left[SU_I(n_l)\right] - \frac{1}{4}(C_1\left[U_Y(1)\right])^2\right), \quad (5.11)$$

where C_1, C_2 are the quadratic Casimirs for each group. In the case of QCD this becomes

$$M = M_0 + C\,S(S+1) + D\,Y + E\left[T(T+1) - \frac{1}{4}Y^2\right] \quad (5.12)$$

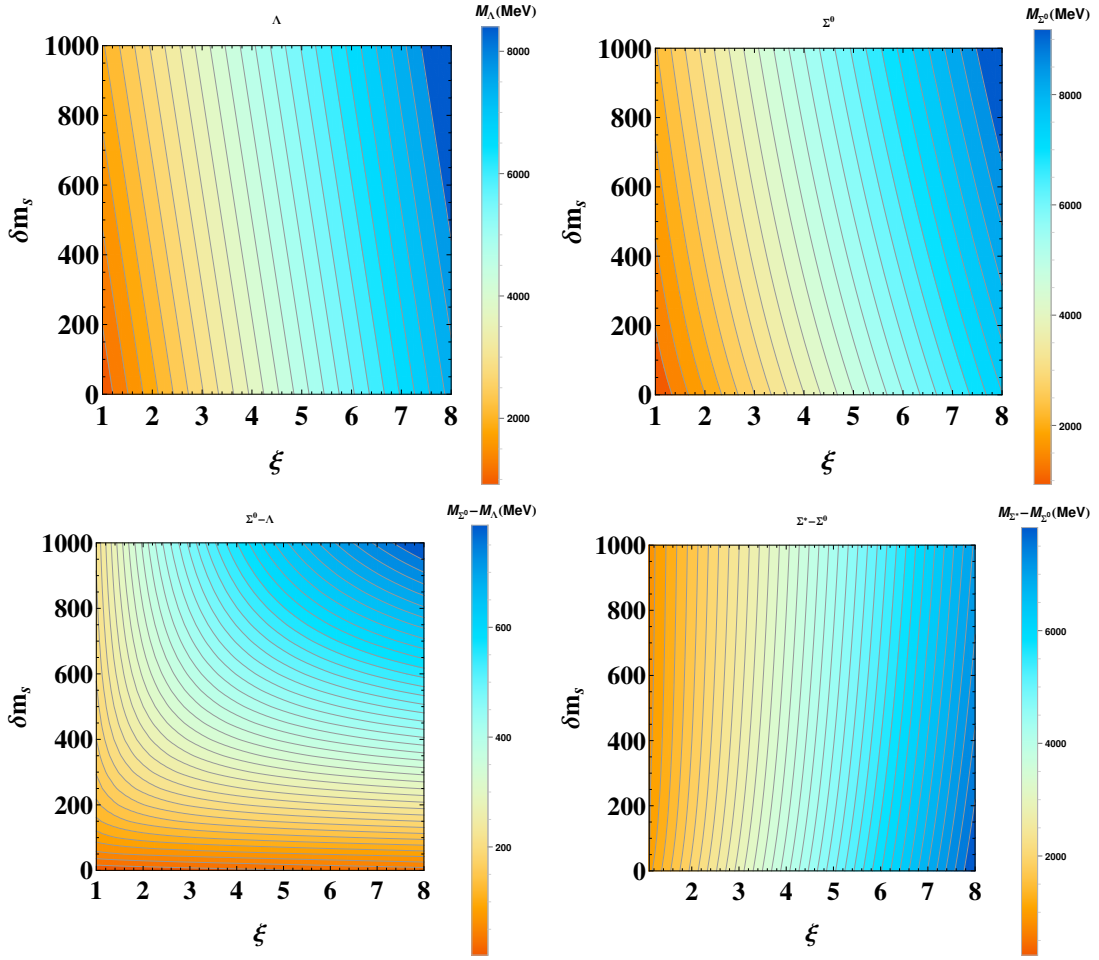

FIGURE 5.6: The top two plots shows the masses of the dark sector Λ^0 and Σ states for a range of values of the semi-light mass splitting δm_s and ξ. The lower plots display the mass differences for the Σ and Σ^* baryons as well as the mass splitting of the two different 3-quark spin-flavour wavefunctions (Λ, Σ) for a range of δm_s and ξ.

and works quite well in reproducing the masses of the octet and decuplet, of ground states in QCD, as shown in Fig. 5.5. In Eq. 5.12 M_0 is a new scale that places the energy of the full baryon spectrum rather than being E_0 itself. However from the hypercentral analysis to find the ground state of a confining theory with n_l light flavours and a given E_0 we can predict the mass of the ground state and working from this result determine the value of M_0. This idea follows the applications to the experimental QCD spectrum in [187] where the $SU(6)$ spin-flavour symmetric Hamiltonian is solved numerically to find the central values for the Gürsey-Radicati formula. The experimental states typically

chosen to fit the parameters are, in terms of ground states,

$$\begin{aligned} \Sigma^* - \Sigma &= 3C \\ \Sigma - N &= \frac{3}{2}E - D \\ \Lambda - N &= -D - \frac{1}{2}E. \end{aligned} \tag{5.13}$$

We can then use Eq. D5 to obtain a minimal number of baryon ground states and refit the above parameters, for a choice of ξ and δm_s, based on our calculated eigenvalues instead of the experimental spectrum. Figure 5.6 shows the masses of the Λ^0 and Σ ground states, as well as the mass differences in spin 1/2 and spin 3/2 Σ ground states, needed to find the parameters of such a formula for a choice of ξ and δm_s while Figure 5.4 shows the lightest $\frac{1}{2}^+$,$\frac{1}{2}^-$ and $\frac{3}{2}^+$ values needed in order to fit the mass difference parameters that use the neutral N and Δ states. Note that as δm_s approaches zero, the dimensional parameters D, E also approach zero, as we expect. This is relevant to the limit of maximum degeneracy. It is through this method that the mass differences within the baryon multiplet for a dark QCD model can then be explored by solving for the Gürsey-Radicati formula parameters each time we generate the resonance spectrum for dark QCD states. Figure 5.7 examines the cases with only two light flavours and in Fig. 5.8 we examine how the spectra of lightest spin-flavour states changes depending on the value of ξ and whether there are any non-degenerate light quarks. Applying this methodology to a dark QCD inherently comes with the caveats that the exact scaling of these parameters in, for instance, one flavour dark QCD may be more complicated than the scaling we employ. In particular the relationship between bare quark mass and constituent quark mass is non-trivial and has been explored in lattice studies such as [188].

5.2.2 Meson spectra

For mesons we are mostly interested in the scaling with confinement scale as their masses can have significant consequences on the stability of baryons. They may additionally impact the cross sections of strong interactions and thus the self-interaction strength of dark matter. In QCD, the application of the constituent quark model meson formula

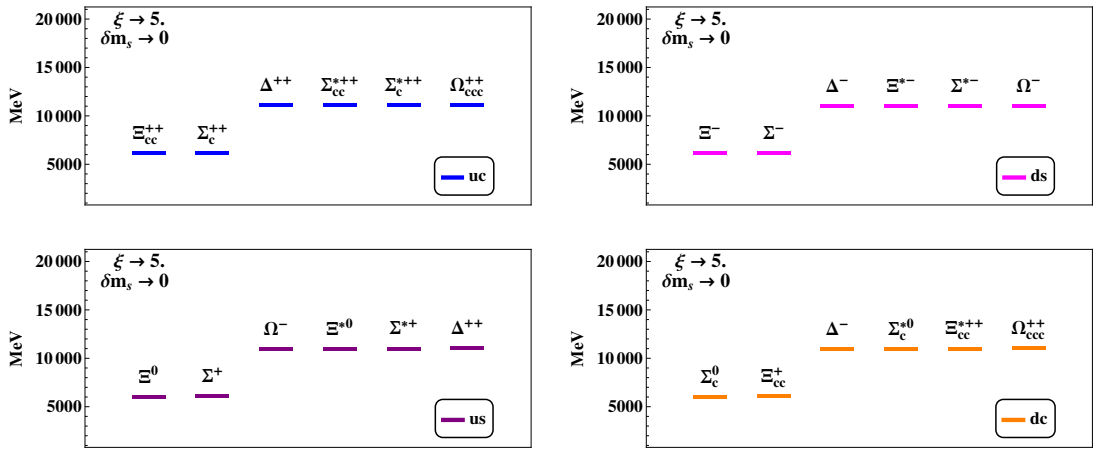

FIGURE 5.7: Gürsey Radicati states for a hidden QCD with two flavours, $\xi = 5$ and degenerate light quark masses in increasing mass values in four flavour combination cases.

[189],

$$M_{\text{meson}} = m_1 + m_2 + \frac{1}{3}\left(\frac{8\pi}{3}\right)\frac{4\pi\alpha_s}{m_1 m_2} S_1.S_2 |\Psi_{\text{meson}}(0)|^2, \tag{5.14}$$

works surprisingly well, where $S.S$ is 1/4 for vector mesons and -3/4 for pseudoscalars. Taking the up and the down to have constituent mass 310 MeV and the strange quark to have 483 MeV reproduces the results in Fig. 5.9. One approach we can then take in exploring a dark analogue is to simply consider the inter-quark potential from the baryon spectrum and solve for the two body wavefunction to find $|\Psi_{\text{meson}}(0)|^2$. This follows the work in [181–183] where the potential and parameter space considered was specifically designed to fit both the baryon and meson spectra.

While Eq. 5.14 is not particularly accurate in the chiral limit as $m_q \to 0$, we observed that the pion scaling with ξ is consistent with the Gell-Mann, Oakes, Renner relation,

$$m_\pi^2 = \frac{(m_u + m_d)\rho}{f_\pi^2}, \tag{5.15}$$

if one assumes a pion decay constant that does not vary with ξ. The parameter ρ is the condensate, $\rho = \langle \bar{q}q \rangle$, that scales directly with ξ. This suggests that the model we employ is taking the degree of explicit chiral symmetry breaking to be of the same magnitude as ordinary QCD as we increase ξ. In other words, while the bare light dark quark masses remain small compared to Λ_{DM}, we are able to analyse the meson spectrum for models where the ratio of light dark quark current masses to Λ_{DM} is similar to standard QCD. This is consistent with models of broken mirror symmetries where the

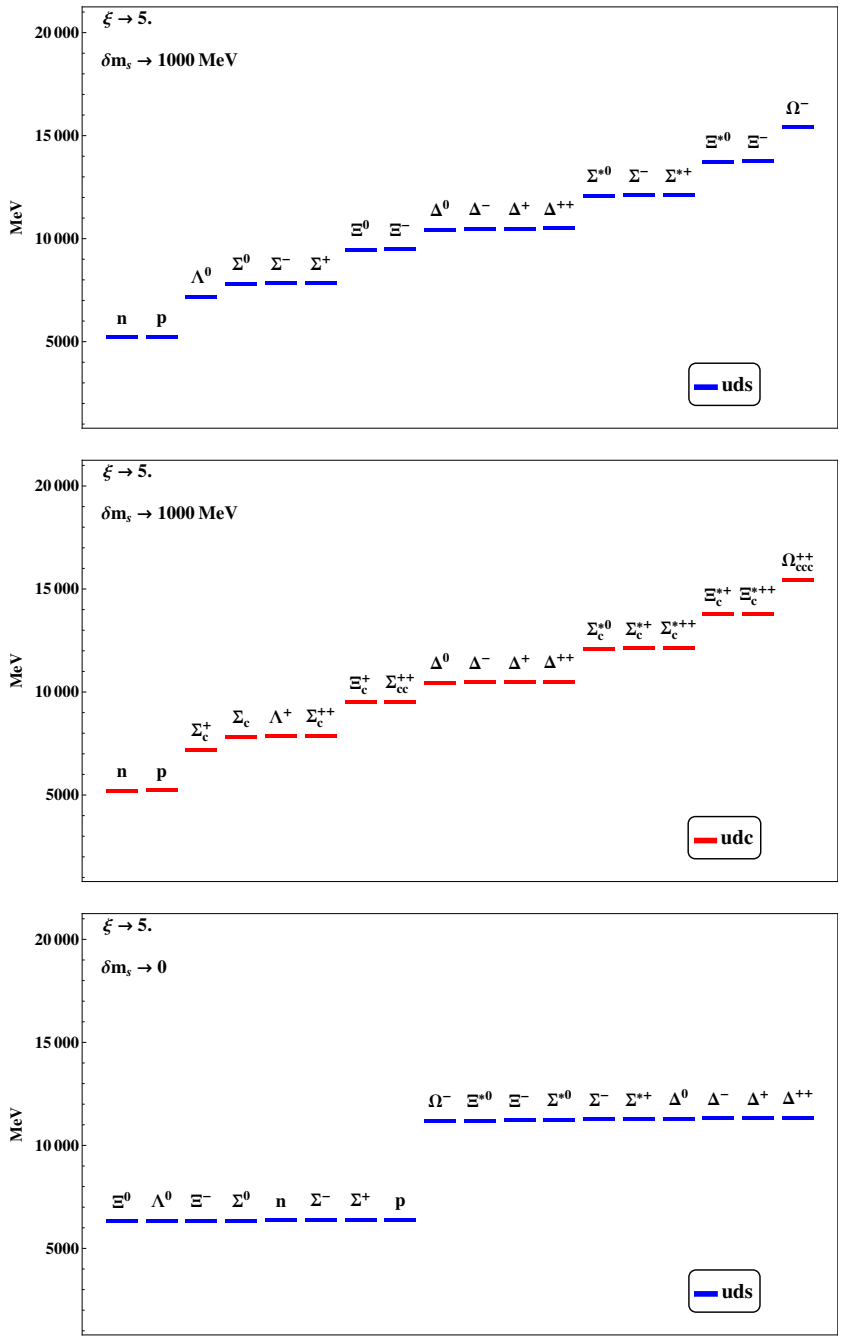

FIGURE 5.8: Spin 1/2 and spin 3/2 baryon ground states for a factor of $\xi = 5$ in the case of three light quarks where one quark may have additional mass. The more massive state is then labelled as the c or s dark quark depending on its quantum charges.

dark EW scale can be a free parameter. This limits the amount of parameter space we can explore in this particular approach to dark hadronic spectra to models of dark QCD with a similar degree of chiral symmetry breaking. We additionally know that in the chiral limit the mesons approach zero mass and so Eq. 5.14 is applied in the context of increasing ξ with meson spectra fitted dressed masses now scaling with ξ along with the

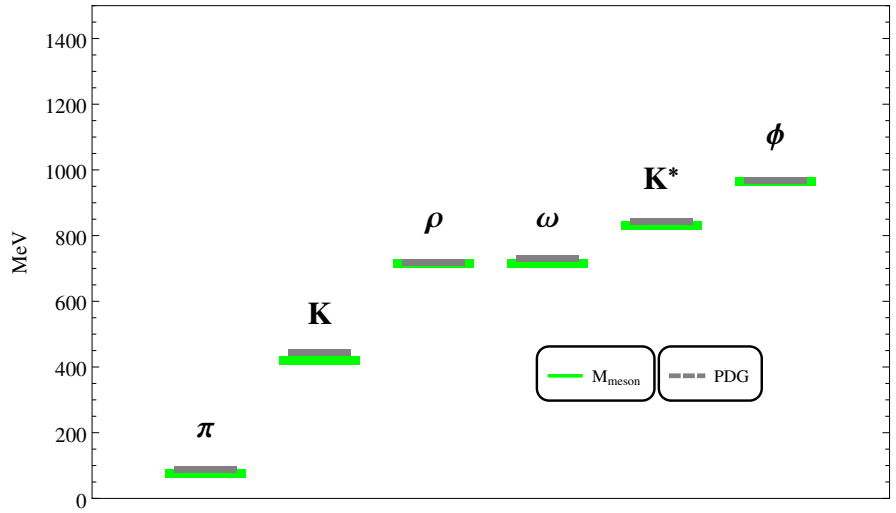

FIGURE 5.9: Meson states from Eq. 5.14 compared to PDG values in QCD. As with the baryon model, these fits will act as the starting point for the scaling of dark meson masses.

inter-quark potential. We can also factor in a value of δm_s to observe the splitting with a semi-light dressed state. The meson spectra are much more sensitive to the masses of the bare dark quarks, which are all free parameters, and thus the spectra and the comparison between meson and baryon mass will depend on the exact model. As noted in [120], choosing a semi-light mass for bare quark masses and a hidden QCD without flavour violating dark electroweak forces, one can make states similar to the Λ baryon stable as Kaons may be too heavy for kinematics to allow decay to lighter baryons.

Figure 5.10 shows the light meson spectra for a small set of different dark QCD cases. As the dark confinement scale is large, we take the anomalous meson to be sufficiently heavy that it is not part of the light set as discussed previously. In Figure 5.11 we examine how a sample of the meson spectra in this model varies with ξ. In particular we see the variation of the mass between the pseudoscalar and vector mesons as ξ increases. As we are assuming a consistent value of the pion decay constant it must be the case that the bare quark masses are similarly increasing with ξ. This reiterates the previous statement that this model is not well suited to exploring the chiral limit and, indeed, exploring the full parameter space of varying the bare quark mass and confinement scale independently for a dark QCD is a task that chiral perturbation theory or lattice QCD studies may have the capacity to accomplish.

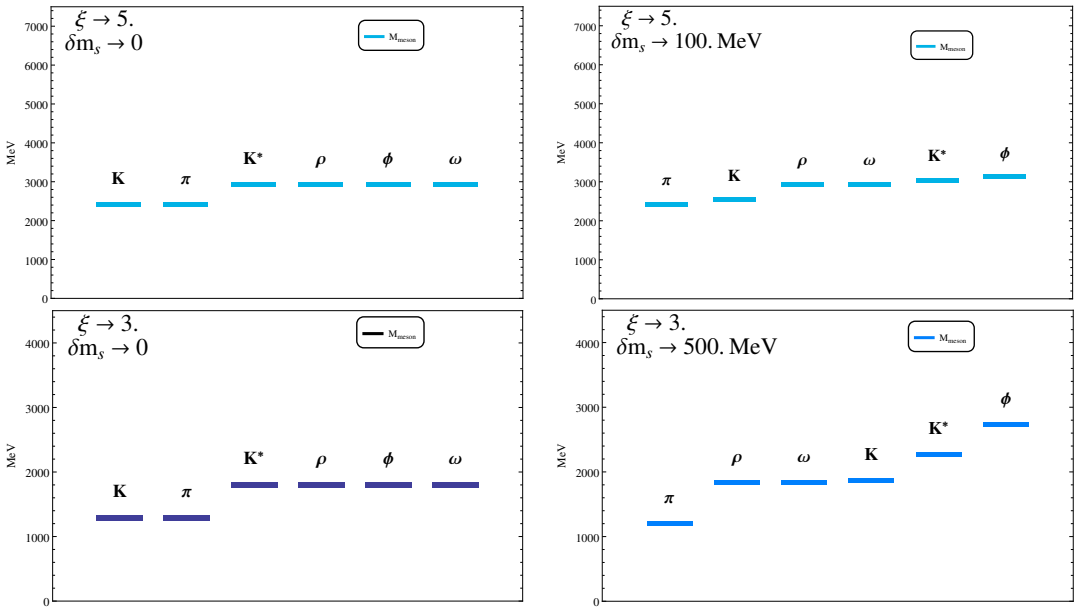

FIGURE 5.10: Three flavour (uds) meson spectra for $\xi = 3, 5$ and semi-light state values given by δm_s.

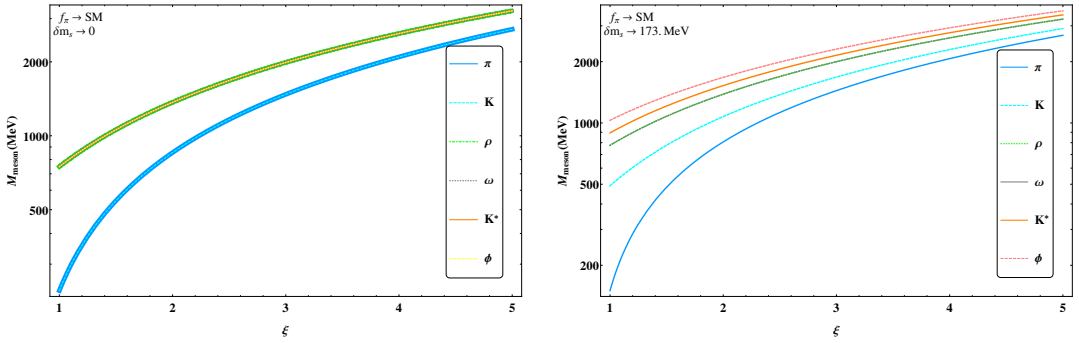

FIGURE 5.11: Scaling of the meson spectra with ξ for a given value of δm_s shown in upper left. The value of the pion decay constant, and thus the strength of chiral symmetry breaking is taken to remain constant.

5.3 Cosmological history of dark QCD

We have seen that asymmetric dark matter models position dark matter as the remaining abundance of matter in a dark sector following the annihilation of near equal amounts of dark matter and dark antimatter, similar to the baryon asymmetry in our own sector [101]. We then require from an asymmetric dark matter model with a dark QCD a number of key features. The first is that dark matter is stable and so a conserved global quantum number is necessary. Dark QCD can provide this in the form of a dark baryon number, however this must be present in the model of the dark quarks themselves, as

is the case in models with a mirror symmetry. Secondly, in order for the dark symmetric matter-antimatter components to be annihilated a form of dark radiation such as dark electromagnetism $U(1)_D$ is needed or annihilation into ordinary radiation must occur. If dark photons fulfil that role this has direct implications as discussed in the previous chapter on the ordering of the hadronic spectra as well as the self-interaction cross section for dark matter. If the dark EM coupling is of the same scale as the SM value, the self-interaction rate for purely charged DM may be above the current bounds. For a recent analysis of constraints see [190] where DM with an $U(1)$ gauge charge was considered and constraints from triaxiality and galaxy cluster mergers were compared to the significant bounds, in particular that for ~ 10 GeV scale DM the dark EM coupling $\alpha_D < 10^{-4}$. Note that these bounds assume no compact object formation in the dark sector. The strength of the dark gauge coupling in this case allows for different fractions of DM to be charged. If the set of light quarks allows for neutral states then we have seen that degenerate quark masses motivate models in which the neutral states are the lightest stable composites and if nuclear forces are sufficiently weak then dark matter can satisfy these constraints. In the case of dark glueball dark matter Ref. [191] considers the relationship derived from the suspected glueball state of QCD that $m_{\rm GB} \sim 5.5\,\Lambda_{\rm DM}$ and estimates a self-interaction cross section $\sigma \sim 4\pi/\Lambda^2_{\rm DM}$.

In order to find a natural explanation for the observed components of the universe, $\rho_{\rm DM} \simeq 5\rho_{\rm M}$, we require both a reason for the similar abundance of baryons and dark baryons as well as the similarity in mass. The relationship in the abundance can be formulated in a large number of different ways and Chapter 4 gives just one fully-worked example. In the case of mass, Section 5.2 has demonstrated how the lightest stable baryon may scale with a dark confinement scale.

In the cases where there is a large mass gap between the lightest baryon and the rest of the spectra we can take the dark matter candidate to be this stable state if dark weak interactions are not suppressed and dark quarks masses are light. If however the mass differences between two or more of the lightest dark QCD states are small then the dark QCD phase transition will produce similar numbers of these states. This can be compared to standard cosmology where the near degeneracy of the neutron and proton produces roughly equal numbers following the quark hadron phase transition. In that case the near equal numbers allows for the process of nucleosynthesis where an array

of stable states of multiple nucleons can be formed. This is in the case where the dark sector has $n + \nu_e \leftrightarrow p + e^-$ interactions that maintain near equal n, p densities prior to the freeze out of weak interactions. This allows for helium to make up a significant fraction ($\sim 26\%$) of the visible mass density. One can then consider dark sectors where two or more near degenerate composite states, that is where $\Delta m \ll \Lambda_{\rm DM}$, are bound by dark nuclear forces into a complex arrangement of nuclei like objects. The complexity may be far greater than standard nuclear theory where there is an approximately linear relationship between the number of protons and neutrons in nuclear bound states, for example; three near degenerate baryons, as in the case of degenerate u,d,s have six possible dibaryon states and the mass hierarchy among these will depend non-trivially on the dark nuclear-like interactions. Compact objects in the form of neutron star-like bodies could also manifest ultimately depending on the model and the self-interaction strength from strong-like interactions.

5.4 Summary

In this chapter we have considered the hypercentral approximation of the constituent quark model and the possible properties of a dark sector with a QCD analogue. In particular we have examined the dependence of the hadron spectra on the number of light chiral fermions and the resulting phenomenology of dark QCD with a confinement scale in the GeV range. As a class of theories to explain the nature of dark matter we have seen that larger confinement scales result in higher degrees of degeneracy in the spectra while the number of flavours has a significant impact on the mass and nature of the lightest baryon and meson for $SU(3)$ theories. Constituent quark models have provided insight into the nature of QCD and while many frameworks for advancing these calculations have sought to better replicate the experimental signatures, potential models still allow us to probe the ground state spectra in a simple manner with fewer parameters and a direct relationship to the confinement scale. By incorporating such descriptions of dark QCD into the asymmetric dark matter models of this work, where the gauge couplings of the SM and hidden sectors are connected in the UV, the similarity in mass scale of DM and the proton finds a natural explanation. The higher confinement scale motivates theories with a neutral ground state in addition to higher degeneracy among the baryons with different total spin and charge. The spin and charge of the

ground state is further dependent on the number of light dark quarks in the theory and the quantum numbers of these quarks that make up the dark matter candidate.

Chapter 6

Conclusion

Common to much of the dark matter literature are models that consider the addition of a single new particle species to fulfil the role of dark matter, in order to explain the majority of mass in the universe. These models assume that the present day knowledge of forces and fields that play a role in the modern universe, despite making up just one sixth of the mass of the universe, is close to complete.

If we consider however that the Standard Model is merely an effective field theory then the possibility is clear that not only is there much more to be found at higher energy scales, but also that the Standard Model could be just one of a number of low energy sets of states that primarily interact gravitationally with each other. The Standard Model does remain however our greatest roadmap for developing theories that seek to explain the currently unexplained features of the cosmos. In this theory of dark matter we have considered the possibility that the gauge group and fermionic content that we observe, governs the dynamics in one of two similar sectors. In particular, drawing on the concept of a $\mathbb{Z}_2$ mirror symmetry connecting two copies of the SM gauge group we have seen how symmetric potentials can break mirror symmetry to create two markedly different sectors.

This type of model can proceed with mirror GUT $SU(5) \times SU(5)$ theories that break this GUT symmetry asymmetrically to give rise to very different mass scales for fermions in the two sectors. The different fermion masses which result from this symmetry breaking can then alter the running of the gauge coupling constants giving rise to similar confinement scales. We demonstrated that this can work with a supersymmetric potential and

a wide range of mass scales for dark fermions. This model can be extended to $SO(10)$ theories, where in the case of $SO(10) \times SO(10)$ we constructed symmetric Lagrangians that induce the mirror GUT group to break asymmetrically through different intermediate gauge theories. This can then generate low energy scale visible and dark sectors that can be similar with respect to the mass scales of matter but have very different thermal histories and forces. In particular, for a wide array of intermediate breaking scales and gauge groups that may have existed along the two sectors' histories, the confining gauge theories at low energy can have very similar confinement scales and thus explain the similar masses of dark matter and the proton.

The similar abundances of matter and dark matter can be explained if the number density asymmetries are generated above the scale of mirror symmetry breaking. This naturally leads us to consider high scale leptogenesis models. We demonstrated models where one sector sets the abundance of visible matter in the universe and a dark copy, with a much higher EW scale, slightly higher confinement scale, and unique fermion flavour mass hierarchy sets the larger density of dark matter mass, made up entirely of dark baryons. Thermal leptogenesis is an ideal model to use for this high scale theory as it also explains the small masses of light neutrinos. In these models of asymmetric symmetry breaking, a lepton asymmetry is generated in each sector by CP violating decays of Majorana neutrinos above the mirror breaking scale after which the two sectors can independently reprocess equal lepton asymmetries into near equal baryon asymmetries. Once antibaryons in our sector and dark antimatter in the hidden sector annihilate away we then have an explanation for a unique dark sector which naturally has a density of dark matter particles near that of the visible baryons and with a mass scale for these particles that is naturally explained to be close to the proton mass. These models can then completely explain the approximate 1:5 ratio of Eq. 1.1.

Lastly we explored the more complicated possibilities of a hidden composite $SU(3)$ theory. Using the hyperspherical constituent quark model of hadronic physics, we explored the spectra of baryons and mesons in a model with a higher energy confinement scale and dark quarks with independent mass scales. In this model we found how the ordering of the hadronic spectra can change depending on whether electromagnetic forces are relevant as well as the effect of the value of the confinement scale and the mass splitting among the dark quarks themselves. This model shows how neutral states are naturally favoured over charged states and how the spin and mass of the lightest stable baryon is

dependent on the number of light dark quarks. This also opened up the discussion to the complexity of possible dark sectors in terms of nuclear binding forces and the possible number of near degenerate dark matter candidates that may co-exist, leading to a rich field of dark matter physics that the hidden sector in our models could be described by.

This thesis has investigated how to solve the fundamental mystery of the matter to dark matter ratio. To that end we have developed the mechanism of asymmetric symmetry breaking and shown in the first five chapters how this can solve the ratio problem in a natural way. The breaking of these high scale mirror symmetries can produce the visible sector, governed by the SM at low energies, and a dark sector with vastly different properties but a similar mass contribution to the universe. These dark sectors are then a compelling explanation for dark matter and offer the possibility that the dark sector itself may be a fascinating landscape of new physics that is eerily similar to the world we know.

Bibliography

[1] F. Zwicky. *Die Rotverschiebung von extragalaktischen Nebeln*. *Helv. Phys. Acta*, 6:110–127, 1933. doi: 10.1007/s10714-008-0707-4. [Gen. Rel. Grav.41,207(2009)].

[2] Matts Roos. *Dark Matter: The evidence from astronomy, astrophysics and cosmology*. *arXiv:*1001.0316 *[astro-ph.CO]*, 2010.

[3] Gianfranco Bertone and Dan Hooper. *A History of Dark Matter*. *arXiv:*1605.04909 *[astro-ph.CO]*, 2016.

[4] P. A. R. Ade et al. *Planck 2015 results. XIII. Cosmological parameters*. *Astron. Astrophys.*, 594:A13, 2016. doi: 10.1051/0004-6361/201525830.

[5] Georges Aad et al. *Observation of a new particle in the search for the Standard Model Higgs boson with the ATLAS detector at the LHC*. *Phys. Lett.*, B716:1–29, 2012. doi: 10.1016/j.physletb.2012.08.020.

[6] Serguei Chatrchyan et al. *Observation of a new boson at a mass of 125 GeV with the CMS experiment at the LHC*. *Phys. Lett.*, B716:30–61, 2012. doi: 10.1016/j.physletb.2012.08.021.

[7] M. Gell-Mann and F. E. Low. *Quantum Electrodynamics at Small Distances. Phys. Rev.*, 95:1300–1312, Sep 1954. doi: 10.1103/PhysRev.95.1300.

[8] Curtis G. Callan. *Broken Scale Invariance in Scalar Field Theory. Phys. Rev. D*, 2:1541–1547, Oct 1970. doi: 10.1103/PhysRevD.2.1541.

[9] K. Symanzik. *Small distance behaviour in field theory and power counting*. *Comm. Math. Phys.*, 18(3):227–246, 1970.

[10] Peter W. Higgs. *Broken Symmetries and the Masses of Gauge Bosons*. *Phys. Rev. Lett.*, 13:508–509, 1964. doi: 10.1103/PhysRevLett.13.508.

[11] F. Englert and R. Brout. *Broken Symmetry and the Mass of Gauge Vector Mesons*. *Phys. Rev. Lett.*, 13:321–323, 1964. doi: 10.1103/PhysRevLett.13.321.

[12] S. L. Glashow. *Partial Symmetries of Weak Interactions*. *Nucl. Phys.*, 22:579–588, 1961. doi: 10.1016/0029-5582(61)90469-2.

[13] Steven Weinberg. *A Model of Leptons*. *Phys. Rev. Lett.*, 19:1264–1266, 1967. doi: 10.1103/PhysRevLett.19.1264.

[14] Jogesh C. Pati and Abdus Salam. *Unified Lepton-Hadron Symmetry and a Gauge Theory of the Basic Interactions*. *Phys. Rev.*, D8:1240–1251, 1973. doi: 10.1103/PhysRevD.8.1240.

[15] Junpei Harada. *Gauge coupling unification with extra Higgs doublets*. *Fortsch. Phys.*, 64(6-7):510–515, 2016. doi: 10.1002/prop.201600022.

[16] David J. Gross, Jeffrey A. Harvey, Emil J. Martinec, and Ryan Rohm. *The Heterotic String*. *Phys. Rev. Lett.*, 54:502–505, 1985. doi: 10.1103/PhysRevLett.54.502.

[17] T.D. Lee and Chen-Ning Yang. *Question of Parity Conservation in Weak Interactions*. *Phys.Rev.*, 104:254–258, 1956. doi: 10.1103/PhysRev.104.254.

[18] I. Kobzarev, L. Okun, and I. Pomeranchuk. *On the possibility of experimental observation of mirror particles*. *Sov. J. Nucl. Phys.*, 3(6):837–841, 1966.

[19] Matej Pavsic. *External inversion, internal inversion, and reflection invariance*. *Int.J.Theor.Phys.*, 9:229–244, 1974. doi: 10.1007/BF01810695.

[20] S.I. Blinnikov and M. Yu. Khlopov. *On possible effects of 'mirror' particles*. *Sov.J.Nucl.Phys.*, 36:472, 1982.

[21] S.Blinnikov and M.Khlopov. *Possible astronomical effects of mirror particles*. *Sov.Astron.Lett.*, 27:371, 1983.

[22] Robert Foot, H. Lew, and R.R. Volkas. *A Model with fundamental improper space-time symmetries*. *Phys.Lett.*, B272:67–70, 1991. doi: 10.1016/0370-2693(91)91013-L.

[23] Robert Foot, H. Lew, and R.R. Volkas. *Possible consequences of parity conservation*. *Mod.Phys.Lett.*, A7:2567–2574, 1992. doi: 10.1142/S0217732392004031.

[24] Robert Foot and Raymond R. Volkas. *Neutrino physics and the mirror world: How exact parity symmetry explains the solar neutrino deficit, the atmospheric neutrino anomaly and the LSND experiment*. *Phys.Rev.*, D52:6595–6606, 1995. doi: 10.1103/PhysRevD.52.6595.

[25] Z. G. Berezhiani. *Mirror world and present neutrino puzzles*. In *Elementary particle physics: Present and future. Proceedings, International Workshop, Valencia, Spain, June 5-9, 1995*, pages 335–342, 1995.

[26] Zurab G. Berezhiani and Rabindra N. Mohapatra. *Reconciling present neutrino puzzles: Sterile neutrinos as mirror neutrinos*. *Phys.Rev.*, D52:6607–6611, 1995. doi: 10.1103/PhysRevD.52.6607.

[27] Z. G. Berezhiani, A. D. Dolgov, and R. N. Mohapatra. *Asymmetric inflationary reheating and the nature of mirror universe*. *Phys. Lett.*, B375:26–36, 1996. doi: 10.1016/0370-2693(96)00219-5.

[28] Z. G. Berezhiani. *Astrophysical implications of the mirror world with broken mirror parity*. *Acta Phys. Polon.*, B27:1503–1516, 1996.

[29] Robert Foot, H. Lew, and R.R. Volkas. *Unbroken versus broken mirror world: A Tale of two vacua*. *JHEP*, 0007:032, 2000. doi: 10.1088/1126-6708/2000/07/032.

[30] Zurab Berezhiani, Denis Comelli, and Francesco L. Villante. *The Early mirror universe: Inflation, baryogenesis, nucleosynthesis and dark matter*. *Phys.Lett.*, B503:362–375, 2001. doi: 10.1016/S0370-2693(01)00217-9.

[31] Luis Bento and Z. Berezhiani. *Baryon asymmetry, dark matter and the hidden sector*. *Fortsch. Phys.*, 50:489–495, 2002. doi: 10.1002/9783527610853.ch8.

[32] A. Yu. Ignatiev and Raymond R. Volkas. *Mirror dark matter and large scale structure*. *Phys.Rev.*, D68:023518, 2003. doi: 10.1103/PhysRevD.68.023518.

[33] Robert Foot and Raymond R. Volkas. *Was ordinary matter synthesized from mirror matter? An Attempt to explain why Omega(Baryon) approximately equal to 0.2 Omega(Dark)*. *Phys.Rev.*, D68:021304, 2003. doi: 10.1103/PhysRevD.68.021304.

[34] Zurab Berezhiani, Paolo Ciarcelluti, Denis Comelli, and Francesco L. Villante. *Structure formation with mirror dark matter: CMB and LSS*. *Int.J.Mod.Phys.*, D14:107–120, 2005. doi: 10.1142/S0218271805005165.

[35] Zurab Berezhiani. *Mirror world and its cosmological consequences*. *Int. J. Mod. Phys.*, A19:3775–3806, 2004. doi: 10.1142/S0217751X04020075.

[36] Robert Foot and Raymond R. Volkas. *Explaining Omega(Baryon) approximately 0.2 Omega(Dark) through the synthesis of ordinary matter from mirror matter: A More general analysis*. *Phys.Rev.*, D69:123510, 2004. doi: 10.1103/PhysRevD.69.123510.

[37] Paolo Ciarcelluti. *Cosmology with mirror dark matter. 1. Linear evolution of perturbations*. *Int.J.Mod.Phys.*, D14:187–222, 2005. doi: 10.1142/S0218271805006213.

[38] Paolo Ciarcelluti. *Cosmology with mirror dark matter. 2. Cosmic microwave background and large scale structure*. *Int.J.Mod.Phys.*, D14:223–256, 2005. doi: 10.1142/S0218271805006225.

[39] Zurab Berezhiani. *Through the looking-glass: Alice's adventures in mirror world*. pages 2147–2195, 2005. doi: 10.1142/9789812775344_0055.

[40] Zurab Berezhiani, Santi Cassisi, Paolo Ciarcelluti, and Adriano Pietrinferni. *Evolutionary and structural properties of mirror star MACHOs*. *Astropart. Phys.*, 24:495–510, 2006. doi: 10.1016/j.astropartphys.2005.10.002.

[41] Zurab Berezhiani. *Marriage between the baryonic and dark matters*. *AIP Conf. Proc.*, 878:195–202, 2006. doi: 10.1063/1.2409087.

[42] Zurab Berezhiani and Angela Lepidi. *Cosmological bounds on the 'millicharges' of mirror particles*. *Phys. Lett.*, B681:276–281, 2009. doi: 10.1016/j.physletb.2009.10.023.

[43] Z. Berezhiani. *Unified picture of ordinary and dark matter genesis*. *Eur. Phys. J. ST*, 163:271–289, 2008. doi: 10.1140/epjst/e2008-00824-6.

[44] Zurab G. Berezhiani, Lilian Kaufmann, Paolo Panci, Nicola Rossi, Andre Rubbia, and Alexander S. Sakharov. *Strongly interacting mirror dark matter*. *CERN-PH-TH-2008-108*, 2008.

[45] Zurab Berezhiani, Luigi Pilo, and Nicola Rossi. *Mirror Matter, Mirror Gravity and Galactic Rotational Curves*. *Eur. Phys. J.*, C70:305–316, 2010. doi: 10.1140/epjc/s10052-010-1457-5.

[46] Zurab Berezhiani and Askhat Gazizov. *Neutron Oscillations to Parallel World: Earlier End to the Cosmic Ray Spectrum?* *Eur. Phys. J.*, C72:2111, 2012. doi: 10.1140/epjc/s10052-012-2111-1.

[47] R. Foot. *Mirror dark matter: Cosmology, galaxy structure and direct detection*. *Int.J.Mod.Phys.*, A29:1430013, 2014. doi: 10.1142/S0217751X14300130.

[48] Zurab Berezhiani. *Shadow dark matter, sterile neutrinos and neutrino events at IceCube*. *Nucl. Part. Phys. Proc.*, 265-266:303–306, 2015. doi: 10.1016/j.nuclphysbps.2015.06.076.

[49] A. Addazi, Z. Berezhiani, R. Bernabei, P. Belli, F. Cappella, R. Cerulli, and A. Incicchitti. *DAMA annual modulation effect and asymmetric mirror matter*. *Eur. Phys. J.*, C75(8):400, 2015. doi: 10.1140/epjc/s10052-015-3634-z.

[50] Zurab Berezhiani. *Anti-dark matter: a hidden face of mirror world*. *arXiv:*1602.08599 *[astro-ph.CO]*, 2016.

[51] R. Cerulli, P. Villar, F. Cappella, R. Bernabei, P. Belli, A. Incicchitti, A. Addazi, and Z. Berezhiani. *DAMA annual modulation and mirror Dark Matter*. *Eur. Phys. J.*, C77(2):83, 2017. doi: 10.1140/epjc/s10052-017-4658-3.

[52] Zurab Berezhiani, Matthew Frost, Yuri Kamyshkov, Ben Rybolt, and Louis Varriano. *Neutron Disappearance and Regeneration from Mirror State*. *Phys. Rev.*, D96(3):035039, 2017. doi: 10.1103/PhysRevD.96.035039.

[53] Z. Berezhiani, R. Biondi, P. Geltenbort, I. A. Krasnoshchekova, V. E. Varlamov, A. V. Vassiljev, and O. M. Zherebtsov. *New experimental limits on neutron - mirror neutron oscillations in the presence of mirror magnetic field*. *arXiv:*1712.05761 *[hep-ex]*, 2017.

[54] Mirza Satriawan. *A Multicomponent Dark Matter in a Model with Mirror Symmetry with Additional Charged Scalars*. *arXiv:*1801.00326 *[hep-ph]*, 2017.

[55] Sidney R. Coleman and J. Mandula. *All Possible Symmetries of the S Matrix*. *Phys. Rev.*, 159:1251–1256, 1967. doi: 10.1103/PhysRev.159.1251.

[56] Hironari Miyazawa. *Baryon Number Changing Currents. Progress of Theoretical Physics*, 36(6):1266–1276, 1966. doi: 10.1143/PTP.36.1266.

[57] Pierre Ramond. *Dual Theory for Free Fermions. Phys. Rev.*, D3:2415–2418, 1971. doi: 10.1103/PhysRevD.3.2415.

[58] A. Neveu and J. H. Schwarz. *Factorizable dual model of pions. Nucl. Phys.*, B31: 86–112, 1971. doi: 10.1016/0550-3213(71)90448-2.

[59] Jean-Loup Gervais and B. Sakita. *Field Theory Interpretation of Supergauges in Dual Models. Nucl. Phys.*, B34:632–639, 1971. doi: 10.1016/0550-3213(71)90351-8.

[60] Yu. A. Golfand and E. P. Likhtman. *Extension of the Algebra of Poincare Group Generators and Violation of p Invariance. JETP Lett.*, 13:323–326, 1971.

[61] J. Wess and B. Zumino. *Supergauge Transformations in Four-Dimensions. Nucl. Phys.*, B70:39–50, 1974. doi: 10.1016/0550-3213(74)90355-1.

[62] Stephen P. Martin. *A Supersymmetry primer*. pages 1–98, 1997. doi: 10.1142/9789814307505_0001.

[63] Alan H. Guth. *The Inflationary Universe: A Possible Solution to the Horizon and Flatness Problems. Phys. Rev.*, D23:347–356, 1981. doi: 10.1103/PhysRevD.23.347.

[64] K. Sato. *First Order Phase Transition of a Vacuum and Expansion of the Universe. Mon. Not. Roy. Astron. Soc.*, 195:467–479, 1981.

[65] A. D. Sakharov. *Violation of CP Invariance, c Asymmetry, and Baryon Asymmetry of the Universe. Pisma Zh. Eksp. Teor. Fiz.*, 5:32–35, 1967. doi: 10.1070/PU1991v034n05ABEH002497.

[66] M. Fukugita and T. Yanagida. *Baryogenesis Without Grand Unification. Phys. Lett.*, B174:45–47, 1986. doi: 10.1016/0370-2693(86)91126-3.

[67] M. A. Luty. *Baryogenesis via leptogenesis. Phys. Rev.*, D45:455–465, 1992. doi: 10.1103/PhysRevD.45.455.

[68] Riccardo Barbieri, Paolo Creminelli, Alessandro Strumia, and Nikolaos Tetradis. *Baryogenesis through leptogenesis. Nucl. Phys.*, B575:61–77, 2000. doi: 10.1016/S0550-3213(00)00011-0.

[69] W. Buchmuller, P. Di Bari, and M. Plumacher. *Leptogenesis for pedestrians*. *Annals Phys.*, 315:305–351, 2005. doi: 10.1016/j.aop.2004.02.003.

[70] Apostolos Pilaftsis and Thomas E. J. Underwood. *Resonant leptogenesis*. *Nucl. Phys.*, B692:303–345, 2004. doi: 10.1016/j.nuclphysb.2004.05.029.

[71] Michael Plumacher. *Baryogenesis and lepton number violation*. *Z. Phys.*, C74: 549–559, 1997. doi: 10.1007/s002880050418.

[72] W. Buchmuller and M. Plumacher. *CP asymmetry in Majorana neutrino decays*. *Phys. Lett.*, B431:354–362, 1998. doi: 10.1016/S0370-2693(97)01548-7.

[73] Koichi Hamaguchi, Hitoshi Murayama, and T. Yanagida. *Leptogenesis from N dominated early universe*. *Phys. Rev.*, D65:043512, 2002. doi: 10.1103/PhysRevD.65.043512.

[74] F. Hahn-Woernle, M. Plumacher, and Y. Y. Y. Wong. *Full Boltzmann equations for leptogenesis including scattering*. *JCAP*, 0908:028, 2009. doi: 10.1088/1475-7516/2009/08/028.

[75] Matthew J. Dolan, Tomasz P. Dutka, and Raymond R. Volkas. *Dirac-Phase Thermal Leptogenesis in the extended Type-I Seesaw Model*. *arXiv:*1802.08373 *[hep-ph]*, 2018.

[76] Tsutomu Yanagida. *Horizontal symmetry and masses of neutrinos*. *Conf. Proc.*, C7902131:95–99, 1979.

[77] Pierre Ramond. *The Family Group in Grand Unified Theories*. In *International Symposium on Fundamentals of Quantum Theory and Quantum Field Theory Palm Coast, Florida, February 25-March 2, 1979*, pages 265–280, 1979.

[78] Rabindra N. Mohapatra and Goran Senjanovic. *Neutrino Mass and Spontaneous Parity Violation*. *Phys. Rev. Lett.*, 44:912, 1980. doi: 10.1103/PhysRevLett.44.912.

[79] Gustavo C. Branco and M. N. Rebelo. *Leptonic CP violation and neutrino mass models*. *New J. Phys.*, 7:86, 2005. doi: 10.1088/1367-2630/7/1/086.

[80] Laura Covi, Esteban Roulet, and Francesco Vissani. *CP violating decays in leptogenesis scenarios*. *Phys. Lett.*, B384:169–174, 1996. doi: 10.1016/0370-2693(96)00817-9.

[81] Apostolos Pilaftsis. *Heavy Majorana neutrinos and baryogenesis*. *Int. J. Mod. Phys.*, A14:1811–1858, 1999. doi: 10.1142/S0217751X99000932.

[82] Frans R. Klinkhamer and N. S. Manton. *A Saddle Point Solution in the Weinberg-Salam Theory*. *Phys. Rev.*, D30:2212, 1984. doi: 10.1103/PhysRevD.30.2212.

[83] Gerard 't Hooft. *Symmetry Breaking Through Bell-Jackiw Anomalies*. *Phys. Rev. Lett.*, 37:8–11, 1976. doi: 10.1103/PhysRevLett.37.8.

[84] Vadim A. Kuzmin. *A Simultaneous solution to baryogenesis and dark matter problems*. *Phys. Part. Nucl.*, 29:257–265, 1998. doi: 10.1134/1.953070. [Phys. Atom. Nucl.61,1107(1998)].

[85] Ryuichiro Kitano and Ian Low. *Dark matter from baryon asymmetry*. *Phys. Rev.*, D71:023510, 2005. doi: 10.1103/PhysRevD.71.023510.

[86] Ryuichiro Kitano and Ian Low. *Grand unification, dark matter, baryon asymmetry, and the small scale structure of the universe*. 2005.

[87] Pei-Hong Gu, Utpal Sarkar, and Xinmin Zhang. *Visible and Dark Matter Genesis and Cosmic Positron/Electron Excesses*. *Phys. Rev.*, D80:076003, 2009. doi: 10.1103/PhysRevD.80.076003.

[88] Hooman Davoudiasl, David E. Morrissey, Kris Sigurdson, and Sean Tulin. *Hylogenesis: A Unified Origin for Baryonic Visible Matter and Antibaryonic Dark Matter*. *Phys. Rev. Lett.*, 105:211304, 2010. doi: 10.1103/PhysRevLett.105.211304.

[89] Pei-Hong Gu, Manfred Lindner, Utpal Sarkar, and Xinmin Zhang. *WIMP Dark Matter and Baryogenesis*. *Phys. Rev.*, D83:055008, 2011. doi: 10.1103/PhysRevD.83.055008.

[90] Jonathan J. Heckman and Soo-Jong Rey. *Baryon and Dark Matter Genesis from Strongly Coupled Strings*. *JHEP*, 06:120, 2011. doi: 10.1007/JHEP06(2011)120.

[91] David H. Oaknin and Ariel Zhitnitsky. *Baryon asymmetry, dark matter and quantum chromodynamics*. *Phys. Rev.*, D71:023519, 2005. doi: 10.1103/PhysRevD.71.023519.

[92] Glennys R. Farrar and Gabrijela Zaharijas. *Dark matter and the baryon asymmetry*. *Phys. Rev. Lett.*, 96:041302, 2006. doi: 10.1103/PhysRevLett.96.041302.

[93] Lawrence J. Hall, John March-Russell, and Stephen M. West. *A Unified Theory of Matter Genesis: Asymmetric Freeze-In*. *arXiv:*1010.0245 *[hep-ph]*, 2010.

[94] Nicole F. Bell, Kalliopi Petraki, Ian M. Shoemaker, and Raymond R. Volkas. *Pangenesis in a Baryon-Symmetric Universe: Dark and Visible Matter via the Affleck-Dine Mechanism*. *Phys. Rev.*, D84:123505, 2011. doi: 10.1103/PhysRevD.84.123505.

[95] Adam Falkowski, Joshua T. Ruderman, and Tomer Volansky. *Asymmetric Dark Matter from Leptogenesis*. *JHEP*, 05:106, 2011. doi: 10.1007/JHEP05(2011)106.

[96] Clifford Cheung and Kathryn M. Zurek. *Affleck-Dine Cogenesis*. *Phys. Rev.*, D84:035007, 2011. doi: 10.1103/PhysRevD.84.035007.

[97] Michael L. Graesser, Ian M. Shoemaker, and Luca Vecchi. *A Dark Force for Baryons*. *arXiv:*1107.2666 *[hep-ph]*, 2011.

[98] Benedict von Harling, Kalliopi Petraki, and Raymond R. Volkas. *Affleck-Dine dynamics and the dark sector of pangenesis*. *JCAP*, 1205:021, 2012. doi: 10.1088/1475-7516/2012/05/021.

[99] John March-Russell and Matthew McCullough. *Asymmetric Dark Matter via Spontaneous Co-Genesis*. *JCAP*, 1203:019, 2012. doi: 10.1088/1475-7516/2012/03/019.

[100] Kalliopi Petraki, Mark Trodden, and Raymond R. Volkas. *Visible and dark matter from a first-order phase transition in a baryon-symmetric universe*. *JCAP*, 1202:044, 2012. doi: 10.1088/1475-7516/2012/02/044.

[101] Kalliopi Petraki and Raymond R. Volkas. *Review of asymmetric dark matter*. *Int.J.Mod.Phys.*, A28:1330028, 2013. doi: 10.1142/S0217751X13300287.

[102] Stephon Alexander, Evan McDonough, and David N. Spergel. *Chiral Gravitational Waves and Baryon Superfluid Dark Matter*. 2018.

[103] Hong-Yee Chiu. *Symmetry between particle and anti-particle populations in the universe*. *Phys. Rev. Lett.*, 17:712, 1966. doi: 10.1103/PhysRevLett.17.712.

[104] G. Steigman. *Cosmology Confronts Particle Physics*. *Ann. Rev. Nucl. Part. Sci.*, 29:313–338, 1979. doi: 10.1146/annurev.ns.29.120179.001525.

[105] Robert J. Scherrer and Michael S. Turner. *On the Relic, Cosmic Abundance of Stable Weakly Interacting Massive Particles*. *Phys. Rev.*, D33:1585, 1986. doi: 10.1103/PhysRevD.33.1585,10.1103/PhysRevD.34.3263. [Erratum: Phys. Rev.D34,3263(1986)].

[106] Scott Dodelson and Lawrence M. Widrow. *Sterile-neutrinos as dark matter*. *Phys. Rev. Lett.*, 72:17–20, 1994. doi: 10.1103/PhysRevLett.72.17.

[107] Xiang-Dong Shi and George M. Fuller. *A New dark matter candidate: Nonthermal sterile neutrinos*. *Phys. Rev. Lett.*, 82:2832–2835, 1999. doi: 10.1103/PhysRevLett.82.2832.

[108] Kalliopi Petraki and Alexander Kusenko. *Dark-matter sterile neutrinos in models with a gauge singlet in the Higgs sector*. *Phys. Rev.*, D77:065014, 2008. doi: 10.1103/PhysRevD.77.065014.

[109] R. D. Peccei and Helen R. Quinn. *CP Conservation in the Presence of Instantons*. *Phys. Rev. Lett.*, 38:1440–1443, 1977. doi: 10.1103/PhysRevLett.38.1440.

[110] R. D. Peccei and Helen R. Quinn. *Constraints Imposed by CP Conservation in the Presence of Instantons*. *Phys. Rev.*, D16:1791–1797, 1977. doi: 10.1103/PhysRevD.16.1791.

[111] Jihn E. Kim. *Weak Interaction Singlet and Strong CP Invariance*. *Phys. Rev. Lett.*, 43:103, 1979. doi: 10.1103/PhysRevLett.43.103.

[112] Pierre Sikivie. *The emerging case for axion dark matter*. *Phys. Lett.*, B695:22–25, 2011. doi: 10.1016/j.physletb.2010.11.027.

[113] Tetsutaro Higaki, Kwang Sik Jeong, and Fuminobu Takahashi. *A Parallel World in the Dark*. *JCAP*, 1308:031, 2013. doi: 10.1088/1475-7516/2013/08/031.

[114] William Detmold, Matthew McCullough, and Andrew Pochinsky. *Dark Nuclei I: Cosmology and Indirect Detection*. *Phys. Rev.*, D90(11):115013, 2014. doi: 10.1103/PhysRevD.90.115013.

[115] Yang Bai and Pedro Schwaller. *The Scale of Dark QCD*. *Phys.Rev.*, D89:063522, 2014. doi: 10.1103/PhysRevD.89.063522.

[116] Jayden L. Newstead and Russell H. TerBeek. *Reach of Threshold-Corrected Dark QCD*. *Phys. Rev. D*, 90:074008, Oct 2014. doi: 10.1103/PhysRevD.90.074008.

[117] Gordan Krnjaic and Kris Sigurdson. *Big Bang Darkleosynthesis*. *Phys. Lett.*, B751:464–468, 2015. doi: 10.1016/j.physletb.2015.11.001.

[118] Kimberly K. Boddy, Jonathan L. Feng, Manoj Kaplinghat, and Tim M. P. Tait. *Self-Interacting Dark Matter from a Non-Abelian Hidden Sector*. *Phys. Rev.*, D89 (11):115017, 2014. doi: 10.1103/PhysRevD.89.115017.

[119] Nodoka Yamanaka, Sho Fujibayashi, Shinya Gongyo, and Hideaki Iida. *Dark matter in the hidden gauge theory*. *arXiv:*1411.2172 *[hep-ph]*, 2014.

[120] Oleg Antipin, Michele Redi, Alessandro Strumia, and Elena Vigiani. *Accidental Composite Dark Matter*. *JHEP*, 07:039, 2015. doi: 10.1007/JHEP07(2015)039.

[121] Ling-Fong Li. *Group Theory of the Spontaneously Broken Gauge Symmetries*. *Phys.Rev.*, D9:1723–1739, 1974. doi: 10.1103/PhysRevD.9.1723.

[122] Graham G. Ross. *Grand Unified Theories*. Frontiers in physics. Benjamin/Cummings Pub. Co., 1984. ISBN 9780805369670.

[123] Goran Senjanovic. *Proton decay and grand unification*. *AIP Conf.Proc.*, 1200: 131–141, 2010. doi: 10.1063/1.3327552.

[124] Ilja Dorsner, Pavel Fileviez Perez, and Ricardo Gonzalez Felipe. *Phenomenological and cosmological aspects of a minimal GUT scenario*. *Nucl.Phys.*, B747:312–327, 2006. doi: 10.1016/j.nuclphysb.2006.05.006.

[125] Haipeng An, Shao-Long Chen, Rabindra N. Mohapatra, and Yue Zhang. *Leptogenesis as a Common Origin for Matter and Dark Matter*. *JHEP*, 1003:124, 2010. doi: 10.1007/JHEP03(2010)124.

[126] Maxim Markevitch, A.H. Gonzalez, D. Clowe, A. Vikhlinin, L. David, et al. *Direct constraints on the dark matter self-interaction cross-section from the merging galaxy cluster 1E0657-56*. *Astrophys.J.*, 606:819–824, 2004. doi: 10.1086/383178.

[127] David N. Spergel and Paul J. Steinhardt. *Observational evidence for selfinteracting cold dark matter*. *Phys.Rev.Lett.*, 84:3760–3763, 2000. doi: 10.1103/PhysRevLett.84.3760.

[128] L. Michel. *Symmetry Defects and Broken Symmetry. Configurations - Hidden Symmetry*. *Rev.Mod.Phys.*, 52:617–651, 1980. doi: 10.1103/RevModPhys.52.617.

[129] R. Slansky. *Group Theory for Unified Model Building*. *Phys.Rept.*, 79:1–128, 1981. doi: 10.1016/0370-1573(81)90092-2.

[130] Zurab Tavartkiladze. *$SU(5)\times SU(5)'$ unification and D_2 parity: Model for composite leptons*. *Phys. Rev.*, D90(1):015022, 2014. doi: 10.1103/PhysRevD.90.015022.

[131] Pei-Hong Gu. *Mirror symmetry: from active and sterile neutrino masses to baryonic and dark matter asymmetries*. *Nucl.Phys.*, B874:158–176, 2013. doi: 10.1016/j.nuclphysb.2013.05.013.

[132] Pei-Hong Gu. *From Dirac neutrino masses to baryonic and dark matter asymmetries*. *Nucl. Phys.*, B872:38–61, 2013. doi: 10.1016/j.nuclphysb.2013.03.014.

[133] Pei-Hong Gu. *Mirror left-right symmetry*. *Phys. Lett.*, B713:485–489, 2012. doi: 10.1016/j.physletb.2012.06.042.

[134] Jogesh C. Pati and Abdus Salam. *Is Baryon Number Conserved?* *Phys.Rev.Lett.*, 31:661–664, 1973. doi: 10.1103/PhysRevLett.31.661.

[135] H. Georgi and S.L. Glashow. *Unity of All Elementary Particle Forces*. *Phys.Rev.Lett.*, 32:438–441, 1974. doi: 10.1103/PhysRevLett.32.438.

[136] H. Georgi. *Lie Algebras in Particle Physics. From Isospin to Unified Theories*. Frontiers in Physics. Avalon Publishing, 1999. ISBN 9780813346113.

[137] Dan-di Wu. *The Symmetry Breaking Pattern of Scalars in Low Dimension Representations*. *Nucl.Phys.*, B199:523, 1982. doi: 10.1016/0550-3213(82)90358-3.

[138] Helena Kolesova and Michal Malinsky. *Proton lifetime in the minimal SO(10) GUT and its implications for the LHC*. *Phys. Rev.*, D90(11):115001, 2014. doi: 10.1103/PhysRevD.90.115001.

[139] K.S. Babu and R.N. Mohapatra. *Coupling Unification, GUT-Scale Baryogenesis and Neutron-Antineutron Oscillation in SO(10)*. *Phys.Lett.*, B715:328–334, 2012. doi: 10.1016/j.physletb.2012.08.006.

[140] Jian-Wei Cui, Hong-Jian He, Lan-Chun Lu, and Fu-Rong Yin. *Spontaneous Mirror Parity Violation, Common Origin of Matter and Dark Matter, and the LHC Signatures*. *Phys. Rev.*, D85:096003, 2012. doi: 10.1103/PhysRevD.85.096003.

[141] Riccardo Barbieri, Lawrence J. Hall, and Keisuke Harigaya. *Minimal Mirror Twin Higgs*. *JHEP*, 11:172, 2016. doi: 10.1007/JHEP11(2016)172.

[142] Pei-Hong Gu. *An $SO(10) \times SO(10)'$ model for common origin of neutrino masses, ordinary and dark matter-antimatter asymmetries*. *JCAP*, 1412(12):046, 2014. doi: 10.1088/1475-7516/2014/12/046.

[143] Pei-Hong Gu. *Mirror symmetry: from active and sterile neutrino masses to baryonic and dark matter asymmetries*. *Nucl. Phys.*, B874:158–176, 2013. doi: 10.1016/j.nuclphysb.2013.05.013.

[144] Marco Farina. *Asymmetric Twin Dark Matter*. *JCAP*, 1511(11):017, 2015. doi: 10.1088/1475-7516/2015/11/017.

[145] G. C. Branco, P. M. Ferreira, L. Lavoura, M. N. Rebelo, Marc Sher, and Joao P. Silva. *Theory and phenomenology of two-Higgs-doublet models*. *Phys. Rept.*, 516: 1–102, 2012. doi: 10.1016/j.physrep.2012.02.002.

[146] Alejandra Melfo, Miha Nemevsek, Fabrizio Nesti, Goran Senjanovic, and Yue Zhang. *Inert Doublet Dark Matter and Mirror/Extra Families after Xenon100*. *Phys. Rev.*, D84:034009, 2011. doi: 10.1103/PhysRevD.84.034009.

[147] Sarah Andreas, Michel H. G. Tytgat, and Quentin Swillens. *Neutrinos from Inert Doublet Dark Matter*. *JCAP*, 0904:004, 2009. doi: 10.1088/1475-7516/2009/04/004.

[148] A. Badertscher, P. Crivelli, W. Fetscher, U. Gendotti, S. Gninenko, V. Postoev, A. Rubbia, V. Samoylenko, and D. Sillou. *An Improved Limit on Invisible Decays of Positronium*. *Phys. Rev.*, D75:032004, 2007. doi: 10.1103/PhysRevD.75.032004.

[149] Edward Hardy and James Unwin. *Symmetric and Asymmetric Reheating*. *JHEP*, 09:113, 2017. doi: 10.1007/JHEP09(2017)113.

[150] Borut Bajc. *High temperature symmetry nonrestoration*. In *Proceedings, 3rd International Conference on Particle Physics and the Early Universe (COSMO*

1999): Trieste, Italy, September 27-October 3, 1999, pages 247–253, 2000. doi: 10.1142/9789812792129_0039.

[151] Lawrence M. Krauss and Soo-Jong Rey. *Spontaneous CP violation at the electroweak scale*. *Phys. Rev. Lett.*, 69:1308–1311, 1992. doi: 10.1103/PhysRevLett.69.1308.

[152] Robert Foot, Archil Kobakhidze, Kristian L. McDonald, and Raymond R. Volkas. *Poincaré protection for a natural electroweak scale*. *Phys. Rev.*, D89(11):115018, 2014. doi: 10.1103/PhysRevD.89.115018.

[153] V. Berezinsky. *Mirror matter and mirror neutrinos*. In *Proceedings of the 2nd NO-VE International Workshop on Neutrino Oscillations*, pages 81–96, 2003.

[154] Robert Foot and R. R. Volkas. *Implications of mirror neutrinos for early universe cosmology*. *Phys. Rev.*, D61:043507, 2000. doi: 10.1103/PhysRevD.61.043507.

[155] Nicole F. Bell. *Mirror matter and heavy singlet neutrino oscillations in the early universe*. *Phys. Lett.*, B479:257–264, 2000. doi: 10.1016/S0370-2693(00)00319-1.

[156] Zackaria Chacko, Nathaniel Craig, Patrick J. Fox, and Roni Harnik. *Cosmology in Mirror Twin Higgs and Neutrino Masses*. *JHEP*, 07:023, 2017. doi: 10.1007/JHEP07(2017)023.

[157] J. A. Casas and A. Ibarra. *Oscillating neutrinos and muon to e, gamma*. *Nucl. Phys.*, B618:171–204, 2001. doi: 10.1016/S0550-3213(01)00475-8.

[158] Jackson D. Clarke, Robert Foot, and Raymond R. Volkas. *Natural leptogenesis and neutrino masses with two Higgs doublets*. *Phys. Rev.*, D92(3):033006, 2015. doi: 10.1103/PhysRevD.92.033006.

[159] Francesco Vissani. *Do experiments suggest a hierarchy problem?* *Phys. Rev.*, D57:7027–7030, 1998. doi: 10.1103/PhysRevD.57.7027.

[160] W. Buchmuller, P. Di Bari, and M. Plumacher. *Some aspects of thermal leptogenesis*. *New J. Phys.*, 6:105, 2004. doi: 10.1088/1367-2630/6/1/105.

[161] Pei-Hong Gu and Utpal Sarkar. *Leptogenesis with Linear, Inverse or Double Seesaw*. *Phys. Lett.*, B694:226–232, 2011. doi: 10.1016/j.physletb.2010.09.062.

[162] Jeffrey A. Harvey and Michael S. Turner. *Cosmological baryon and lepton number in the presence of electroweak fermion number violation*. *Phys. Rev.*, D42:3344–3349, 1990. doi: 10.1103/PhysRevD.42.3344.

[163] Edward W. Kolb and Michael S. Turner. *The Early Universe*. Frontiers in physics. Perseus, 1994. ISBN 9788187169543.

[164] Eugene Golowich. *Unbinding the Deuteron*. *arXiv*:0803.3329 *[hep-ph]*, 2008.

[165] Dominik J. Schwarz and Maik Stuke. *Lepton asymmetry and the cosmic QCD transition*. *JCAP*, 0911:025, 2009. doi: 10.1088/1475-7516/2009/11/025,10.1088/1475-7516/2010/10/E01. [Erratum: JCAP1010,E01(2010)].

[166] David J. Griffiths. *Introduction to elementary particles*. Physics textbook. Wiley, 2008. ISBN 9783527406012.

[167] Shung-ichi Ando, Fred Myhrer, and Kuniharu Kubodera. *Capture rate and neutron helicity asymmetry for ordinary muon capture on hydrogen*. *Phys. Rev.*, C63:015203, 2001. doi: 10.1103/PhysRevC.63.015203.

[168] Andrzej Czarnecki, William J. Marciano, and Alberto Sirlin. *Electroweak radiative corrections to muon capture*. *Phys. Rev. Lett.*, 99:032003, 2007. doi: 10.1103/PhysRevLett.99.032003.

[169] Sean Tulin and Hai-Bo Yu. *Dark Matter Self-interactions and Small Scale Structure*. *Phys. Rept.*, 730:1–57, 2018. doi: 10.1016/j.physrep.2017.11.004.

[170] Murray Gell-Mann. *A Schematic Model of Baryons and Mesons*. *Phys. Lett.*, 8:214–215, 1964. doi: 10.1016/S0031-9163(64)92001-3.

[171] M. M. Giannini and E. Santopinto. *The hypercentral constituent quark model*. *AIP Conf. Proc.*, 1488:257–265, 2012. doi: 10.1063/1.4759406.

[172] J. M. Richard. *The Nonrelativistic three-body problem for baryons*. *Phys. Rept.*, 212:1–76, 1992. doi: 10.1016/0370-1573(92)90078-E.

[173] Nathan Isgur and Gabriel Karl. *Hyperfine Interactions in Negative Parity Baryons*. *Phys. Lett.*, B72:109, 1977. doi: 10.1016/0370-2693(77)90074-0.

[174] Nathan Isgur and Gabriel Karl. *P Wave Baryons in the Quark Model*. *Phys. Rev.*, D18:4187, 1978. doi: 10.1103/PhysRevD.18.4187.

[175] Lindsay Forestell, David E. Morrissey, and Kris Sigurdson. *Non-Abelian Dark Forces and the Relic Densities of Dark Glueballs*. *Phys. Rev.*, D95(1):015032, 2017. doi: 10.1103/PhysRevD.95.015032.

[176] Amarjit Soni and Yue Zhang. *Hidden SU(N) Glueball Dark Matter*. *Phys. Rev.*, D93(11):115025, 2016. doi: 10.1103/PhysRevD.93.115025.

[177] Kimberly K. Boddy, Jonathan L. Feng, Manoj Kaplinghat, Yael Shadmi, and Timothy M. P. Tait. *Strongly interacting dark matter: Self-interactions and keV lines*. *Phys. Rev.*, D90(9):095016, 2014. doi: 10.1103/PhysRevD.90.095016.

[178] Michael D. Scadron, Frieder Kleefeld, and George Rupp. *Small strange quark content of protons*. *arXiv:hep-ph/*0609024, 2006.

[179] C. J. Horowitz and J. Piekarewicz. *Quark Coulomb interactions and the mass difference of mirror nuclei*. *Phys. Rev. C*, 63:011303, Dec 2000. doi: 10.1103/PhysRevC.63.011303.

[180] A. De Rujula, Howard Georgi, and S. L. Glashow. *Hadron Masses in a Gauge Theory*. *Phys. Rev.*, D12:147–162, 1975. doi: 10.1103/PhysRevD.12.147.

[181] Kalman Varga, Marco Genovese, Jean-Marc Richard, and Bernard Silvestre-Brac. *Isospin mass splittings of baryons in potential models*. *Phys. Rev.*, D59:014012, 1999. doi: 10.1103/PhysRevD.59.014012.

[182] C. Semay and B. Silvestre-Brac. *Potential models and meson spectra*. *Nucl. Phys.*, A618:455–482, 1997. doi: 10.1016/S0375-9474(97)00060-2.

[183] B. Silvestre-Brac. *Spectrum and static properties of heavy baryons*. *Few Body Syst.*, 20:1–25, 1996. doi: 10.1007/s006010050028.

[184] R. K. Bhaduri, L. E. Cohler, and Y. Nogami. *A Unified Potential for Mesons and Baryons*. *Nuovo Cim.*, A65:376–390, 1981. doi: 10.1007/BF02827441.

[185] K. A. Olive et al. *Review of Particle Physics*. *Chin. Phys.*, C38:090001, 2014. doi: 10.1088/1674-1137/38/9/090001.

[186] F. Gursey and L. A. Radicati. *Spin and unitary spin independence of strong interactions*. *Phys. Rev. Lett.*, 13:173–175, 1964. doi: 10.1103/PhysRevLett.13.173.

[187] M. M. Giannini, E. Santopinto, and A. Vassallo. *A New application of the Gursey and Radicati mass formula*. *Eur. Phys. J.*, A25:241–247, 2005. doi: 10.1140/epja/i2005-10113-4.

[188] Elmar P. Biernat, M. T. Pena, J. E. Ribeiro, Alfred Stadler, and Franz Gross. *Chiral-symmetry breaking and confinement in Minkowski space*. *AIP Conf. Proc.*, 1701:040003, 2016. doi: 10.1063/1.4938620.

[189] Robert Mann. *An Introduction to Particle Physics and the Standard Model*. CRC Press, 1 edition, 2011. ISBN 9781420082982.

[190] Prateek Agrawal, Francis-Yan Cyr-Racine, Lisa Randall, and Jakub Scholtz. *Make Dark Matter Charged Again*. *JCAP*, 1705(05):022, 2017. doi: 10.1088/1475-7516/2017/05/022.

[191] James M. Cline, Zuowei Liu, Guy Moore, and Wei Xue. *Composite strongly interacting dark matter*. *Phys. Rev.*, D90(1):015023, 2014. doi: 10.1103/PhysRevD.90.015023.

Appendix A

$SU(5) \times SU(5)$ Potentials

A.1 Scalar potential for non-supersymmetric $SU(5)\times SU(5)$ model

In Chapter 2 we outlined the construction of an $SU(5)\times SU(5)$ potential with asymmetric minima. Here we discuss its features in more detail and explore some of the possibilities in regard to breaking to various subgroups. The full $SU(5) \times SU(5)$ potential can be written as

$$\begin{aligned} V &= \lambda_{a1}(\phi_v{}^i_j\phi_v{}^j_i + \phi_d{}^i_j\phi_d{}^j_i - \mu_a^2)^2 + \kappa_a(\phi_v{}^i_j\phi_v{}^j_i\phi_d{}^h_k\phi_d{}^k_h) + \lambda_{a2}(\phi_v{}^i_j\phi_v{}^j_k\phi_v{}^k_h\phi_v{}^h_i + \phi_d{}^i_j\phi_d{}^j_k\phi_d{}^k_h\phi_d{}^h_i) \\ &+ \lambda_{t2}(\chi_{vij}\chi_v{}^{ji} + \chi_{dij}\chi_d{}^{ji} - \mu_t^2)^2 + \kappa_t(\chi_{vij}\chi_v{}^{ji}\chi_{dij}\chi_d{}^{ji}) \\ &+ \lambda_{t2}(\chi_{vij}\chi_v{}^{ij}\chi_{vij}\chi_v{}^{ij} + \chi_{dij}\chi_d{}^{ij}\chi_{dij}\chi_d{}^{ij}) + C_0(\chi_{vij}\chi_v{}^{ij}\phi_v{}^i_j\phi_v{}^j_i + \chi_{dij}\chi_d{}^{ji}\phi_d{}^i_j\phi_d{}^j_i) \\ &+ C_1(\chi_{vij}\chi_v{}^{jk}\phi_v{}^l_k\phi_v{}^j_l + \chi_{dij}\chi_d{}^{jk}\phi_d{}^l_k\phi_d{}^j_l) + C_2(\chi_{vlq}\chi_v{}^{ij}\phi_v{}^l_j\phi_v{}^q_i + \chi_{dlq}\chi_d{}^{ij}\phi_d{}^l_j\phi_d{}^q_i) \\ &+ C_3(\chi_{vsu}\chi_v{}^{pq}\phi_v{}^n_m\phi_v{}^i_j\epsilon^{smujt}\epsilon_{pnqit} + \chi_{dsu}\chi_d{}^{pq}\phi_d{}^n_m\phi_d{}^i_j\epsilon^{smujt}\epsilon_{pnqit}) \\ &+ C_4(\phi_v{}^i_j\phi_v{}^j_i\chi_{dij}\chi_d{}^{ji} + \phi_d{}^i_j\phi_d{}^j_i\chi_{vij}\chi_v{}^{ji}). \end{aligned} \tag{A.1}$$

The parameters are $\lambda_{t1}, \mu_t, \lambda_{t2}$ as well as $\lambda_{a1}, \mu_a, \lambda_{a2}$, κ_a and κ_t. In addition to these there are five cross terms arising from nontrivial contractions between our representations, with parameters $(C_0, C_1, C_2, C_3, C_4)$. In general the asymmetry required can be attained by making these additional cross term parameters smaller than C_0 and the other parameters of the model. In minimising this potential we can reduce the total number of parameters by placing all of our fields in a simplified VEV form. The adjoint

can be represented by the traceless matrix

$$\langle \phi_v \rangle = v_v \begin{pmatrix} \alpha_1 & 0 & 0 & 0 & 0 \\ 0 & \alpha_2 & 0 & 0 & 0 \\ 0 & 0 & \alpha_3 & 0 & 0 \\ 0 & 0 & 0 & \alpha_4 & 0 \\ 0 & 0 & 0 & 0 & \alpha_5 \end{pmatrix}, \tag{A.2}$$

with $\alpha_1 + \alpha_2 + \alpha_3 + \alpha_4 + \alpha_5 = 0$. For the **10** we have

$$\langle \chi_d \rangle = v_d \begin{pmatrix} 0 & \rho_1 & 0 & 0 & 0 \\ -\rho_1 & 0 & 0 & 0 & 0 \\ 0 & 0 & 0 & \rho_2 & 0 \\ 0 & 0 & -\rho_2 & 0 & 0 \\ 0 & 0 & 0 & 0 & 0 \end{pmatrix}, \tag{A.3}$$

with $\rho_{1,2}$ complex. The **24** and **10** are both reduced to just four total different degrees of freedom each in this form. Working numerically we can however quickly compare the results of using just these 16 degrees of freedom or the full 68; they were found to agree in all cases. The parameter space is directly comparable to that of the simple model of Sec. 2.3. The positive definite terms act exactly like collections of additional fields that one could add to that previous model with the same-sector and cross-sector couplings needed to generate asymmetric VEVs that differentiate entire sets of fields within these multiplets. That is, if κ_a is large enough then if all $(\phi_{v_j}^{\ i})$ fields gain a nonzero VEV, all of the fields $(\phi_{d_j}^{\ i})$ are encouraged to become zero. Together with (C_1, C_2, C_3, C_4) there is a greater variability for the signs of quartic terms of the potential. Scaling any of these additional quartics too high may alter the VEV pattern from the desired asymmetric pattern. A larger value of C_0 will however ensure the breaking is the extension of that in Sec. 2.3. To be concrete, we display an example of some parameters set along these guidelines and the VEVs that are produced. The parameters

$$\begin{gathered} \lambda_{a1} \simeq 0.4,\ \kappa_a \simeq 0.4,\ \kappa_t \simeq 0.4,\ \lambda_{t1} \simeq 0.8, \\ \mu_t \simeq 0.2,\ \mu_a \simeq 0.1,\ \lambda_{a2} \simeq 0.1,\ \lambda_{t2} \simeq -0.1, \\ C_0 \simeq 0.5,\ C_1 \simeq -0.1,\ C_2 \simeq -0.1,\ C_3 \simeq -0.1,\ C_4 \simeq -0.1 \end{gathered} \tag{A.4}$$

give rise to the VEVs

$$
\begin{aligned}
\langle \phi_v \rangle &\simeq 0.24 \begin{pmatrix} 1 & 0 & 0 & 0 & 0 \\ 0 & 1 & 0 & 0 & 0 \\ 0 & 0 & 1 & 0 & 0 \\ 0 & 0 & 0 & -3/2 & 0 \\ 0 & 0 & 0 & 0 & -3/2 \end{pmatrix}, \\
\langle \chi_v \rangle &\simeq 0, \\
\langle \phi_d \rangle &\simeq 0, \\
\langle \chi_d \rangle &\simeq 0.1 \begin{pmatrix} 0 & 1+i & 0 & 0 & 0 \\ -1-i & 0 & 0 & 0 & 0 \\ 0 & 0 & 0 & 0 & 0 \\ 0 & 0 & 0 & 0 & 0 \\ 0 & 0 & 0 & 0 & 0 \end{pmatrix}. \qquad \text{(A.5)}
\end{aligned}
$$

A.2 Scalar potential for supersymmetric $SU(5) \times SU(5)$ model

In this section we will discuss further the results of the supersymmetric version of asymmetric symmetry breaking. The analysis here only serves to demonstrate that such asymmetric patterns are possible within the constraints inherent in supersymmetric theories.

Positive definite couplings between fields of different sectors are required to create the anti-correlation between sectors. This is what necessitates a field which transforms into itself under the discrete symmetry. An alternative to this could be to arm the theory with a pair of complete singlets under the discrete symmetry, i.e. S_v, S_d. Without such additions we are unable to create gauge invariant terms in the superpotential which can allow for cross-sector couplings to appear in the F-terms. The other addition we made of the multiplet Y was based on our choice of complex representations.[1] We wish, however, to demonstrate that the theory which we used previously can be adopted into a supersymmetric form with the same gauge group breaking chains. The terms that we wish to highlight that are derived from the superpotential are the contractions of the form

$$s_4^2(\Phi_v\Phi_v X_v X_v + \Phi_v\Phi_v Y_v Y_v + \Phi_d\Phi_d X_d X_d + \Phi_d\Phi_d Y_d Y_d). \tag{A.6}$$

It is clear that the parameter s_4 being larger can help lead to asymmetric VEVs. The other important parameter is s_5 which affects the term

$$s_5^2(\Phi_d\Phi_d\Phi_v\Phi_v). \tag{A.7}$$

With just these terms and the additional soft masses one can generate an asymmetric VEV pattern. For the parameter example

$$\begin{aligned} &s_4 = s_5 \simeq 0.02, \qquad g_5 \simeq 0.037, \qquad s_9 \simeq 0.001, \\ &m_X = m_Y \simeq 0.001, \qquad m_\Phi \simeq 0.1, \qquad m_S = 0, \end{aligned} \tag{A.8}$$

[1] This may of course not be necessary, if one was working with two different real representations to facilitate different symmetry breaking in each sector. In that case the procedure would be more straightforward.

and all trilinear terms and other parameters set at or close to zero, we obtain nonzero VEVs for the adjoint in one sector and for the fields X_v and Y_d in the other sector which serve to break $SU(5)_v$ to the Standard Model gauge group and $SU(5)_d$ to the dark sector gauge group with VEVs

$$
\begin{aligned}
\langle \Phi_v \rangle &\simeq 2.1 \begin{pmatrix} 1 & 0 & 0 & 0 & 0 \\ 0 & 1 & 0 & 0 & 0 \\ 0 & 0 & 1 & 0 & 0 \\ 0 & 0 & 0 & -3/2 & 0 \\ 0 & 0 & 0 & 0 & -3/2 \end{pmatrix}, \\
\langle X_v \rangle &\simeq 0, \\
\langle Y_v \rangle &\simeq 0, \\
\langle \Phi_d \rangle &\simeq 0, \\
\langle S \rangle &\simeq 0, \\
\langle X_d \rangle &\simeq \begin{pmatrix} 0 & 1.2+2.9i & 0 & 0 & 0 \\ -1.2-2.9i & 0 & 0 & 0 & 0 \\ 0 & 0 & 0 & -1.53-2.1i & 0 \\ 0 & 0 & 1.5+2.1i & 0 & 0 \\ 0 & 0 & 0 & 0 & 0 \end{pmatrix}, \\
\langle Y_d \rangle &\simeq \begin{pmatrix} 0 & 1.2-2.9i & 0 & 0 & 0 \\ -1.2+2.9i & 0 & 0 & 0 & 0 \\ 0 & 0 & 0 & -1.53+2.1i & 0 \\ 0 & 0 & 1.5i-2.1i & 0 & 0 \\ 0 & 0 & 0 & 0 & 0 \end{pmatrix}. \qquad \text{(A.9)}
\end{aligned}
$$

This demonstrates the capacity for supersymmetric models to display the same asymmetric symmetry breaking as non-SUSY models. There are other terms which can contribute to the asymmetric pattern, i.e. contractions of the style $(X_d X_d X_v X_v)$, but scaling these up to be larger also scales upwards terms that we would need to contend with to maintain the asymmetry.

Appendix B

$SO(10) \times SO(10)$ Potentials

In this appendix we expand on the potential discussed in Section 3.4. We firstly consider the two representations of $SO(10)$ independently. These are the adjoint **45**, denoted by ϕ_{ij} which can be formed from the antisymmetric product of two fundamental representations, and the **54** which we label χ_{ij} which is formed from the completely symmetric product of two fundamentals. The most general quartic potential for a rank two antisymmetric tensor in $SO(10)$ is

$$-\frac{\mu^2}{2}\phi_{ij}\phi_{ji} + \frac{\lambda}{4}(\phi_{ij}\phi_{ji})^2 + \frac{\alpha}{4}\phi_{ij}\phi_{jk}\phi_{kl}\phi_{li}. \tag{B.1}$$

For this potential the symmetry breaking pattern is as follows. For $\lambda > 0$ and $\alpha > 0$ we have

$$SO(10) \to SU(5) \times U(1), \tag{B.2}$$

while for $\lambda > 0$ and $\alpha < 0$ we find

$$SO(10) \to SO(8) \times U(1). \tag{B.3}$$

In the case of the symmetric rank two representation we have a similar equation but with the added cubic term $\mathrm{Tr}(\chi^3)$ so that the potential reads

$$-\frac{\mu^2}{2}\chi_{ij}\chi_{ji} + \frac{\lambda}{4}(\chi_{ij}\chi_{ji})^2 + \frac{\alpha}{4}\chi_{ij}\chi_{jk}\chi_{kl}\chi_{li} + \frac{\beta\mu}{3}\chi_{ij}\chi_{jk}\chi_{ki}. \tag{B.4}$$

For this potential the parameter space is such that without the cubic term the possible breaking chains are, for $\lambda < 0$ and $\alpha < 0$,

$$SO(10) \to SO(9), \tag{B.5}$$

while for $\lambda > 0$ and $\alpha > 0$ we have

$$SO(10) \to SO(5) \times SO(5). \tag{B.6}$$

For the parameter space where $\lambda > 0$ and $\alpha > 0$ and the cubic term is nonzero we have

$$SO(10) \to SO(10-n) \times SO(n), \tag{B.7}$$

where for values of $\beta = 0$ we recover the above result in Eq. B6 and for $\beta > 0$, n increases as β does until the breaking chain of Eq. B5 is recovered. The generation of the potential in Eq. 3.18 then results from the addition of the two potentials given above in Eq. B1 and Eq. B4, as well as the analogue terms of the toy potential that mix the fields of the two sectors and the new non-trivial same-sector contractions afforded by the choice of the **45** and **54** representations. Using this potential our numerical results align with the expected minima from the above potentials in the case where the cross terms and the additional cubic terms are sufficiently small. For the choice of parameter space where $\lambda_\phi > 0, \alpha_\phi > 0, \lambda_\chi > 0, \alpha_\chi > 0, \beta > 0, \kappa_\phi > 0, \kappa_\chi > 0, c_2 > c_1 > 0, c_3 \ll c_2, c_4 \ll c_2, c_5 \ll c_2$ we will obtain a potential which breaks asymmetrically with the specific choice of breaking chain for each sector. This agrees with our numerical analysis where for a sample choice of parameters,

$$\lambda_\phi \simeq 1,\ \kappa_\phi \simeq 0.75,\ \kappa_\chi \simeq 0.75,\ \lambda_\chi \simeq 1.6,$$
$$\mu_\phi \simeq 1,\ \mu_\chi \simeq 1,\ \alpha_\phi \simeq 0.5,\ \alpha_\chi \simeq 1,$$
$$\beta_\chi \simeq 0.35,\ c_1 \simeq 0.25,\ c_2 \simeq 0.75,\ c_3 \simeq 0,\ c_4 \simeq 0,\ c_5 \simeq 0,$$

we find that minimum preserves the VEVs

$$
\begin{aligned}
\langle \phi_V \rangle &= 0.3 \begin{pmatrix}
0 & 1 & 0 & 0 & 0 & 0 & 0 & 0 & 0 & 0 \\
-1 & 0 & 0 & 0 & 0 & 0 & 0 & 0 & 0 & 0 \\
0 & 0 & 0 & 1 & 0 & 0 & 0 & 0 & 0 & 0 \\
0 & 0 & -1 & 0 & 0 & 0 & 0 & 0 & 0 & 0 \\
0 & 0 & 0 & 0 & 0 & 1 & 0 & 0 & 0 & 0 \\
0 & 0 & 0 & 0 & -1 & 0 & 0 & 0 & 0 & 0 \\
0 & 0 & 0 & 0 & 0 & 0 & 0 & 1 & 0 & 0 \\
0 & 0 & 0 & 0 & 0 & 0 & -1 & 0 & 0 & 0 \\
0 & 0 & 0 & 0 & 0 & 0 & 0 & 0 & 0 & 1 \\
0 & 0 & 0 & 0 & 0 & 0 & 0 & 0 & -1 & 0
\end{pmatrix}, \\
\langle \phi_D \rangle &= 0, \\
\langle \chi_V \rangle &= 0, \\
\langle \chi_D \rangle &= 0.3 \begin{pmatrix}
1 & 0 & 0 & 0 & 0 & 0 & 0 & 0 & 0 & 0 \\
0 & 1 & 0 & 0 & 0 & 0 & 0 & 0 & 0 & 0 \\
0 & 0 & 1 & 0 & 0 & 0 & 0 & 0 & 0 & 0 \\
0 & 0 & 0 & 1 & 0 & 0 & 0 & 0 & 0 & 0 \\
0 & 0 & 0 & 0 & 1 & 0 & 0 & 0 & 0 & 0 \\
0 & 0 & 0 & 0 & 0 & 1 & 0 & 0 & 0 & 0 \\
0 & 0 & 0 & 0 & 0 & 0 & -6/4 & 0 & 0 & 0 \\
0 & 0 & 0 & 0 & 0 & 0 & 0 & -6/4 & 0 & 0 \\
0 & 0 & 0 & 0 & 0 & 0 & 0 & 0 & -6/4 & 0 \\
0 & 0 & 0 & 0 & 0 & 0 & 0 & 0 & 0 & -6/4
\end{pmatrix},
\end{aligned}
\tag{B.8}
$$

which breaks the symmetry according to

$$
SO(10)_V \times SO(10)_D \to [SU(4) \times SU(2) \times SU(2)]_V \times [SU(5) \times U(1)]_D. \tag{B.9}
$$

The analysis discussed here describes just the first step in asymmetrically breaking an $SO(10)$ mirror symmetric potential to different subgroups for each sector and at different energy scales. While many other possible breaking chains that have been discussed in this work could be analysed, we leave such work to future efforts to create a detailed model of an $SO(10)$ GUT model where the choice of representations aligns with choices for fermion mass generation models and considerations of minimality. Due to the complexity

in analysing such Higgs potentials for large gauge groups we content ourselves at the present juncture with the demonstration of the versatility of such asymmetric symmetry breaking in the context of GUT models. With this specific example and the principles given in the toy model, many of the other breaking chains could be realised in potentials constructed in a like manner.

Appendix C

Leptogenesis Rates and Mass Eigenstates of a Mirror 2HDM

C.1 Interaction rates in mirror leptogenesis

The decay terms in Eq 4.44 are given by

$$D_{+}^{\phi_1} = z\frac{(Y_1^{\dagger}Y_1)_{11}}{H(z=1)}\frac{K_1(z)}{K_2(z)}, \quad D_{+}^{\phi_2} = z\frac{(Y_2^{\dagger}Y_2)_{11}}{H(z=1)}\frac{K_1(z)}{K_2(z)}, \tag{C.1}$$
$$D_{-}^{\phi_1} = z\frac{(F_1^{\dagger}F_1)_{11}}{H(z=1)}\frac{K_1(z)}{K_2(z)}, \quad D_{-}^{\phi_2} = z\frac{(F_2^{\dagger}F_2)_{11}}{H(z=1)}\frac{K_1(z)}{K_2(z)},$$

with K_1, K_2 modified Bessel functions of the second kind with order one and two respectively. For scatterings and washout we also have additional terms from the additional decay channels to each sector and via the second Higgs doublet,

$$S_{\pm}^{s,t} = \frac{\Gamma_{\pm}^{s,t}}{Hz}, \tag{C.2}$$

with $S_{\pm} = 2(S_{\pm}^{s} + 2S_{\pm}^{t})$. The scattering rate is

$$\Gamma_{\pm}^{s,t} = \frac{M_1}{24\zeta(3)g_N\pi^2}\frac{I_{\pm}^{s,t}}{K_2(z)z^3}, \tag{C.3}$$

where

$$
\begin{aligned}
I_{\pm}^{s,t} &= \int_{z^2}^{\infty} d\Psi\, \hat{\sigma}_{\pm}^{s,t}(\Psi)\, \sqrt{\Psi}\, K_1(\sqrt{\Psi}), \\
\hat{\sigma}_{+}^{s,t} &= \frac{3}{16\pi} \left[(\eta_1^t)^2 (Y_1^\dagger Y_1)_{ii} + (\eta_2^t)^2 (Y_2^\dagger Y_2)_{ii} \right] \chi^{s,t}(x), \\
\hat{\sigma}_{-}^{s,t} &= \frac{3}{16\pi} \left[(\eta_1^t)^2 (F_1^\dagger F_1)_{ii} + (\eta_2^t)^2 (F_2^\dagger F_2)_{ii} \right] \chi^{s,t}(x).
\end{aligned}
\tag{C.4}
$$

The functions $\chi^{s,t}$ are the same as in [74] and the η^t is the top Yukawa coupling. The washout from inverse decays is then given by

$$
W_{ID} = \frac{1}{2}(D_+^{\phi_1} + D_+^{\phi_2} + D_-^{\phi_1} + D_-^{\phi_2}) \frac{\mathcal{N}_{N_1^{\rm Eq}}}{\mathcal{N}_{l^{\rm Eq}}}, \tag{C.5}
$$

and the total washout rate by

$$
W_T = W_{ID} \left[1 + \frac{\left(2 \left(\frac{\mathcal{N}_{N_1^+}}{\mathcal{N}_{N_1^{\rm Eq}}} S_+^s + \frac{\mathcal{N}_{N_1^-}}{\mathcal{N}_{N_1^{\rm Eq}}} S_-^s \right) + 4(S_+^t + S_-^t) \right)}{(D_+^{\phi_1} + D_+^{\phi_2} + D_-^{\phi_1} + D_-^{\phi_2})} \right]. \tag{C.6}
$$

C.2 Mirror Higgs potentials

In Chapter 4 we examined the general Higgs potential of a mirror symmetric model with two Higgs doublets in each sector. In the asymmetric limit where neutral states G_1 and G_2 are massless Goldstone bosons following the breaking to QED in each sector we can examine the mixing among all six neutral bosons. The neutral squared mass matrix in the mirror symmetric Φ basis among states, $(\phi_1, \phi_2, a_2, \phi_1', \phi_2', a_1)$, is

$$
\begin{pmatrix}
m_{\phi_1\phi_1} & m_{\phi_1\phi_2} & m_{\phi_1 a_2} & m_{\phi_1\phi_1'} & m_{\phi_1\phi_2'} & m_{\phi_1 a_1} \\
m_{\phi_2\phi_1} & m_{\phi_2\phi_2} & m_{\phi_2 a_2} & m_{\phi_2\phi_1'} & m_{\phi_2\phi_2'} & m_{\phi_2 a_1} \\
m_{a_2\phi_1} & m_{a_2\phi_2} & m_{a_2 a_2} & m_{a_2\phi_1'} & m_{a_2\phi_2'} & m_{a_2 a_1} \\
m_{\phi_1'\phi_1} & m_{\phi_1'\phi_2} & m_{\phi_1' a_2} & m_{\phi_1'\phi_1'} & m_{\phi_1'\phi_2'} & m_{\phi_1' a_1} \\
m_{\phi_2'\phi_1} & m_{\phi_2'\phi_2} & m_{\phi_2' a_2} & m_{\phi_2'\phi_1'} & m_{\phi_2'\phi_2'} & m_{\phi_2' a_1} \\
m_{a_1\phi_1} & m_{a_1\phi_2} & m_{a_1 a_2} & m_{a_1\phi_1'} & m_{a_1\phi_2'} & m_{a_1 a_1}
\end{pmatrix}.
\tag{C.7}
$$

This consists of the 21 elements, which in the asymmetric limit become

$$m_{\phi_1\phi_1} \simeq m_{11}^2 + (3v_1^2 z_1)\frac{1}{2} + (w_2^2 z_{12})\frac{1}{2} + (v_2^2 z_3)\frac{1}{2} + (v_2^2 z_4)\frac{1}{2} + (w_1^2 z_8)\frac{1}{2} + w_1 w_2 \mathrm{Re}[z_{13}]$$
$$+ \frac{1}{2}v_2^2 \mathrm{Re}[z_5] + 3v_1 v_2 \mathrm{Re}[z_6],$$
$$m_{\phi_2\phi_2} \simeq m_{22}^2 + (w_1^2 z_{12})\frac{1}{2} + (3v_2^2 z_2)\frac{1}{2} + (v_1^2 z_3)\frac{1}{2} + (v_1^2 z_4)\frac{1}{2} + (w_2^2 z_9)\frac{1}{2} + w_1 w_2 \mathrm{Re}[z_{14}]$$
$$+ \frac{1}{2}v_1^2 \mathrm{Re}[z_5] + 3v_1 v_2 \mathrm{Re}[z_7],$$
$$m_{a_2 a_2} \simeq m_{22}^2 + (w_1^2 z_{12})\frac{1}{2} + (v_2^2 z_2)\frac{1}{2} + (v_1^2 z_3)\frac{1}{2} + (v_1^2 z_4)\frac{1}{2} + (w_2^2 z_9)\frac{1}{2} + w_1 w_2 \mathrm{Re}[z_{14}]$$
$$- \frac{1}{2}v_1^2 \mathrm{Re}[z_5] + v_1 v_2 \mathrm{Re}[z_7],$$
$$m_{\phi_1'\phi_1'} \simeq m_{11}^2 + (3w_1^2 z_1)\frac{1}{2} + (v_2^2 z_{12})\frac{1}{2} + (w_2^2 z_3)\frac{1}{2} + (w_2^2 z_4)\frac{1}{2} + (v_1^2 z_8)\frac{1}{2} + v_1 v_2 \mathrm{Re}[z_{13}]$$
$$+ \frac{1}{2}w_2^2 \mathrm{Re}[z_5] + 3w_1 w_2 \mathrm{Re}[z_6],$$
$$m_{\phi_2'\phi_2'} \simeq m_{22}^2 + (v_1^2 z_{12})\frac{1}{2} + (3w_2^2 z_2)\frac{1}{2} + (w_1^2 z_3)\frac{1}{2} + (w_1^2 z_4)\frac{1}{2} + (v_2^2 z_9)\frac{1}{2} + v_1 v_2 \mathrm{Re}[z_{14}]$$
$$+ \frac{1}{2}w_1^2 \mathrm{Re}[z_5] + 3w_1 w_2 \mathrm{Re}[z_7],$$
$$m_{a_1 a_1} \simeq m_{22} + (v_1^2 z_{12})\frac{1}{2} + (w_2^2 z_2)\frac{1}{2} + (w_1^2 z_3)\frac{1}{2} + (w_1^2 z_4)\frac{1}{2} + (v_2^2 z_9)\frac{1}{2} + v_1 v_2 \mathrm{Re}[z_{14}]$$
$$- \frac{1}{2}w_1^2 \mathrm{Re}[z_5] + w_1 w_2 \mathrm{Re}[z_7],$$
$$m_{\phi_1\phi_2} \simeq v_1 v_2 z_3 + v_1 v_2 z_4 + \mathrm{Re}[Y_3] + \frac{1}{2}w_1 w_2 \mathrm{Re}[z_{10}] + \frac{1}{2}w_1 w_2 \mathrm{Re}[z_{11}] + \frac{1}{2}w_1^2 \mathrm{Re}[z_{13}]$$
$$+ \frac{1}{2}w_2^2 \mathrm{Re}[z_{14}] + v_1 v_2 \mathrm{Re}[z_5] + \frac{3}{2}v_1^2 \mathrm{Re}[z_6] + \frac{3}{2}v_2^2 \mathrm{Re}[z_7],$$
$$m_{\phi_1 a_2} \simeq \mathrm{Im}[m_{12}^2] + \frac{1}{2}w_1 w_2 \mathrm{Im}[z_{10}] + \frac{1}{2}w_1 w_2 \mathrm{Im}[z_{11}] + \frac{1}{2}w_1^2 \mathrm{Im}[z_{13}] + \frac{1}{2}w_2^2 \mathrm{Im}[z_{14}]$$
$$- v_1 v_2 \mathrm{Im}[z_5] - \frac{3}{2}v_1^2 \mathrm{Im}[z_6] - \frac{1}{2}v_2^2 \mathrm{Im}[z_7],$$
$$m_{\phi_1\phi_1'} \simeq v_1 w_1 z_8 + \frac{1}{2}v_2 w_2 \mathrm{Re}[z_{10}] + \frac{1}{2}v_2 w_2 \mathrm{Re}[z_{11}] + v_2 w_1 \mathrm{Re}[z_{13}]$$
$$+ v_1 w_2 \mathrm{Re}[z_{13}],$$
$$m_{\phi_1\phi_2'} \simeq v_1 w_2 z_{12} + \frac{1}{2}v_2 w_1 \mathrm{Re}[z_{10}] + \frac{1}{2}v_2 w_1 \mathrm{Re}[z_{11}] + v_1 w_1 \mathrm{Re}[z_{13}]$$
$$+ v_2 w_2 \mathrm{Re}[z_{14}],$$
$$m_{\phi_1 a_1} \simeq \frac{1}{2}v_2 w_1 \mathrm{Im}[z_{10}] - \frac{1}{2}v_2 w_1 \mathrm{Im}[z_{11}] + v_1 w_1 \mathrm{Im}[z_{13}],$$
$$m_{\phi_2 a_2} \simeq -(\frac{1}{2})v_1^2 \mathrm{Im}[z_5] - v_1 v_2 \mathrm{Im}[z_7],$$
$$m_{\phi_2\phi_1'} \simeq v_2 w_1 z_{12} + \frac{1}{2}v_1 w_2 \mathrm{Re}[z_{10}] + \frac{1}{2}v_1 w_2 \mathrm{Re}[z_{11}] + v_1 w_1 \mathrm{Re}[z_{13}] + v_2 w_2 \mathrm{Re}[z_{14}],$$
$$m_{\phi_2\phi_2'} \simeq v_2 w_2 z_9 + \frac{1}{2}v_1 w_1 \mathrm{Re}[z_{10}] + \frac{1}{2}v_1 w_1 \mathrm{Re}[z_{11}] + v_2 w_1 \mathrm{Re}[z_{14}] + v_1 w_2 \mathrm{Re}[z_{14}],$$
$$m_{\phi_2 a_1} \simeq \frac{1}{2}v_1 w_1 \mathrm{Im}[z_{10}] - \frac{1}{2}v_1 w_1 \mathrm{Im}[z_{11}] + v_2 w_1 \mathrm{Im}[z_{14}],$$

$$
\begin{aligned}
m_{a_2\phi_1'} &\simeq \frac{1}{2}v_1w_2\mathrm{Im}[z_{10}] + \frac{1}{2}v_1w_2\mathrm{Im}[z_{11}] + v_1w_1\mathrm{Im}[z_{13}],\\
m_{a_2\phi_2'} &\simeq \frac{1}{2}v_1w_1\mathrm{Im}[z_{10}] + \frac{1}{2}v_1w_1\mathrm{Im}[z_{11}] + v_1w_2\mathrm{Im}[z_{14}],\\
m_{a_2a_1} &\simeq -(\frac{1}{2})v_1w_1\mathrm{Re}[z_{10}] + \frac{1}{2}v_1w_1\mathrm{Re}[z_{11}],\\
m_{\phi_1'\phi_2'} &\simeq w_1w_2z_3 + w_1w_2z_4 + \mathrm{Re}[Y3] + \frac{1}{2}v_1v_2\mathrm{Re}[z_{10}] + \frac{1}{2}v_1v_2\mathrm{Re}[z_{11}] + \frac{1}{2}v_1^2\mathrm{Re}[z_{13}]\\
&+ \frac{1}{2}v_2^2\mathrm{Re}[z_{14}] + w_1w_2\mathrm{Re}[z_5] + \frac{3}{2}w_1^2\mathrm{Re}[z_6] + \frac{3}{2}w_2^2\mathrm{Re}[z_7],\\
m_{\phi_1'a_1} &\simeq \mathrm{Im}[m_{12}^2] + \frac{1}{2}v_1v_2\mathrm{Im}[z_{10}] - \frac{1}{2}v_1v_2\mathrm{Im}[z_{11}] + \frac{1}{2}v_1^2\mathrm{Im}[z_{13}] + \frac{1}{2}v_2^2\mathrm{Im}[z_{14}]\\
&- w_1w_2\mathrm{Im}[z_5] - \frac{3}{2}w_1^2\mathrm{Im}[z_6] - \frac{1}{2}w_2^2\mathrm{Im}[z_7],\\
m_{\phi_2'a_1} &\simeq -(\frac{1}{2})w_1^2\mathrm{Im}[z_5] - w_1w_2\mathrm{Im}[z_7].
\end{aligned}
$$

In the dual Higgs basis we can express a new set of six fields that are in terms of only v and w. We can then move to the mass eigenstate basis by rotating these fields or, working from the initial basis, rotate the 8×8 matrix including G_1 and G_2. This results in two zero eigenvalues for the solutions in Table 4.2 and Table 4.3 as expected. Either case yields the same physical mass eigenstates which we find numerically. These solutions to the mass eigenstates, in terms of the parameters of the mirror symmetric basis, are given in Table 4.2 and Table 4.3 for particular choices of the parameter space that produce asymmetric symmetry breaking.

C.3 Feynman diagrams in mirror leptogenesis

We list here the relevant $\Delta L = 1$ scattering interaction channels in the case of mirror leptogenesis considered in Chapter 4.

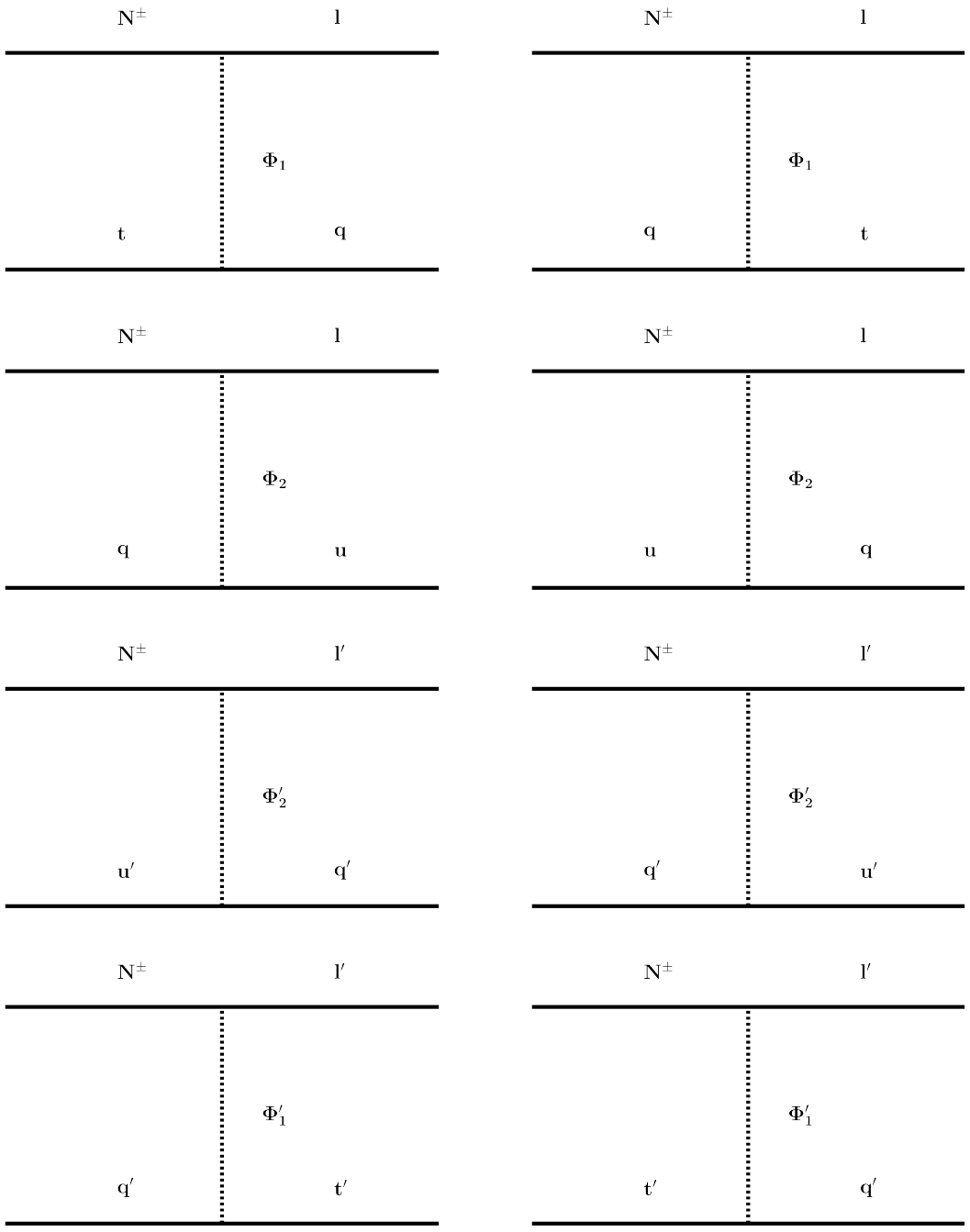

FIGURE C.1: Scattering channels considered in the Boltzmann equations of Chapter 4.

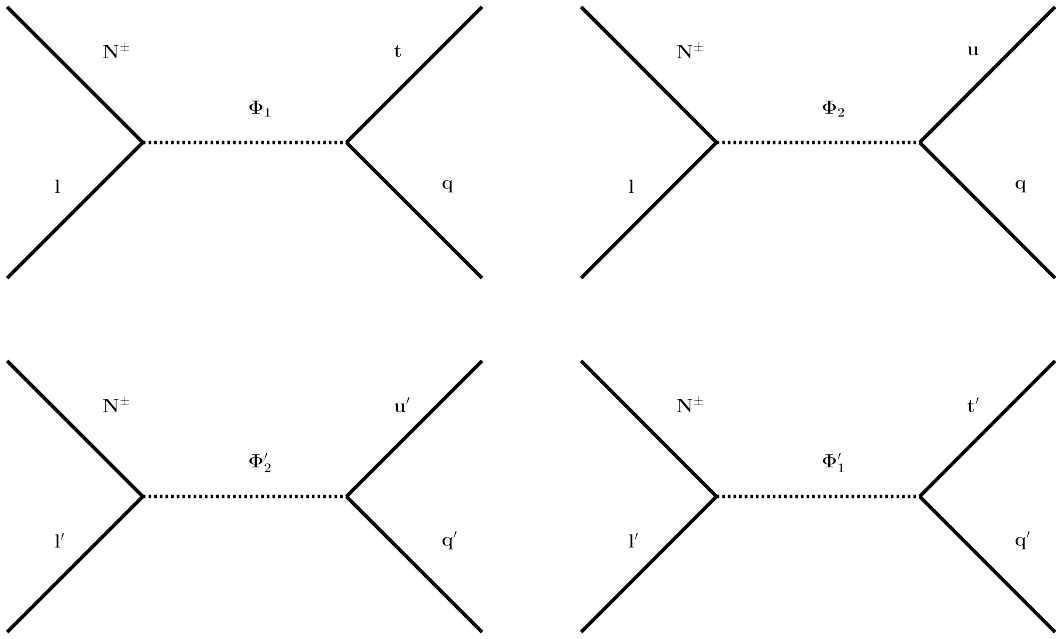

FIGURE C.2: Decay and scattering channels considered in the Boltzmann equations of Chapter 4.

Appendix D

Hypercentral Schrödinger Equation

The full potential including additional spin-spin interactions, isospin-isospin and spin-isospin interactions has the form

$$H_V = V(\vec{r_{ij}}) + V_{SS}(\vec{r_{ij}})\,\vec{\sigma}_1 \cdot \vec{\sigma}_2 + V_{II}\,(\vec{r_{ij}})\vec{t}_1 \cdot \vec{t}_2 + V_{SI}\,(\vec{r_{ij}})(\vec{t}_1 \cdot \vec{t}_2)(\vec{\sigma}_1 \cdot \vec{\sigma}_2) \tag{D.1}$$

and the full non-relativistic Hamiltonian is then [173, 174]

$$H = \sum_i m_i + H_0 + H_V \tag{D.2}$$

with $H_0 = \sum_i \frac{p_i^2}{2m_i}$. As the spin-spin interaction has a larger contribution to the potential than the remaining hyperfine interactions and the spin-orbit term is taken to be negligible as in [171] we similarly focus on a model with the spin-spin effect contributing the most important effects to mass differences. It has the form [180]

$$H_{HI}^{ij} = A\left[(\frac{8\pi}{3})\,\vec{S}_i \cdot \vec{S}_j\,\delta^3(r_{ij})\right], \tag{D.3}$$

where $A = \frac{2\alpha_s}{3m_i m_j}$. In the case of the confining potentials of Eq. 5.10 where analytic solutions are not obtainable we use the matrix methods of [172]. This then uses the expansion of the 6D hyperspherical Schrodinger equation using the Fourier expansion of the spatial wavefunctions over the hyperradius x. Following the matrix methods converts

this to a scaled coordinate $y = \frac{x}{x+r_0}$ where r_0 remains as a scaling estimate of the radius of the spatial wavefunction. We can then express the hypercentral wavefunctions as

$$\psi(y) = \sum_{i=1}^{N} a_i \, \sin(i\pi y). \tag{D.4}$$

This reduces the differential equation to a matrix eigenvalue problem that gives the first N levels for a given value of γ,

$$\begin{aligned} \sum_j \Bigg[& \left[\frac{1}{2m} \frac{(1-y_i)^4}{r_0^2} \sum_k \left(\frac{2}{N+1}\right) \sin(k\pi y_j) \, k^2\pi^2 sin(k\pi y_i) \right] \\ & - \left[\frac{1}{2m} \frac{5}{r_0^2} \frac{(1-y_i)^3}{y_i} \sum_c \frac{2}{N+1} \sin(c\pi y_j) \, c\pi \cos(c\pi y_i) \right] \\ & + \left(\frac{1}{2m} \frac{\gamma(\gamma+4)}{x(y_j)^2} + V(x(y_j)) \right) \delta_{ij} \Bigg] \psi_j = E_{N[\gamma]} \psi(y_i). \end{aligned} \tag{D.5}$$

This can be compared to the numerical solution of the case without the hypercentral approximation. In that calculation, a similar change of variables allows for the calculation of the complete set of coupled hyperspherical differential equations. In our case we apply it to a variety of non-analytic potentials that scale to dark sector parameters and that use the hypercentral approach.